Università degli Studi di Ferrara

Uniwersytet Wrocławski

DOCTORAL COURSE IN
"CHEMISTRY"

CYCLE XXXVIII

International Joint Doctoral Study Programme in Chemistry
with University of Wroclaw (Wroclaw, Poland)

COORDINATOR Prof. Massi Alessandro

# *Novel metallo-peptides to combat antimicrobial resistance: from design to functional characterization through a multi-technique analytical approach*

Scientific/Disciplinary Sector (SDS) CHIM/01


**Candidate**
Dr. Leveraro Silvia

_____
*(signature)*

**Supervisor**
Prof. Remelli Maurizio

_____
*(signature)*

**Co-Supervisor**
Prof. Rowińska-Żyrek Magdalena

_____
*(signature)*

**Co-Supervisor**
Dr. Bellotti Denise

_____
*(signature)*


Years 2022/2025

*Niente nella vita va temuto, dev'essere solamente compreso.*
*Ora è tempo di comprendere di più, così possiamo temere di meno.*

Maria Salomea Skłodowska-Curie

# Contents

# Abstract

The discovery of antibiotics changed modern medicine, both drastically reducing the severity of many bacterial diseases and allowing progress in other medical fields, like surgery. However, the abuse and misuse of these drugs has led to an increase of antimicrobial resistance (AMR). AMR calls for the continuous discovery and introduction of new antibiotics. A promising substrate for the development of new drugs is represented by antimicrobial peptides (AMPs), which are characterized by a broad spectrum of activities and a low attitude to induce AMR.[1] In fact, they can act through different mechanisms, such as the interaction with cell membranes or the innate immune response named "nutritional immunity". Through the latter mechanism, AMPs can sequester metallic nutrients such as zinc, copper or iron, interfering with the homeostasis of the pathogens. However, they present some drawbacks, including metabolic instability and relatively lower antimicrobial activity, compared to traditional antibiotics. To overcome these limitations, a rational design approach, employing peptidomimetics, is fruitful. Peptidomimetics are peptide derivatives obtained by introducing some chemical modification in the peptide sequence, e.g. the incorporation of unnatural or D-amino acids. In this thesis, the effects of incorporating terminal protections,[2] amino acid substitutions [3-4] or D-amino acids on the metal binding ability, the enzymatic stability and the antimicrobial activity of different natural peptides have been thoroughly examined.

The comprehensive characterization of metal-complexes solution-equilibria requires a multi-technique approach. Mass spectrometry and potentiometric titrations have been used to determine the stoichiometry and the thermodynamic stability of the formed complexes, under different experimental conditions; spectroscopic techniques, including UV-Vis spectrophotometry, circular dichroism (CD) and electron paramagnetic resonance, gave hints on coordination geometry and binding sites. Moreover, Far-UV CD measurements provided information on the secondary structure (e.g., α-helices formation). Resistance to enzymatic degradation was tested through incubation in human plasma followed by HPLC measurements; biological studies complemented the structural and thermodynamic data by evaluating the antimicrobial activity and clarifying the mechanism of action, particularly the role of metal ion sequestration in nutritional immunity. Moreover, the comparison between different peptide analogues helped clarify the role of specific residues of the peptide sequence, not always directly involved in complexation but rather influencing the complex geometry and contributing to its stability.

The findings demonstrate the efficacy of the used strategies to enhance peptide stability against proteolytic enzymes, finely tune structure and stability of their metal complexes and increase antimicrobial activity and selectivity towards fungi, bacteria and also viruses. Antimicrobial assays confirmed the crucial role of metal-peptide complex-formation.[5] Overall, these results prove that the investigated peptides and their complexes represent promising candidates as potential therapeutic agents. In addition, the detailed thermodynamic and structural description of metal ion coordination has significantly advanced the general knowledge of bioinorganic chemistry,[6] partially elucidating the role of

these metals in antimicrobial activity and paving the way for strategies to modulate the efficacy and selectivity of new antimicrobial drugs.

## References:


[1] Browne, *et al.*, International journal of molecular sciences **2020**, 21(19).
[2] D'Accolti, *et al.*, Scientific Reports **2023**, 13(1), 18228.
[3] Leveraro, *et al.*, Dalton Transactions **2024**.
[4] Leveraro, *et al*, Journal of Inorganic Biochemistry **2025**, 262, 112761.
[5] Caproni, *et al.* Analytical Biochemistry **2025**, 700, 115784.
[6] Leveraro, *et al.* Inorganic Chemistry **2025**, 64(13), 6751-6760.

# Acknowledgments

I would like to express my deepest gratitude to my supervisors, Prof. Maurizio Remelli and co-supervisor Prof. Magdalena Rowińska-Żyrek, for their invaluable support, expert guidance, and continuous encouragement throughout my doctoral journey. In particular, I would like to thank them for encouraging me to step out of my comfort zone, which was fundamental for my personal growth. I am truly grateful for the professional and personal development opportunities they provided. They are invaluable teachers and people.

I owe a special debt of gratitude to Dr. Denise Bellotti, who served as my primary guide and mentor in the laboratory. Her technical expertise and hands-on guidance were essential for executing the experiments of my research. I am deeply thankful for her patient instruction, meticulous attention to detail, and tireless availability whenever I encountered challenges. She not only taught me what to do but also how to become an independent and confident researcher in the laboratory. Her intellectual rigor and commitment to excellence set a high standard that I aspire to maintain in my future career.

My deepest *dziękuję bardzo* to all the colleagues of the group of Biological Inorganic Chemistry of Wrocław University. I am thankful for their warm welcome and continuous support during my mobility period. The opportunity to work in such a stimulating and collaborative environment was invaluable to my scientific growth and significantly contributed to this thesis.

A special thanks to Kinga, for all the support and the time we spent together around Poland. You have become like a sister to me.

A big thank you to my friends and relatives for the necessary distractions, the spontaneous adventures and the deep understanding during these three years.

To Riccardo, thank you for your support and understanding. You saw me at my most stressed and most elated, and you handled both with patience. Having you by my side to keep me grounded, remind me to take breaks and not to overthink when I was under stress, made these three years easier. Thank you for being my greatest supporter.

To my family, thank you for teaching me the value of hard work and perseverance. Your faith in my potential was a constant source of inspiration. I am eternally grateful for your sacrifices and look forward to the next chapter we can share together. I dedicate this work to you.

*Grazie. Thank you. Dziękuję.*

# List of publications

This research work includes the following publications:

**Journal articles**

1. S. Leveraro, V. Dzyhovskyi, K. Garstka, A. Szebesczyk, F. Zobi, D. Bellotti, K. Stokowa-Soltys, M. Remelli, M. Rowińska-Żyrek, *Inorg. Chem.* **2025**, 64, 6751-6760.

2. S. Leveraro, M. D'Accolti, E. Marzola, E. Caselli, R. Guerrini, M. Rowińska-Żyrek, M. Remelli, D. Bellotti, *J. Inorg. Biochem.* **2025**, 112761.

3. A. Caproni, S. Leveraro, K. Szarszoń, C. Nordi, R. Fontana, M. Buratto, P. Marconi, M. Remelli, M. Sicurella, D. Bellotti, *Anal. Biochem*. **2025**, 700, 115784.

4. S. Leveraro, K. Garstka, P. Śliwka, T. Janek, M. Rowińska-Żyrek, M. Remelli, D. Bellotti, *Dalton Trans.*, **2024**, 53, 1267-12687.

5. M. D'Accolti, D. Bellotti, E. Dzień, C. Leonetti, S. Leveraro, V. Albanese, E. Marzola, R. Guerrini, E. Caselli, M. Rowińska-Żyrek, M. Remelli. *Sci. Rep*., **2023**, 13 (1), 18228.

6. D. Bellotti, S. Leveraro, A. Hecel, M. Remell, *Anal*. *Biochem.*, **2023**, 680, 115315.

7. D. Bellotti, S. Leveraro, M. Remelli, *Methods in enzymology*, **2023**, 687, 279-341.

**Conference proceedings – Oral presentations**

8. S. Leveraro, D. Bellotti, K. Szarszoń, M. Rowińska-Żyrek, M. Remelli. "Microplusin: a strong copper-chelating and effective antimicrobial natural peptide". XV International Symposium on Inorganic Biochemistry. September 10th-13th 2025, Wrocław (Poland), pp 77-78, Oral presentation (OC-3).

9. S. Leveraro, V. Dzyhovskyi, K. Garstka, A. Szebesczyk, F. Zobi, D. Bellotti, K. Stokowa-Soltys, M. Remelli, M. Rowińska-Żyrek. "Metal-induced amide deprotonation and binding of model peptides to Cu(II), Zn(II) and Fe(II) metal ions". Acta of the International Symposia on Metal Complexes. ISMEC GROUP SERIES, June 10th-13th 2025, Granada (Spain), pp 38, Oral presentation (OC-3).

10. S. Leveraro, D. Bellotti, M. Remelli. "Optimization of enzymatic stability of the antimicrobial peptide calcitermin". Merck Young Chemists' Symposium, November 13th-15th 2024, Rimini (Italy). Oral presentation (OR014).

11. S. Leveraro, M. D'Accolti, D. Bellotti, E. Dzień, C. Leonetti, V. Albanese, E. Marzola, R. Guerrini, E. Caselli, M. Rowińska-Żyrek, M. Remelli. "How terminal protection affects the chemical and biological properties of the antimicrobial calcitermin". Acta of the International Symposia on Metal Complexes. ISMEC GROUP SERIES, June 10th-13th 2024, Nizza (France), pp 56, Oral presentation.

12. S. Leveraro, D. Bellotti, M. Rowińska-Żyrek, R. Guerrini, M. Remelli. "Does the Ala-to-Ser substitution affect the metal binding and biological properties of the antimicrobial peptide calcitermin?", Merck Young Chemists' Symposium, November 13th-15th 2023, Rimini (Italy), pp 100. Flash presentation (FL11).

**Conference proceedings – Other contributions**

13. D. Bellotti, S. Leveraro, G. Adami, V. Albanese, S. Berto, R. Bonsignore, E. Garribba, R. Guerrini, A. Merlino, S. Pacifico, M. Remelli. "Thermodynamic and spectroscopic analysis of peptide-based enzyme mimics containing the ATCUN site". XV International Symposium on Inorganic Biochemistry. September 10th-13th 2025, Wrocław (Poland), pp 128-128, poster presentation (P-1).

14. D. Bellotti, S. Leveraro, M. Remelli. "Analytical multi-technique approach to successfully tackle the complexity of metal-peptide interaction: the case of copper-microplusin". Atti del XXXI Congresso Nazionale della Divisione di Chimica Analitica Italiana. September 7th-11th 2025, Pisa (Italy), pp 215-216, Oral presentation (O-EQS-2).

15. S. Berto, M. Marafante, S. Leveraro, M. Remelli, E. Garribba, R. Bonsignore, G. Adami, A. Merlino, D. Bellotti. "Design and redox properties characterization of metal/tetrabranched peptide adducts as possible superoxide dismutase mimics". Acta of the International Symposia on Metal Complexes. ISMEC GROUP SERIES, June 10th-13th 2025, Granada (Spain), pp 138-139, poster presentation (P-2).

16. D. Bellotti, S. Leveraro, G. Adami, V. Albanese, S. Berto, R. Bonsignore, E. Garribba, R. Guerrini, A. Merlino, S. Pacifico, M. Remelli. "Thermodynamic and spectroscopic analysis of peptide-based enzyme mimics containing the ATCUN site". Acta of the International Symposia on Metal Complexes. ISMEC GROUP SERIES, June 10th-13th 2025, Granada (Spain), pp 101-102, poster presentation (P-22).

17. S. Leveraro, D. Bellotti, M. Remelli. "Aminoacids substitution can deeply affect the activity and stability of antimicrobial peptides". XXIII Giornata della Chimica dell'Emilia-Romagna: la chimica per le sfide future. December 19th 2024, Modena (Italy), pp 78, Poster presentation (P053).

18. D. Bellotti, S. Leveraro, K. Garstka, M. Rowińska-Żyrek, M. Remelli. "Beyond the thermodynamics of metal-peptide complexes: new perspectives for antimicrobial agents". Atti del XXVIII Congresso Società Chimica Italiana. August 26th-30th 2024, Milano(Italy), pp 238 vol2., oral presentation ANA-PO-067.
19. S. Leveraro, D. Bellotti, K. Garstka, V. Dzyhovskyi, M. Rowińska-Żyrek, M. Remelli. "Does the proline residue affect the coordination of divalent metal ions?". Atti del XXVIII Congresso Società Chimica Italiana. August 26th-30th 2024, Milano (Italy), pp 356, vol2., poster presentation ANA-PO-087.

20. D. Bellotti, S. Leveraro, K. Garstka, M. Rowińska-Żyrek, M. Remelli. "Insight into the role of metal coordination in the bioactivity of calcitermin derivatives". 2nd International Metal-Binding Peptides conference. MBP24, July 10th-12th 2024, Tolosa (France), pp 59, oral presentation.

21. S. Leveraro, D. Bellotti, K. Garstka, V. Dzyhovskyi, M. Rowińska-Żyrek, M. Remelli. "Investigating the effect of proline residues on the coordination of divalent metal ions". 2nd International Metal-Binding Peptides conference. MBP24, July 10th-12th 2024, Tolosa (France), poster presentation.

22. D. Bellotti, S. Leveraro, K. Garstka, M. Rowińska-Żyrek, M. Remelli. "Exploring the thermodynamics of metal-peptide complexes: unveiling promising perspective for antimicrobial innovation". Acta of the International Symposia on Metal Complexes. ISMEC GROUP SERIES, June 10th-13th 2024, Nizza (France), pp 42, Oral presentation.

23. D. Bellotti, S. Leveraro, M. Marafante, M. Remelli, S. Berto, E. Garribba, R. Bonsignore, G. Adami, A. Merlino. "Design and study of metal complexes with tetrabranched peptide systems as surrogates of superoxide dismutase". Acta of the International Symposia on Metal Complexes. ISMEC GROUP SERIES, June 10th-13th 2024, Nizza (France), pp 100, Poster presentation.

24. D. Bellotti, S. Leveraro, M. Remelli. "From biological systems to metal binding tools: the case of polyhistidine peptides". 4$^{th}$ European NECTAR Conference and Final Action Meeting, February 26$^{th}$-27$^{th}$ 2024, Milazzo (Italy), pp 47-48, oral presentation (P03).

25. S. Leveraro, D. Bellotti, M. Rowińska-Żyrek, R. Guerrini, M. Remelli. "The importance of being positive! Ala-to-Arg substitution in the antimicrobial peptide calcitermin", XXII Giornata della Chimica dell'Emilia-Romagna: Chimica e salute. December 18th 2023, Parma (Italy), pp 49, Poster presentation (P22).

26. D. Bellotti, S. Leveraro, M. Rowińska-Żyrek, M. Remelli. "Be positive! More than a state of mind behind the thermodynamic study of metal complexes with novel calcitermin peptide derivatives". In Atti del XXX Congresso della Divisione Chimica Analitica della Società Chimica Italiana, Vasto (Italy), pp 231, September 17th-21th 2023, Oral presentation (O6-Eq).

27. S. Leveraro, D. Bellotti, M. Rowińska-Żyrek, R. Guerrini, M. Remelli. "The effect of Ala-to-Ser substitution on calcitermin derivatives". Acta of the International Symposia on Metal Complexes. ISMEC GROUP SERIES, June 11th-14th 2023, Urbino (Italy), pp 137, Poster presentation (P17).

28. L.R. Magnaghi, D. Bellotti, S. Leveraro, G. Alberti, M. Remelli, R. Biesuz. "Dyes in food chemistry: empirical use versus descriptor-based design", Acta of the International Symposia on Metal Complexes, ISMEC GROUP SERIES, June 11th-14th 2023, Urbino (Italy), pp 113, Poster presentation (P4).

29. D. Bellotti, S. Leveraro, E. Dzień, M. Rowińska-Żyrek, M. Remelli, "THE IMPACT OF METAL COORDINATION ON CALCITERMIN ANTIMICROBIAL PROPERTIES", XXIX Congresso della Divisione di Chimica Analitica, September 11th-15th 2022, Milazzo (Italy), pp 145, Oral presentation (EQ-OR08).

30. S. Leveraro, D. Bellotti, M. Rowińska-Żyrek, R. Guerrini, M. Remelli. "Sympathy for the serine: the effect of Ala-to-Serine substitution on the metal binding affinity of calcitermin peptide", XXI Giornata della Chimica dell'Emilia-Romagna: Sostenibile, eco, green: le nuove strade della chimica. December 19th 2022, Bologna (Italy). Poster presentation (P9).

# 1. Chapter One: Introduction

## 1.1 Antimicrobial resistance

The introduction of antibiotics in medicine was likely the most important medical breakthrough of the 20th century. It made possible many previously unavailable medical procedures, such as chemotherapy, organ transplantation and open-heart surgery.

The first discovered antibiotic in 1910 was Salvarsan, used in the syphilis treatment. Afterwards, Alexander Fleming discovered penicillin in 1928, giving birth to the antibiotic "golden age", which peaked in the middle of the 1950s. Within just over 100 years, the use of these drugs has extended human life by not less than 23 years.[1] Due to their immense potential, antibiotics have been overused and often misused, thus leading to an increasing spread of the antimicrobial resistance phenomenon (AMR). Antimicrobial resistance leads to a loss of effectiveness of the antibiotics in use, with the risk of making some diseases untreatable.[1] AMR is a condition that occurs when microorganisms such as bacteria, viruses, fungi or parasites develop the capacity to adapt and grow in the presence of drugs that were previously effective against them. The immune-system ability to combat infectious diseases is compromised by this phenomenon, which results in a variety of complications for patients that are most vulnerable, like e.g. during chemotherapy treatments, organ transplants or surgical operations. Moreover, due to the diminished antibiotic efficacy, physicians necessitate the use of last-choice drugs, which are prohibitively expensive, not always available in developing countries and may induce a variety of adverse effects.[2] Nevertheless, the development of antimicrobial resistance mechanisms cannot be ascribed to the development of antimicrobial drugs. Indeed, samples obtained from a cave ecosystem that remained isolated for over 4 million years, have showed the existence of bacteria presenting resistance factors.[3]

Certainly, the conditions of use of these antimicrobial drugs have favoured the rapid diffusion of genes and resistance mechanisms. We must also consider the rapidity in bacteria replication: ten generations of bacteria replications can be achieved in less than 12 hours by a strain of *Staphylococcus aureus*. Each replication cycle has the potential to produce a mutation, leading to the emergence of effective resistance mechanisms.[3]

Resistance mechanisms adopted by bacteria can be different:
- inactivation or modifications of antimicrobial molecules;
- modification of target site on bacteria;
- reduction in drug penetration and/or accumulation;
- biofilm formation.[4]

Among the many factors that contribute to the development of AMR, there is the lack of accurate information not only among patients but also among physicians. Different surveys conducted around the world demonstrate that patients think antimicrobial drugs can help in case of viral diseases, such as a cold or flu.[2] In countries where antibiotics require a medical prescription, most of them turn out to be inappropriate. In absence of rapid diagnostic test, physicians sometimes only presume the need of antibiotic drugs in case of any infection

disease. Furthermore, physicians prescribe antibiotics to patients with viral infection in order to prevent the development of secondary microbial diseases.[5, 6] Contrary to the principle of restricting antibiotic access to prescription-base dispensing, in many developing countries their availability as self-medication drugs facilitate the widespread use with the population.[2]

Another critical aspect to consider is their extensive application in agricultural and livestock management. For instance, in the United States, approximately 80% of all antibiotics sold are components of animal feed. In fact, beyond treatment of disease, subtherapeutic doses are every day incorporated into animal feed and water as a prophylactic measure against bacterial infections.[2] This routine use favours the survival and proliferation of antibiotic-resistant bacteria within the animal gut. These resistant bacteria can then transfer to humans through different mechanisms from food consumption to environmental contamination.

While precise mortality data are challenging to obtain, recent estimations indicate that antimicrobial resistance potentially can cause 10 million deaths per years globally by 2050 if strong and impactful measures are not taken.[2] In addition, it is worth nothing the decline in the discovery of new antibiotic drugs over recent decades. The US Food and Drug Administration (FDA) approved 16 new antibiotics between 1983 and 1987, but this number decreased to just 2 between 2008 and 2012.[3] More recently, between 2017 and 2019, FDA approved 11 new antibiotics, though the European Medicine Agencies (EMA) approved only 4 of these. The reason behind this slowdown can be attributed to the decrease in investments. This is largely due to the nature of these drugs, which are typically used for short treatment durations and are susceptible to the development of resistance, leading to an uncertain long-term stay on the market.[4]

Despite the taken measures in recent decades, the trend of global AMR shows no sign of slowing down. Due to this phenomenon, the interest in exploring novel therapeutic strategies has emerged, considering both pharmacological and non-pharmacological approaches. Among the non-pharmacological therapies, research is focusing on the use of bacteriophages, monoclonal antibody therapy, and vaccine development.[3, 4] Regarding pharmacological therapies, the study and use of antimicrobial peptides, indicated by the acronym AMPs, is gaining increasing consensus.[7-9] Due to the general lack of resistance towards antimicrobial peptides, these are considered a new class of drugs useful for combating the phenomenon of bacterial and fungal resistance. [8]

## 1.2 Antimicrobial peptides

Antimicrobial peptides (AMPs), small peptides identified in every kingdom of life, are a key component of the innate immune systems. Indeed, in plants and insects, they represent the principal defence mechanisms against pathogens. Bacteria and other microorganisms also produce antimicrobial peptides to protect themselves from threats from their surrounding environment. In complex eukaryotes, AMPs play a different role, regulating both innate and adaptive immune responses. [6]

Antimicrobial peptides (AMPs), typically ranging from 10 to 40 amino acids in length, are generally characterized by a net positive charge and an amphiphilic nature, since generally they possess both hydrophobic and hydrophilic regions.[10] These peptides are classified into

various groups according to their structure, which can range from entirely α-helical or β-sheet conformations to more complex structures.[6] The AMPs are of significant interest due to their broad spectrum of activity. Indeed, their characteristic features - charge, hydrophobicity and structure - enable them to fight both Gram-positive and Gram-negative bacteria, as well as fungi and certain encapsulated viruses. Furthermore, AMPs can also exhibit some role as anticancer agents, drug delivery agents, signalling molecules or mitogenic agents.[11]

Peptides found in nature can be classified into two main categories: those synthesized by ribosomes and those not synthesized by ribosomes. The latter group is produced by bacteria and fungi; some examples are bacitracin, daptomycin and vancomycin. On the contrary, peptides synthesized by ribosomes are produced by plants, animals and some bacteria, with defensin, lactoferricin and magainins being some examples.[6]

Among naturally derived peptides, there are insulin and adrenocorticotropic hormone (ACTH), who became life-saving drugs in the early twentieth century. Notably, both of these important molecules possess a peptide structure.[11]

The main mechanisms of action of AMPs are reported in Figure 1.1:

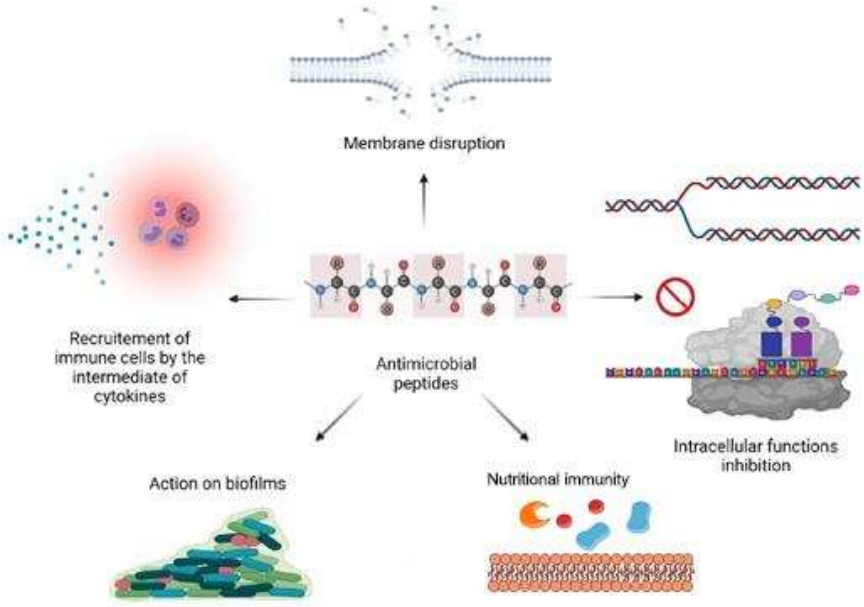


**Figure 1.1 -** AMPs mechanisms of action.[12]

1. Disruption of the bacterial cell membrane: their net positive charge facilitates an initial electrostatic interaction with anionic groups on the bacterial surface. This interaction enables the peptide to insert itself into the membrane, subsequently forming pores. The resulting loss of membrane integrity leads to the leakage of essential metabolites, causing bacterial cell death.[5]

2. Inhibition of intracellular functions: some peptides cross the membrane and interfere with processes essential for pathogens' survival. Their mechanism of action are diverse, encompassing the inhibition of DNA replication, protein synthesis, nucleic acid biosynthesis, metabolism or even cell division.[12]

3. Action on biofilm: the exact mechanism by which AMPs act on biofilm remains uncertain but their ability to inhibit various staged of biofilm formation has been established. Biofilm structure allows bacteria to tolerate high concentrations of antibiotics, even though the same bacteria are fully susceptible to these drugs in their planktonic conditions.[12]

4. Immunomodulatory activity: they achieve this activity by exerting a chemotactic effect on leukocytes, enhancing leukocytes and monocytes activity, and increasing the expression of pro-inflammatory cytokines.[5]

5. Nutritional immunity: AMPs can coordinate metal ions, such as zinc, iron and copper from their surroundings, effectively depriving pathogens of these essential micronutrients necessary for their survival.[13-18]

### *1.2.1 Therapeutic potential of antimicrobial peptides*

The efficacy of antimicrobial peptides is attributed to their capacity to act through multiple and distinct mechanisms and pathways. This multi-approach of action not only enhances their antimicrobial potency but also diminishes the potential for resistance mechanisms to emerge. A drug that acts simultaneously via several pathways, makes it much harder for bacteria to acquire the multiple mutations needed for resistance.[5]

The strategy of combining antibiotics with antimicrobial peptides represents an additional method to decrease the probability of antimicrobial resistance emerging. Studies have highlighted the synergistic activity between these two types of drugs, offering several significant advantages:

- lower antibiotic dosages: less medication is needed to achieve the desired effect;
- reduced drug toxicity: the overall harmful impact on the body is minimized;
- fewer side effects.[5]

Furthermore, unlike other active compounds that can produce potentially harmful metabolites, AMPs are degraded into amino acids during metabolism, making them safer for the human body.[12]

### *1.2.2 Problems and limitations of antimicrobial peptides*

The challenge in current research studies is the development of effective antimicrobial peptides. While numerous peptides exhibit promising activity in *in vitro* experiments and in animal models, most often their efficacy does not translate to humans due to the high complexity of human pathologies. [5]

Moreover, it is also important to consider the potential toxicity of antimicrobial peptides to eukaryotic cells. In fact, some AMPs have shown nephrotoxic properties, primarily due to the high dosages required for administration. Additionally, AMPs are susceptible to proteases in the serum, therefore they get degraded quite easily.[5] For these reasons, many AMPs have been developed as topical applications. Bacitracin and gramicidin, for instance, are exclusively used as topical agents because of their degradation by proteases and their haemolytic side effects. However, topical applications also have their challenges, as they require sufficient tissue penetration to be effective against skin diseases.[5] Furthermore, other challenges arise from high extraction costs, limited bioavailability, a short half-life,

cytotoxicity, and a general lack of specificity. Moreover, AMPs show lower direct antimicrobial activity compared to antibiotics.[12]

Finally, the potential development of resistance mechanisms cannot be completely excluded, particularly when microorganisms are repeatedly exposed to the drug. Currently, only a few examples have been noted, including bacteria using enzymes to sequester the drug and efflux pumps to expel it from the cell.[12]

Researchers have investigated various strategies to tackle these issues. Encapsulation has emerged as a method to prevent protease degradation and improve peptide stability. Moreover, laboratory synthesis, using natural peptides as templates, can significantly reduce extraction costs and improve the yield of synthetic AMPs. A wide range of potential modifications can be introduced to generate novel antimicrobial peptides. For instance, peptoids, which are proteolysis-resistant peptidomimetics, have been developed to extend their half-life. Structural changes like dimerization or methylation have been introduced to increase bioavailability and half-life, while reducing cytotoxicity. For better specificity, target-specific AMPs (STAMPs) have been developed. These involve linking the AMPs to a carrier peptide that specifically binds to the pathogen, ensuring controlled drug release at the target site.[12]

## 1.3 Nutritional immunity

The primary defence mechanism developed by vertebrate organisms, including humans, to combat pathogen infection is nutritional immunity. This process involves the host organism sequestering essential micronutrients, especially metal ions, in an attempt to limit pathogenicity during an infection. Pathogens such as Gram-negative bacteria, Gram-positive bacteria, viruses and fungi, need to acquire trace minerals, like zinc and copper, to replicate and, consequently, cause disease. However, sufficient levels of these metal ions are also crucial for the proper functioning of the human body. Therefore, it is clear that some competitive mechanisms for acquiring these metal ions emerge between the host and the pathogen during an infection.[19]

The human body is equipped to produce many molecules that coordinate and bind various metal ions. For instance, lactoferrin, a glycoprotein secreted by neutrophils during infection, can bind iron and reduce its free levels. In response to the host's metal ion sequestration, pathogens have simultaneously developed their own mechanisms.[16, 20] They might, for example, secrete siderophores, small molecules capable of binding and chelating iron with a higher affinity than human proteins.[19]

The main metal ions involved in the process of nutritional immunity are iron, manganese, copper and zinc. The last two are fundamental for pathogen subsistence and virulence.

### *1.3.1 Copper*

Copper is an essential metal ion that can exist in both oxidized ($Cu^{2+}$) and reduced ($Cu^{+}$) form. It plays a crucial role in enzymes involved in cellular respiration, iron transport, superoxide dismutation, and other crucial processes involved in virulence. Notably, copper

ability to undergo redox reactions can lead to the production of reactive oxygen species (ROS), which are useful in pathogen elimination.[8]

The precise role of copper ion in the innate immune response still needs to be fully explored, but the current hypothesis suggests that phagocytes may directly use the copper ion as an antibacterial agent.[21]

The exact mechanism by which bacteria import copper ions into the cell is not entirely clear, as bacterial cuproproteins are primarily expressed in the periplasmic and extracellular spaces. However, studies have shown that copper efflux components are critical determinants of bacterial virulence. The CopA and CopB efflux systems present a histidine-rich N-terminal domain and a Cys-Pro-Cys binding sequence, both of which participate in copper ion binding. Their function is to move copper from the intracellular to the extracellular space. Indeed, excessive copper levels inside the bacterium could be fatal. Although the success in determining the virulence by the pathogen seems linked to efficient removal of copper excess from the cytoplasm, copper levels in periplasmic space should not be neglected. [21, 22] Research indicates that inactivation of the CopA efflux systems gene leads to the accumulation of copper within bacterium cytoplasm, achieving toxic concentrations.[21]

In response to bacterial infections like the pathogenic *Salmonella*, the host increases expression of the ATP7A gene. This gene codes for ATP-dependent copper ion transporters, and its expression is particularly enhanced in macrophages. This boost in ATP7A expression is coupled with a significant rise in the expression of CTR1 and CTR2 genes. These genes code for transporter proteins responsible for moving copper into the cell cytoplasm. These changes in the expression of genes involved in copper metabolism lead to increased copper absorption within the host cell.[22]

Copper, therefore, plays a dual role in the host's response to microbial infections:

- nutritional immunity: the host sequesters copper, reducing its availability for the pathogen;
- "bombardment": copper concentrations are increased within the pathogen to reach toxic levels.

### *1.3.2 Zinc*

Zinc is one of the most important metal ions for all the species, essential for the survival of both pathogenic microorganisms and their hosts. It plays a crucial role in cell growth, development and homeostasis, transcription, oxidative stress, apoptosis and aging. In humans, it is fundamental for proper bone mineralization, blood coagulation, cognitive functions, foetal growth, and sperm production. Alterations in zinc homeostasis can cause growth delays, hypogonadism, immunodeficiency, and neuronal dysfunctions.[23]

*In vitro* and *in vivo* studies reveal that bacteria maintain extremely low intracellular levels of free zinc. This tight control is crucial because excessive levels of free zinc can be toxic. Zinc can compete with other essential metal ions for binding site; for instance, it has a higher affinity than magnesium for magnesium-dependent enzymes. For this reason, the intracellular zinc concentration must be kept a million times lower than that of magnesium. Yet, it must also be high enough to support critical biological functions. To achieve this delicate balance, bacteria have evolved a sophisticated array of mechanisms. These include

specialized sensors, transporters, and other molecules that regulate cellular zinc levels. These control systems are categorized into high- or low-affinity influx and efflux systems, enabling precise regulation of zinc concentration. Furthermore, bacteria can implement zinc storage systems, allowing them to stock the metal for later use, such as during periods of zinc starvation caused by "nutritional immunity".[23]

In bacteria, zinc efflux and influx are primarily carried out by ABC transporters, which are ATPases. These transporters typically consist of one or two transmembrane domains that form a pore in the membrane, allowing the passage of specific substrates from one side to the other. They also have two ATP-binding cassette domains located in the cytoplasm, which give energy from ATP hydrolysis to transport substrates across the cell membrane.[23]

In humans, zinc availability is quite limited. Only 0.1% of the total zinc is found in plasma, and most of that is bound to proteins, which further reduces the amount of available zinc. Sequestrating this very small amount of free zinc is a clever way to deprive pathogens of this essential ion. This mechanism is employed by the immune response during pathogen infections, a process known as nutritional immunity.[23] Bacteria have evolved additional mechanisms to contrast the host's zinc sequestration. They secrete specific zinc-selective chelators that bind the metal ion and transport it to specific membrane transporters. These chelators function similarly to siderophores.[23]

Similarly to copper, macrophages can employ two different mechanisms, based on zinc, to fight pathogens. They can kill microorganisms by either zinc starvation or zinc intoxication (an excess of the ion). Zinc intoxication within the macrophage has been observed in bacterial species like *M. tuberculosis* and *S. pneumoniae*. However, it is not yet clear which criteria macrophages use to decide whether to employ zinc deprivation or intoxication to kill pathogen.[19, 23]

An example of an antimicrobial peptide capable of chelating zinc, and thus limiting its free availability, is calprotectin. This S100 family peptide can inhibit the growth of *S. aureus* by sequestrating both zinc and manganese. It is the most abundant antimicrobial peptide found in the cytoplasm of neutrophils and it is secreted at the site of inflammation. Calprotectin has two metal-binding sites: one binds zinc, while the other binds either manganese or zinc with low affinity.[19, 23]

### *1.3.3 Role of copper and zinc metal ions in the AMPs antimicrobial activity*

Studies have revealed the existence of certain antimicrobial peptide whose activity and mode of action are closely tied to the presence of divalent metal ions, specifically Cu(II) and Zn(II). The binding of these peptides to such ions triggers structural or charge changes within the peptide itself, leading to increased antimicrobial activity. Examples include the AMPs psoriasin, calcitermin, microplusin and histatin.[8]

### *1.3.4 AMPs as antiviral agents*

Some antimicrobial peptides are not only active against bacteria, but they can also target other pathogens, such as viruses. Also in this case, they can act trough a range of mechanisms of action. One primary mechanism involves direct interaction with the viral envelope or capsid. Many AMPs can bind to and disrupt the integrity of the viral membrane (for

enveloped viruses) or the capsid structure (for non-enveloped viruses). This direct disruption can prevent viral entry into host cells, inhibit viral uncoating, or even lead to the degradation of viral particles, thus making them non-infectious. Beyond direct viral targeting, AMPs can also interfere with the viral life cycle at various intracellular stages. Some peptides have been shown to block viral adsorption or penetration by interacting with specific cellular receptors that viruses typically use for entry. Furthermore, certain AMPs can internalize into host cells and inhibit viral replication by targeting essential viral enzymes or interfering with the synthesis of viral nucleic acids (DNA/RNA) or proteins. Finally, AMPs often possess immunomodulatory properties, which contribute indirectly to their antiviral effects. They can modulate the host's immune response by recruiting immune cells, enhancing cytokine production, or dampening excessive inflammation, thereby promoting a more effective antiviral defence.[24] Moreover, analogously to antibacterial peptides, the antiviral power can be enhanced by metal ions and formation of metal complexes.[25-27]

## 1.4 Formation of metal-peptide complexes

Potential metal-binding sites of proteins and peptides correspond to specific amino acid side-chains and the C- and N-terminal ends. The chemical groups that most commonly bind metals are the imidazole ring of histidine, the carboxyl group of glutamic and aspartic acid, the thiol group of cysteine and the phenolic hydroxyl of tyrosine. Less frequently, the coordination can involve the thioether of methionine, the amino group of lysine or ornithine, the guanidinium group of arginine and the amides of asparagine and glutamine.

The imidazole nitrogen of the histidine side chain, in particular, is an excellent binding site for metals classified as "borderline" according to Pearson's classification,[28] such as Cu(II) and Zn(II). Although the latter ions can form coordination bonds with other donor atoms (like oxygen), they show a marked preference for nitrogen. The imidazole group of histidine is partially deprotonated at physiological pH (p$K_a$ approximately 6.5), thus exerting a buffering action and becoming available for coordination with the metal. Therefore, when a His residue is located in a solvent-exposed site or in an unstructured portion of the peptide, Cu(II) and Zn(II) can easily anchor and coordinate the imidazole.[29]

### *1.4.1 Copper complexes*

The most common oxidation state of copper is +2. The Cu element has an $[Ar]3d^{10}4s^1$ electronic configuration, while Cu(II) ion is a $3d^9$ and it can form complexes with a coordination number of 4, 5 or 6. These complexes are characterized by the Jahn-Teller effect; in fact, the geometry of the complex is often not symmetrical but tetragonally distorted, stretched or compressed along a quaternary axis (this stabilizes the system). In particular, the complexes of Cu(II) with coordination 4 are essentially square planar (due to the tetragonal deformation).[30]

In simple peptides with the lack of coordinating side chains (such as poly- alanines or poly-glycines), at acidic pH, Cu(II) coordinates the nitrogen of the N-terminal amino group and the oxygen of the neighbouring carbonyl group to form the complex $[CuL]^+$ (species 1N). At around pH 5, the Cu(II) ion can displace the proton of a peptide group of the backbone,

thus leading to the formation of an additional Cu-$N^-$ bond in the complex $[CuLH_{-1}]$ (species 2N). At higher pH, the nitrogens of a second and a third peptide group can bind the copper ion to form the $[CuLH_{-2}]^-$ (species 3N) and the $[CuLH_{-3}]^{2-}$ (species 4N) complexes, respectively. When a peptide forms complexes of type 3N and 4N with Cu(II), its conformation changes drastically, which affects its physical and biological properties.[30]

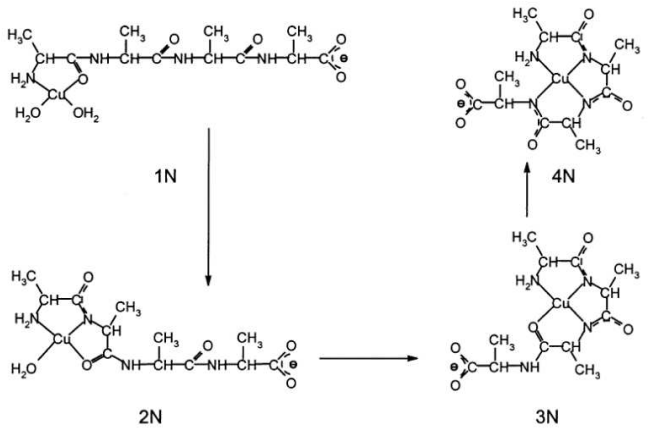


**Figure 1.2 -** The stepwise complex formation between $Cu^{2+}$ and tetraalanine (AAAA) at increasing pH.

As a general rule, the coordination of Cu(II) to peptides begins with the terminal amino nitrogen and then continues with other donor sites, but the imidazole nitrogen ($N_{Im}$) of histidine is able to compete for the first coordination bond. Systematic studies on complexes of tetra- (or more) peptides have shown that the presence of a single histidine residue can lead to the formation of a macrochelate. The largest number of macrochelates has been identified with peptides containing histidines in different number and positions.[30]

In order to give an example of the geometry of these complexes, some structures corresponding to the Cu(II) complexes with the tripeptide Ac-HGH-NH-Me are described below. In the cited peptide, two histidine residues are separated by another amino acid (Gly). The coordination begins with the formation of the species $[CuLH]^{3+}$, in which an imidazole nitrogen is deprotonated and coordinated to the metal ion. The second step is the deprotonation of a second imidazole nitrogen, which leads to the species $[CuL]^{2+}$ (**Figure 1.3**).

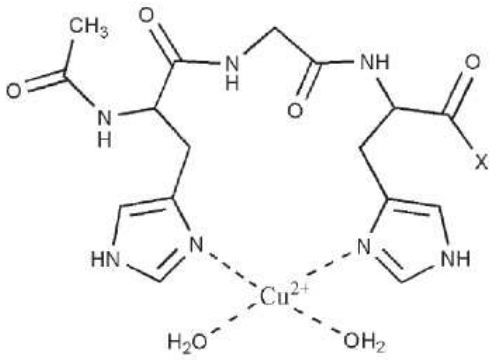


**Figure 1.3 -** Hypothesized solution structure for the species $[CuL]^{2+}$ in the system Cu(II) / Ac-HGH-NH-Me (X= NHMe).

The subsequent deprotonation and coordination of an amide nitrogen give rise to the species $[CuLH_{-1}]^{+}$. The next species is the complex $[CuLH_{-2}]$, in which two amide nitrogens are coordinated to the metal ion. In this case, the set of donors is ($N_{Im}$, $N^{-}$, $N^{-}$, $N_{Im}$), with the formation of three chelated rings (7, 5 and 6 members) (**Figure 1.4**).

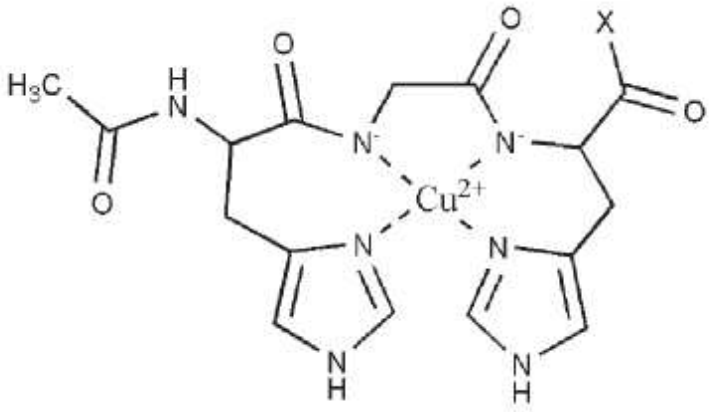


**Figure 1.4 -** Hypothesized solution structure for the species $[CuH_{-2}L]$ in the system Cu(II) / Ac-HGH-NH-Me (X= NHMe).

At higher pH, a further deprotonation of an amide nitrogen occurs. N-amide moves one imidazole to an axial position of the complex; the corresponding species, $[CuLH_{-3}]^{-}$, has a square pyramidal geometry (**Figure 1.5**).

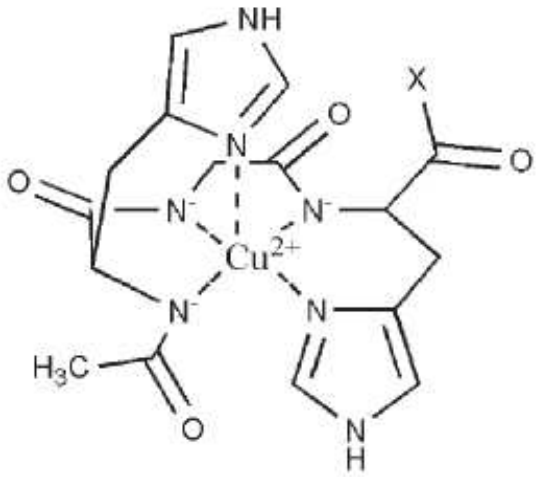


**Figure 1.5 -** Hypothesized solution structure for the species $[CuH_{-3}L]^{-}$ in the system Cu(II) / Ac-HGH-NH-Me (X= NHMe).

*1.4.2 Zinc complexes*

The most common oxidation state for zinc is +2. The zinc element has a [Ar]$3d^{10}4s^2$ electron configuration, while Zn(II) ion is a $d^{10}$; this is the reason why its complexes do not adsorb visible light, since *d-d* transitions are not possible.[30]

The Zn(II) ion has high rate of ligand exchange and its polarizing power makes the p$K_a$ of coordinated $H_2O$ molecules quite low. Combining a strong binding ability to protein ligands, a fast ligand-exchange (coordinated $H_2O$ or substrate molecules), a reasonably high electron affinity, a flexibility of coordination geometry (mostly tetrahedral or octahedral) and a not complicated redox chemistry, zinc is well suited to its role of catalysing specific acid-base reactions.[30] The large family of Zn-enzymes includes carbonic anhydrase, carboxypeptidases, alkaline phosphatase, beta-lactamase and alcohol dehydrogenases.

The zinc ion can easily coordinate several imidazole side chains that are close together; it is likely that more consecutive histidines cooperate in the coordination to Zn(II). Typically, the zinc ion is coordinated to three amino acid ligands and one exchangeable $H_2O$ molecule, as it happens in the cavity of carbonic anhydrase enzyme (Figure 1.6).[30]

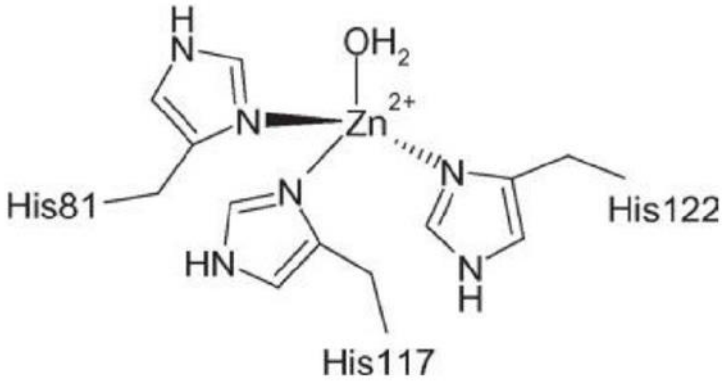


**Figure 1.6 -** Typical zinc(II) coordination to His-rich peptides.[31]

*1.4.3 Nickel complexes*

Nickel element has a [Ar]$3d^8s^2$ electron configuration and its most common oxidation state is +2, although in certain conditions it can present a +1 or +3 oxidation state. The resulting $Ni^+$ and $Ni^{3+}$, however, are unstable species and do not contribute to noticeable redox activity in living organisms. Ni(II) is thus the most stable and common ion, with a $3d^8$ electronic configuration. The formation of Ni(II) complexes with peptides proceeds in a way similar to Cu(II), displaying a preference for nitrogen and oxygen donor atoms and being able to promote the deprotonation of N-backbone amides. In contrast with Cu(II), increasing the pH value, the coordination of the peptide chain (namely the deprotonation of N-amides) occurs cooperatively and promotes the transition from an initial octahedral distorted arrangement (most frequent with amine ligands) to a square-planar geometry. An important limitation of Ni(II) ion is the relatively slow kinetic of ligand exchange and complexation reactions, the first-order water exchange rate constant for Ni(II) is 100 times slower than for Cu(II) and 1000 times slower than for Zn(II).[32]

## 1.5 S100 proteins

The S100 family protein comprises 25 members that share a high degree of structural and sequence similarity. Members of this family regulate various intracellular and extracellular processes, including proliferation, differentiation, inflammation, apoptosis, Ca(II) homeostasis, and energy metabolism.[33]

Given their broad modulatory roles across numerous cellular functions, specific members of this family have been assigned additional nomenclature. For instance, S100A8 (calgranulin A), S100A9 (calgranulin B), and S100A12 (calgranulin C) are recognized as intracellular Ca(II) sensors.[33] Notably, S100A8 and S100A9 form a heterodimeric complex known as calprotectin, which exhibits established fungicidal and bactericidal activities.[34]

All the S100 family members have a molecular mass between 10 and 12 kDa and share 25-65% amino acid sequence similarity. Three-dimensional structural studies show that Ca(II) binding triggers a conformational change, enabling interactions with target proteins.[33]

Following cellular damage/stress or activation of immune system cells, S100A8/A9 proteins are released into the extracellular space. Here, they play a critical role in regulating immune and inflammatory processes. S100A12 also plays an essential role in mediating inflammation.[33]

Due to their involvement in mediating inflammatory processes and modulating the immune system, these proteins can be used as biomarkers for specific diseases. High expression of these proteins indicates microbial infection or other conditions like rheumatoid arthritis, atherosclerosis, Alzheimer's disease, or diabetes. Beyond their role as markers, they also hold potential as therapeutic agents.[33, 35]

### *1.5.1 S100A12: calgranulin C*

The mature S100A12 protein consists of 91 amino acids, and its expression has been observed exclusively in vertebrates. The protein conformation and function are influenced by intracellular and extracellular concentrations of calcium, zinc and copper. [35]

In humans, the expression of the S100A12 gene is almost entirely limited to neutrophil granulocytes. The protein expression has also been recorded in monocytes, but in a lower rate. In healthy individuals, this protein, also known as calgranulin C, can be found primarily in the spleen and lungs, where granulocytes and monocytes are abundant. After the protein secretion by granulocytes into the extracellular environment, S100A12 becomes a danger signal molecule, exhibiting characteristics similar to cytokines and chemokines.[35] The constitutive genes for S100A12 expression in human tissues are mostly present in neutrophil granulocytes. In the absence of intracellular calcium, S100A12 is predominantly found in the cytosol, and upon calcium addition, translocation to the membrane occurs.[35]

The antimicrobial peptide calcitermin consists of the C-terminal domain of calgranulin C, in particular the 77-91 domain of the mature protein.[35]


**Figure 1.7-** Amino acidic sequence of the S100A12. The box contains the calcitermin sequence.[35]

## 1.6 Calcitermin

A fluid layer rich in antimicrobial effector molecules protects human airways from bacterial colonization. Numerous antimicrobial peptides (AMPs) are present here, ranging from large, abundant molecules like lysozyme and lactoferrin to smaller, less common ones like defensins.

Among various uncharacterized components, in 2001 Cole and colleagues isolated a peptide that showed activity against Gram-negative bacteria. This peptide was called "calcitermin". This peptide corresponds to the last 15 amino acids of the C-terminus of calgranulin C, with the sequence: VAIALKAAHYHTHKE.[34] Calcitermin antimicrobial activity is highly dependent on environmental conditions. At pH 7.4, the peptide shows no microbicidal activity against tested bacterial species like *E. coli*, *P. aeruginosa*, *C. albicans*, *S. aureus*, and *L. monocytogenes*.[34] However, under the acidic conditions frequently encountered during inflammation (pH = 5.4), calcitermin demonstrates activity against *E.coli*, *P. aeruginosa* and *C. albicans*, though not against *S. aureus* and *L. monocytogenes*. This pH-dependent activity is likely attributed to the protonation of three histidine residues within its sequence, leading to an increase in cationic charges. This enhanced positive charge facilitates a stronger interaction between calcitermin and the negatively charged surfaces of bacteria.[34, 36] Furthermore, calcitermin antimicrobial activity is modulated by the presence of metal ions. In fact, studies conducted in presence of zinc(II), a metal ion abundant in human nasal fluids, have revealed an enhanced antimicrobial effect, likely attributable to the conformational changes induced by zinc interaction that stabilize the peptide structure.[36] Beyond zinc, calcitermin ability to interact with other metal ions, such as copper, is also linked to the presence of histidine residues. Replacing one of these histidines with an alanine residue significantly alters both the thermodynamic stability and the structure of the resulting metal complex. Despite these observations, the precise relationship between calcitermin antimicrobial activity and the specific structure, charge and coordination mode of the interacting metal has not yet been clarified.[36]

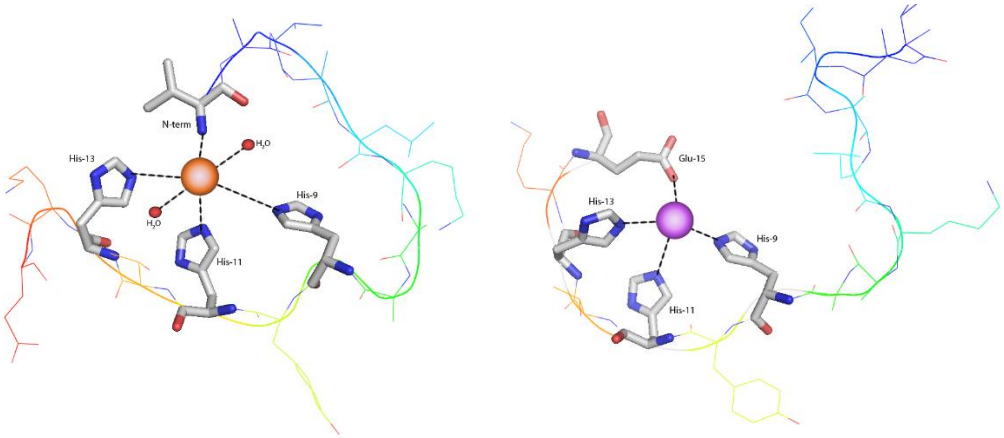


**Figure 1.8 -** Hypothesized coordination modes of Cu(II)\VAIALKAAHYHTHKE (left) and Zn(II)\VAIALKAAHYHTHKE (right) complexes.

## 1.7 Microplusin

Another example of naturally occurring antimicrobial peptide is microplusin, originally isolated from the cattle tick *Rhipicephalus (Boophilus) microplus*. Microplusin exists both in a precursor and mature form; the former presents an N-terminal 20 aa peptide signal.[37] Once reached its final target, the signal sequence is cut and the protein becomes mature. The mature microplusin is characterized by a 90 amino acids sequence containing six cysteine residues that form three disulphide bonds and five α-helices with unfolded N- and C-termini. It also contains histidine-rich regions in its N- and C-termini. The presence of disulphide bonds is extremely important to determine the peptide antimicrobial activity. In fact, studies have shown that the reduced and alkylated peptide exhibits no activity against bacteria.[37] Since the peptide presents several histidine residues (2 at the N-terminus, 1 at position 74 and 4 at the C-terminus), scientists have tested its ability to bind different kinds of metal ions ($Mg^{2+}$, $Cl^{-}$, $Ca^{2+}$, $Fe^{2+}$, $SO_4^{2-}$, $Mn^{2+}$, $Zn^{2+}$, $Cu^{2+}$, $Co^{2+}$, $Na^{+}$ and $MoO_4^{2-}$). For most of them, there was no evidence of peptide binding, except for copper and iron.[37]

Microplusin has demonstrated antimicrobial activity primarily against Gram-positive bacteria, such as *Micrococcus luteus*, and various fungi, including *Cryptococcus neoformans*.[38] Interestingly, its mechanism of action is distinct from many pore-forming AMPs; instead of permeabilizing bacterial membranes, microplusin exerts a bacteriostatic and fungistatic effect by binding and sequestering copper(II) ions. This copper-chelating ability directly influences essential copper-dependent cellular processes, particularly microbial respiration, as evidenced by its effect on *M. luteus* and *C. neoformans* respiration, which can be reversed by copper supplementation. Furthermore, microplusin has been shown to inhibit critical virulence factors in *C. neoformans*, such as melanisation (by inhibiting laccase) and polysaccharide capsule formation, highlighting its potential as an anti-infective agent.[39]

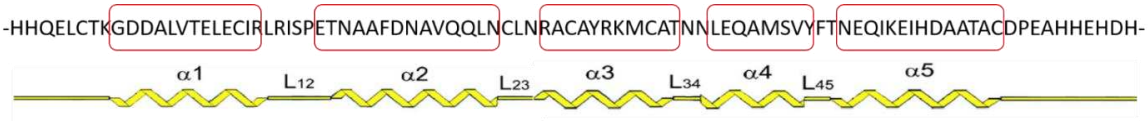


**Figure 1.9 -** Microplusin amino acids sequence. Amino acids forming helices are boxed.

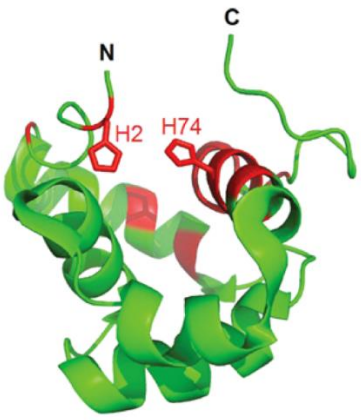


**Figure 1.10 -**Mapping of the microplusin suggested binding region for Cu(II) ions (in red).[40]

## 1.8. Overview of the presented research

The work of this thesis is justified by the increasing need of innovative pharmacological therapies against infectious diseases. The phenomenon of antimicrobial resistance still represents a clinical and financial burden on the world health care system. Antimicrobial peptides (AMPs) are a promising class of new drugs, mostly thanks to their scarce attitude to induce antimicrobial resistance. Moreover, several studies have shown that divalent metal ions, such as Zn(II) and Cu(II), can modulate the efficacy of antimicrobial peptides. These two metal ions are essential for the virulence and survival of pathogenic species in the human organism, being crucial in the expression of many metal-proteins, enzymes and transcription factors. Although a precise explanation of how exactly the metal ions participate in the expression or in the enhancement of antimicrobial activity is not yet achieved, two hypothesis have been put forward: (*i*) the metal sequestration operated by the AMP starves the pathogen of its metal nutrients and prevent its growth (nutritional immunity); or (*ii*) the metal binding involves changes in the peptide charge and structure, modifying its properties.[41] However, AMPs presents some drawbacks, such as their low proteolytic stability: the AMPs activity depends on degradation by both human and pathogenic proteolytic enzymes, since many endo- and exo-peptidases can transform high molecular weight peptides into shorter oligopeptides, making them inactive. Another challenge to overcome is the decrease of biological activity *in vivo*, compared to the *in vitro* experiments due to many factors as differences in the pH and salt concentrations and the presence of a variety of interacting molecules which can inhibit the AMPs efficacy.[42, 43] These problems altogether translate into short half-lives and low bioavailability. A useful strategy to improve the therapeutic potential of AMPs, is the rational design of "peptidomimetics", aimed at optimizing their chemical and biological properties. Peptidomimetics are derivative peptides built up using unnatural amino acids or chemical alterations, which confer resistance to proteolysis and degradation.[44-46]

A deep knowledge of both the thermodynamic and structural aspects concerning the metal coordination chemistry of AMPs can be crucial to design new effective drugs, while the improvement of their proteolytic stability can guarantee adequate properties for the clinical use. For that reason, we tried to elucidate metal-peptide interactions, which is an extremely important aspect of bioinorganic chemistry, also in the view of designing novel therapeutic agents. While the Cu(II)-peptide coordination chemistry is extensively documented,[47-53] the coordination behaviour of other biologically relevant metal ions, like Zn(II) or Fe(II), particularly concerning the backbone amide deprotonation and binding, still remains controversial.[54-56] In fact, in the case of Cu(II) ions, while histidine or terminal amine often act as anchoring sites at acidic pH, increasing the alkalinity of the solution, metal coordination might involve the backbone amides. Theoretically, a similar behaviour is also possible for Zn(II) and Fe(II) metal ions. In order to clarify this point, we also studied metal complexing thermodynamic and spectroscopic behaviour of some short model peptides.

The investigation presented in this thesis is mainly devoted to calcitermin peptidomimetics and their ability to bind Zn(II) and Cu(II) metal ions, since they are crucial for the virulence and survival of pathogenic species in the human organism and they have been reported to

enhance the antimicrobial activity of calcitermin against *Candida albicans* and common bacteria like *Staphylococcus aureus* and *Enterococcus faecalis*.[36]

The systematic study includes: (*i)* terminal protections on the native peptide, (*ii*) introduction of additional serine residues, (*iii*) introduction of additional arginine or histidine residues and (*iv*) substitution of L- with D-amino acids. In addition, (*v*) the antiviral activity of the native peptide has been studied in presence of the Ni(II), Cu(II) or Zn(II) metal ions and (*vi*) its potential to generate ROS species has been evaluated in presence of Cu(II).

Finally, another antimicrobial peptide has caught our attention and curiosity, microplusin. In this case, only Cu(II) complexes have been investigated, since the peptide exerts bacteriostatic and fungistatic effect in presence of the named metal ion by sequestering it.[39] In this case, we focused on the unstructured N- and C-terminal domains, which are rich in histidine residues, with the aim of determining the residues involved in copper binding.

The thermodynamic data obtained with these studies allowed a comparison of the complexing ability of wild-type calcitermin and some of its most stable peptidomimetics towards the Cu(II) and Zn(II) ions. Furthermore, to evaluate the impact of the number and position of histidine residues in the peptide sequence on copper complex stability, we also compared calcitermin with microplusin fragments and other biologically relevant peptides.

In order to have a complete description of the complex-formation equilibria between model peptides and metal ions it is crucial the use of a sufficient number of independent investigation techniques, able to provide information both on the stability and structure of the formed species. From the thermodynamic point of view, the most used technique is potentiometry, which can provide, with high accuracy, the stoichiometry and thermodynamic stability of formed species. In this context, mass spectrometry is often used to confirm both formation and stoichiometry of the species revealed in solution by potentiometry. Depending on the specific properties of the involved metal(s) and peptide(s), it is possible to apply a wide choice of spectroscopic techniques that give detailed information on the complex structure and coordination geometry. In this PhD work the main used techniques are solid-phase peptide synthesis, potentiometric titrations, electrospray ionization mass spectrometry, UV-Vis spectrophotometry, circular dichroism (CD), electron paramagnetic resonance (EPR) and reverse-phase high-performance liquid chromatography (RP-HPLC).

The totality of the obtained results represents a robust foundation for the rational development of novel strategies against various human pathologies which involve metal ions (infections, neurodegenerative diseases, cancers). [57-60] Moreover, we presented a multi-technique approach that covers the most widely used thermodynamic and spectroscopic methods for investigating the interaction between metal ions and peptides in solutions.

# 1.9 References


[1] Hutchings, M. I., Truman, A. W. & Wilkinson, B., *Current opinion in microbiology*, **2019,** *51*, 72-80.

[2] Dadgostar, P., *Infect Drug Resist*, **2019,** *12*, 3903-3910.

[3] Marston, H. D., Dixon, D. M., Knisely, J. M., Palmore, T. N. & Fauci, A. S., *Jama*, **2016,** *316*, 1193-1204.

[4] De Oliveira, D. M. P., Forde, B. M., Kidd, T. J., Harris, P. N. A., Schembri, M. A., Beatson, S. A., Paterson, D. L. & Walker, M. J., *Clinical microbiology reviews*, **2020,** *33*.

[5] Browne, K., Chakraborty, S., Chen, R., Willcox, M. D., Black, D. S., Walsh, W. R. & Kumar, N., *International journal of molecular sciences*, **2020,** *21*.

[6] Roope, L. S. J., Smith, R. D., Pouwels, K. B., Buchanan, J., Abel, L., Eibich, P., Butler, C. C., Tan, P. S., Walker, A. S., Robotham, J. V. & Wordsworth, S., *Science (New York, NY)*, **2019,** *364*.

[7] Battersby, A. J., Khara, J., Wright, V. J., Levy, O. & Kampmann, B., *Frontiers in immunology*, **2016,** *7*, 309.

[8] Łoboda, D., Kozłowski, H. & Rowińska-Żyrek, M., *New Journal of Chemistry*, **2018,** *42*, 7560-7568.

[9] Wang, S., Zeng, X., Yang, Q. & Qiao, S., *International journal of molecular sciences*, **2016,** *17*.

[10] Malmsten, M., *Upsala journal of medical sciences*, **2014,** *119*, 199-204.

[11] Datta, S. & Roy, A., *International Journal of Peptide Research and Therapeutics*, **2021,** *27*, 555-577.

[12] Rima, M., Rima, M., Fajloun, Z., Sabatier, J. M., Bechinger, B. & Naas, T., *Antibiotics (Basel, Switzerland)*, **2021,** *10*.

[13] Hood, M. I. & Skaar, E. P., *Nature reviews Microbiology*, **2012,** *10*, 525-37.

[14] Maret, W., *International journal of molecular sciences*, **2016,** *17*.

[15] Porcheron, G., Garénaux, A., Proulx, J., Sabri, M. & Dozois, C. M., *Frontiers in cellular and infection microbiology*, **2013,** *3*, 90.

[16] Ma, Z., Jacobsen, F. E. & Giedroc, D. P., *Chem Rev*, **2009,** *109*, 4644-81.

[17] Fukada, T., Yamasaki, S., Nishida, K., Murakami, M. & Hirano, T., *Journal of biological inorganic chemistry : JBIC : a publication of the Society of Biological Inorganic Chemistry*, **2011,** *16*, 1123-34.

[18] Weinberg, E. D., *Jama*, **1975,** *231*, 39-41.

[19] Hennigar, S. R. & McClung, J. P., *American journal of lifestyle medicine*, **2016,** *10*, 170-173.

[20] Capdevila, Daiana A., Edmonds, Katherine A. & Giedroc, David P., *Essays in Biochemistry*, **2017,** *61*, 177-200.

[21] Djoko, K. Y., Ong, C. L., Walker, M. J. & McEwan, A. G., *The Journal of biological chemistry*, **2015,** *290*, 18954-61.

[22] Li, C., Li, Y. & Ding, C., *International journal of molecular sciences*, **2019,** *20*.

[23] Wątły, J., Potocki, S. & Rowińska-Żyrek, M., *Chemistry – A European Journal*, **2016,** *22*, 15992-16010.

[24] Lee, Y.-C. J., Shirkey, J. D., Park, J., Bisht, K. & Cowan, A. J., *BioDesign Research*, **2022,** *2022*, 9898241.

[25] Hutchinson, D. W., *Antiviral Research*, **1985,** *5*, 193-205.

[26] Pinkham, A. M., Yu, Z. & Cowan, J. A., *Journal of Medicinal Chemistry*, **2018,** *61*, 980-988.

[27] Abate, C., Carnamucio, F., Giuffrè, O. & Foti, C., *Biomolecules*, **2022,** *12*.

[28] Pearson, R. G., *Journal of the American Chemical Society*, **1963,** *85*, 3533-3539.

[29] Farkas, E., Csapó, E., Buglyó, P., Damante, C. A. & Di Natale, G. J. I. C. A., **2009,** *362*, 753-762.

[30] Smith, D. W., *Annual Reports Section "A" (Inorganic Chemistry)*, **2005,** *101*, 231-252.

[31] Atkins, P., *ed by Oxford University Press Oxford*, **2010,** *5th edition*, 21,22,27.

[32] Martin, R. B., *Metal ions in Biological Systems: Nickel and Its Role in Biology*, **1988,** *23*, 123-164.

[33] Gonzalez, L. L., Garrie, K. & Turner, M. D., *Biochimica et biophysica acta Molecular cell research*, **2020,** *1867*, 118677.
[34] Cole, A. M., Kim, Y. H., Tahk, S., Hong, T., Weis, P., Waring, A. J. & Ganz, T., *FEBS letters*, **2001,** *504*, 5-10.
[35] Pietzsch, J. & Hoppmann, S., *Amino acids*, **2009,** *36*, 381-9.
[36] Bellotti, D., Toniolo, M., Dudek, D., Mikołajczyk, A., Guerrini, R., Matera-Witkiewicz, A., Remelli, M. & Rowińska-Żyrek, M., *Dalton Transactions*, **2019,** *48*, 13740-13752.
[37] Silva, F. D., Rezende, C. A., Rossi, D. C., Esteves, E., Dyszy, F. H., Schreier, S., Gueiros-Filho, F., Campos, C. B., Pires, J. R. & Daffre, S., *The Journal of biological chemistry*, **2009,** *284*, 34735-46.
[38] Alexander, J. L., Thompson, Z. & Cowan, J. A., *ACS Chemical Biology*, **2018,** *13*, 844-853.
[39] Silva, F. D., Rossi, D. C., Martinez, L. R., Frases, S., Fonseca, F. L., Campos, C. B., Rodrigues, M. L., Nosanchuk, J. D. & Daffre, S., *FEMS microbiology letters*, **2011,** *324*, 64-72.
[40] Libardo, M. D. J. & Angeles-Boza, A. M., *Comments on Inorganic Chemistry*, **2014,** *34*, 42-58.
[41] Jiang, H., Hu, X.-Y., Mosel, S., Knauer, S. K., Hirschhäuser, C. & Schmuck, C., *ChemBioChem*, **2019,** *20*, 1410-1416.
[42] Brogden, K. A., *Nature reviews Microbiology*, **2005,** *3*, 238-50.
[43] Agbale, C. M., Sarfo, J. K., Galyuon, I. K., Juliano, S. A., Silva, G. G. O., Buccini, D. F., Cardoso, M. H., Torres, M. D. T., Angeles-Boza, A. M., de la Fuente-Nunez, C. & Franco, O. L., *Biochemistry*, **2019,** *58*, 3802-3812.
[44] Qvit, N., Rubin, S. J. S., Urban, T. J., Mochly-Rosen, D. & Gross, E. R., *Drug discovery today*, **2017,** *22*, 454-462.
[45] Gentilucci, L., De Marco, R. & Cerisoli, L., *Current pharmaceutical design*, **2010,** *16*, 3185-203.
[46] Lenci, E. & Trabocchi, A. J. C. S. R., **2020,** *49*, 3262-3277.
[47] Bellotti, D., Rowińska-Żyrek, M. & Remelli, M., *Dalton Transactions*, **2020,** *49*, 9393-9403.
[48] Kozłowski, H., Kowalik-Jankowska, T. & Jeżowska-Bojczuk, M., *Coordination Chemistry Reviews*, **2005,** *249*, 2323-2334.
[49] Faller, P. & Hureau, C., *Dalton Transactions*, **2009**, 1080-1094.
[50] Millhauser, G. (2023) The Rich Chemistry of the Copper and Zinc Sites in PrPC in pp. 25-43.
[51] Grenács, Á. & Sóvágó, I., *J Inorg Biochem*, **2014,** *139*, 49-56.
[52] Zawisza, I., Rózga, M. & Bal, W., *Coordination Chemistry Reviews*, **2012,** *256*, 2297-2307.
[53] Raics, M., Sanna, D., Sóvágó, I. & Kállay, C., *Inorganica Chimica Acta*, **2015,** *426*, 99-106.
[54] Garstka, K., Dzyhovskyi, V., Wątły, J., Stokowa-Sołtys, K., Świątek-Kozłowska, J., Kozłowski, H., Barceló-Oliver, M., Bellotti, D. & Rowińska-Żyrek, M., *Molecules*, **2023,** *28*.
[55] Dzyhovskyi, V., Remelli, M. & Stokowa-Sołtys, K., *Journal of Inorganic Biochemistry*, **2025,** *263*, 112769.
[56] Dzyhovskyi, V. & Stokowa-Sołtys, K., *Journal of Inorganic Biochemistry*, **2023,** *244*, 112203.
[57] Gaggelli, E., Kozlowski, H., Valensin, D. & Valensin, G., *Chem Rev*, **2006,** *106*, 1995-2044.
[58] Giampietro, R., Spinelli, F., Contino, M. & Colabufo, N. A., *Molecular pharmaceutics*, **2018,** *15*, 808-820.
[59] Gerega, K., Kozlowski, H., Masiukiewicz, E., Pettit, L. D., Pyburn, S. & Rzeszotarska, B., *J Inorg Biochem*, **1988,** *33*, 11-8.
[60] Tokar, E. J., Benbrahim-Tallaa, L. & Waalkes, M. P., *Metal ions in life sciences*, **2011,** *8*, 375-401.

# 2. Chapter Two: Instrumental techniques

## 2.1 Complex formation equilibria in solution

A metal complex can be defined as a species resulting from the interaction of one or more metal ions (M) with another species (ligand, L) able to independently exist in solution. Their interaction is based on Lewis theory of electron pairs donors and acceptors. According to the type and number of metal ions (acceptors) and ligand (donors), a complex can be: positively or negatively charged, neutral, mononuclear (one metal ion), polynuclear (multiple metal ions), bis-, tris, etc. complex (multiple ligand molecules), etc. The required parameters for the characterization of simultaneous complex-formation equilibria in solution are contained in the so-called "speciation model", which provides the stoichiometry of the different formed species and their formation constants at a given temperature (*T*) and ionic strength (*I*). The speciation model allows to calculate the composition of a system in different conditions of pH, absolute concentrations of the components and metal to ligand ratios. For a generic system constituted by the metal ion M, the ligand L and a proton H, the stoichiometry and the stability constant are described by the following equations:

$$pM + qL + rH \leftrightarrows M_pL_qH_r \tag{2.1}$$

$$\beta_{pqr} = \frac{[M_p L_q H_r]}{[M]^p[L]^q[H]^r} \tag{2.2}$$

where the terms in square brackets in equation (2.2) represent the molar concentrations of the different species present at equilibrium (2.1). The charges and the solvent molecules are omitted for the sake of simplicity. $\beta_{pqr}$ is the global (or cumulative) formation constant and provides quantitative information about the interaction between the metal ion M and ligand L. The stoichiometric coefficient r for the proton may also be negative if the number of protons dissociated from the ligand is greater than the maximum number of dissociated protons in the absence of metal ion. A detailed description of the different equilibria in solution can be obtained by stepwise constants, $K_n$ (or $X_n$, when they refer to the ligand protonation, equations 2.3). The overall formation constants is equal to the product of the individual stepwise constants (equations 2.4 and 2.5).

When working in aqueous solutions, besides the complex-formation equilibria, the metal ion and the ligand participate in other equilibria that are influenced by the pH value, *i.e.* they are involved in acid/base reactions: the metal ion can form complexes with the hydroxide ion ($[M^{m+}(OH^-)_n]^{m-n}$ and/or become insoluble and precipitate in solution, while the ligand can undergo protonation equilibria. The first step to determine the speciation model of a system is to experimentally determine such equilibria and measure the corresponding equilibrium constants. The metal hydrolysis constants are often available from literature and calculated at specific value of *T* and *I*. Ligand protonation (stepwise or cumulative) constants must instead be determined and refer to the following equilibria:

$$\mathrm{L} + \mathrm{H} \rightleftarrows \mathrm{HL} \qquad X_1 = \frac{[\mathrm{HL}]}{[\mathrm{H}][\mathrm{L}]}$$

$$\mathrm{HL} + \mathrm{H} \rightleftarrows \mathrm{H_2L} \qquad X_2 = \frac{[\mathrm{H_2L}]}{[\mathrm{H}][\mathrm{HL}]}$$

$$\mathrm{H_{n-1}L} + \mathrm{H} \rightleftarrows \mathrm{H_nL} \qquad X_n = \frac{[\mathrm{H_nL}]}{[\mathrm{H}][\mathrm{H_{n-1}L}]} \tag{2.3}$$

$$\mathrm{L} + \mathrm{H} \rightleftarrows \mathrm{HL} \qquad \beta_{011} = \frac{[\mathrm{HL}]}{[\mathrm{H}][\mathrm{L}]} = X_1$$

$$\mathrm{L} + 2\mathrm{H} \rightleftarrows \mathrm{H_2L} \qquad \beta_{012} = \frac{[\mathrm{H_2L}]}{[\mathrm{H}][\mathrm{HL}]} = X_1X_2$$

$$\mathrm{L} + \mathrm{nH} \rightleftarrows \mathrm{H_nL} \qquad \beta_{01n} = \frac{[\mathrm{H_nL}]}{[\mathrm{H}][\mathrm{H_{n-1}L}]} = X_1X_2 \dots \dots X_n \tag{2.4}$$

Once the protonation equilibria are described, it is possible to move forward to the determination of complex-formation constants.

$$\mathrm{M} + \mathrm{L} \rightleftarrows \mathrm{ML} \qquad \beta_{110} = \frac{[\mathrm{ML}]}{[\mathrm{L}][\mathrm{M}]} = K_1$$

$$\mathrm{L} + 2\mathrm{H} \rightleftarrows \mathrm{H_2L} \qquad \beta_{120} = \frac{[\mathrm{ML_2}]}{[\mathrm{L}]^2[\mathrm{M}]} = K_1K_2$$

$$\mathrm{L} + \mathrm{nH} \rightleftarrows \mathrm{H_nL} \qquad \beta_{1n0} = \frac{[\mathrm{ML_n}]}{[\mathrm{L}]^n[\mathrm{M}]} = K_1K_2 \dots \dots K_n \tag{2.5}$$

The stepwise constants are usually sought in order to understand the relationship between structure and reactivity; while to calculate the concentration of the final product (the complex $ML_n$) the overall formation constants are frequently used.

A system with *n* components (metal/s, ligand/s and proton) can be described by following equations:

a) *n* mass balances of the *n* components,
b) charge balance,
c) *N* formation constants $\beta_i$ for the present species,

For a binary system, there are three mass balances:

$$C_M = [M] + [ML] \dots + [ML_n] = [M] + \sum \beta_n[M][L]^n \tag{2.6}$$

$$C_L = [L] + [HL] \dots + [ML] \dots + N[ML_n] = [L] + \sum X_r[L][H]^r + \sum N\beta_n[M][L]^n \tag{2.7}$$

$$C_H = [H] - [OH] + [HL] \dots + r[H_rL] = [H] - K_w[H]^{-1} + \sum rX_r[L][M]^r \tag{2.8}$$

where $C_M$, $C_L$ and $C_H$ are the stoichiometric (total) concentration of the metal, the ligand and the proton respectively, and [M], [L], [H] are the corresponding free concentrations. $C_M$, $C_L$ and $C_H$ are usually known, as they are properly established by the experimenter, while the *N* formation constants and the *n* free concentrations of the components are unknown quantities.

To properly describe the solution behaviour of the three components, under the selected experimental conditions, first of all it is necessary to hypothesize a speciation model, which represent the system and considers all the possible species in which the components are distributed. Therefore, the system of equations 2.6, 2.7 and 2.8 must be built up; it contains 3+$N$ unknowns, i.e. the free concentrations of the components and the overall formation constants. Since the number of unknown variables is higher than that of equations, the system is not univocally solvable. However, if the free concentration of one component can be measured and the protonation constants are known (from the literature or from previous experiments), by repeating the measurement under slightly different experimental conditions – as it happens in a titration – the resulting set of simultaneous equations can be solved and the $N$ overall formation constants, $\beta_i$, can be obtained

Experimental methods for the study of these systems are, thus, based on the determination of the free concentration of at least one component and re-test to different conditions in which the formation constants remain unchanged (temperature and ionic strength are kept constant). In the case of labile complexes, *i.e.* for those complexes in which the ligands are not irreversibly bound to the metal but may be replaced by other ligands with fast kinetics and there is competition between the metal ion and the proton for the donor sites of the ligand, an experiment can be performed through an acid-base potentiometric titration. For each titration point, the concentration of free proton can be estimated. For each of the $N_p$ titration points, a system of three mass balances can be written. The results is a total system of $3N_p$ equations and (3-1) $N_p + N$ unknown, because for every point we have 3-1 unknown free concentrations and the same $N$ formation constants for all the points. The system can be solved if the number of unknowns equals the number of equations, namely the number of experimental points ($N = N_p$). Normally, the exact solution of these systems can be achieved only in very simple cases. For systems with an equation order higher than one, it is possible to get a good approximate result with statistical methods and a greater number of experimental points will increase the accuracy of the result. Nowadays, there are several available software programs which are able to process hundreds of experimental points related to systems with several metals and ligands, where there are many simultaneous equilibria. The program usually gives a statistical analysis of the goodness of fit, which provides an assessment of the model reliability. Although potentiometry is the most widely used technique for this purpose, thanks to its simplicity and accuracy, this method of calculation may be coupled to any analytical technique capable of measuring the free concentration of at least one component of the system in variable experimental conditions.

### *2.1.1. Potentiometry*

In potentiometry, the determination of the free concentration of the hydrogen ion, a component of the solution which is in equilibrium with both the metal(s) and the ligand(s), is performed using a glass electrode. A glass electrode is a type of ion-selective electrode made of a doped glass membrane, which is sensitive to the changes of solution pH, although it is also sensitive to other cations, like $Na^+$. The potentiometric method can be used for the determination of both the protonation and the complex-formation constants. It is important that the ligand is involved in both acid/base equilibria and complex-formation equilibria (*i.e.* there must be competition between metal ion and proton for the ligand binding sites). A glass

electrode measures the potential $E$ of the system, which correlates with the activity of the hydrogen ions through the Nernst equation:

$$E = E^0 + \frac{RT}{nF} \ln \alpha_{H^+} + E_j \quad (2.9)$$

where $E^0$ is the standard potential, $E_j$ represents any liquid junction potential of the system, $R$ is the universal gas constant (8.314 J $K^{-1}$ $mol^{-1}$), $T$ is the absolute temperature (in Kelvin, K), $F$ is the Faraday constant (96840 C $mol^{-1}$), $n$ is the number of transferred electrons and for the glass electrode is 1 and $\alpha_{H+}$ is the activity of the $H^+$ ion. $E_j$ can be minimized to negligible and reproducible values by providing a salt bridge (conventional saturated KCl solution) and a constant ionic medium. Corrections for the effect of the liquid junction can be included in the calibration procedure in the region of low pH;[1] $E_j$ is then revealed as a deviation from the linearity of the observed potential as a function of pH, since the liquid junction potential in a solution of constant ionic strength can be defined as:

$$E_j = j_\alpha [H^+] + j_\beta K_w [H^+]^{-1} \quad (2.10)$$

where $j_\alpha$ and $j_\beta$ are the so-called parameters of the ionic medium: the acidic liquid junction coefficient and the basic liquid junction coefficient, respectively, and $K_w$ is the water self-ionisation constant. Converting now the Neperian logarithm into the decimal one, at room temperature $T$ = 25°C, and approximating the effect of $E_j$ to a negligible value, equation 2.9 can be written as:

$$E = E^0 + 0.05916 \log \alpha_{H^+} \quad (2.11)$$

The rigorous thermodynamic equilibrium constant is expressed in terms of activities, which are quite impractical. For the sake of convenience and reproducibility, concentrations are preferred. The proton activity can then be expressed as:

$$\alpha_{H^+} = [H^+]\gamma_{H^+} \quad (2.12)$$

and thus, considering both equations 2.9 and 2.12:

$$E = E^0 + \frac{RT}{nF} \ln[H^+] + \frac{RT}{nF} \ln \gamma_{H^+} \quad (2.13)$$

where $[H^+]$ is the proton molar concentration and $\gamma_{H^+}$ is the activity coefficient, which is related to the interactions occurring between the solute molecules. γ describes the deviation from the solution ideal behaviour and its value tend to unity in very dilute conditions (*i.e.* when particles encounter approach zero). Experimentally, the Debye-Hückel limiting law is valid only for very dilute solutions (C ≤ $10^{-3}$ M). According to the Debye-Hückel limiting law, the log $\gamma_i$ should also decrease with the square root of increasing ionic strength, $I$:

$$\log \gamma_i = -\frac{Az_i^2\sqrt{I}}{1+Ba_i\sqrt{I}} \quad (2.14)$$

A and B are constants depending on the ionic charge, the temperature, the density and the dielectric constant of the solvent, for aqueous solutions at $T$= 25°C, A = 0.509 and B = 0.3284, $z_i$ is the ionic charge number, and $a_i$ is the effective diameter of the hydrated ion. The most significant aspect of equation 2.14 is the prediction that the activity coefficient is a function of ionic strength rather than the electrolyte concentration. Hence, for high and constant concentrations of ionic strength, the activity coefficients remain constant with respect to the variation of the other species in solution, where their concentration is 10% lower than the ionic medium concentration. Therefore, in order to avoid complications due to variation of activity coefficients, it is customary to perform stability constants determinations in solutions of relatively high and constants ionic strength (~ 0.1M).

In condition of constant temperature and ionic strength, the activity coefficient is constant, and it could be incorporated into the standard potential $E^0$:

$$E = E^{0\prime} + \frac{RT}{nF}\ln[H^+] \quad (2.15)$$

with

$$E^{0\prime} = E^0 + \frac{RT}{nF}\ln \gamma_{H^+} \quad (2.16)$$

The Nernst equation applies to an ideal situation, and a real system can actually undergo some slight deviations from the theoretical Nernstian behaviour due to experimental fluctuations. Thus, it is convenient to introduce the slope factor $\beta_{sl}$, an experimental parameter that takes into account the deviation from the theoretical slope of Nernst equation (~ 59.16 mV, see equation 2.11). The resulting equation is:

$$E = E^{0\prime} + \beta_{sl}\frac{RT}{nF}\ln[H^+] \quad (2.17)$$

The values of $\beta_{sl}$ and $E^{0'}$ are obtained through a specific daily calibration consisting in a strong acid titration using a strong base as titrant. In this way, the measured values of potential $E$ can be directly related to the concentration of the proton [$H^+$] and the obtained equilibrium constants can be expressed in terms of concentration.

*2.1.2 Data analysis and processing*

The analysis of potentiometric data are performed using the following computer programs: OMNIS, Microsoft EXCEL, GLEE,[2] HYPERQUAD[3] and HYSS.[4]

OMNIS is the software package interfaced with the potentiometric instrument OMNIS; it allows to acquire titration curves and to modify the experimental measuring parameters. GLEE is exploited mainly to process the calibration curves of the electrode. Indeed, if the

hydrogen ion concentration, indicated by $[H^+]$ in equation 2.17, is known for a series of measurements of electrode potential it is possible to determine both the standard potential and the slope factor. Calculations proceed using Gran's method (**Figure 2.1**)[5]. The perfect linearity is a good estimate of the proper electrode function and the absence of convergence between the acidic and basic lines (ideally the end point of the titration) allows to calculate the amount of impurity of the solutions, often corresponding to the carbonate contamination of the alkaline titrant. The acceptable error on the alkaline concentration is about 2-3%.

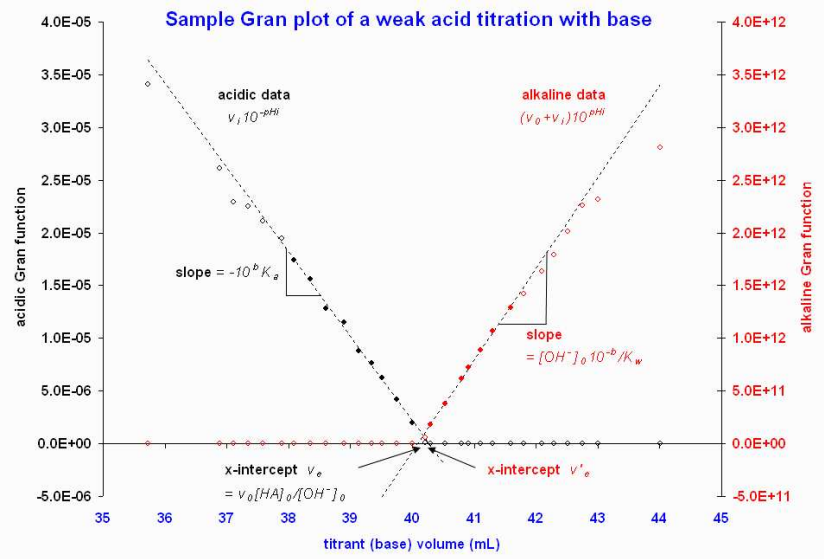


**Figure 2.1 -** Gran's linearization

Microsoft EXCEL software is used to derive the exact concentration of the ligand in the prepared solutions, once again taking advantage of the Gran's method: applying the Gran plot theory, it is possible to precisely detect the end-points of the potentiometric titration curve. The first end-point corresponds to the volume at which the number of equivalents of strong base (NaOH or KOH) are equal to those of the previously added strong acid (HCl or $HClO_4$):

$$n^0_{eq}\ acid = n^0_{eq}\ base \tag{2.18}$$

The second end-point indicates the volume at which the sum of equivalents of acid and ligand is equal to the equivalents of the added base:

$$n^0_{eq}\ ligand\ + n^0_{eq}\ acid\ \ = n^0_{eq}\ base \tag{2.19}$$

Therefore, the difference between the above two points is the volume of strong base necessary to titrate the ligand. Then, multiplying this volume for the base concentration and

dividing it by the number of protonable sites, it is possible to obtain the concentration of the ligand in the solution.

The above calculated parameters and the titration curve points can be also processed with the HYPERQUAD program, to compute the protonation constants for the ligand and the stability constants for the complexes. HYPERQUAD input file contain a list of parameters that describe the sample analysis: millimoles of ligand, acid and metal, titrant base concentration, electrode standard potential $E^{0'}$ and slope factor $\beta_{sl}$, initial volume of the analysed sample and temperature. The data refinement is a least-squares based procedure, in which the sum of squared residual is minimized. The results of a least-squares calculation include the standard deviations and correlation coefficients of the refined parameters, giving information on the goodness of fit. In the input speciation model for HYPERQUAD calculations, hydrolysis constants for metal ions are also included.

## 2.2 UV-Vis spectrophotometry

Ultraviolet-visible spectrophotometer is a technique widely used to analyse complex formation in solution. The interpretation of the absorption spectra, and hence the analysis of the position and intensity of the experimental bands, provides information about number and nature of the donor sites involved in the metal coordination. UV-Vis spectrophotometry allows to determine the concentration of a species in solution, since it is linearly related to the absorbance of the solution (equation 2.20). The quantitative analysis in spectrophotometric methods is based on the Beer-Lamber law. According to Beer, for a dilute solution the absorption intensity is proportional to the number of the attenuating species, and therefore, to their concentration, while Lambert's law states that the fraction of absorbed radiation is independent of the radiation intensity. Combining these two laws, we can derive the Beer-Lambert law:

$$A = \log\frac{I_0}{I} = \varepsilon\, l\, C \qquad (2.20)$$

where $A$ is the observable absorbance of the solution, $I_0$ is the intensity of the incident monochromatic radiation, $I$ is the intensity of the transmitted radiation, ε represents the molar extinction coefficient, an intrinsic property of the absorbing species independent of the other parameters, $l$ is the path length of the absorbing solution expressed in cm and $C$ the concentration of the absorbing species expressed in molarity. The value of $\log(I_0/I)$ is commonly known as the absorbance $A$ of the solution and it can be directly read from the experimentally recorded spectrum; $A$ is often expressed as "absorbance units". The absorbance is an additive property of the system, therefore when more than one absorbing species coexist in solution; the measured total absorbance is a sum of each single component contribution.

$$A = l\,(\varepsilon_1\, C_1 + \varepsilon_2\, C_2 \ldots + \varepsilon_n\, C_n) \qquad (2.21)$$

In the field of inorganic chemistry, UV-Vis spectral range is usually associated with metal-centred d-d electronic transitions. Indeed, transition metals appear coloured because they are able to absorb visible light (wavelength range: 400-800 nm). Higher energy transition may also occur in the ultraviolet range (200-400 nm). When a complex absorbs enough energy in form of quantized ultraviolet or visible light, the valence electrons can be excited to higher energy orbitals depending on the energetic separation between them (ΔE). Different compound will have unique energy spacing between electronic levels and therefore changes in the absorption spectra of a metal complex solution can provide information about the type of ligand and the metal coordination sphere under different experimental conditions (*e.g.* pH, metal-ligand ratio). The value of c can be directly correlated to the frequency of the absorbed light (υ) and thus to its wavelength (λ). The higher the energy gap ΔE the smaller the value of $\lambda$:

$$\Delta E = h\upsilon = h\frac{c}{\lambda} \tag{2.22}$$

$h$ is Planck's constant ($6.626 \cdot 10^{-34}$ J s), and $c$ is the speed of light in vacuum ($3.00 \cdot 10^{8}$ m $s^{-1}$). However, the rigorous discussion of electronic transitions must take into account that light-induced electronic excitation also causes many rotational and vibrational transitions of the molecule, and the results is a gaussian band-shape absorption instead of a single line corresponding to the expected ΔE energy (Franck-Condon principle). The maximum of the absorption band is centred on a $\lambda_{max}$ value which gives information on the $\Delta E$ and therefore on the energy distribution and electron occupancy of the complex orbitals. Besides $\lambda_{max}$, another important parameter provided by absorption spectra is the molar absorptivity ε at a given wavelength. It is an estimate of the probability that a specific transition between two states separated by $\Delta E \propto \lambda^{-1}$occurs. Indeed, certain transitions are allowed, and certain transitions are forbidden depending on the nature of the involved orbitals and electrons. Without going into the details of the theory, it is possible to distinguish between allowed and forbidden transitions simply investigating the interaction of the complex with the electromagnetic moment induced by the incident photon. The resulting spectroscopic selection rules impose (*i*) a symmetry requirement of the involved orbitals on the basis of the representation of the point group to which the molecule belongs, this also includes the Laporte rule for centrosymmetric complexes, which states that allowed electronic transitions cause a change of the parity (*Germ.* G, *gerade* and u, *ungerade*); (*ii*) a spin state requirement by which electronic transitions which cause a change of the electron spin state are forbidden ($\varepsilon_{max} < 1$ $M^{-1}cm^{-1}$). Nevertheless, selection rules may undergo some exceptions. The spin selection rule may be broken by the coupling of spin and orbital angular momenta, which is greater for heavy atoms. The symmetry/Laporte selection rule can be circumvented by molecular vibrations, which can perturb the symmetry and destroy the centre of inversion, or by intrinsic asymmetry of the complex structure due to distorted arrangements of the ligand around the metal ion. The breakdown of Laporte rule allows to detect roughly intense d-d bands in the absorption spectra of transition metal complexes, which are instead expected to be forbidden ($t_{2g} \rightarrow e_g$). To briefly summarise, the types of electronic transition which are possible to detect by means of UV-Vis absorption (**Figure 2.2**) are:

- transition between orbitals mostly localized on the metal ion (MC, *i.e.* d-d transitions; $\varepsilon_{max} \sim 100\text{-}200\ M^{-1}cm^{-1}$), typically observable in the visible spectral range;
- transitions between orbitals mostly localized on the ligands (LC), whose UV-Vis bands are almost independent of the presence of the metal;
- transitions between orbitals that are predominantly ligand in character and orbitals that are predominantly metal in character (metal-to-ligand charge transfer MLCT, ligand-to-metal charge transfer LMCT), which are characterized by extremely intense bands ($\varepsilon_{max} \sim 1000\text{-}50000\ M^{-1}cm^{-1}$) in the ultraviolet spectral range, although may have a tail into the visible.

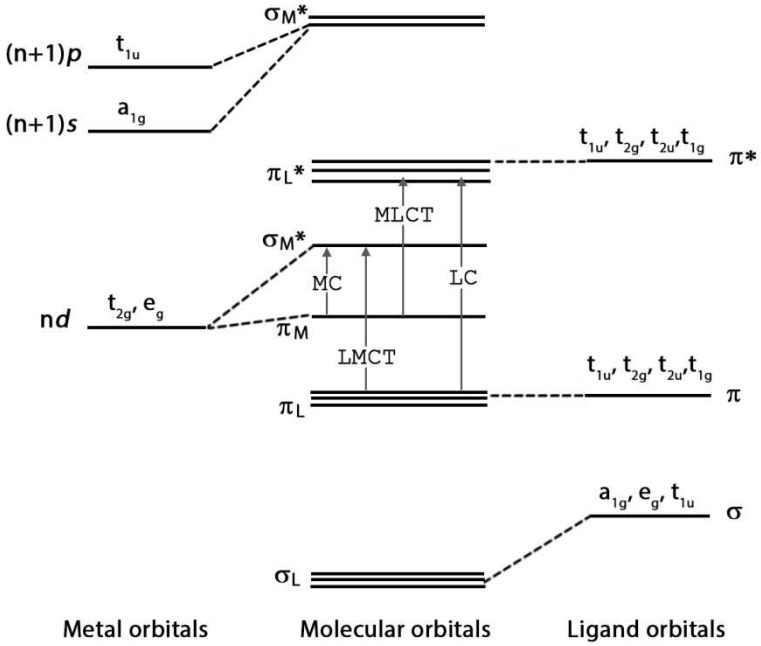


**Figure 2.2 –** Molecular orbital diagram for a generic $ML_6$ complex with $O_h$ symmetry representing various types of electronic transitions.

### *2.2.1 Crystal Field (CF) and Ligand Field (LF) Theories*

The above considerations arise from a specific theoretical background that allows rationalising the absorption spectra of a metal complex by means of both the crystal-field theory (CFT) and the ligand-field theory (LFT). A transition-metal ion in a compound or complex is supposed to be subjected to an electrostatic field produced by molecules and ion in its environment. According to the crystal field theory, the ligands are either negative ions or molecules with unshared electron pairs directed towards the metal. When forming a complex, the electrons from the ligands will be closer to some of the metal d-orbitals and farther away from others, causing a loss of degeneracy in the orbital energetic levels. The electrons in the d-orbitals and those in the ligands repel each other due to repulsion between charges on the same sign. Thus, the d-electrons closer to the ligands will have a higher energy than those farther away, which results in the d-orbitals splitting in energy. The magnitude of the energy separation between the d-orbitals, and hence the colour of the complex (that is due to the d-d transition), depends on: (*i*) the nuclear charge and the identity of the central

metal ion, (*ii*) the ligand charge density, (*iii*) the geometry of the complex ion (the electric field created by the lone-pair of the ligand depends on the geometry of the complex ion), (*iv*) the number of d-electrons, and (*v*) the oxidation number of the central ion. CFT focuses on the d-orbital energy separation, being crucial to understand and rationalize experimental spectra, thermodynamics stability and magnetic properties of the metal complexes. In an octahedral model six ligands (*i.e.* six point charges) are located around the metal ion and cause a lowering of the $d_{xy}$, $d_{xz}$ and $d_{yz}$ orbital energy and the increase of the $d_{z2}$ and $d_{x2-y2}$ one, as shown in Figure 2.3.The differences in energy between the two sets of the d-orbitals is called the ligand-field splitting parameter $\Delta_o$ where the subscript "o" stand for octahedral.

Tetrahedral complexes are the second most common type of complexes for the first-row transition metals (*i.e* Zn(II)) after the octahedral ones; they are characterized by four ligands that form a tetrahedron around the metal ion. In a tetrahedral distribution of charges, metal d-orbitals split again into two groups, with an energetic gap of $\Delta_t$. The lower energy orbitals are $d_{z2}$ and $d_{x2-y2}$, while the higher energy orbitals are $d_{xy}$, $d_{xz}$ and $d_{yz}$, opposite to the octahedral situation. Furthermore, since in the ligand electrons in the tetrahedral symmetry are not oriented directly towards the d-orbitals, the energy splitting is lower than in the octahedral field ($\Delta_t = 0.44\ \Delta_o$). Crystal-field theory is also successful in describing square planar and other geometries, including the tetragonal distortion due to Jahn-Teller effect (**Figure 2.3**) and allows introducing the concept of high-spin and low-spin configurations for $d^4$, $d^5$, $d^6$ and $d^7$ metal ions. Depending on the ligand-field splitting parameter, $\Delta$, and on the pairing energy (electron-electron Coulombic repulsion), the d-electrons may occupy all the available (not degenerate) five d-orbitals with parallel spin (high-spin) or proceed first filling the lower degenerate d-orbitals, allocating two paired electrons per orbital (low-spin), fully in accordance with Pauli exclusion principle.

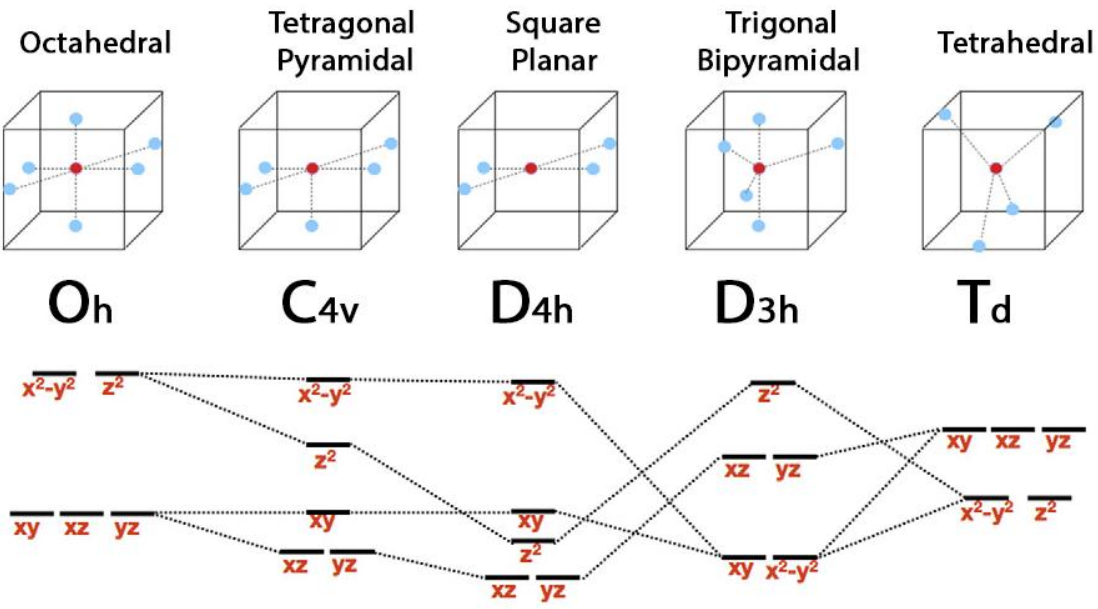


**Figure 2.3** – Distribution of the five d-orbitals in different ligand fields. The elongation on one axis causes the decrease in energy of the orbitals lying along the axis direction.

The splitting of d-orbitals in the crystal-field model not only depends on the geometry of the complex, but also on the nature of the metal ion, its charge and the surrounding ligands. For instance, the higher the oxidation state of the metal or the stronger the ligand, the larger the splitting. A list of ligands ranked in order of their ability to cause large orbital separations is known as spectrochemical series. In case of octahedral field:

$$- \text{ increasing } \Delta_0 \rightarrow$$

$$I^- < Br^- < Cl^- < \underline{S}CN^- < F^- < OH^- < \underline{O}NO^- < H_2O < SC\underline{N}^- < NH_3 < \underline{N}O_2^- < CN^- < CO$$

*weak-field ligands* *strong-field ligands*

When the geometry and the ligands are held constant, the metal spectrochemical series is approximately the following one:

$$- \text{ increasing } \Delta_0 \rightarrow$$

$$Mn^{2+} < Ni^{2+} < Co^{2+} < Fe^{2+} < V^{2+} < Fe^{3+} < Ru^{3+} < Pd^{4+} < Pt^{4+}$$

In an octahedral field, the value of $\Delta_0$ increases as the oxidation state increases and moving down the group. This trend agrees with the decrease of the atomic radius in higher oxidation state ions, that means smaller distances between metal and ligands and larger interaction energies.

An advanced theory to explain the spectroscopic properties of metal complexes is based on the ligand-field model, which takes into account the overlap between the orbitals of the metal ion and of the ligands. LFT arises from the application of the molecular orbital theory and allows to build-up a molecular orbital energy level diagram from metal atom orbitals and symmetry-adapted linear combinations (SALC) of ligand orbitals. In an octahedral complex, the result is an electronic rearrangement which is qualitatively the same as in crystal-field theory with five molecular orbitals which are mainly metal-orbital in character (three triply degenerate nonbonding orbitals with $t_{2g}$ symmetry and two doubly degenerate antibonding $e_g$ orbitals). Moreover, when ligands have orbitals with local π symmetry with respect to the M-L axis, it is possible to form SALCs of $t_{2g}$ symmetry and to combine them with the three metal $t_{2g}$ orbitals. With respect to the atomic nonbonding orbitals, the resulting $t_{2g}$ molecular orbitals of the complex can have higher or lower energy (depending on the relative energies of the ligand and metal orbitals) and $\Delta_0$ is decreased or increased, respectively (**Figure 2.4**). The ligands can be then classified as π-donor or π-acceptor depending on the presence (π-donor) or absence (π-acceptor) of electrons in their available π orbitals; this also affects the energy of such orbitals and therefore the $\Delta_0$ gap. The spectrochemical series introduced by CFT can be then explained on the basis of the π bonding effect, when feasible, and most of the above considerations on the frontier orbitals are also reflected in LFT model, but with

the advantage of a detailed description (and prediction) of the complex molecular orbital energy diagram which rigorously clarify most of the observable absorption phenomena.

| | − increasing $\Delta_0$ → | |
|---|---|---|
| LFT | π donor < weak π donor < no π effects < π acceptor | |
| CFT | *weak-field ligands* | *strong-field ligands* |

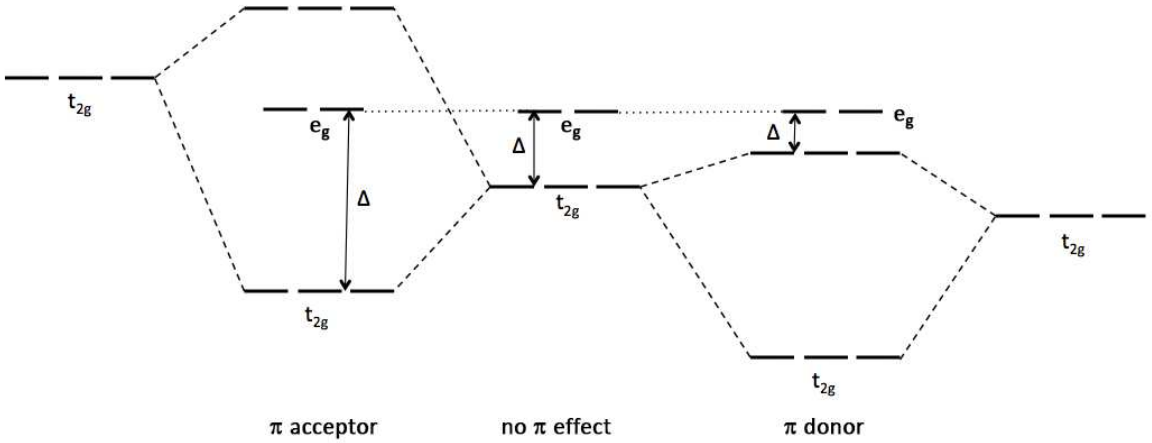


**Figure 2.4** – Effect of π-donor and π-acceptor ligands on the energy gap between HOMO and LUMO orbitals of a generic metal complex with $O_h$ symmetry.

*2.2.2 Data analysis and processing*

The UV-Vis spectra are acquired in the spectral range 200-900 nm at a temperature of 25°C, in a quartz cuvette with an optical path of 1 cm. Spectrophotometric titrations allowed to follow the changes in absorbance throughout the pH range 2-12. The pH was varied approximately half unit for each measurement by manual addition of a little amount of HCl and KOH 0.1 M. Obtained UV-Vis spectra at different pH values were analysed using the Origin software. For each spectrum, the absorbance were converted in ε ($M^{-1}$ $cm^{-1}$) dividing it by the overall metal concentration and the optical pathway ($\varepsilon = A/Cl$). Molar extinction coefficient values are reported on y-axis, while wavelengths are maintained on x-axis. The position and the intensity of the main bands were derived and the corresponding values of wavelength of maximum absorption ($\lambda_{max}$, nm), absorbance ($\varepsilon_{max}$, $M^{-1}$ $cm^{-1}$) were obtained. In literature it is possible to find the value of $\lambda_{max}$ expected for a d-d transition of Cu(II) and Ni(II) complexes. In **Tables 2.1** and **2.2** are listed some values that will be useful for the interpretation of the spectrophotometric results in the visible spectral range. In particular, the method here employed to analyse the spectroscopic data is based on the "rule of average environment" (Billo's method).[6-8]

**Table 2.1** – Expected $\lambda_{max}$ for Cu(II) complexes with different coordination modes.

| **Donor atoms** | **$\lambda_{max}$ (nm)** |
|---|---|
| $N_{Im}$, $COO^-$ | 731 |
| 2 $N_{Im}$ | 687 |
| 3 $N_{Im}$ | 627 |
| 2 $N_{Im}$, $N^-$ | 604 |
| 4 $N_{Im}$ | 576 |
| 3 $N_{Im}$, $N^-$ | 557 |
| 2 $N_{Im}$, 2 $N^-$ | 539 |
| $N_{Im}$, 3 $N^-$ | 522 |
| 4 $N^-$ | 506 |

**Table 2.2** – Expected $\lambda_{max}$ for Ni(II) complexes with different coordination geometries.

| **Coordination geometry** | **$\lambda_{max}$ (nm)** |
|---|---|
| Square planar | 420 – 600 |
| Octahedral | ≈ 650; ≈ 380 |

For Cu(II) complexes the wavelength related to the maximum absorption $\lambda_{max}$ can also be estimated using the following empirical equation:

$$\lambda_{max} = \frac{10^3}{[\,0.294\, n_{\frac{CO}{H_2O}} + 0.346\, n_{COO^-} + 0.434\, n_{N_{Im}} + 0.460\, n_{NH_2} + 0.494\, n_{N^-}]} \qquad (2.23)$$

where $n_{COO^-}$ refers to the number of carboxyl groups, $n_{N_{Im}}$ is the number of imidazole moieties, $n_{NH_2}$ represents the number of amines and $n_{N^-}$ the number of amides coordinated to the metal ion.[8] As already mentioned above, unfortunately, Zn(II) complexes are not spectrophotometrically active.

## 2.3 Circular Dichroism (CD)

Asymmetric chromophores or symmetric chromophores in an asymmetric environment can interact differently with right- and left-circularly polarized light. When a circularly polarized light beam passes through an optically active medium, it experiences different velocities depending on the different refraction indices for right- and left-circularly polarized light ($n_r \neq n_l$); this phenomenon is called optical rotation, and it results in the rotation of the polarized axis. The variation of optical rotation as function of wavelength is known as optical rotatory dispersion (ORD). Similarly, right- and left-circularly polarized light at certain wavelength can be differently absorbed due to differences in the extinction coefficients ($\varepsilon_r \neq \varepsilon_l$) for the two polarized rays, giving rise to the phenomenon called circular dichroism (CD). Therefore, two types of circularly polarized light interact in different ways with optically active chiral molecules. In a CD experiment, right- and left-handed circularly polarized light at different wavelength pass through the sample and the difference in the two light components absorption is measured. The interaction with the sample usually causes an elliptically polarised vector of the transmitted radiation, due to the different interaction with the left- and right- circularly polarized components. If one component is completely absorbed, the resultant wave will be circularly polarized. A circular dichroism signal can be positive or negative, depending on whether L-CPL (left-circularly polarized light) is absorbed to a greater extent than R-CPL (right-circularly polarized light) or to a lesser extent, giving rise to a positive or negative CD signal, respectively. A schematic representation of the instrumental apparatus for a generic CD experiment is shown in **Figure 2.5**.

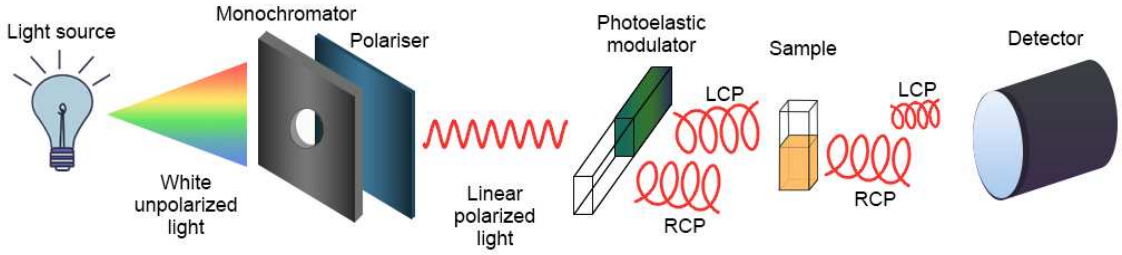


**Figure 2.5 -** Schematic representation of a CD instrument. The incident radiation passes through a modulating device, usually a photoelastic modulator (PEM), which transforms the linear light to circular polarized light. The PEM is able to let pass either the left (L-CPL) and the right (R-CPL) light component depending on the applied alternating electric field. The direction of polarization and the absorption changes are measured by a detector and circular dichroism is calculated.

### *2.3.1 Data analysis and processing*

The CD spectra were acquired in the spectral range 200-900 nm. Analogously to UV-Vis measurements, spectrophotometric titrations have been performed to follow the changes in the CD signals throughout the pH range 2-11. The pH was varied approximately half unit for each measurement, by manual addition of a little amount of HCl and KOH 0.1 M. Obtained CD spectra at different pH values were analysed using the software Origin. In

general, any electronic transition that give rise to a UV-Vis absorption also give rise to a CD band, with the maximum (or minimum) located at approximately the same wavelength of the maximum absorption on UV-Vis spectra (**Figure 2.6**).

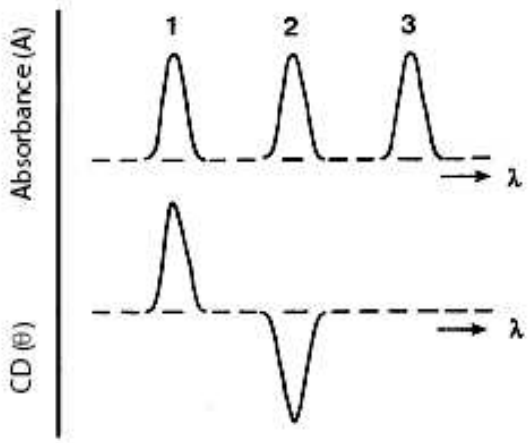


**Figure 2.6 -** The relationship between UV-Vis absorption and CD spectra. Band 1 has a positive CD spectrum with L-CPL absorbed more than R-CPL; band 2 has a negative CD spectrum with R-CPL absorbed more than L-CPL; band 3 is due to an achiral chromophore.

Historically, circular dichroism is represented in terms of ellipticity (θ), which is defined as the tangent of the ratio of minor to major elliptical axis. Modern CD instruments are capable of millidegree precision. Molar ellipticity can also be defined as $\theta = 3298\ \Delta\varepsilon$. The unit ellipticity persists even though CD is now measured as the difference in absorbance between right- and left-circularly polarized light as a function of wavelength ($\Delta A = A_l - A_r$). The Beer-Lambert law ($\Delta\varepsilon = \Delta A/lC$) states that the difference in extinction coefficients ($\Delta\varepsilon = \varepsilon_l - \varepsilon_r$ , where $\varepsilon_l$ and $\varepsilon_r$ are the molar extinction coefficients expressed as $M^{-1}cm^{-1}$ for left- and right-circularly polarized light, respectively), at a given wavelength, is equal to the difference in absorbance divided by the product of the path-length and the concentration. Therefore, circular dichroism spectra usually present Δε along y-axis and $\lambda$ along x-axis. Besides d-d transitions in the visible region, circular dichroism allows to detect intense bands in the ultraviolet region mostly due to charge transfer transitions between metal and ligand. **Table 2.3** reports the maximum wavelengths of absorption for CD bands of Cu(II) and Ni(II) complexes, which can help predicting the coordination modes of the studied complexes.

**Table 2.3** – Expected $\lambda_{max}$ for the most characteristic CD bands of Cu(II) and Ni(II) complexes with different donor atoms.[9]

| **Metal ion** | **Donor** | **$\lambda_{max}$ (nm)** |
|---|---|---|
| **Cu(II)** | $N_{Im}$ | 220 |
| | | 245 - 260 |

| | | |
|---|---|---|
| | | 280 - 345 |
| | $N^-$ | 295 - 315 |
| | OH | 285 |
| | $O_{tyr}^-$ | 300 - 310 |
| | $NH_2$ | 233 - 245 |
| | $COO^-$ | 255-265 |
| **Ni(II)** | S | 220 – 270<br>320 - 350 |
| | $N^-$ | 250 - 270 |
| | $N_{Im}$ | 260 - 270 |

It is also worth to mention that the chirality of the molecule can arise from both its conformation and its structure. This means, for instance, that the CD spectra of a protein molecule with a specific secondary structure can undergo some variations if its conformation changes (for example from random coil to β-sheet). Such analyses are commonly performed in the far-ultraviolet spectroscopic range (180-350 nm) and require a low concentrated solution of the interested biomolecule (or peptide with an adequate large sequence of amino acids) and a quartz cuvette with 0.1 mm path length. It is useful to measure far-UV CD spectra for both the apo-peptide and the metal-ligand complexes in order to verify possible conformational changes in the peptide folding, which may occur upon the metal coordination. CD signals for specific secondary structures are shown in **Figure 2.7**.

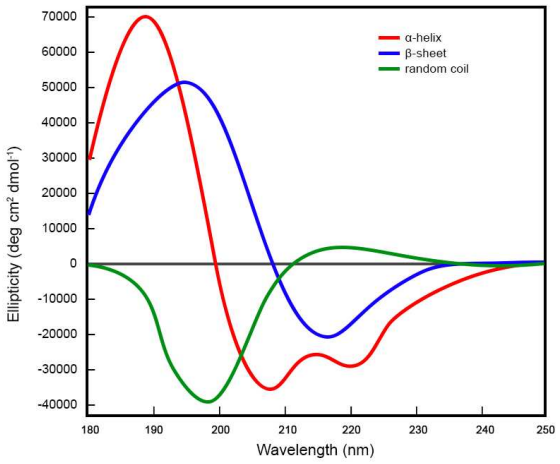


**Figure 2.7** – Typical CD bands for α-helix (yellow), β-sheet (blue) and random coil (red) conformations.[10]

## 2.4 Nuclear Magnetic Resonance Spectroscopy (NMR)

Nuclear magnetic resonance (NMR) is a spectroscopic technique widely used for the determination of molecular structures in solution and pure liquids. This spectroscopic method applies to atomic nuclei which are sensitive to an external magnetic field, $B_0$, and it measures the absorption of radiofrequency electromagnetic radiation. Atomic nuclei are characterised by nuclear spin quantum number, *I*. When an atomic nucleus possesses a non-zero net nuclear spin ($I \neq 0$), it can be investigated by NMR. Examples of nuclei relevant for biomolecular NMR include $^{1}H$ (spin = ½), deuterium $^{2}H$ or d (spin = 1), $^{13}C$ (spin = ½), $^{14}N$ (spin = 1), $^{15}N$ (spin = ½), $^{31}P$ (spin = ½). A rotating particle possesses an angular momentum, **J**, and a magnetic moment, **μ**; these vectorial quantities are related by the giromagnetic ratio, γ, which is constant and typical for each nucleus.

$$\boldsymbol{\mu} = \gamma \boldsymbol{J} \tag{2.24}$$

When a nucleus interacts with an external magnetic field, the motion of the electrons around the atom generates an opposite magnetic field and the nucleus precesses about the direction of the field. The angular momentum vector **J** precesses about the external field axis with an angular frequency known as the Larmor frequency, ω, which is proportional to γ and $B_0$ (Larmor equation, 2.26). Therefore, in the presence of an external magnetic field, nuclei with different gyromagnetic ratios can be discriminated by means of their precession frequency.

$$\omega = \gamma B_0 \tag{2.25}$$

In the presence of an external magnetic field, two spin states exist for a nucleus. The magnetic moment of the lower energy +1/2 state is aligned with the external field, while the higher -1/2 spin state is opposite. The nuclear magnetic moment, oscillating at the Larmor frequency, can be in resonance with the magnetic component of an incident electromagnetic radiation of frequency equal to ω. Under these conditions, the radiation is absorbed (its energy exactly corresponds to the spin state separation of a specific set of nuclei) and the nuclear spin rotates changing orientation from the +1/2 state to the higher -1/2 spin state. The frequency of a NMR transition depends on the local magnetic field experienced by the nucleus and is expressed in terms of the chemical shift, δ, that is the difference between the resonance frequency of nuclei in the sample and that of a reference compound, usually tetramethylsilane $Si(CH_3)_4$. Chemical shift are different for the same element in inequivalent positions within a molecule, therefore NMR can be used to study the structure of a molecule and the interaction with a metal ion. Moreover, the use of two-dimensional nuclear magnetic resonance spectroscopy allows the dispersion of the signals in various dimensions and the observation of correlations between different signals. Interactions between nuclear spins is also possible and can be observed by NMR. The so-called spin-spin coupling, which is reported as the spin-spin gives rise to multiplets due to small changes in the resonance energy associated to a nucleus affected by the orientation of the spin of a nearby nucleus. The

strength of spin-spin coupling, which is reported as the spin-spin coupling constant, J (in hertz, Hz), decreases rapidly with distance through chemical bonds. Chemically equivalent nuclei, however, do not display the effects of their mutual spin-spin coupling.

### *2.4.1 Data analysis and processing*

The TOCSY (Total Correlation Spectroscopy) experiment has been the most employed method to record NMR spectra in this work; it shows the correlations (cross peaks) for nuclei which are directly coupled and nuclei which are connected by a chain of subsequent couplings. A comparison between the observed chemical shifts of a peptide sample in absence and presence of metal ion allows to identify which proton signals are more affected by the addition of the metal and therefore which residues are most likely involved in the interaction with it. In the case of paramagnetic metals, like Cu(II), NMR proton signals of the residues close to the metal ion undergo an intense line broadening, therefore the selective signal disappearance can give information on the involved donor groups. Spectral processing and analysis was performed using Bruker TOPSPIN 2.1

## 2.5 Electrospray Ionization Mass Spectrometry (ESI-MS)

Mass spectrometry is an analytical technique that can provide both qualitative and quantitative information (such as structure, molecular mass, concentration and isotopic ratios of atoms) on organic and inorganic analytes in complex mixtures after their conversion to positively or negatively charged ion. A mass spectrum is a graphical representation of the relative abundance of the obtained ions as a function of their mass/charge (*m/z*) ratio. The most intense peak has 100% of abundance and it is called base peak. Since a mass spectrometer separates and detects ions of slightly different masses (modern instrumentations can resolve ions differing by only a single atomic mass unit), it distinguishes different isotopes of a given element.

Mass spectrometers can be divided into three fundamental parts, namely the ionization source, the analyser and the detector system. Since ions are easier to manipulate than natural molecules, the sample must be first introduced into the ionization source where the ionization process takes place. The obtained ions are sent to the analyser region of the mass spectrometer, where they are separated according to their *m/z* values. The separated ions are thus detected to generate the signal and plot the spectrum. The analyser and detector components, and often the ionisation source too, are maintained under high vacuum to prevent any hindrance from air molecules and let ions travel throughout the instrument. The main function of the mass analyser is to separate the formed ions according to their mass-to-charge ratios. There are a large number of currently available mass analysers, which include quadrupoles, time-to-flight analysers (TOF), magnetic sectors, Fourier transform ion cyclotron resonance (FT-ICR) and quadrupole ion traps. These mass analysers have different features, including the *m/z* range that can be covered, the mass accuracy and the achievable resolution. The analysers listed above can be used in conjunction with electrospray ionization source (ESI). ESI is suitable for polymers, proteins, peptides and small polar molecules, allowing very high sensitivity and an easy coupling to high-performance liquid chromatography HPLC, μ-HPLC or capillary electrophoresis. The transfer of ionic species

from solution to the gas phase by ESI involves three steps: (1) dispersion of a fine spray of charged droplets, followed by (2) solvent evaporation and (3) ion ejection from the highly charged droplets (**Figure 2.8**).

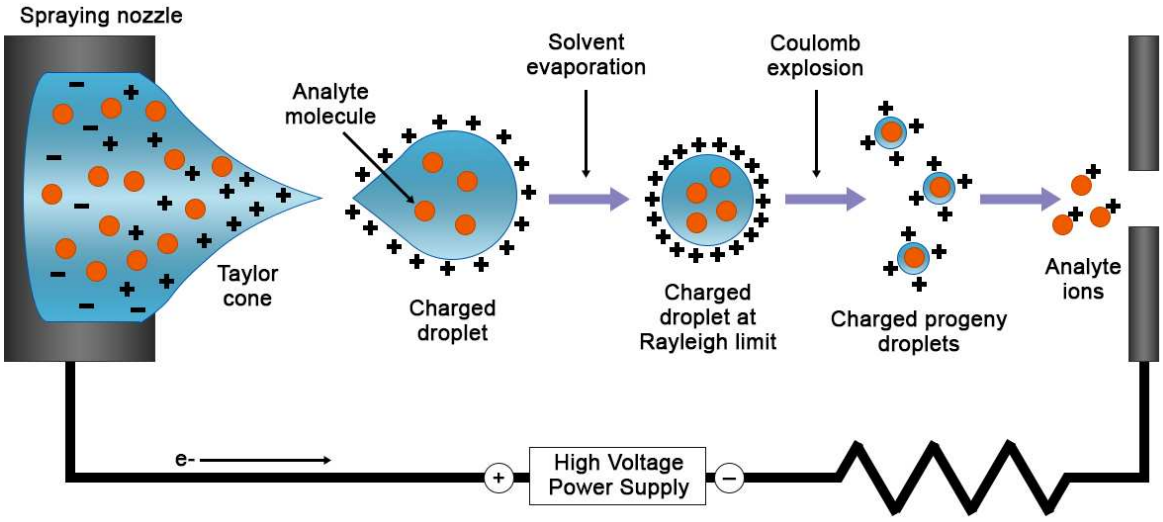


**Figure 2.8** – Schematic representation of the electrospray ionization process.

Spray is produced by applying a strong electric field (3 – 6 kV), under atmospheric pressure, to a liquid passing through a capillary tube with a weak flux. The applied electric field induces a charge accumulation at the liquid surface, which then results in the formation of highly charged droplets, which are carried by a nebulising gas (*e.g.* nitrogen) and pass down pressure potential gradients toward the analyser region. With the aid of temperature and/or stream of drying gas, the charged droplets are continuously reduced in size by evaporation of the solvent, with consequent increase of surface charge density until the reach of their Rayleigh limit. At this point the surface tension cannot compensate for the electrostatic repulsion and the droplets undergo a "Coulomb explosion" creating many smaller and more stable droplets. Finally, the electric field strength within the charged droplet reaches a critical point and the formation of ions in gaseous phase becomes kinetically and energetically favourable. The ions are then accelerated into the analyser for subsequent analysis.

A brief description of one of the analysers used for the ESI-MS measurements of this work is also given. The Quadrupole-time-of-flight analyser is high mass accuracy and high-resolution instrument, ideal for peptide sequencing, where a time-of-flight analyser is coupled with a linear series of two quadrupoles. The first quadrupole can be used as a precursor mass selector, *i.e.* an ion mass filter, while the second quadrupole is employed as a collision cell using Ar, He, or $N_2$ gas, in order to produce further fragmentations. A mass spectrum is obtained by monitoring the ions passing through the quadrupole filter as the voltages on the four paired rods, which composed it, are varies. The two opposite rods have an applied potential of $\pm (U + V\cos(\omega t))$, where U is a direct current voltage and V cos(ωt) is an alternating current voltage. There are two operating procedures: varying ω and holding U and V constants, or varying U and V with the ratio U/V fixed for a constants angular frequency, ω. Then the product ions are analysed in the TOF analyser. Resolution for such instrument can be higher than 18000. In a time-to-flight analyser ions "drift" down an

evacuated tube of a suitable length (usually 1 m) with different velocities depending on their mass-to-charge ratios (heavier ions of the same charge reach low speeds, while ions with higher charge have an increased velocity). For a tube of known length, velocity is inversely proportional to the time of flight, $t_F$, of the ions:

$$t_F = \frac{L}{\upsilon} = L\sqrt{\frac{m}{2zeV}} \tag{2.26}$$

where $L$ is the distance between the source and the detector, $\upsilon$ is the ion rate after acceleration, $m$ is the mass, $e$ is the electron charge ($e$ = 1.60 $\cdot 10^{-19}$ C) and $V$ is the accelerating electric field potential. Times of flight are typically on the order of microseconds (1-50 μs) for a drift tube ($L$) of 1 meter long. TOF instrument offers a wide number of advantages respect to other types of mass spectrometers, as it is simple to use and study enough. Furthermore, TOF is the fastest MS analyser, it is well suited for pulsed ionization methods (*i.e.* MALDI ion source), and it has high ion transmission and the highest practical mass range (theoretically unlimited). However, it requires fast digitizers which can have limited dynamic range, and it has limited resolution and sensitivity.

### *2.5.1 Data analysis and processing*

The interpretation of mass spectra was achieved using the program Bruker Compass Data Analysis 4.0; with this software, it was possible to compare the experimental spectrum with the isotopic pattern of a simulated spectrum, in order to obtain a validation of the ion attribution. The physical property of ions that is measured is the mass-to-charge ratio rather than the simple mass. Therefore, it should be mentioned that for multiply charged ions the apparent *m/z* values are fractional parts of their actual masses. ESI-MS is a soft ionization technique which allows a gentle handling of a sample ions, this is a great advantage since it prevents the molecule fragmentation. As a consequence, ESI mass spectra of peptides and proteins usually appear as a collection of various multiply charged ions of the intact analyte molecule forming adducts with other metal ions (such as $K^+$ or $Na^+$) or protons deriving from the chosen experimental conditions (*e.g.* pH).

## 2.6 Electron Paramagnetic Resonance (EPR)

Electron paramagnetic resonance spectroscopy (EPR) corresponds to the observation of a resonant absorption by unpaired electrons in a magnetic field. It is suitable for paramagnetic species. The application of an external magnetic field $B_0$ produces a difference in energy between the possible spin states of the unpaired electrons (Zeeman effect) and the absorption of the microwave radiation can cause the excitation of the particle from its low energy state to a higher energy state:

$$\Delta E = g\mu_B B_0 \tag{2.27}$$

where $\mu_B$ is the Bohr magneton ($9.2740 \cdot 10^{-24}$ J $T^{-1}$) and g is a numerical factor known as the "g value". Usually the resonance conditions are obtained at a fixed incident radiation ($\Delta E = h\upsilon$, with constant $\upsilon$), by varying the intensity of the magnetic field. The most used frequencies are the microwave range (9.5 GHz). The proportionally constant g is the primary empirical parameter which is determined in an EPR experiment: this value is specific for the molecule under investigation and contains information on the chemical environment, *e.g.* the coordination sphere of a paramagnetic metal ion. For a free electron in vacuum $g_e$ = 2.00232, but in compounds this value is affected by spin-orbit coupling, which alters the local magnetic field experienced by the electron. The unpaired electron of a paramagnetic molecule does not only experience the external magnetic field, but it is also affected by the molecular electronic structure. Then, the g values can be highly anisotropic so that the resonance condition depends on the rotation of the molecule in the applied field (or, alternatively, rotation of the field around the magnet). A metal ion at the centre of a perfect octahedron with six identical ligands with identical metal-to-ligand bond lengths will give a single (derivative) line EPR spectrum, called an isotropic pattern, with $g_z = g_y = g_x$. An axial pattern with $g_z \neq g_y \neq g_x$ can occur when a perfect octahedron is elongated or compressed along one of the axes. More generally, if one, or two of the ligands along this axis are different from the others the structure and the spectrum are (near) axial and it is possible to define two g values, $g_{//}$ (for the component parallel to the applied magnetic field) and $g_\perp$ (for the other two components, which are perpendicular to the field).

The coupling of the electron spin to any magnetic nucleus with $I \neq 0$ gives rise to hyperfine interaction, which results in the multiplet (2I+1) structure of each EPR line. The hyperfine interaction parameter, A, expressed in gauss, represents the magnitude of the splitting and is also generally anisotropic. Taking a metal complex as an example, besides the hyperfine structure, which describes the coupling of the unpaired electron to the atom on which it is primarily located, the superhyperfine structure refers to the coupling to ligands nuclei and gives further information about the formed complexes (*e.g.* the extent electron delocalization and covalence in metal complexes).

### *2.6.1 Data analysis and processing*

The EPR parameters, g and A, for Cu(II) complexes were obtained by means of computer simulation of the experimental spectra using the WIN-EPR SIMFONIA software (Bruker). Since these parameters are determined by the chemical composition and the position of the atoms nearest to the metal ion, they provide information on the coordination sphere and the donor atom set. The metal-ligand interaction can be predicted by a comparison with literature values for the EPR parameters (**Table 2.4**).[11] EPR analyses can also give information on the possible formation of bi-nuclear copper complexes, since the magnetic interaction between the two metal centres – unless very distant in the molecule – produces an antiferromagnetic coupling that renders Cu(II) ions silent.

**Table 2.4** – Expected values of $g_{//}$ and $A_{//}$ in Cu(II) complexes with different equatorial donor atoms.

| **Donor atoms** | **$g_{//}$** | **$A_{//}$ (G)** |
|---|---|---|
| 1N, 3O | 2.34 – 2.32 | 140 – 160 |
| 2N, 2O | 2.30 – 2.27 | 160 – 180 |
| 3N, 1O | 2.25 – 2.19 | 170 – 200 |
| 4N | 2.21 – 2.16 | 190 - 215 |

## 2.7 Reverse-Phase High-Performance Liquid Chromatography

Reverse-Phase High-Performance Liquid Chromatography (RP-HPLC) separates molecules based on their hydrophobicity. In this technique, the stationary phase inside the column is non-polar, typically made of silica bonded with long-chain hydrocarbons (like C18). The mobile phase, a mixture of polar (*e.g.* water) and less polar (*e.g.* acetonitrile) solvents plus pH modifiers (like trifluoroacetic acid), flows through this column. As the sample passes through, more hydrophobic molecules interact strongly with the non-polar stationary phase and are retained longer, while more polar molecules interact less and elute faster. By gradually increasing the concentration of the less polar solvent in the mobile phase, even highly hydrophobic molecules can be eluted and detected, allowing for precise separation and analysis of complex mixtures like peptides. The resolution and accuracy of the separation depend on the correct selection of the column (*e.g.* C18), and pH conditions. The elution of analytes is detected by a UV-Vis detector.

The study of peptide enzymatic stability is a crucial step in the development of new drugs, with plasma incubation representing the most physiologically relevant *in vitro* model to assess their resistance to proteolytic degradation. The process begins with incubating the peptide of interest in plasma samples (human or animal) at physiological temperature (typically 37°C) for a total time of 120 minutes, during which plasma enzymes act. At established time points, aliquots of the sample are withdrawn, and enzymatic activity is immediately quenched, usually by adding denaturing agents like acids (*e.g.* perchloric acid) to prevent the degradation state at the sampling moment. Prior to analysis, samples often undergo deproteinization (centrifugation and filtering) which is essential to remove abundant plasma protein that could interfere with subsequent chromatographic separation and damage the column. To enhance the reproducibility and accuracy of quantification, it is common practice to use an internal standard (IS): a compound chemically similar to the peptide of interest but not naturally present in the biological sample (*e.g.* L-phenylalaninol), added in known quantities to the peptide stock solution. Although less sensitive and selective than mass spectrometry for metabolite identification, the use of a UV-Vis detector allows for the quantification of the intact peptide and, in some cases, the main degradation products, provided they possess suitable chromophores (*e.g.* tryptophan, tyrosine or phenyalanine residues) and are present in sufficient concentrations. By monitoring the ratio of the intact

peptide's peak area to that of the internal standard over time, its plasma half-life can be calculated, providing valuable insights into its *in vivo* stability.[12]

## 2.8 Solid-phase peptide synthesis

Solid-Phase Peptide Synthesis (SPPS) is a common technique for peptide synthesis. The method is based on the use of a solid resin as support material, the use of an excess of reagents in order to promote a faster synthetic process with high purity, and the construction of the peptide from the carbonyl group side (C-terminus) to amino group side (N-terminus) of the amino acid chain. The employed synthetic strategy is Sheppard's α-Fmoc strategy, where the α-amino group is protected with the Fmoc (9-fluorenylmethoxycarbonyl) labile base protecting group. The Fmoc strategy is overall accessible, simple and inexpensive and it allows a wide choice of both resins and amino acid side chains protecting groups, ensuring high yields. The general synthetic scheme is shown in **Figure 2.9**: the first amino acid, which is protected at its α-amino group and the reactive lateral group (Fmoc-Xaa), is anchored to the resin through its C-terminus; the Fmoc group is then removed and the unprotected amino group can react with a second Fmoc-amino acid (Fmoc-Xbb) to form a peptide bond. The use of coupling reagents (*e.g.* carbodiimides) is also crucial to activate the reactive groups and enhance the efficiency of amide bond formation. The above steps are repeated for each amino acid added to the peptide chain. Under strong acidic conditions, the peptide chain in then cleaved from the resin and the side chains protecting groups are removed.

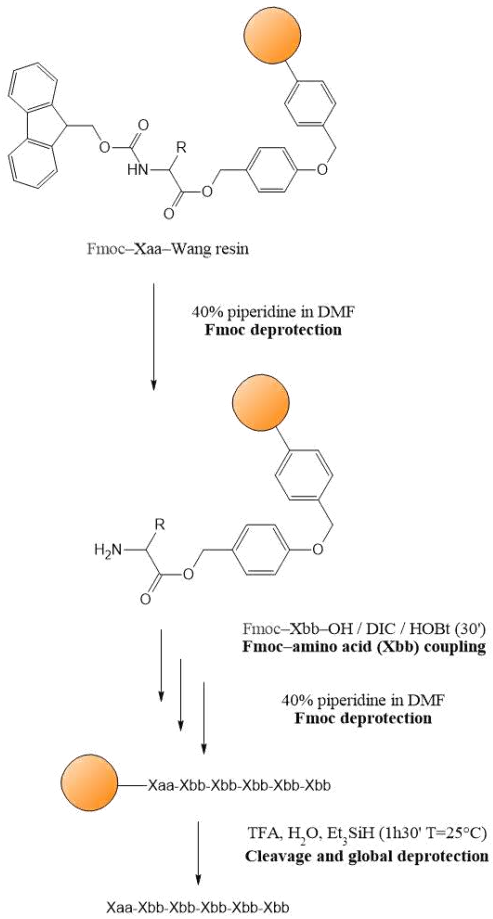


**Figure 2.9 -** Schematic procedure of Solid-Phase Peptide Synthesis.

## 2.8 References


[1] A. Braibanti, G. O., P. Paoletti, L. D. Pettit, S. Sammartano, *Pure and Applied Chemistry*, **1987,** *59*, 1721 - 1728.
[2] Gans, P. & O'Sullivan, B., *Talanta*, **2000,** *51*, 33-7.
[3] Gans, P., Sabatini, A. & Vacca, A., *Talanta*, **1996,** *43*, 1739-1753.
[4] Alderighi, L., Gans, P., Ienco, A., Peters, D., Sabatini, A. & Vacca, A. J. C. C. R., **1999,** *184*, 311-318.
[5] Gran, G., Dahlenborg, H., Laurell, S. & Rottenberg, M. J. A. C. S., **1950,** *4*, 559-577.
[6] Billo, E. J., *Inorganic and Nuclear Chemistry Letters*, **1974,** *10*, 613-617.
[7] Prenesti, E., Daniele, P. G., Prencipe, M. & Ostacoli, G., *Polyhedron*, **1999,** *18*, 3233-3241.
[8] Sigel, H. & Martin, R. B., *Chemical Reviews*, **1982,** *82*, 385-426.
[9] Daniele, P. G., Prenesti, E. & Ostacoli, G., *Journal of the Chemical Society, Dalton Transactions*, **1996**, 3269-3275.
[10] Greenfield, N. J., *Nature protocols*, **2006,** *1*, 2876-90.
[11] Peisach, J. & Blumberg, W. E., *Arch Biochem Biophys*, **1974,** *165*, 691-708.
[12] Benovitz, D. E. & Spatola, A. F., *Peptides*, **1985,** *6*, 257-261.

# 3. Chapter Three: Amide deprotonation and binding

## 3.1 Outline of the work

Metal-protein interactions are a core area of study in bioinorganic chemistry. While the binding of Zn(II) and Cu(II) to proteins and peptides has been extensively researched for decades,[1-5] data on the thermodynamics of Fe(II)-peptide binding is sparse and has only recently gained attention.[6-8]

Amide dissociation constant (p$K_a$), typically between 15 and 18,[9] can be lowered by metal ions like Cu(II) and Ni(II). These ions can displace the amide proton and bind to the amide nitrogen at relatively low pH (pH > 6.0 for Cu(II) and pH > 9.5 for Ni(II)).[10-12] The binding of the metal ion to a peptide ligand often starts with a histidine imidazole ring at acidic pH. Subsequently, increasing the solution pH value, the amide preceding the histidine (N-terminal direction) deprotonates and binds to the metal ion. If solution pH is increased, further amides can be involved in complexation, forming stable five- and six-membered fused chelate rings.[13-15]

There is an emergence of conflicting opinions regarding the ability of other divalent metal ions to bind amide nitrogens. Driven by literature discussion on Zn(II) and Fe(II)-induced amide deprotonation and binding, a study of short model peptides has been undertaken with the aim of determining if these two metal ions can induce the mentioned phenomenon. The three model peptides are: Ac-AAAHAAA-$NH_2$ (AHA), Ac-AAPHAAA-$NH_2$ (PHA) and Ac-AAPHPAA-$NH_2$ (PHP). They are short peptides protected at both terminal ends, containing only one histidine residue. In the second and third peptide, one or two neighboring alanines have been replaced with prolines. The presence of proline residues in the peptide sequence acts as a sort of "breaking point" in the progressive deprotonation and binding of backbone amides by metal ions.[16] Proline is the only natural amino acid having a secondary amino nitrogen. Therefore lack of a replaceable amide proton, prevents the typical stepwise coordination of consecutive amide nitrogens. However, if a proline precedes a histidine (N-terminal direction), the deprotonation and coordination of amide nitrogens by metal ion can proceed in the opposite (C-terminal) direction, as seen in the Prion protein,[17] although the resulting metal chelates have reduced stability. A deep thermodynamic and spectroscopic investigation of the formed metal complexes, conducted by means of different techniques, helped us elucidate the possible differences among the complexing behaviors of the Cu(II), Zn(II) and Fe(II)-metal ions.

## 3.2 Experimental procedure

Analyses performed on the above-mentioned peptides follow the scheme:

- Potentiometric determination of ligand protonation and Fe(II), Zn(II) and Cu(II) complex-formation constants.

- Mass spectrometric analysis to evaluate the stoichiometry of the formed Fe(II), Zn(II) and Cu(II) complexes.
- Spectrophotometric (UV-Vis and CD) analyses of Cu(II) complexes.
- EPR measurements of Cu(II) complexes.
- Calorimetric titration of Zn(II) and Cu(II) complexes.
- Density Functional Theory calculations of the Fe(II), Zn(II) and Cu(II) complexes.

From the obtained equilibrium constants, it is possible to plot the species distribution diagram for each system. It shows the formation percentage of each complex as a function of pH. Both the equilibrium constants and the spectroscopic data from UV-Vis and CD measurements help defining the most probable coordination modes for the Cu(II) ion by comparing the observed wavelength of absorption of a certain complex (corresponding to the pH value at which the species reaches its maximum of formation in solution) with the expected theoretical $\lambda_{max}$ value obtained from the literature. EPR $g_{//}$ and $A_{//}$ parameters also give information on the metal coordination sphere. Calorimetric titration helped defining the number of nitrogen atoms coordinated to Zn(II) and Cu(II) metal ions. Finally, DFT calculations helped us supporting our experimental results.

The employed experimental conditions, instruments and material are reported in details in Leveraro *et al.*, 2025.[18]

## 3.3 Results and discussion

The overall stability constants (log$\beta$) and acid dissociation constants (p$K_a$) for the formed metal complexes are reported in **Table 3.1** together with the proposed coordination mode for each species. In case of Cu(II) systems, increasing the pH value, a general shift of the visible absorption bands towards shorter wavelength is observed (**Figure 3.1**); this behavior typically indicates the increase of the number of coordinated nitrogen atoms around the Cu(II) ion. Therefore, moving to alkaline conditions, Cu(II) is able to gradually form complexes where 2, 3 or 4 nitrogen atoms are coordinated to the metal center. However, looking at the three UV-Vis spectra some differences between the three peptides complexes are already visible. Starting from the peptide AHA: it exhibits the most extensive amide coordination, with the first, second and third amides deprotonating and coordinating to copper progressively as pH increases. The last species $[CuH_{-3}L]^-$ achieves a $N_{Im}$, 3 $N^-$ binding mode with a square planar geometry at alkaline pH, resulting in a significantly blue-shifted $\lambda_{max}$ around 517 nm. The progressive amide coordination is suggested to proceed in the N-terminal direction, starting from the histidine-anchoring site. In the case of the peptide PHA, the coordination proceed in a slightly different way. After the deprotonation and binding of the histidine residue, the deprotonation of the first amide nitrogen is not detected by potentiometry. Instead, the simultaneous deprotonation and binding of a two amide nitrogens, that could shift the already bound imidazole to an axial position of the distorted octahedron, has been observed. Lastly, at very alkaline pH, the deprotonation and coordination of a third backbone amide occurs. Due to the presence of a proline residue before the His anchoring site, the amide coordination is forced to proceed in the C-terminal direction. Finally, the PHP peptide displays the most restricted amide coordination. Only

one backbone amide is available next to the His and its deprotonation and binding was not detectable by potentiometry. However, the formation of the [$CuH_{-2}L$] species has been observed with the proposed release of a proton from a coordinated water molecule, leading to a $N_{Im}$, $N^-$, $OH^-$ coordination mode. The presence of two proline residues creates significant structural rigidity around the metal binding site. This rigidity hinders the binding of other backbone amides located further from the His anchoring site.

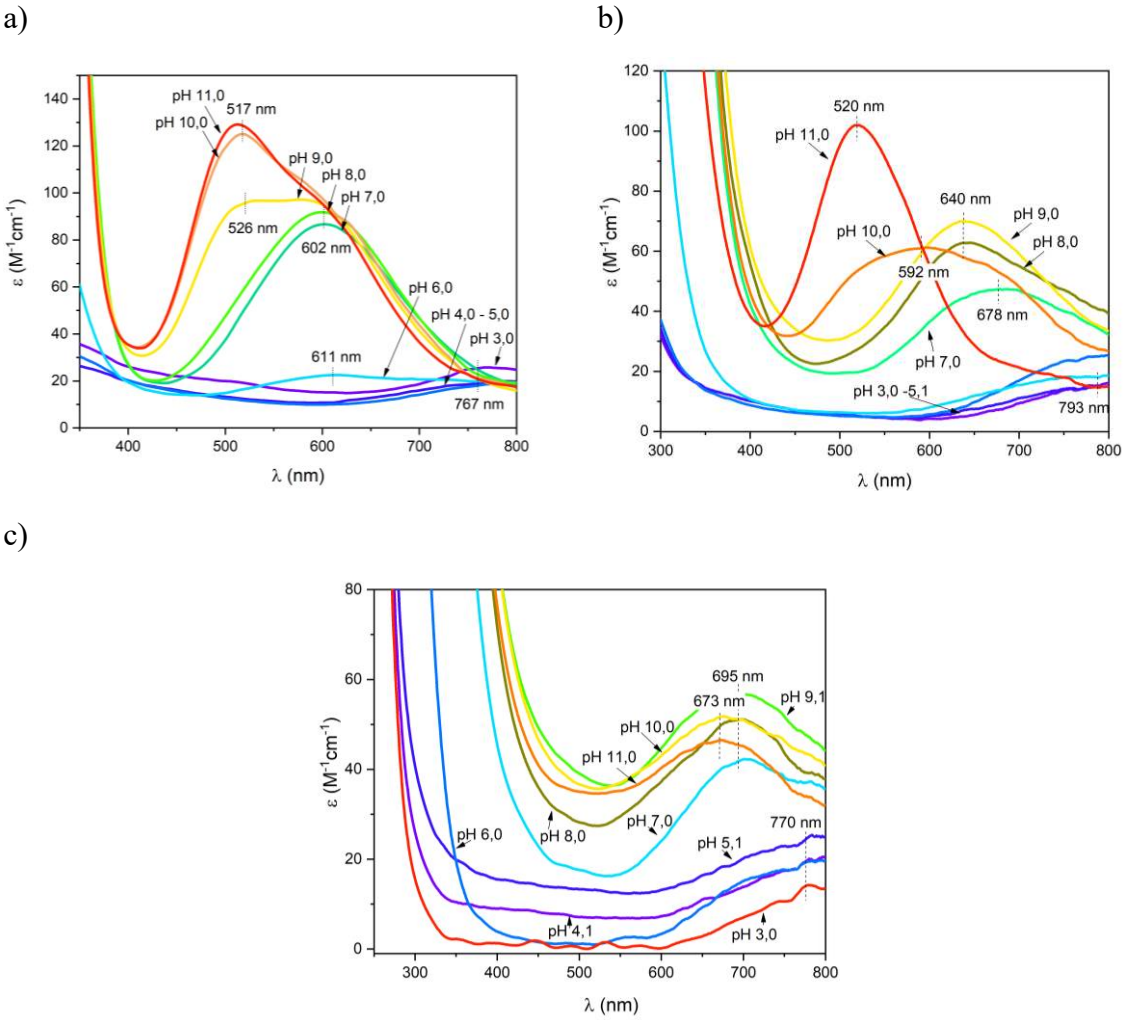


**Figure 3.1 -** UV-Vis absorption of: (a) Cu(II)/AHA, (b) Cu(II)/PHA, (c) Cu(II)/PHP complexes, M:L ratio 0.9:1; $C_M = 0.44 \cdot 10^{-3}$ M, optical path 1 cm.

Those differences between the complexing behaviors of copper towards the three peptides can be also deduced from the CD spectra. Under physiological and alkaline conditions, the binding of a larger number of N-amides to the Cu(II) ion in the equatorial coordination plane, is confirmed by the increased intensity of the CD signals. The interaction with the peptide backbone, in fact, usually produces a stronger CD absorption, due to the proximity of the N-amide donor groups to the peptide chiral centers. In the case of Cu(II)/AHA, a higher intensity is achieved than that of Cu(II)/PHA, supporting our hypothesis of coordination. While in case of PHP, the CD spectra remain unchanged across the whole pH range, and no typical coordinated nitrogen signals are detected, but this is not uncommon in case of just one coordinated amide nitrogen.

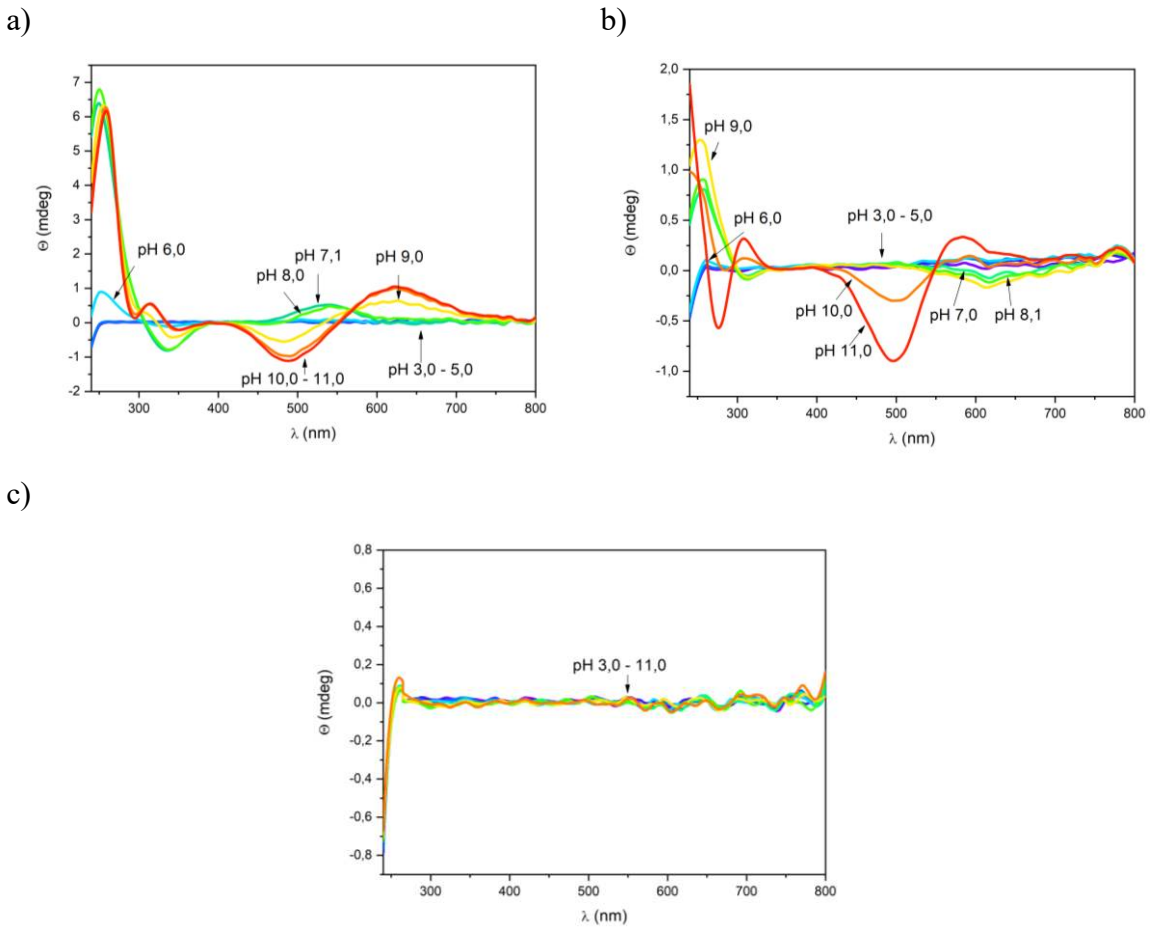


**Figure 3.2 -** CD spectra of Cu(II) complexes with (a) AHA, (b) PHA and (c) PHP at different pH values; M:L ratio 0.9:1, $C_M$= 0.44· $10^{-3}$ M, optical path 1 cm.

**Table 3.1** – Equilibrium constants and proposed coordination modes for Cu(II), Zn(II) and Fe(II) complexes at $T$ = 298 K and $I$ = 0.1 M (NaCl). Values in parentheses are standard deviations on the last significant figure.

| **Species** | **log**β | **p*K*a** | **Coord.** | **log**β | **p*K*a** | **Coord.** |
|---|---|---|---|---|---|---|
| | **AHA** | | | **PHA** | | |
| $[CuL]^{2+}$ | 3.44(6) | 6.07 | $N_{Im}$ | 3.56(4) | - | $N_{Im}$ |
| $[CuH_{-1}L]^{+}$ | -2.63(3) | 6.14 | $N_{Im}$, $N^-$ | - | - | - |
| $[CuH_{-2}L]$ | -8.77(1) | 8.68 | $N_{Im}$, $2N^-$ | -9.65(2) | 9.73 | $2N^-$ |
| $[CuH_{-3}L]^{-}$ | -17.45(2) | - | $N_{Im}$, $3N^-$ | -19.38(2) | - | $3N^-$ |
| | **PHP** | | | | | |
| $[CuL]^{2+}$ | 3.81(5) | - | $N_{Im}$ | | | |
| $[CuH_{-2}L]$ | -9.66(3) | - | $N_{Im}$,$N^-$, $OH^-$ | | | |
| | **AHA** | | | **PHA** | | |
| $[ZnL]^{2+}$ | 3.70(6) | - | $N_{Im}$ | 3.60(1) | - | $N_{Im}$ |

| | | | | | | |
|---|---|---|---|---|---|---|
| $[ZnH_{-2}L]$ | -12.27(6) | 8.02 | $N_{Im}$, $2OH^-$ | -12.00(1) | 8.01 | $N_{Im}$, $2OH^-$ |
| $[ZnH_{-3}L]^-$ | -20.29(4) | - | $N_{Im}$, $3OH^-$ | -20.01(8) | - | $N_{Im}$, $3OH^-$ |

| | **PHP** | | |
|---|---|---|---|
| $[ZnL]^{2+}$ | 3.70(6) | - | $N_{Im}$ |
| $[ZnH_{-2}L]$ | -12.13(6) | 8.06 | $N_{Im}$, $2OH^-$ |
| $[ZnH_{-3}L]^-$ | -20.19(4) | - | $N_{Im}$, $3OH^-$ |

| | **AHA** | | | **PHA** | | |
|---|---|---|---|---|---|---|
| $[FeL]^{2+}$ | 3.41(6) | 7.75 | $N_{Im}$ | 3.15(6) | 7.64 | $N_{Im}$ |
| $[FeH_{-1}L]^+$ | -4.34(3) | - | $N_{Im}$, $2OH^-$ | -4.49(3) | - | $N_{Im}$, $2OH^-$ |
| $[FeH_{-3}L]^-$ | -22.28(3) | 10.25 | $N_{Im}$, $3OH^-$ | -21.98(3) | 9.66 | $N_{Im}$, $3OH^-$ |
| $[FeH_{-4}L]^{2-}$ | -32.53(3) | | $N_{Im}$, $4OH^-$ | -31.64(4) | - | $N_{Im}$, $3OH^-$ |

| | **PHP** | | |
|---|---|---|---|
| $[FeL]^{2+}$ | 3.30(5) | 7.79 | $N_{Im}$ |
| $[FeH_{-1}L]$ | -4.49(3) | - | $N_{Im}$, $2OH^-$ |
| $[FeH_{-3}L]^-$ | -22.28(2) | 10.05 | $N_{Im}$, $3OH^-$ |
| $[FeH_{-4}L]^{2-}$ | -32.33(3) | - | $N_{Im}$, $4OH^-$ |

In case of Zn(II) complexes, potentiometric data shows how the three peptides behave in a very similar way towards the Zn(II) ion: they start binding the metal ion from pH 4, and proceed with deprotonation and binding of the histidine residue when pH is increased. Subsequently, the release of protons from the coordinated water molecules occurs.

For Fe(II) complexes, the precipitation of iron hydroxide was observed at pH values higher than 9.5. The coordination pattern for Fe(II) is very similar to that observed for Zn(II) binding. This pattern involves the deprotonation and binding of the histidine residue, followed by the stepwise deprotonation of the coordinated water molecules. The Fe(II) system is particularly challenging to analyze and work with due to the redox activity of the Fe(II) ion. Despite these difficulties, we can conclude that the potential deprotonation and binding of backbone amides by Fe(II) is remote according to our results.

The thermodynamic results unequivocally demonstrate that the availability or not of backbone amides near to the His binding site makes no differences in the complexing behavior of Zn(II) and Fe(II) ion towards the three different peptides.

Support for the proposed coordination hypotheses of the three complex-peptides is also derived from EPR spectroscopy, which identify the number of coordinated nitrogen atoms to copper ion across the pH range. Further support for the previous hypotheses comes from calorimetric titration, giving a complete thermodynamic picture of Cu(II) and Zn(II) complex-formation equilibria.

High resolution mass spectra confirmed the formation of Zn(II) and Cu(II) complexes under the employed experimental conditions. Signals corresponding to various sodium and potassium adducts, together with the differently protonated free ligand and metal complexes

have been detected. No poly-nuclear or bis-complexes have been identified. An exemplificative mass spectrum is given in **Figure 3.3**.

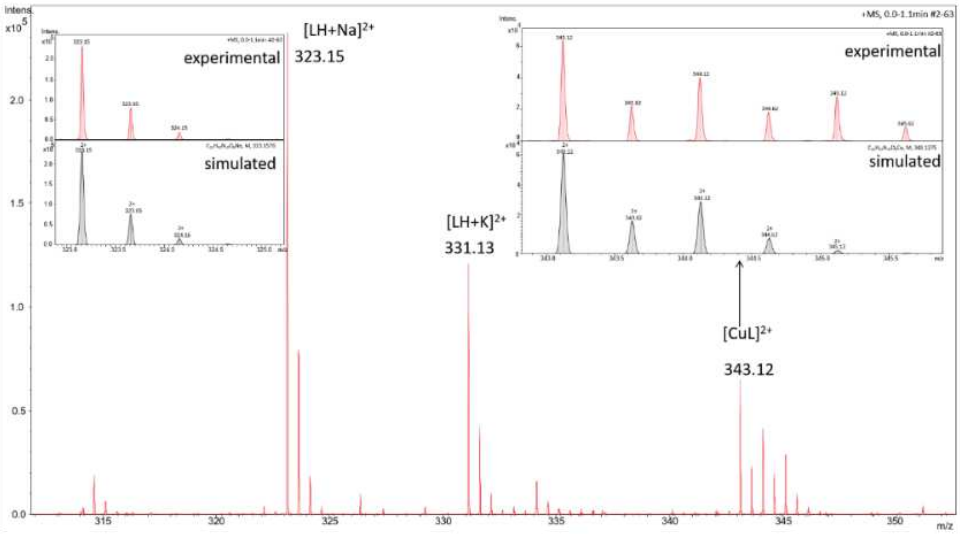


**Figure 3.3** – ESI-MS spectrum for Cu(II)/AHA system at L:M molar ratio = 1:0.9 in MeOH:$H_2O$ (1:1) mixture solution, and comparison between the experimental and simulated isotopic patterns of chosen metal complex $[CuL]^{2+}$.

Finally, to further understand the experimental findings, computational studies were conducted on metal-peptide complexes ($MH_{-x}L$) of the AHA peptide at various pH conditions. The aim is to compare the stability of complexes where the peptide is deprotonated at an amide group ($N_{Im}$, $nN^-$) versus those where deprotonation occurred from a coordinated water molecule, forming a hydroxyl complex ($N_{Im}$, $nOH^-$). In the case of copper(II) ions, the computational results aligned well with the experimental data: as pH increased, amide deprotonation and coordination to copper ion consistently led to more stable complexes compared to the hydroxyl forms. However, for zinc(II) ions binding to the peptide AHA, the computational data indicated a different scenario. It has been suggested that amide-deprotonated complexes ($N_{Im}$, $nN^-$) are unlikely to form in solution. This is because the tetrahedral geometry of the zinc(II) ion would experience significant strain. Instead, the most probable species are those where protons are simply released from coordinated water molecules. This is further supported by the fact that attempts to computationally model amide-deprotonated zinc complexes ($[ZnH_{-2}L]$ and $[ZnH_{-3}L]^-$) repeatedly failed to converge, suggesting their instability.

a)

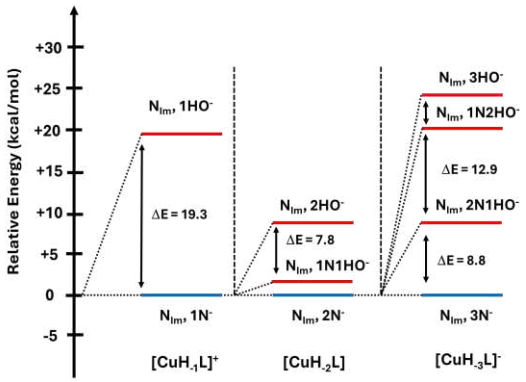


b)

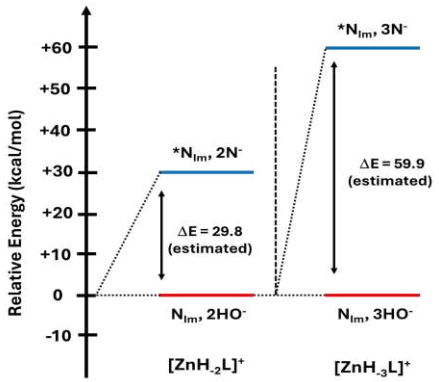

**Figure 3.4** – Correlative energies of mononuclear 1:1 metal peptide $MH_{-x}L$ species formed as a function of the deprotonation degree with increasing solution pH. In all cases, the relative energies of complexes were evaluated for the $OH^-$ vs the corresponding amide-deprotonated structures.

Nevertheless, the obtained thermodynamic equilibrium constants designate the AHA as the best metal binding domain. We calculated two competition plots to qualitatively evaluate the ligand affinity for Cu(II) and Zn(II) (**Figure 3.5**). They represent a simulation of a solution containing equimolar concentrations of the metal and the chosen ligands, admitting that all the peptides compete for the metal recruitment and that they form only the binary complexes described in the speciation models (**Table 3.1**). The AHA peptide is the best ligand for Cu(II) ion, confirming the assumption that a higher number of available amide nitrogens, near the metal binding site, favors the metal complexation. In case of Cu(II), according to the proposed speciation models, AHA complexes exhibit significantly greater stability compared to complexes formed by its proline derivatives, particularly in alkaline solutions. This enhanced stability is attributed to the ability of the AHA peptide to coordinate the Cu(II) ion with up to four nitrogen atoms. In contrast, the substitution of alanine with proline in the PHA and PHP peptides reduces the number of available amide nitrogens for complexation, limiting their coordination to only two or three nitrogen atoms. The competition curve for the Cu(II)-PHP system has been stopped at pH 7.5 due to precipitation. Despite the marked differences observed in the stability of the copper complexes, the stabilities of the corresponding Zn(II) complexes are nearly identical across all the three peptides (**Figure 3.5 b**). This striking observation suggests a fundamental difference in the coordination modes. Since the stability of the Zn(II) complexes is not affected by the proline substitution, it is evident that their coordination does not involve the amide nitrogens of the peptide backbone. Therefore, the native AHA peptide and its alanine-substituted analogues must employ a similar coordination mode for zinc, which does not rely on amide nitrogen involvement.

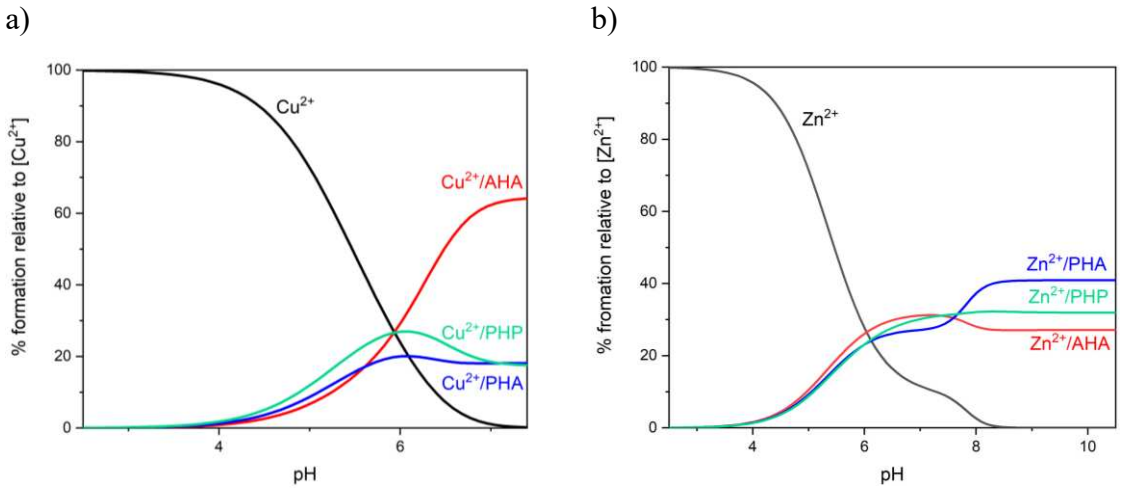


**Figure 3.5** – Competition plots for a solution containing equimolar concentration of metal ion, AHA: Ac-AAAHAAA-$NH_2$, PHA: Ac-AAPHAAA-$NH_2$ and PHP: Ac-AAPHPAA-$NH_2$. (a) Cu(II), and (b) Zn(II).

## 3.4. Conclusions

This study provides the first detailed investigation into the formation equilibria and metal coordination mode of Cu(II) and Zn(II) complexes with the model peptide Ac-AAAHAAA-$NH_2$ and its two mutants. The primary objective wat to determine if Zn(II) ion, like Cu(II), can induce the deprotonation of backbone amide protons and subsequently bind to the amide nitrogens. Both experimental and computational data conclusively show that Zn(II) ion does not induce amide deprotonation or forms complexes with amide nitrogens in the model peptide Ac-AAAHAAA-$NH_2$. This is supported by the observation that the complex-formation behavior of Ac-AAAHAAA-$NH_2$ with the metal ion is nearly identical to that of its proline-substituted analogues, Ac-AAPHAAA-$NH_2$ and Ac-AAPHPAA-$NH_2$. The proline residues in these mutant peptides introduce tertiary amide nitrogens that are sterically unable to bind to metal ions, serving as a clear control. This straightforward study directly addresses the ongoing debate regarding the potential for Zn(II)-amide binding, clarifying that such binding is not likely for these peptides.

The research on amide deprotonation and binding induced by metal ions has been published in the paper "S. Leveraro, V. Dzyhovskyi, K. Garstka, A. Szebesczyk, F. Zobi, D. Bellotti, K. Stokowa-Sołtys, M. Remelli, M. Rowińska-Żyrek, *Inorganic Chemistry* **2025,** *64* (13), 6751-6760".

## 3.5. References


[1] Kozłowski, H., Kowalik-Jankowska, T. & Jeżowska-Bojczuk, M., *Coordination Chemistry Reviews*, **2005,** *249*, 2323-2334.
[2] Faller, P. & Hureau, C., *Dalton Transactions*, **2009**, 1080-1094.
[3] Grenács, Á. & Sóvágó, I., *J Inorg Biochem*, **2014,** *139*, 49-56.
[4] Zawisza, I., Rózga, M. & Bal, W., *Coordination Chemistry Reviews*, **2012,** *256*, 2297-2307.
[5] Bellotti, D., Rowińska-Żyrek, M. & Remelli, M., *Dalton Transactions*, **2020,** *49*, 9393-9403.
[6] Garstka, K., Dzyhovskyi, V., Wątły, J., Stokowa-Sołtys, K., Świątek-Kozłowska, J., Kozłowski, H., Barceló-Oliver, M., Bellotti, D. & Rowińska-Żyrek, M., *Molecules*, **2023,** *28*.
[7] Dzyhovskyi, V. & Stokowa-Sołtys, K., *Journal of Inorganic Biochemistry*, **2023,** *244*, 112203.
[8] Dzyhovskyi, V., Remelli, M. & Stokowa-Sołtys, K., *Journal of Inorganic Biochemistry*, **2025,** *263*, 112769.
[9] Sigel, H. & Martin, R. B., *Chemical Reviews*, **1982,** *82*, 385-426.
[10] Farkas, E., Csapó, E., Buglyó, P., Damante, C. A. & Di Natale, G. J. I. C. A., **2009,** *362*, 753-762.
[11] Remelli, M., Brasili, D., Guerrini, R., Pontecchiani, F., Potocki, S., Rowinska-Zyrek, M., Watly, J. & Kozlowski, H., *Inorganica Chimica Acta*, **2018,** *472*, 149-156.
[12] Bellotti, D., Sinigaglia, A., Guerrini, R., Marzola, E., Rowińska-Żyrek, M. & Remelli, M., *J Inorg Biochem*, **2021,** *214*, 111304.
[13] Kozłowski, H., Bal, W., Dyba, M. & Kowalik-Jankowska, T., *Coordination Chemistry Reviews*, **1999,** *184*, 319-346.
[14] Bellotti, D., Łoboda, D., Rowińska-Żyrek, M. & Remelli, M., *New Journal of Chemistry*, **2018,** *42*, 8123-8130.
[15] Kastal, Z., Balabán, A., Vida, S., Kállay, C., Nagy, L., Várnagy, K. & Sóvágó, I. (2024) Copper(II), Nickel(II) and Zinc(II) Complexes of Peptide Fragments of Tau Protein in *Molecules*

[16] Formicka-Kozlowska, G., Kozlowska, H., Siemion, I. Z., Sobczyk, K. & Nawrocka, E., *Journal of Inorganic Biochemistry*, **1981,** *15*, 201-212.
[17] Gralka, E., Valensin, D., Porciatti, E., Gajda, C., Gaggelli, E., Valensin, G., Kamysz, W., Nadolny, R., Guerrini, R., Bacco, D., Remelli, M. & Kozlowski, H., *Dalton transactions (Cambridge, England : 2003)*, **2008**, 5207-19.
[18] Leveraro, S., Dzyhovskyi, V., Garstka, K., Szebesczyk, A., Zobi, F., Bellotti, D., Stokowa-Sołtys, K., Remelli, M. & Rowińska-Żyrek, M., *Inorganic Chemistry*, **2025,** *64*, 6751-6760.

# 4. Chapter Four: Impact of C- and N-terminal protection on calcitermin chelating properties

## 4.1 Outline of the work

Calcitermin is a 15 amino acids antimicrobial peptide (AMPs) (VAIALKAAHYHTHKE, WT) isolated from the mucosal secretions of human airways. It corresponds to the terminal domain of calgranulin C, a proinflammatory protein of the S100 family. It is of great interest due to its ability of binding metal ions such as Cu(II) and Zn(II),[1] which leads to the enhancement of its antimicrobial activity against fungi like *Candida albicans*[2] and bacteria like *Staphylococcus aureus* and *Enterococcus faecalis*, especially in the acidic environments, typical in case of inflammation.[3] The peptide metal-binding ability is mainly due to its three alternated histidine residues (His9, His11 and His13) and its free amino and carboxyl terminal groups. Its antimicrobial properties are also enhanced by its ability to adopt a helical structure within membranes and by the protonation of its histidine residues at low pH. In fact, the presence of positive charges on the peptide sequence favors the interaction with the negatively charged surface of bacterial cells.[1, 3] [4] With the aim of improving the microbicidal activity of the peptide, several strategies can be employed: (*i*) extending its half-life increasing its resistance to proteases; (*ii*) enhancing its sequestering ability towards metal micronutrients, thus hampering pathogen growth; (*iii*) modifying its structure and charge before and/or after metal interaction. An outstanding example of the latter mentioned strategy is the study of three calcitermin His-to-Ala mutants: H9A, H11A and H13A. In these mutants, a histidine residue is replaced with alanine. The change in metal coordination modes results in significant alterations to their antimicrobial properties.[3]

A primary goal of this work is to modify the peptide structure to achieve a longer half-life and lower proteolytic susceptibility while maintaining its antimicrobial properties. Several strategies to improve the stability of peptides have been explored in the last forty years.[5] To enhance resistance to exo-peptidases (enzymes that catalyze the cleavage of the terminal peptide bonds), a common strategy is to introduce chemical modifications on one or both peptide ends. Examples of such modifications include: N-acylation, C-amidation, cyclization or binding to polyethylenglycol.[6] On the other hands, to prevent degradation by endo-peptidases, the replacement of one or more amino acid residues with non-proteinogenic amino acids (that are not typically recognized by enzymes) can be employed. These can include D-amino acids,[7] N-methyl-α-amino acids,[8] β- and γ- amino acids,[9-11] α-alkylated amino acids[12] and N-substituted glycines.[13]

We decided to focus on the degradation processes carried out by exo-peptidases, introducing the amino and carboxyl terminal protections on calcitermin. [14] We introduced acetylation on amino terminus and amidation on the carboxyl terminus, yielding three derivatives: Ac-VAIALKAAHYHTHKE (L1), Ac-VAIALKAAHYHTHKE-$NH_2$ (L2) and VAIALKAAHYHTHKE-$NH_2$ (L3). The introduction of terminal protections is expected to confer higher proteolytic stability and preserve the principal metal-binding site, the –HxHxH- motif. Furthermore, studying these protected peptides the role of the terminal

groups in calcitermin antimicrobial and metal-chelating properties will be clarified. An in-depth investigation into the complex-formation equilibria of these derivatives with Zn(II) and Cu(II) ions will provide further insight into their mechanism of action.

## 4.2 Experimental procedure

Analyses performed on the above mentioned peptides follow the scheme:

- Potentiometric determination of ligand protonation and Zn(II) and Cu(II) complex-formation constants.
- Mass spectrometric analysis to evaluate ligand purity and the stoichiometry of the formed Zn(II) and Cu(II) complexes.
- Spectrophotometric (UV-Vis and CD) analyses of Cu(II) complexes.
- EPR measurements of Cu(II) complexes.
- Far-UV CD spectroscopy to investigate the structural conformations of apo-peptides, Cu(II) and Zn(II) complexes.
- Peptide stability in human plasma.

For the sake of brevity, the employed experimental conditions, instruments and materials are reported in details in D'Accolti *et al.*, 2023, [2] along with the ligand protonation constants and distribution diagrams of the ligands as a function of pH, both in the absence and in the presence of metal ions.

## 4.3 Results and discussion

All the formed Cu(II) complexes correspond to 1:1 metal/peptide stoichiometry (**Table 4.1**). L1 is the only ligand with free carboxyl terminus, and its first formed species, $[CuH_2L]^{4+}$, is likely characterized by a coordination mode ($N_{Im}$, $COO^-$). Then, the complex is rapidly substituted by the species $[CuHL]^{3+}$, where a second histidine residue is involved in the coordination sphere, giving rise to a ($2N_{Im}$, $COO^-$) complex. In the case of the two peptides presenting the C-terminal protection, L2 and L3, the stoichiometry of the first formed complexes ($[CuH_2L]^{4+}$ for L2 and $[CuH_5L]^{5+}$ for L3) suggests that two histidine residues are already deprotonated and bound to the metal center. At the most acidic pH, the protection of the C-terminus likely favors the initial formation of a 2N complex where Cu(II) ion binds two imidazole groups of the histidine side chain. Indeed, EPR spectra recorded at pH values between 4 and 5.5 show the presence of 2N complexes in solution. Increasing the pH value, the coordination proceeds with the deprotonation and binding of a third histidine residue by copper ion, leading to the formation of a ($3N_{Im}$) species, which is prevalent in solution at pH around 6 in all the studied systems. Indeed, the recorded wavelengths of maximum absorption at pH 6 ($\lambda_{max}$ = 626 nm for L1, $\lambda_{max}$ = 630 nm for L2 and $\lambda_{max}$ = 635 nm for L3) are in good agreement with the expected value of 627 nm[15] for a complex with the proposed coordination mode.

Moving to alkaline pH, two different situations can be distinguished. In case of L3, the further metal-binding step involves the free amino terminal group, while, in the case of L1 and L2, which present N-acetylation at the C-terminus, the deprotonation and binding of an amide group of the peptide backbone occurs. Spectroscopic analyses, including EPR, confirmed the formation of a 4N species, since the spectra above pH 7 show the same superhyperfine structure and the following EPR parameters: $A_{//}$=182–198; $g_{//}$=2.20–2.21; $g_{\perp}$=2.02–2.05, which agree with the expected literature values.[16] Going deeper, starting at pH 5.5, both L1 and L2 form complexes where copper ion is coordinated by three imidazole nitrogens from the histidine residues and one deprotonated amide nitrogen ($3N_{Im}$, $N^-$). The maximum absorbance at 557 nm and the emergence of strong signals in the circular dichroism (CD) spectra are in good agreement with this coordination mode. As the pH becomes more alkaline, the intensity of the CD bands increases. This indicates the binding of a second amide nitrogen, which displaces a histidine residue from the coordination sphere to form a ($2N_{Im}$, $2N^-$) species and increase the square-planar character of the corresponding complex. Under the most alkaline conditions, a third amide proton is displaced, leading to a ($N_{Im}$, $3N^-$) species. The formation of this last complex species is characterized by a shift in the wavelength of maximum absorption to 525 nm, reflecting the change in the coordination sphere (**Figure 4.1**).

While the study provides a detailed understanding of the coordination steps, the specific histidine residues and backbone amides involved in the complex formation could not be uniquely identified by the used experimental techniques.

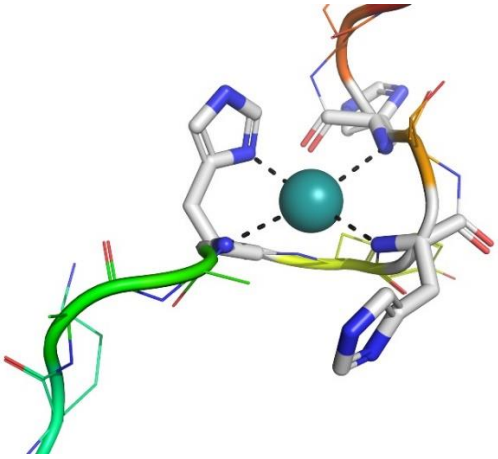

**Figure 4.1** – Coordination hypothesis ($N_{Im}$, $3N^-$) of the predominant Cu(II) complex at alkaline pH. Molecular structure is generated with Pymol. [17]

L3 is the only derivative presenting the free terminal amino group and this is reflected in a different coordination behavior. At a pH close to neutral, specifically around pH 6.5, the dominant formed Cu(II) complex is $[CuH_3L]^{3+}$. As the pH increases from 5.5 to 6.5, the UV-Vis spectra shows a shift to a shorter wavelength value (blue-shift). However, the wavelength of maximum absorption remains above 600 nm, which is not characteristic of complexes where the copper ion is bound by four nitrogen atoms in a square-planar geometry. This suggests that as the pH rises, the free terminal amino group coordinates with the copper ion, moving one of the coordinated histidine residues to the axial position. At physiological pH, the dominant copper complex in solution is $[CuH_2L]^{2+}$. The detected wavelength of maximum absorption at pH 7.5 is 553 nm, which is strikingly similar to the

expected value for two distinct coordination modes: ($3N_{Im}$, $N^-$) (557 nm) and ($2N_{Im}$, $NH_2$, $N^-$) (549 nm). [15] This suggests that both complexes can exist simultaneously in solution, or that they rapidly interconvert due to the labile nature of copper coordination bonds. As the pH increases beyond 7.5, the complex undergoes further changes. Three backbone amides are gradually deprotonated and coordinated with the copper ion, forming ($2N_{Im}$, $2N^-$) and ($N_{Im}$, $3N^-$) species. Finally, the side chains of tyrosine and two lysine residues simply release their protons at higher pH without participating in the copper coordination.

**Table 4.1** – Equilibrium constants and proposed coordination modes for Cu(II) and Zn(II) complexes at $T$ = 298 K and $I$ = 0.1 M (KCl). Values in parentheses are standard deviations on the last significant figure.

| **Species** | **logβ** | **p$K_a$** | **Coord.** | **logβ** | **p$K_a$** | **Coord.** |
|---|---|---|---|---|---|---|
| | **Ac-VAIALKAAHYHTHKE (L1)** | | | **Ac-VAIALKAAHYHTHKE-NH₂ (L2)** | | |
| $[CuH_2L]^{4+}$ | 18.21(3) | 4.40 | $N_{Im}$, $COO^-$ | 23.06(4) | 5.49 | $2N_{Im}$ |
| $[CuHL]^{3+}$ | 13.81(2) | 5.38 | $2N_{Im}$, $COO^-$ | 17.57(5) | 6.30 | $3N_{Im}$ |
| $[CuL]^{2+}$ | 8.43(2) | 6.59 | $3N_{Im}$ | 11.27(7) | 6.70 | $3N_{Im}$, $N^-$ |
| $[CuH_{-1}L]^{+}$ | 1.84(3) | 6.88 | $3N_{Im}$, $N^-$ | 4.57(6) | 9.44 | $2N_{Im}$, $2N^-$ |
| $[CuH_{-2}L]$ | -5.04(3) | - | $2N_{Im}$, $2N^-$ | -4.87(9) | 9.91 | $2N_{Im}$, $2N^-$ |
| $[CuH_{-3}L]^{-}$ | - | - | - | -14.78(7) | - | $N_{Im}$, $3N^-$ |
| | **VAIALKAAHYHTHKE-NH₂ (L3)** | | | | | |
| $[CuH_5L]^{5+}$ | 51.38(2) | 5.16 | $2N_{Im}$ | | | |
| $[CuH_4L]^{4+}$ | 46.21(2) | 6.21 | $3N_{Im}$ | | | |
| $[CuH_3L]^{3+}$ | 40.00(3) | 6.90 | $2N_{Im}$, $NH_2$ | | | |
| $[CuH_2L]^{2+}$ | 33.11(2) | 7.75 | $2N_{Im}$,$NH_2$, $N^-$ | | | |
| $[CuHL]^{+}$ | 25.36(3) | 9.53 | $2N_{Im}$, $2N^-$ | | | |
| $[CuL]$ | 15.83(5) | 10.01 | $2N_{Im}$, $2N^-$ | | | |
| $[CuH_{-1}L]^{-}$ | 5.82(4) | - | $N_{Im}$, $3N^-$ | | | |
| $[CuH_{-3}L]^{3-}$ | -15.03(9) | - | $N_{Im}$, $3N^-$ | | | |
| | **Ac-VAIALKAAHYHTHKE (L1)** | | | **Ac-VAIALKAAHYHTHKE-NH₂ (L2)** | | |
| $[ZnH_2L]^{4+}$ | - | - | - | 20.29(6) | 6.14 | $2N_{Im}$ |
| $[ZnHL]^{3+}$ | 11.00(5) | 5.80 | $2N_{Im}$ | 14.15(4) | 7.63 | $3N_{Im}$ |
| $[ZnL]^{2+}$ | 5.21(2) | 7.33 | $3N_{Im}$ | 6.52(5) | 8.93 | $3N_{Im}$, $OH^-$ |
| $[ZnH_{-1}L]^{+}$ | -2.12(3) | - | $3N_{Im}$, $OH^-$ | -2.41(7) | 9.44 | $3N_{Im}$, $2OH^-$ |
| $[ZnH_{-2}L]$ | - | - | - | -11.85(3) | - | $3N_{Im}$, $2OH^-$ |
| | **VAIALKAAHYHTHKE-NH₂ (L3)** | | | | | |
| $[ZnH_5L]^{5+}$ | 48.7(1) | 5.6 | $2N_{Im}$ | | | |

| | | | |
|---|---|---|---|
| $[ZnH_4L]^{4+}$ | 43.07(3) | 7.32 | $3N_{Im}$ |
| $[ZnH_3L]^{3+}$ | 35.75(6) | 7.69 | $3N_{Im}$, $OH^-$ |
| $[ZnH_2L]^{2+}$ | 28.06(4) | 8.65 | $3N_{Im}$, $OH^-$ |
| $[ZnHL]^{+}$ | 19.40(5) | 9.47 | $3N_{Im}$, $2OH^-$ |
| [ZnL] | 9.94(4) | - | $3N_{Im}$, $2OH^-$ |
| $[ZnH_{-2}L]^{2-}$ | -10.70(7) | - | $3N_{Im}$, $2OH^-$ |

Also the coordination of Zn(II) ion leads to the formation of only mononuclear complexes (**Table 4.1**). Starting from the most acidic pH values, the first formed species involves the coordination of two imidazole nitrogens from histidine residues. The geometry of this complex is likely tetrahedral. [18] In the case of L1 derivative, it is also possible the binding of the terminal carboxyl group of the glutamic acid residue, replacing a water molecule in the coordination sphere. As the pH increases, the deprotonation and coordination of a third histidine residue occurs, with a p$K_a$ values between 5.6 and 6.14, leading to the formation of a ($3N_{Im}$) species (**Figure 4.2**). Subsequently, a proton is released by one of the coordinated water molecules, with a p$K_a$ value ranging from 7.3 to 7.6. At higher pH, the coordination patterns for the acetylated derivatives (L1 and L2) are similar. The zinc complexes likely remain tetrahedral, with either two or three coordinated histidines and water molecules filling the remaining coordination sites. The only difference consists of the observance of the deprotonation of the tyrosine residue, in case of L2 derivative, which does not participate in the coordination. This step was not detected in case of L1 peptide. Instead, in case of L3 derivative, we observed the mere deprotonation of four basic sites of the ligand, in the order: the terminal amino group ($pK_a = 7.69$), the tyrosine ($pK_a = 9.47$) and the two lysine residues. Finally, at very alkaline pH (above pH 9), the amidated peptides L2 and L3 show evidence of a second coordinated water molecule releasing a proton. This suggests a change in geometry to a trigonal bipyramidal complex.

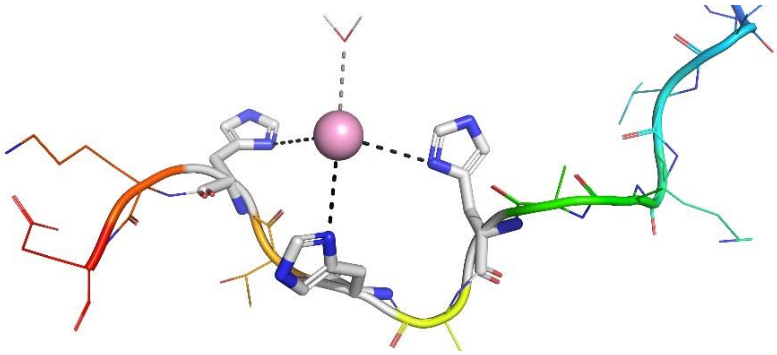

**Figure 4.2** - Coordination hypothesis for the ($3N_{Im}$) $Zn^{2+}$ complexes. Molecular structure generated with PyMol.[17]

In order to compare the metal binding affinity of different peptides towards the studied metal ions, we can build up some competition plots (**Figure 4.3**). While these graphs provide only a qualitative comparison, they are useful for evaluating the overall capacity of these peptides to coordinate with Cu(II) and Zn(II) ions. These diagrams help assess the stability of the

formed complexes across the entire pH range, regardless of their specific stoichiometry or structure.

For copper, WT calcitermin shows the strongest binding ability above pH 4.5. This enhanced stability can be attributed to the presence of both the free terminal amino and carboxyl groups, which provide a greater number of potential donor sites. Under acidic conditions, the chelating ability of WT and L1 (N-acetylated) is comparable, thus suggesting a role for the free carboxyl terminus as first copper anchoring site. The protected derivatives have comparable copper-binding abilities above pH 5, as their coordination behavior is very similar, involving the progressive binding of three histidine residues, followed by the terminal amino group (in L2) and backbone amides.

In case of Zn(II), WT calcitermin is consistently a slightly better ligand than its protected counterparts across the entire pH range. The protected peptides behave similarly up to pH 6. However, above the mentioned pH, the N-acetylated peptide (L1) shows greater stability than L2 and L3. This suggests that the terminal amino group is not essential for zinc complexation. The C-terminal carboxyl group appears to be important for stabilizing the zinc complexes, indicating that the terminal carboxyl group of the glutamic acid participates in the coordination.

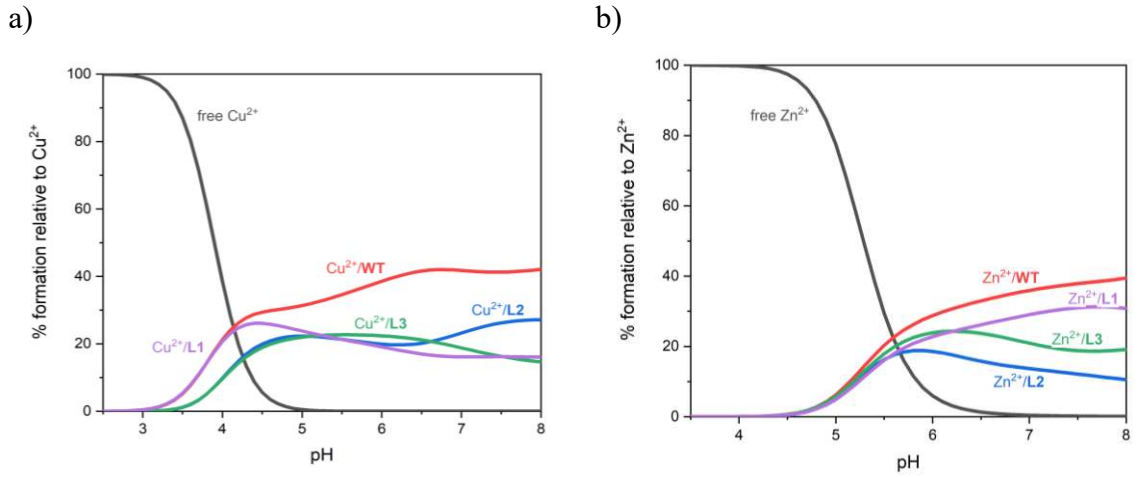


**Figure 4.3 –** Competition plots for a solution containing equimolar concentrations ($1 \cdot 10^{-3}$ M) of metal ion, WT calcitermin, L1, L2 and L3. (a) Cu(II); (b) Zn(II).

Finally, we evaluated the influence of the introduction of terminal protections on the peptide stability in human plasma. The stability of the three derivatives has been compared to the susceptibility of wild-type calcitermin (WT) (**Figure 4.4a**). The concentration of all the peptides decreases with an approximately exponential decay, and the half-lives ($t_{1/2}$) of the peptides are the following: WT 18 min, L1 135 min, L2 68 min and L3 20 min. The degradation profile of L3 is comparable to the one of WT calcitermin. Instead, the acetylated peptides L1 and L2, show an enhanced resistance to degradation, with L1 showing a half-life higher than two hours. These results highlight that the introduction of the N-terminus protection is an efficient method to increase the resistance to proteolytic degradation of antimicrobial peptides.[6] On the contrary, the C-terminus amidation does not seem to affect the resistance of peptides in human plasma. Therefore, we can suggest that the main

contribution to peptide degradation is due to aminopeptidases or dipeptidylaminopeptidases acting on the N-terminus.

The effect of metal complex formation on the peptide stability has been evaluated for WT and L1 (**Figures 4.4b and 4.4c**). The complexation of Cu(II) and Zn(II) increases the half-life of WT from 18 min to about 33 min, while the half-life increased from 135 min to ≈ 150 min (Zn(II)) or ≈ 160 min (Cu(II)) in the case of L1. This suggests that metal coordination is a promising strategy for improving peptide stability in biological fluids.

a)

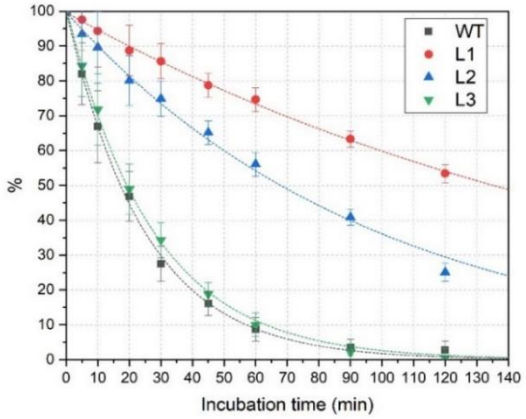


b)

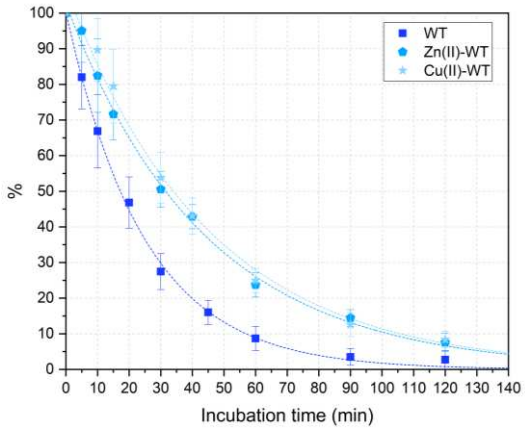


c)

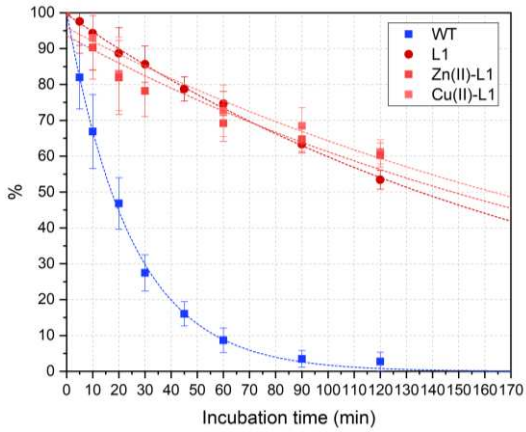


**Figure 4.4** – (a) Stability of wild-type calcitermin (WT) and its derivatives (L1, L2 and L3) in human plasma; (b) Stability in human plasma of wild-type calcitermin and its Zn(II) and Cu(II) complexes; (c) Stability in human plasma of wild-type calcitermin WT, its N-terminal protected analogue L1 and the Zn(II) and Cu(II) complexes with L1.

All compounds were tested for their antimicrobial activity against *Candida albicans*, *Staphylococcus aureus* and *Escherichia coli*, respectively representative of human pathogens of fungal and bacterial origin. Each peptide has been tested alone and in presence of $CuCl_2$ or $ZnCl_2$ and what emerged is the strong antifungal effect of $ZnCl_2$ alone and the significant role it plays in enhancing the peptide activity, whereas $CuCl_2$ has a limited effect.

WT calcitermin showed remarkable antifungal activity on its own, significantly reducing yeast colonies of *C. albicans* within just three hours. The addition of $ZnCl_2$ dramatically boosted WT antifungal effect, leading to a significant 96% reduction in yeast colonies after 24 hours. On the other hand, the Cu(II) complexes with WT did not show any significant reduction in yeast colonies. Tests on both L1 (N-acetylated) and L3 (C-amidated) showed limited antifungal activity on their own, while it is significantly enhanced by the addition of $ZnCl_2$, mirroring the powerful synergy seen with WT. Both derivatives in addition of $ZnCl_2$ achieved substantial reductions of 88% and 76% respectively after 24 hours. L1 and L3 showed only a modest increase in antifungal activity when combined with $CuCl_2$.The most promising results have been obtained with the L2 derivative (N- and C-terminal protections). The combination of the peptide with $ZnCl_2$ is highly effective, resulting in a 97% reduction after 24 hours. This is comparable with of WT in the presence of $ZnCl_2$.

Tests conducted on *E.coli* show that WT calcitermin presented antimicrobial activity primarily when combined with either zinc or copper. At 3 hours, both metal complexes caused a significant dose-dependent reduction in bacterial colonies. As for the protected derivatives, L1, is the only derivative that show significant anti-*E. coli* activity on its own, even without added metals, particularly at 3 hours. Its activity is enhanced by the presence of both zinc and copper. This derivative also shows sustained activity at 24 hours when combined with copper. This prolonged effect is possibly linked to its higher resistance to proteolytic enzymes. On the other hand, both L2 and L3 are essentially inactive on their own. Their activity is observed only in the presence of zinc or copper, but it is limited to the three hours. After 24 hours, there is no significant CFU reduction.

Lastly, the peptides have been tested against *S. aureus* and the results show that WT calcitermin, L1 and L2 do not present activity on their own. Their antibacterial action is only observed at the highest concentration (0.128 mg/ml) in the presence of zinc, resulting in a reduction around 50%. None of them shows any significant activity in the presence of copper. Different results have been obtained for the L3 derivative, which is the only one showing significant antibacterial activity on its own, even without added metals. Its effectiveness increased with concentration, reaching a 49% reduction at 0.128 mg/ml. The addition of zinc boosted its activity leading to a 73% reduction at the highest concentration. Furthermore, it is also the only derivative showing a detectable effect with copper, achieving a 47% reduction at 0.128 mg/ml.

## 4.4 Conclusions

The primary aim of this work was to enhance calcitermin resistance against proteolytic degradation and examining how these modifications affect its chemical and biological properties. Among several strategies that can be employed, the introduction of peptide amino and/or carboxyl terminal protection has been adopted. Three different derivatives have been investigated: the first presenting only the acetylation (L1), the second presenting both the terminal protections (L2) and the third presenting only the amidation (L3). What emerged from the coordination chemistry of these three derivatives is that the free amino and carboxyl termini in the native peptide WT provide a secondary contribution to coordination, resulting in the most stable metal complexes compared to the modified derivatives. Conversely, the

studies conducted in human plasma demonstrated that the introduction of terminal protections is a highly effective approach to enhance calcitermin resistance to proteolytic enzymes. In particular, the acetylation of the N-terminus results in a much longer half-life, which is a critical understanding for the development of peptide-based drugs with a prolonged duration of action.

Finally, while the derivatives themselves showed limited direct antimicrobial activity, their metal-complexes proved to be promising, especially in combination with zinc.

This research work includes the publication " M. D'Accolti, D. Bellotti, E. Dzień, C. Leonetti, S. Leveraro, V. Albanese, E. Marzola, R. Guerrini, E. Caselli, M. Rowińska-Żyrek, M. Remelli, *Scientific Reports* 2023, 13(1), 18228".

## 4.5 References


[1] Cole, A. M., Kim, Y. H., Tahk, S., Hong, T., Weis, P., Waring, A. J. & Ganz, T., *FEBS letters*, **2001,** *504*, 5-10.

[2] D'Accolti, M., Bellotti, D., Dzień, E., Leonetti, C., Leveraro, S., Albanese, V., Marzola, E., Guerrini, R., Caselli, E., Rowińska-Żyrek, M. & Remelli, M., *Scientific Reports*, **2023,** *13*, 18228.

[3] Bellotti, D., Toniolo, M., Dudek, D., Mikołajczyk, A., Guerrini, R., Matera-Witkiewicz, A., Remelli, M. & Rowińska-Żyrek, M., *Dalton Transactions*, **2019,** *48*, 13740-13752.

[4] Bellotti, D., D'Accolti, M., Pula, W., Huang, N., Simeliere, F., Caselli, E., Esposito, E. & Remelli, M., *Gels (Basel, Switzerland)*, **2023,** *9*.

[5] Lenci, E. & Trabocchi, A. J. C. S. R., **2020,** *49*, 3262-3277.

[6] Bellotti, D. & Remelli, M. (2022) Lights and Shadows on the Therapeutic Use of Antimicrobial Peptides in *Molecules*

[7] Mutter, M. & Tuchscherer, G., *Cellular and Molecular Life Sciences CMLS*, **1997,** *53*, 851-863.

[8] Sandberg, B. E. B., Lee, C.-M., Hanley, M. R. & Iversen, L. L., *European Journal of Biochemistry*, **1981,** *114*, 329-337.

[9] Porter, E. A., Weisblum, B. & Gellman, S. H., *Journal of the American Chemical Society*, **2002,** *124*, 7324-7330.

[10] Cabrele, C., Martinek, T. A., Reiser, O. & Berlicki, Ł., *Journal of Medicinal Chemistry*, **2014,** *57*, 9718-9739.

[11] Robinson, J. A., **2019,** *Volume 7 - 2019*.

[12] Degenkolb, T. & Brückner, H., *Chemistry & Biodiversity*, **2008,** *5*, 1817-1843.

[13] Dancs, Á., May, N. V., Selmeczi, K., Darula, Z., Szorcsik, A., Matyuska, F., Páli, T. & Gajda, T., *New Journal of Chemistry*, **2017,** *41*, 808-823.

[14] Jois, S. D. (2022) *Peptide Therapeutics : Fundamentals of Design, Development, and Delivery*, 1st ed. 2022. edn, Springer International Publishing, Cham.

[15] Sigel, H. & Martin, R. B., *Chemical Reviews*, **1982,** *82*, 385-426.

[16] Peisach, J. & Blumberg, W. E., *Arch Biochem Biophys*, **1974,** *165*, 691-708.

[17] The PyMOL Molecular Graphics System, V. r. p., Schrödinger, LLC.

[18] Alberts, I. L., Nadassy, K. & Wodak, S. J., *Protein science : a publication of the Protein Society*, **1998,** *7*, 1700-16.

# 5. Chapter Five: Study of the metal-binding site of the antimicrobial peptide calcitermin

## 5.1 Outline of the work

After conducting a comprehensive analysis of the terminal protections' impact on the thermodynamic, spectroscopic and antimicrobial properties of calcitermin, we decided to focus our attention on the metal-binding domain of the peptide calcitermin, represented by the three alternated histidine residues -HYHTH-. We designed the calcitermin variant truncated between position 7 and 8 (VAIALKAAHYHTHKE) and protected the fragment at both terminal ends Ac-AHYHTHKE-$NH_2$ (WT(8-15)). The aim of this investigation is to determine if the metal-binding region alone is sufficient to form copper and zinc metal complexes presenting antimicrobial activity. This fragment, protected at both ends, excludes the more lipophilic portion of the original peptide, focusing the study on the core coordination site.

## 5.2 Experimental procedure

Analyses performed on the above mentioned peptide follow the scheme:

- Peptide synthesis by means of solid-phase technique.
- Potentiometric determination of ligand protonation and Zn(II) and Cu(II) complex-formation constants.
- Mass spectrometric analysis to evaluate ligand purity and the stoichiometry of the formed Zn(II) and Cu(II) complexes.
- Spectrophotometric (UV-Vis) analyses of the Cu(II) complexes.

The employed experimental conditions, instruments and materials are reported in details in Leveraro *et al.*, 2024.[1]

## 5.3 Results and discussion

Analogously to previous discussed systems (see Chapter 3 and 4), by means of titrimetric and spectrophotometric techniques the speciation model for the studied fragment has been obtained: the complex-formation constants are reported in **Table 5.1** together with the most probable coordination environment for the formed species.

**Table 5.1 –** Equilibrium constants and proposed coordination modes for Cu(II) and Zn(II) complexes at $T$ = 298 K and $I$ = 0.1 M (KCl). Values in parentheses are standard deviations on the last significant figure.

| Species | logβ | p$K_a$ | Coord. |
|---|---|---|---|
| | **WT(8-15)** | | |
| $[CuH_3L]^{3+}$ | 32.96(3) | 5.07 | $2N_{Im}$ |
| $[CuH_2L]^{2+}$ | 27.89(3) | 6.27 | $3N_{Im}$ |
| $[CuHL]^{+}$ | 21.62(5) | 6.55 | $3N_{Im}$, $N^-$ |
| [CuL] | 15.07(4) | 9.31 | $2N_{Im}$, $2N^-$ |
| $[CuH_{-1}L]^{-}$ | 5.77(6) | 10.45 | $2N_{Im}$, $2N^-$ |
| $[CuH_{-2}L]^{2-}$ | -4.68(6) | 10.78 | $N_{Im}$, $3N^-$ |
| $[CuH_{-3}L]^{3-}$ | -15.46(7) | - | $N_{Im}$, $3N^-$ |
| | **WT(8-15)** | | |
| $[ZnH_2L]^{2+}$ | 24.88(3) | 7.43 | $3N_{Im}$, $COO^-$ |
| $[ZnHL]^{+}$ | 17.45(5) | 8.24 | $3N_{Im}$, $OH^-$ |
| [ZnL] | 9.20(5) | 9.74 | $2N_{Im}$, $2OH^-$ |
| $[ZnH_{-1}L]^{-}$ | -0.53(6) | 10.76 | $2N_{Im}$, $2OH^-$ |
| $[ZnH_{-2}L]^{2-}$ | -11.29(7) | - | $2N_{Im}$, $2OH^-$ |

As already discussed in the previous chapters, both the equilibrium constants and the spectroscopic data from UV-Vis and CD measurements can help defining the most probable coordination mode for the Cu(II) ion. The observed wavelength of maximum absorption at a given pH value (corresponding to the conditions at which a selected species reaches its maximum of formation in solution) can be compared with the expected $\lambda_{max}$ value obtained from literature.[2-4] From UV-Vis spectra of the fragment (**Figure 5.1**), it is possible to clearly distinguish the gradual shift of the $\lambda_{max}$ value towards higher energies (blue-shift) with the increase of the pH. This trend agrees with the hypothesis that, moving to alkaline conditions, a general increase of the number of coordinated nitrogen atoms is observed. The acidic residue (Glu) present in the fragment sequence may also participate in the coordination at acidic pH, however in the employed experimental techniques leave this point questionable. As a general trend, Cu(II) coordination occurs with the progressive binding of the available histidine residues, followed by the deprotonation and coordination of three backbone N-amides, which gradually substitute the donor groups in the equatorial plane of Cu(II) complexes (**Table 5.1**). A comparison between the obtained thermodynamic constants for copper complexes and for ligand protonation, together with the absence of changes in the UV-Vis absorption at specific pH values, suggest that the oxygen of tyrosine and the nitrogen of the lysine amino group in lateral chain do not participate in the metal complexation with the peptide.

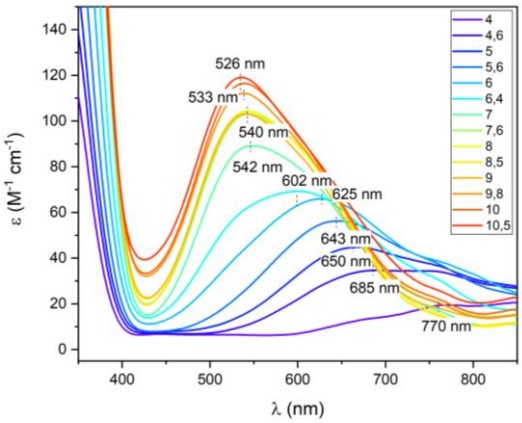


**Figure 5.1** – Vis absorption spectra of Cu(II)/Ac-AHYHTHKE-$NH_2$ system; M:L ratio = 0.8:1; $C_M = 0.4 \cdot 10^{-3}$ M, optical path 1 cm.

In the case of zinc complexes, a tetrahedral coordination geometry is expected where up to three imidazole nitrogens, belonging to the His residues, participate in the complexation forming (3Nim, O) species, where the oxygen atom may be a carboxylic O- or may belong to a coordinated water molecule. The coordination steps correspond to the release of a proton from two coordinated water molecules and after that from tyrosine and lysine residues, with tyrosine and lysine not being involved in the coordination sphere.

The competition diagrams in **Figure 5.2** allow us to compare the metal binding ability of the fragment WT(8-15) with wild-type calcitermin[5] and its terminal protected analogue, Ac-VAIALKAAHYHTHKE-$NH_2$ (see previous chapter);[5] these competition plots give information on the possible contribution of residues 1–7 in the stabilization of metal complexes, even if they are not directly involved in coordination. Furthermore, the comparison allows us to evaluate the impact of the amino- and carboxyl-terminal groups in the complexation of the metal ion. In the case of copper, in the whole pH range, wild-type calcitermin presents the best metal binding affinity. This behavior can be explained by the presence of the free terminal groups, in particular the terminal amino group, which are available as donor groups able to coordinate the metal ion. The competition diagram shows that the short fragment WT(8-15) coordinates copper ion with less efficacy even compared to the protected calcitermin (Ac-VAIALKAAHYHTHKE-$NH_2$), although the proposed coordination modes are the same for both the systems. This behavior opens the way to the hypothesis (which would require support from quantum mechanical calculations and molecular dynamics studies) that the N-terminal hydrophobic domain of calcitermin contributes to the stability of the complexes, protecting the metal from solvent interference, for example through long-range non-bonding interactions or forming a sort of "hydrophobic cage" around copper ion. In the case of zinc, wild-type calcitermin is again the best ligand, most likely due to the presence of the free carboxyl and amino terminal groups, which also confer a different net charge to the peptide. This may have an effect on the stability of the formed complexes and therefore justify the higher metal-binding affinity. The lipophilic N-terminal fragment, however, does not exert a stabilization effect as in the case of copper, since WT(8-15) is able to chelate zinc ion better than Ac-VAIALKAAHYHTHKE-$NH_2$. This is not surprising, considering that zinc is able to bind up to two solvent molecules and form stable complexes at pH higher than 7.

a) b)

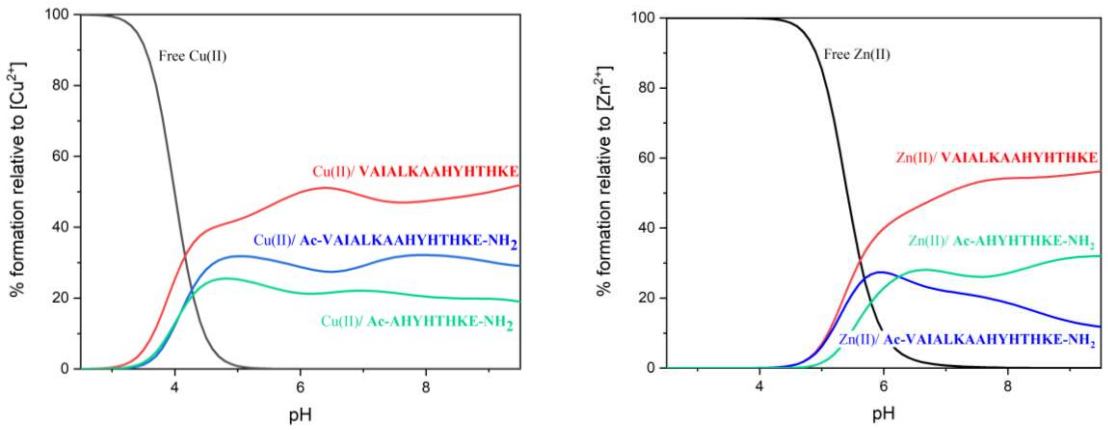


**Figure 5.2** – Competition plots for a solution containing equimolar concentrations ($1 \cdot 10^{-3}$ M) of metal ion, WT calcitermin, Ac-VAIALKAAHYHTHKE-$NH_2$ and WT(8-15). (a) Cu(II); (b) Zn(II).

Finally, the fragment has been tested for its antimicrobial activity against a representative panel of pathogenic organisms: *Staphylococcus aureus* ATCC 25923, *Staphylococcus epidermidis* KCTC 1917, *Enterococcus faecalis* ATCC 29212, *Pseudomonas aeruginosa* ATCC 15422, *Escherichia coli* ATCC 25922, *Klebsiella rhinoscleromatis* 13884, *Klebsiella pneumoniae* 13882, *Proteus mirabilis* ATCC 21100, *Candida albicans* 10231. The minimal inhibitory concentration (MIC) has been determined for free ligand and metal complexes at pH 5.4 (**Table 5.2**). Comparing the antimicrobial results with those of WT calcitermin, the first observation is that the WT(8-15) fragment shows activity against *E. faecalis* and *P. aeruginosa*, not observed for WT. In particular, the metal complexes exhibit an enhanced capacity to kill these bacteria with respect to the free peptide. Furthermore, the WT(8-15)-Zn(II) complexes were particularly effective against *K. rhinoscleromatis,* with a very low inhibitory concentration, MIC= 8 μg/ml. It also proved to be the best antimicrobial agent against *S. epidermidis*, especially when complexed with metal ions.

**Table 5.2** – *In vitro* antimicrobial activity expressed as minimal inhibitory concentration (MIC) at pH=5.4. MIC [μg/ml]. For *E.coli* ATCC 25922, no MIC was determined for peptide and its metal complexes at the maximum concentration tested. The results represent the averages of triplicate experiments ± SD.

| **Strain** | **WT(8-15)** | | | **WT** | | |
|---|---|---|---|---|---|---|
| | **L** | **$LZn^{2+}$** | **$LCu^{2+}$** | **L** | **$LZn^{2+}$** | **$LCu^{2+}$** |
| *S. aureus* ATCC 25923 | >256 | >256 | >256 | 128±4 | >256 | 128±4 |
| *S. epidermidis* KCTC 1917 | 32±1 | 16±1 | 8±2 | >256 | 256±2 | 256±2 |
| *E. faecalis* ATCC 29212 | >256 | 128±2 | 128±2 | >256 | >256 | >256 |
| *P. aeruginosa* ATCC 15422 | >256 | 128±3 | 256±3 | >256 | >256 | >256 |
| *K. rhinoscleromatis* ATCC 13884 | 16±1 | 8±1 | 32±2 | 128±2 | 256±4 | 128±4 |
| *K. pneumoniae* ATCC 13882 | >256 | >256 | >256 | 128±2 | >256 | >256 |
| *K. ozaenae* ATCC 11298 | 128±2 | >256 | 32±3 | 256±3 | >256 | 128±2 |
| *P. mirabilis* ATCC 21100 | >256 | >256 | >256 | >256 | >256 | >256 |
| *C. albicans* ATCC 10231 | >256 | 256±4 | 128±4 | >256 | 4±1 | 4±1 |

## 5.4 Conclusions

The studied fragment of calcitermin, Ac-AHYHTHKE-$NH_2$, corresponding to the metal binding site with the addition of terminal protections, has be synthetized and studied in order to evaluate if the sequence alone is able to form metal complexes with antimicrobial activity. The study began with the determination of the thermodynamic constants of the ligand, proceeding with the determination of the formation constants of copper and zinc complexes. Comparing the coordination mode of the species formed by the fragment with those obtained by wild type calcitermin,[5] it is possible to affirm that both peptides lead to the formation of metal complexes with the same coordination mode. Subsequently, the bioactivity of the fragment WT(8-15) was investigated to determine its antimicrobial potential. The results show that WT(8-15) exhibits better antimicrobial activity against two specific bacteria than calcitermin wild type: *S. epidermidis* MIC = 32 μg/ml for the fragment alone; MIC = 16 μg/ml for Zn(II)-WT(8-15) and MIC = 8 μg/ml for Cu(II)- WT(8-15); *K. rhinoscleromatis* MIC = 16 μg/ml for the fragment alone; MIC = 8 μg/ml for Zn(II)-WT(8-15) and MIC = 32 μg/ml for Cu(II)- WT(8-15). These findings suggest that the lipophilic portion of calcitermin is not strictly essential for its antimicrobial activity. Instead, the interaction with metal ions appears to be crucial for the peptide microbicidal activity, opening the door for future peptide design aimed at enhancing proteolytic stability.

This research work includes the publication "S. Leveraro, K. Garstka, P. Śliwka, T. Janek, M. Rowińska-Żyrek, M. Remelli, D. Bellotti, *Dalton Trans.* 2024, 53,12676-12687".

## 5.5 References


[1] Leveraro, S., Garstka, K., Śliwka, P., Janek, T., Rowińska-Żyrek, M., Remelli, M. & Bellotti, D., *Dalton Transactions*, **2024**.

[2] Prenesti, E., Daniele, P. G., Prencipe, M. & Ostacoli, G., *Polyhedron*, **1999,** *18*, 3233-3241.

[3] Daniele, P. G., Prenesti, E. & Ostacoli, G., *Journal of the Chemical Society, Dalton Transactions*, **1996**, 3269-3275.

[4] Sigel, H. & Martin, R. B., *Chemical Reviews*, **1982,** *82*, 385-426.

[5] D'Accolti, M., Bellotti, D., Dzień, E., Leonetti, C., Leveraro, S., Albanese, V., Marzola, E., Guerrini, R., Caselli, E., Rowińska-Żyrek, M. & Remelli, M., *Scientific Reports*, **2023,** *13*, 18228.

# 6. Chapter Six: Calcitermin derivatives containing serine residues

## 6.1 Outline of the work

As already mentioned in Chapter 1.2.2, antimicrobial peptides present some drawbacks as decrease of biological activity *in vivo*, limited bioavailability, high susceptibility to proteases and therefore short half-lives. Hence, a systematic study has been conducted on the peptide calcitermin in order to design and develop derivatives with improved properties. The study investigated how specific modifications affects the peptide stability in plasma, its metal coordination and its antimicrobial activity. Based on studies present in literature, [1-3] we have replaced one or two alanine residues at position 7 and/or 8 with serine residues. The presence of serine near the histidine anchoring site should favour the binding of backbone N-amides by copper ion, affecting the metal peptide coordination and antimicrobial activity.[4-7] The three obtained derivatives are: VAIALKSAHYHTHKE (A7S), VAIALKASHYHTHKE (A8S) and VAIALKSSHYHTHKE (A7S/A8S).

## 6.2 Experimental procedure

Analyses performed on the above mentioned peptides follow the scheme:

- Peptide synthesis by means of solid-phase technique.
- Potentiometric determination of ligand protonation and Zn(II) and Cu(II) complex-formation constants.
- Mass spectrometric analysis to evaluate ligand purity and the stoichiometry of the formed Zn(II) and Cu(II) complexes.
- Spectrophotometric (UV-Vis and CD) analyses of the Cu(II) complexes.
- EPR measurements of the Cu(II) complexes.
- Far-UV CD spectroscopy to investigate the structural conformations of apo-peptides, Cu(II) and Zn(II) complexes.
- Peptide stability in human plasma.

The employed experimental conditions, instruments and materials are reported in details in Leveraro *et al.*, 2024.[8]

## 6.3 Results and discussion

The investigated peptides proved to be able to form stable 1:1 complexes with Zn(II) and Cu(II); no poly-nuclear or bis-complexes have been detected either by potentiometry, mass spectrometry or EPR in the case of copper. In all the systems the Cu(II) coordination begins at about pH 3-3.5. The two derivatives A7S and A8S behave in a very similar way, while A7S/A8S presents only small differences. The coordination starts with the binding of

histidine residues (1 or 2 $N_{Im}$) and one of the carboxyl groups of the C-terminal glutamic acid. It follows the coordination of a third histidine residue ($3N_{Im}$), and the binding of a first backbone amide which substitutes one histidine residue in the equatorial plane of Cu(II) complex. Subsequently, the coordination follows with the binding of the free amino terminal group, forming a 4N complex. Afterward, it occurs the coordination of a second amide nitrogen, which most likely replaces the amine group in the equatorial plane of the complex. At this point, the coordination of the A7S and A8S derivatives involves a third amide of the peptide backbone. This does not seem to occur with the A7S/A8S derivative, which is able to coordinate only up to two amides at very alkaline pH values (**Table 6.1**). A comparison between the obtained thermodynamic constants for copper complexes and for ligands protonation, together with the absence of changes in the Vis absorption and CD spectra at alkaline pH values, suggest that the tyrosyl-$O^-$, and the two lysil ε-$NH_2$ groups do not participate in the metal complexation with all the investigated peptides. Spectroscopic data are in good agreement with the proposed speciation models; in fact, with the increase of pH, a blue-shift of Vis spectra is observed (**Figure 6.1a**), suggesting the increase of the number of coordinated nitrogen atoms. Considering the A8S system as an example, the wavelength of maximum absorption shifts from 737 nm at pH 4.0, corresponding to the $[Cu(H_2O_2)_6]^{2+}$ species, to 625 nm at pH 6.1, corresponding to the $[CuH_4L]^{3+}$ complex, which reaches almost 55% of formation. The reached $\lambda_{max}$ value supports the hypothesis of a ($3N_{Im}$) coordination (expected $\lambda_{max}$ = 625 nm)[9] with a distorted octahedral geometry. Moving to alkaline conditions, the wavelengths shift continues due to the formation of 4N complexes with all the studied peptides. Under physiological and alkaline conditions, the binding of a larger number of N-amides is also confirmed by the increased intensity of the CD signals (**Figure 6.1b**).[10]

a)

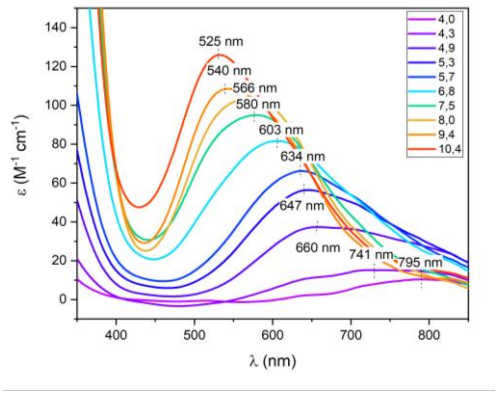


b)

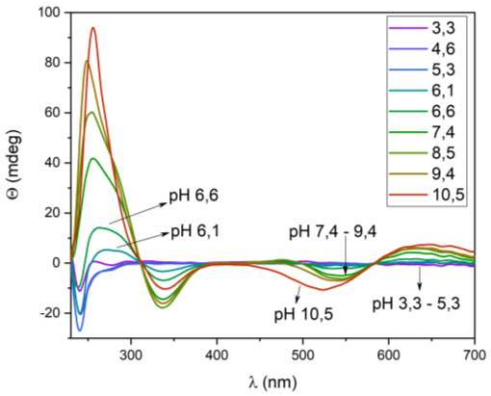

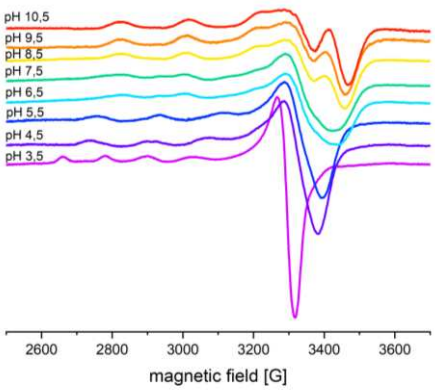


c)

**Figure 6.1** – (a) Vis absorption spectra, (b) CD spectra of Cu(II)/A8S system; M:L ratio = 0.8:1; $C_M = 0.4 \cdot 10^{-3}$ M, optical path 1 cm; (c) X-band EPR spectra of frozen solution (77K) of Cu(II)/A8S system; M:L ratio = 0.8:1; $C_M = 1.00 \cdot 10^{-3}$ M.

**Table 6.1** – Equilibrium constants and proposed coordination modes for Cu(II) and Zn(II) complexes at *T*= 298 K and *I*= 0.1 M (KCl). Values in parentheses are standard deviations on the last significant figure.

| **Species** | **logβ** | **p*K*a** | **Coord.** | **logβ** | **p*K*a** | **Coord.** |
|---|---|---|---|---|---|---|
| | **A7S** | | | **A8S** | | |
| $[CuH_6L]^{5+}$ | 55.3(1) | 4.00 | $N_{Im}$, $COO^-$ | 55.4(1) | 4.4 | $N_{Im}$, $COO^-$ |
| $[CuH_5L]^{4+}$ | 51.27(4) | 5.02 | $2N_{Im}$, $COO^-$ | 51.04(6) | 4.84 | $2N_{Im}$, $COO^-$ |
| $[CuH_4L]^{3+}$ | 46.25(4) | 6.13 | $3N_{Im}$ | 46.19(5) | 5.98 | $3N_{Im}$ |
| $[CuH_3L]^{2+}$ | 40.12(5) | 7.05 | $2N_{Im}$, $N^-$ | 40.21(6) | 7.02 | $2N_{Im}$, $N^-$ |
| $[CuH_2L]^{+}$ | 33.07(6) | 7.45 | $2N_{Im}$,$N^-$,$NH_2$ | 33.19(8) | 7.36 | $2N_{Im}$,$N^-$, $NH_2$ |
| [CuHL] | 25.62(5) | 9.33 | $2N_{Im}$, $2N^-$ | 25.83(7) | 9.16 | $2N_{Im}$, $2N^-$ |
| $[CuL]^-$ | 16.29(8) | 9.83 | $2N_{Im}$, $2N^-$ | 16.7(1) | 9.7 | $2N_{Im}$, $2N^-$ |
| $[CuH_{-1}L]^{2-}$ | 6.46(6) | - | $N_{Im}$, $3N^-$ | 6.99(8) | - | $N_{Im}$, $3N^-$ |
| $[CuH_{-3}L]^{4-}$ | -14.80(8) | - | $N_{Im}$, $3N^-$ | -14.20(9) | - | $N_{Im}$, $3N^-$ |
| | **A7S/A8S** | | | | | |
| $[CuH_5L]^{4+}$ | 51.35(2) | 5.42 | $2N_{Im}$, $COO^-$ | | | |
| $[CuH_4L]^{3+}$ | 45.93(3) | 6.36 | $3N_{Im}$ | | | |
| $[CuH_3L]^{2+}$ | 39.57(5) | 7.17 | $2N_{Im}$, $N^-$ | | | |
| $[CuH_2L]^{+}$ | 32.40(5) | 7.83 | $2N_{Im}$,$N^-$,$NH_2$ | | | |
| [CuHL] | 24.58(6) | 9.21 | $2N_{Im}$, $2N^-$ | | | |
| $[CuL]^-$ | 15.37(7) | - | $2N_{Im}$, $2N^-$ | | | |
| $[CuH_{-2}L]^{3-}$ | -4.98(8) | - | $2N_{Im}$, $2N^-$ | | | |
| | **A7S** | | | **A8S** | | |
| $[ZnH_5L]^{4+}$ | 48.6(1) | 5.5 | $2N_{Im}$, $COO^-$ | 48.1(1) | 5.3 | $2N_{Im}$, $COO^-$ |
| $[ZnH_4L]^{3+}$ | 43.07(3) | 6.84 | $3N_{Im}$ | 42.74(4) | 7.18 | $3N_{Im}$ |
| $[ZnH_3L]^{2+}$ | 36.24(5) | 7.74 | $3N_{Im}$, $OH^-$ | 35.57(8) | 7.52 | $3N_{Im}$, $OH^-$ |
| $[ZnH_2L]^{+}$ | 28.49(5) | 8.28 | $3N_{Im}$, $2OH^-$ | 28.04(6) | 8.55 | $3N_{Im}$, $2OH^-$ |
| [ZnHL] | 20.21(5) | 9.32 | $3N_{Im}$, $2OH^-$ | 19.49(7) | 9.33 | $3N_{Im}$, $2OH^-$ |

| | | | | | | |
|---|---|---|---|---|---|---|
| $[ZnL]^-$ | 10.89(5) | - | $3N_{Im}$, $2OH^-$ | 10.16(7) | - | $3N_{Im}$, $2OH^-$ |
| $[ZnH_{-2}L]^{3-}$ | -9.57(5) | - | $3N_{Im}$, $2OH^-$ | -11.15(8) | - | $3N_{Im}$, $2OH^-$ |

| | **A7S/A8S** | | |
|---|---|---|---|
| $[ZnH_4L]^{3+}$ | 43.10(2) | 7.06 | $3N_{Im}$ |
| $[ZnH_3L]^{2+}$ | 36.04(4) | 7.64 | $3N_{Im}$, $OH^-$ |
| $[ZnH_2L]^+$ | 28.40(5) | 8.29 | $3N_{Im}$, $OH^-$ |
| [ZnHL] | 20.11(5) | 9.30 | $3N_{Im}$, $2OH^-$ |
| $[ZnL]^-$ | 10.81(4) | - | $3N_{Im}$, $2OH^-$ |
| $[ZnH_{-2}L]^{3-}$ | -9.54(5) | - | $3N_{Im}$, $2OH^-$ |

As for zinc complexes, the metal coordination is very similar with all the three ligands: Zn(II) binding occurs by means of all the available histidine residues, giving rise to tetrahedral complexes. The N-terminus, the tyrosine and the two lysine residues are not involved in complexes formation. Furthermore, approaching the physiological/alkaline pH, the deprotonation of a coordinated water molecule leads to the formation of bis-hydroxo species with all the investigated peptides (**Table 6.1**).

To better understand the capacity of the investigated peptides to stably coordinate metal ions, it is useful to compare their metal-binding ability with that of wild-type calcitermin (WT) by means of competition diagrams (**Figure 6.2**). In case of Cu(II), the chelating ability of the A8S derivative is comparable to that of WT calcitermin. Interestingly, the A8S copper complexes are more stable than those of A7S, suggesting that the effect of the serine substitution is dependent on its spatial proximity to the coordinated histidines. Whereas, in the case of A7S/A8S derivative, the plot shows that its binding ability decreases rapidly above pH 5, precisely when amides begin to coordinate the metal ion. Therefore, the presence of two consecutive serine residues appears to hinder the interaction of a third amide with Cu(II) ion, even under the most alkaline conditions. This suggests that the reduced affinity of A7S/A8S peptide for Cu(II) is primarily due to steric and/or electronic effects from the two consecutive serine residues.

A different behaviour is observed in case of Zn(II) complexes. All four peptides behave similarly up to a neutral pH. After this point, the complexes formed by the two peptides containing the A7S substitution show improved stability. This behaviour is not easily rationalized and necessitates further investigations, as the effect of Ala-to-Ser substitutions on the stability of Zn(II)-peptide complexes remains a controversial topic in the literature.[1-3]

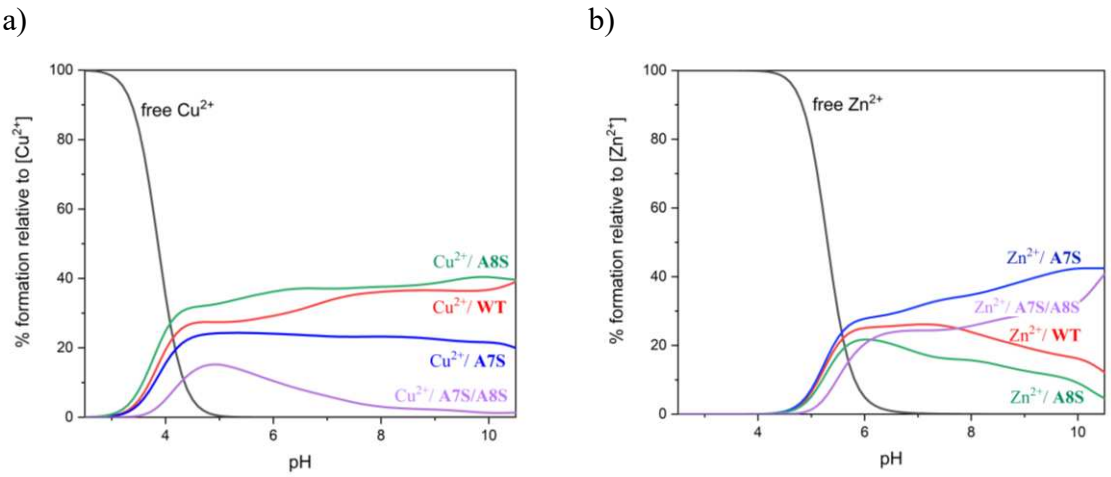


**Figure 6.2 –** Competition plots for a solution containing equimolar concentrations ($1 \cdot 10^{-3}$ M) of metal ion, WT calcitermin, A7S, A8S and A7S/A8S. (a) Cu(II); (b) Zn(II).

Subsequently, the stability of the peptide derivatives in human plasma has been investigated to determine whether specific amino acid substitutions in the peptide sequence influence their plasma stability. The stability of the three peptides has been assessed and compared to the wild-type (WT) calcitermin, which has a half-life ($t_{1/2}$) of 18 minutes.[11] The degradation profiles of the three Ala-to-Ser derivatives mirror that of the native peptide, characterized by an exponential decrease (19±4 min for A7S/A8S, 21±4 min for A7S and 22±4 min for A8S). These experimental results indicate that the substitution of alanine residue with serine residue in position 7 and/or 8 does not significantly increase calcitermin resistance to degradation in human plasma. This outcome is consistent with the known susceptibility of unmodified N-terminal L-amino acid peptides to cleavage by aminopeptidases or dipeptidyl aminopeptidases.[12] Some strategies to enhance peptide stability against proteolysis have already been investigated in the chapter four.

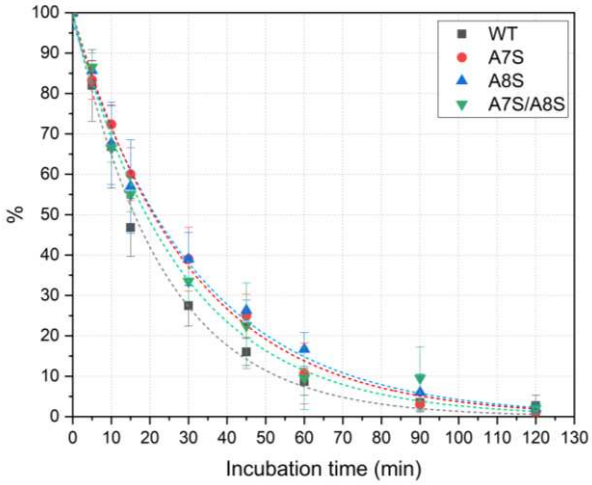


**Figure 6.3** – Stability of wild-type calcitermin (WT) and its derivatives (A7S, A8S and A7S/A8S) in human plasma.

All compounds were tested for their antimicrobial activity against a representative panel of pathogenic organisms: *Staphylococcus aureus* ATCC 25923, *Staphylococcus epidermidis* KCTC 1917, *Enterococcus faecalis* ATCC 29212, *Pseudomonas aeruginosa* ATCC 15422, *Escherichia coli* ATCC 25922, *Klebsiella rhinoscleromatis* 13884, *Klebsiella pneumoniae* 13882, *Proteus mirabilis* ATCC 21100, *Candida albicans* 10231. The minimal inhibitory concentration (MIC) has been determined for free ligand and metal complexes at pH 5.4 (**Table 6.2**). Comparing the antimicrobial results with those of WT calcitermin, the first observation is that A7S/A8S derivative shows activity against *E. faecalis* and *P. aeruginosa*, not observed for WT. In particular, the metal complex exhibits an enhanced capacity to kill these bacteria with respect to the free peptide. Furthermore, this system is the only one active against *S. aureus*. Moreover, its Cu(II) complex showed a significantly enhanced effect against *K. pneumoniae*, with a very low minimum inhibitory concentration (MIC) of 4 μg/ml. All the calcitermin derivatives and their complexes are active against *K. rhinoscleromatis*, especially in the case of A7S-Cu(II). In the case of *K. ozaenae*, activity has been observed for A8S and A7S/A8S, the latter being the best, as both free peptide and Cu(II) complexes (MIC = 4 μg/ml). Activity against *C. albicans* has been also detected: the presence of metal ions enhanced the antifungal activity of all tested peptides against the fungi. While WT showed the best overall performance, the three mutants also showed promising results. The results suggest that Ala-to-Ser substitutions near the calcitermin coordination site, -HYHTH-, may improve the interaction of the peptide with microbial cell membranes, potentially leading to cell lysis or the pore formation.

**Table 6.2**. *In vitro* antimicrobial activity expressed as minimal inhibitory concentration (MIC) at pH=5.4. MIC [μg/ml]. For *E. coli* ATCC 25922, no MIC was determined for all peptides and their metal complexes at the maximum concentration tested. The results represent the averages of triplicate experiments ± SD.

| **Strain** | **A7S** | | | **A8S** | | | **A7S/A8S** | | | **WT** | | |
|---|---|---|---|---|---|---|---|---|---|---|---|---|
| | **L** | **$LZn^{2+}$** | **$LCu^{2+}$** | **L** | **$LZn^{2+}$** | **$LCu^{2+}$** | **L** | **$LZn^{2+}$** | **$LCu^{2+}$** | **L** | **$LZn^{2+}$** | **$LCu^{2+}$** |
| *S. aureus* | >256 | >256 | >256 | >256 | >256 | >256 | 256±1 | 128±1 | 128±3 | 128±4 | >256 | 128±4 |
| *S. epidermidis* | 128±3 | 32±2 | 32±1 | 128±3 | 32±1 | 64±2 | >256 | 128±1 | 128±1 | >256 | 256±2 | 256±2 |
| *E. faecalis* | >256 | >256 | 128±2 | >256 | >256 | 128±4 | 256±2 | 128±3 | 128±2 | >256 | >256 | >256 |
| *P. aeruginosa* | >256 | >256 | >256 | >256 | >256 | >256 | >256 | 128±2 | 128±2 | >256 | >256 | >256 |
| *K. rhinoscleromatis* | 128±1 | 256±3 | 16±1 | 64±2 | 128±2 | 32±1 | 128±4 | 32±2 | 32±1 | 128±2 | 256±4 | 128±4 |
| *K. pneumoniae* | 128±2 | >256 | 256±3 | >256 | >256 | >256 | 128±3 | >256 | 4±1 | 128±2 | >256 | >256 |
| *K. ozaenae* | >256 | >256 | >256 | 32±1 | >256 | 16±1 | 4±1 | >256 | 4±1 | 256±3 | >256 | 128±2 |
| *P. mirabilis* | 32±1 | 32±1 | >256 | >256 | >256 | >256 | >256 | >256 | >256 | >256 | >256 | >256 |
| *C. albicans* | >256 | 128±1 | 128±2 | >256 | 256±4 | 256±2 | 256±4 | 256±5 | 128±1 | >256 | 4±1 | 4±1 |

Finally, the three derivatives and their copper and zinc complexes have been tested in aqueous solutions and SDS solutions by means of FAR-UV CD spectroscopy in order to investigate their structural conformation. Measurements conducted in water revealed a disordered structure for all the systems (ligands and their complexes), while they adopt a helical-like structure in the presence of membrane mimicking SDS.

## 6.4 Conclusions

The present work is a comprehensive description of the thermodynamics, structure, coordination chemistry, stability in plasma and antimicrobial activity of the studied metal-calcitermin derivatives complexes. Novel antimicrobial derivatives presenting Alanine-to-Serine substitutions are presented. First of all, the stability of the serine derivatives was tested in human plasma, highlighting no enhanced resistance to proteases, with respect to wild-type calcitermin. The comparison of the stabilities of metal complexes with the three mutants shows two interesting facts: (*i*) the presence of two consecutive serine residues (A7S/A8S) negatively impacted the thermodynamic stability of the Cu(II) complexes, particularly at alkaline pH. In fact, this peptide does not involve a third amide in the coordination sphere; (*ii*) all serine mutants showed similar affinity towards Zn(II) ion at physiological pH, while some differences emerged at lower pH for the A8S derivative which had the lowest affinity.

Considering their antimicrobial activity, their efficacy against pathogens were significantly enhanced in the presence of Zn(II) or, more notably, Cu(II) ions. This suggests a synergistic effect where the metal-peptide complex is more effective than the peptide alone. This effect was more evident for the A7S/A8S mutants and in general against the Gram-positive bacteria and the fungi *C. albicans*. While it was less evident against the Gram-negative bacteria, especially those of the *Klebsiella* species.

In conclusion, while the Ala-to-Ser substitutions did not improve the peptide stability in human plasma, they did alter its metal-binding properties, and, most importantly, significantly enhanced its antimicrobial activity in the presence of Cu(II) and Zn(II), particularly against Gram-positive bacteria.

This research work includes the publication "S. Leveraro, K. Garstka, P. Śliwka, T. Janek, M. Rowińska-Żyrek, M. Remelli, D. Bellotti, *Dalton Trans.* 2024, 53,12676-12687".

## 6.5 References


[1] Bellotti, D., Miller, A., Rowińska-Żyrek, M. & Remelli, M. (2022) Zn2+ and Cu2+ Binding to the Extramembrane Loop of Zrt2, a Zinc Transporter of Candida albicans in *Biomolecules*

[2] Bellotti, D., Tocchio, C., Guerrini, R., Rowińska-Żyrek, M. & Remelli, M., *Metallomics*, **2019,** *11*, 1988-1998.

[3] Bellotti, D., Łoboda, D., Rowińska-Żyrek, M. & Remelli, M., *New Journal of Chemistry*, **2018,** *42*, 8123-8130.

[4] Alexander, J. L., Thompson, Z. & Cowan, J. A., *ACS Chemical Biology*, **2018,** *13*, 844-853.

[5] Łoboda, D., Kozłowski, H. & Rowińska-Żyrek, M., *New Journal of Chemistry*, **2018,** *42*, 7560-7568.

[6] Wilson, M., Tillery, L., Tabaie, E., Beery, G., Preusker, J., Bhola, I. & Frato, K., *JBIC Journal of Biological Inorganic Chemistry*, **2020,** *25*, 1-12.

[7] Wezynfeld, N., Fraczyk, T. & Bal, W., *Coordination Chemistry Reviews*, **2016,** *327-328*, 166-187.

[8] Leveraro, S., Garstka, K., Śliwka, P., Janek, T., Rowińska-Żyrek, M., Remelli, M. & Bellotti, D., *Dalton Transactions*, **2024**.

[9] Sigel, H. & Martin, R. B., *Chemical Reviews*, **1982,** *82*, 385-426.

[10] Stanyon, H. F., Cong, X., Chen, Y., Shahidullah, N., Rossetti, G., Dreyer, J., Papamokos, G., Carloni, P. & Viles, J. H., *The FEBS journal*, **2014,** *281*, 3945-54.

[11] D'Accolti, M., Bellotti, D., Dzień, E., Leonetti, C., Leveraro, S., Albanese, V., Marzola, E., Guerrini, R., Caselli, E., Rowińska-Żyrek, M. & Remelli, M., *Scientific Reports*, **2023,** *13*, 18228.
[12] Powell, M. F., *Annu Rep Med Chem*, **1993,** *28*, 285-294.

# 7. Chapter Seven: Introduction of positively charged residues and their effect on the calcitermin antimicrobial activity

## 7.1 Outline of the work

Eukaryotic antimicrobial peptides (AMPs) are typically cationic and amphiphilic, possessing both lipophilic and hydrophilic regions.[1] This structure, particularly their positive charge, facilitates their initial interaction with the negatively charged bacterial membranes. This electrostatic attraction can lead to the peptide insertion into the membrane, which can results in the formation of pores or channels, leading to the pathogen death.[2] In order to enhance the antimicrobial activity of calcitermin, we adopted a strategy consisting of the increment of the number of positively charged residues, thereby strengthening the electrostatic interaction with bacterial membranes. A common and effective method for achieving this increment, it is the introduction of arginine residue into the peptide sequence.[3] This amino acid is known to play a crucial role in the membrane-permeabilization mechanism of many AMPs.[4-6] Based on this strategy, new calcitermin derivatives were developed by substituting an alanine residue with an arginine residue at either position 7 or 8. The resulting peptides are VAIALKRAHYHTHKE (A7R) and VAIALKARHYHTHKE (A8R). Additionally, a mutant has been designed where alanine at position 7 has been replaced by a histidine residue, VAIALKHAHYHTHKE (A7H). This modification not only increases the peptide positive charge under acidic conditions but also introduces a fourth potential metal-coordination site, creating the –HxHxHxHx- motif, for Cu(II) and Zn(II) ions.

These new derivatives have been studied by means of different techniques with the aim of understanding how their modified sequences affect their metal-coordination abilities, structural properties and antimicrobial activity.

## 7.2 Experimental procedure

Analyses performed on the above mentioned peptides follow the scheme:

- Peptide synthesis by means of solid-phase technique.
- Potentiometric determination of ligand protonation and Zn(II) and Cu(II) complex-formation constants.
- Mass spectrometric analysis to evaluate ligand purity and the stoichiometry of the formed Zn(II) and Cu(II) complexes.
- Spectrophotometric (UV-Vis and CD) analyses of the Cu(II) complexes.
- EPR measurements of Cu(II) complexes.
- Far-UV CD spectroscopy to investigate the structural conformations of apo-peptides, Cu(II) and Zn(II) complexes.
- Peptide stability in human plasma.
- NMR measurements of apo-peptides and Zn(II) complexes.

The employed experimental conditions, instruments and materials are reported in details in Leveraro *et al.*, 2025.[7]

## 7.3 Results and discussion

All the formed Cu(II) complexes correspond to 1:1 metal/peptide stoichiometry. The obtained thermodynamic data for the two derivatives containing arginine residues, A7R and A8R (**Table 7.1**), show very high consistency with those of wild-type calcitermin[8] and its derivatives containing serine residues described in the previews chapter.[9] Therefore, substituting alanine residues with arginines would not appear to significantly impact the thermodynamic data and coordination modes of calcitermin.

On the contrary, the substitution of one alanine residue with a histidine residue in position 7 (A7H) has influenced calcitermin thermodynamic and spectroscopic properties. As a result of the introduction of an additional histidine, the metal-binding site has been expanded, resulting into an alteration of the peptide coordination mode. At the lowest pH, the initial formed complex is $[CuH_6L]^{5+}$, this species is characterized as a 2N complex, where copper is coordinated by two histidine residues and potentially the carboxylate groups of the C-terminal glutamic acid. As the pH increases, two additional histidine residues deprotonate and coordinate with the metal, which is supported by their significantly lower $pK_a$ values compared to the free peptide. This leads to a complex with a distorted octahedral geometry, where the copper is coordinated by three histidine imidazole nitrogens in the equatorial plane of the complex and a fourth histidine in an axial position. We supposed the presence of the fourth histidine in axial position since in the UV-Vis spectra we detected a $\lambda_{max}$ = 589 nm, which presents a bathochromic deviation of +13 nm from the expected value of 576 nm.[10, 11] As the pH increases beyond 7.6, a significant blue-shift is observed in UV-Vis spectra, indicating a change in the coordination mode. This change is also present in the recorded CD spectra from pH 7.6 to 10.5 where they are characterized by a different shape. This change is attributed to the increasing square-planar character of the complex as the terminal amino group and the backbone amides begin to coordinate with the copper ion. In the pH range 8.6-9.2 (**Figure 7.1d**), where the three species are present in solution ($[CuH_3L]^{2+}$, $[CuH_2L]^{+}$ and [CuHL]), there is the detection of a broad band which can indicate the presence of isomeric species, where the donor groups mutually exchange in the copper coordination sphere. Increasing the alkalinity of the solution the deprotonation and coordination of a second backbone amide leads to the formation of species with increased square-planar character. Subsequently, the deprotonation of tyrosine, lysine and the third amide occurs, with tyrosine and lysine not involved in the complexation.

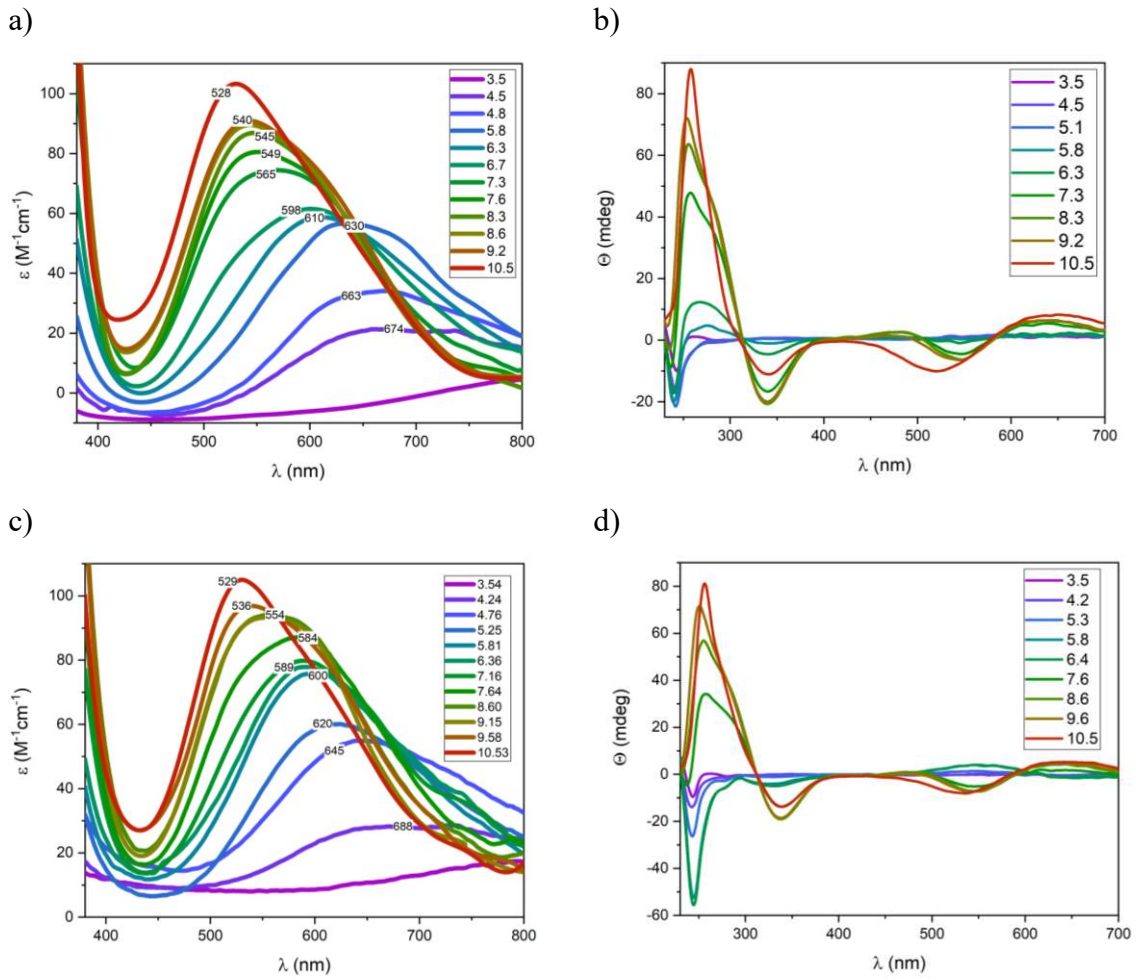


**Figure 7.1** – Vis absorption spectra of (a) Cu(II)/A8R and (c) Cu/A7H system; CD spectra of (b) Cu(II)/A8R and (d) Cu(II)/A7H system; M:L ratio = 0.8:1; $C_M = 0.4 \cdot 10^{-3}$ M, optical path 1 cm.

**Table 7.1** – Equilibrium constants and proposed coordination modes for Cu(II) and Zn(II) complexes at $T$ = 298 K and $I$= 0.1(KCl). Values in parentheses are standard deviations on the last significant figure.

| **Species** | **logβ** | **p$K_a$** | **Coord.** | **logβ** | **p$K_a$** | **Coord.** |
|---|---|---|---|---|---|---|
| | **A7R** | | | **A8R** | | |
| $[CuH_6L]^{6+}$ | 56.69(5) | 4.47 | $N_{Im}$, $COO^-$ | 55.96(3) | - | $N_{Im}$, $COO^-$ |
| $[CuH_5L]^{5+}$ | 52.22(3) | 5.13 | $2N_{Im}$, $COO^-$ | - | - | $2N_{Im}$, $COO^-$ |
| $[CuH_4L]^{4+}$ | 47.09(4) | 6.44 | $3N_{Im}$ | 46.50(3) | 6.35 | $3N_{Im}$ |
| $[CuH_3L]^{3+}$ | 40.65(5) | 6.85 | $2N_{Im}$, $N^-$ | 40.15(7) | 6.74 | $2N_{Im}$, $N^-$ |
| $[CuH_2L]^{2+}$ | 33.81(5) | 7.96 | $2N_{Im}$,$N^-$,$NH_2$ | 33.41(6) | 7.58 | $2N_{Im}$,$N^-$, $NH_2$ |
| $[CuHL]^+$ | 25.85(6) | 9.53 | $2N_{Im}$, $2N^-$ | 25.83(6) | 9.25 | $2N_{Im}$, $2N^-$ |
| [CuL] | 16.32(7) | 10.13 | $2N_{Im}$, $2N^-$ | 16.58(9) | 9.97 | $2N_{Im}$, $2N^-$ |
| $[CuH_{-1}L]^-$ | 6.19(6) | - | $N_{Im}$, $3N^-$ | 6.61(8) | - | $N_{Im}$, $3N^-$ |
| $[CuH_{-3}L]^{3-}$ | -14.53(6) | - | $N_{Im}$, $3N^-$ | -14.21(9) | - | $N_{Im}$, $3N^-$ |

| | A7H | | |
|---|---|---|---|
| $[CuH_6L]^{5+}$ | 56.84(5) | 5.00 | $2N_{Im}$, $COO^-$ |
| $[CuH_5L]^{4+}$ | 51.84(8) | 5.06 | $3N_{Im}$, $COO^-$ |
| $[CuH_4L]^{3+}$ | 46.78(5) | 7.2 | $3N_{Im}$, $N_{Im\ (ax)}$ |
| $[CuH_3L]^{2+}$ | 39.6(1) | 7.3 | $3N_{Im}$, $NH_2$ |
| $[CuH_2L]^{+}$ | 32.33(8) | 7.82 | $2N_{Im}$,$NH_2$,$N^-$ |
| [CuHL] | 24.51(9) | 9.26 | $2N_{Im}$, $2N^-$ |
| $[CuL]^-$ | 15.25(9) | - | $2N_{Im}$, $2N^-$ |
| $[CuH_{-2}L]^{3-}$ | -5.2(1) | 10.8 | $N_{Im}$, $3N^-$ |
| $[CuH_{-3}L]^{4-}$ | -16.0(2) | - | $N_{Im}$, $3N^-$ |

| | A7R | | | A8R | | |
|---|---|---|---|---|---|---|
| $[ZnH_5L]^{5+}$ | 49.14(8) | 6.03 | $2N_{Im}$, $COO^-$ | - | - | |
| $[ZnH_4L]^{4+}$ | 43.11(4) | - | $3N_{Im}$, $COO^-$ | 42.45(2) | 7.43 | $3N_{Im}$, $COO^-$ |
| $[ZnH_3L]^{3+}$ | - | - | | 35.02(6) | 7.56 | $3N_{Im}$, $OH^-$ |
| $[ZnH_2L]^{2+}$ | 27.57(5) | 9.52 | $3N_{Im}$, $OH^-$ | 27.37(4) | 8.64 | $3N_{Im}$, $OH^-$ |
| $[ZnHL]^{+}$ | 18.04(9) | 9.60 | $3N_{Im}$, $2OH^-$ | 18.72(5) | 9.15 | $3N_{Im}$, $2OH^-$ |
| [ZnL] | 8.44(7) | - | $3N_{Im}$, $2OH^-$ | 9.58(4) | - | $3N_{Im}$, $2OH^-$ |
| $[ZnH_{-2}L]^{2-}$ | -13.0(1) | - | $3N_{Im}$, $2OH^-$ | -11.10(4) | - | $3N_{Im}$, $2OH^-$ |

| | A7H | | |
|---|---|---|---|
| $[ZnH_6L]^{5+}$ | 54.7(1) | - | $2N_{Im}$ ($COO^-$) |
| $[ZnH_4L]^{3+}$ | 43.42(4) | 7.2 | $4N_{Im}$ |
| $[ZnH_3L]^{2+}$ | 36.2(1) | 7.4 | $3N_{Im}$, $OH^-$ |
| $[ZnH_2L]^{+}$ | 28.79(7) | 8.36 | $3N_{Im}$, $OH^-$ |
| [ZnHL] | 20.43(9) | 9.18 | $3N_{Im}$, $2OH^-$ |
| $[ZnL]^-$ | 11.26(9) | - | $3N_{Im}$, $2OH^-$ |
| $[ZnH_{-2}L]^{3-}$ | -9.26(9) | - | $3N_{Im}$, $2OH^-$ |

As in case of copper complexes, the obtained thermodynamic data for the three derivatives show high consistency with those of WT calcitermin[8] and its derivatives.[9] Zn(II) binding occurs by means of all the available histidine residues and the glutamic acid, supported by NMR results, where $H_\delta$-$H_\varepsilon$ and $H_\alpha$-$H_\beta$ protons signals of all the histidine residues and the proton correlations of the glutamic acid are broadened to baseline in the presence of the metal ion (**Figure 7.2**). Actually, the interaction with the glutamic acid is an option in case of A7H derivative since the broadening of its proton is less intense. Subsequently, the release of a proton from a coordinated water molecule and the deprotonation of the terminal amino group occurs. The latter binding to zinc ion cannot be excluded, since a significant shift of the $H_\alpha$-$H_\beta$ correlations of Val1 is present in the NMR spectra (**Figure 7.2b**). Lastly, the deprotonation of coordinated water molecule, the tyrosine and the two lysine residues occurs. Tyrosine and lysines are not involved in complexes formation.

a)

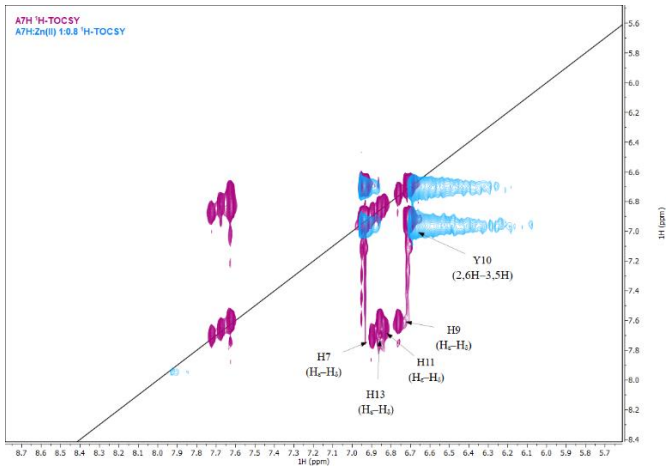


b)

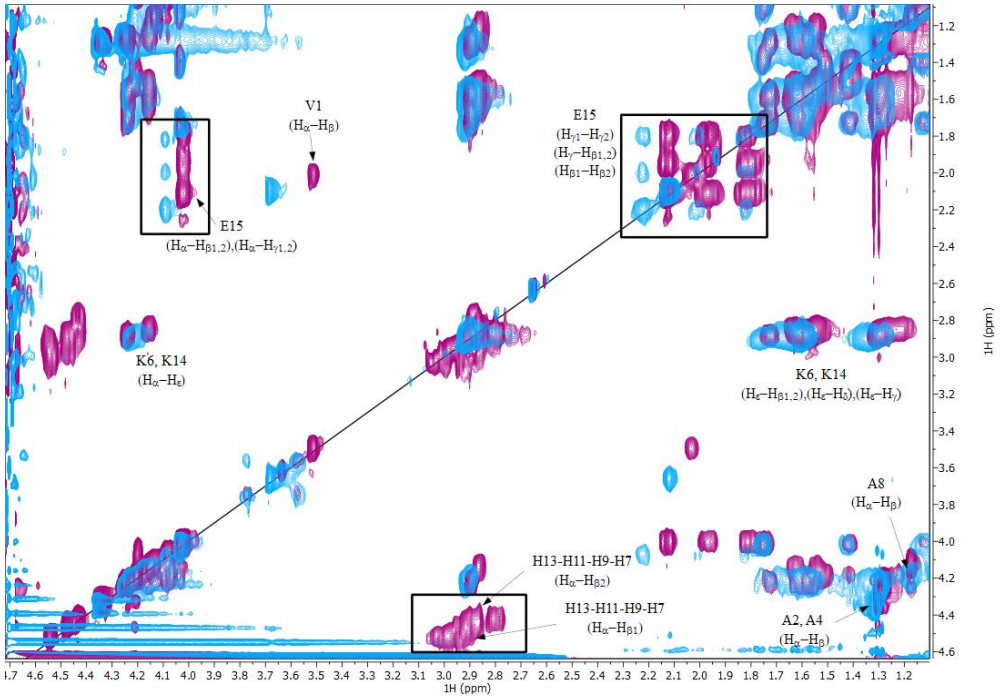


**Figure 7.2** - (a) Aromatic and (b) aliphatic region of 1H-1H TOCSY NMR spectra of 1.0 mM A7H peptide, T = 298 K, in the absence (purple) and in the presence (cyan) of 0.8 eq. of Zn(II), pH 7.4.

Alanine-to-Arginine derivatives show very similar binding affinity with copper metal ion, compared to wild-type calcitermin (**Figure 7.3a**). The coordination involves three histidine residues at acidic pH, followed by the terminal amino group and backbone amides at more physiological pH. Interestingly, A8R forms slightly more stable copper complexes than A7R, a difference which is not easily explained by the metal-binding site. This increased stability, along with its higher proteolytic resistance, suggests that the arginine at position 8 may exert a slight effect, likely through electrostatic interactions or hydrogen bonding with one of the terminal carboxyl groups or weak interactions with coordinated solvent molecules. The A7H derivative, which contains a fourth histidine, shows a similar copper-binding affinity to WT and A7R up to pH 6.5. Above this pH, A7H becomes the least effective

ligand. This is likely because the fourth histidine hinders the coordination of backbone amides, which are known to be crucial for forming highly stable copper complexes at higher pH, and it shifts their coordination at more alkaline pH.[12, 13]

On the contrary, A7H results to be the most effective ligand with zinc metal ion (**Figure 7.3b**). The presence of a fourth histidine residue increases its zinc-binding affinity that can be attributed to two main factors. The first is the formation of a very stable complex with four histidine residues involved in the coordination sphere and the second can be the formation of polymorphic binding states. In this case zinc ion can move "back and forth" between different sets of histidine residues along the peptides chain. This type of dynamic binding enhances the overall stability of the complex. In contrast, the A7R and A8R derivatives, which present non-coordinating arginine residues, do not show this enhanced zinc-binding effect.[14]

a) b)

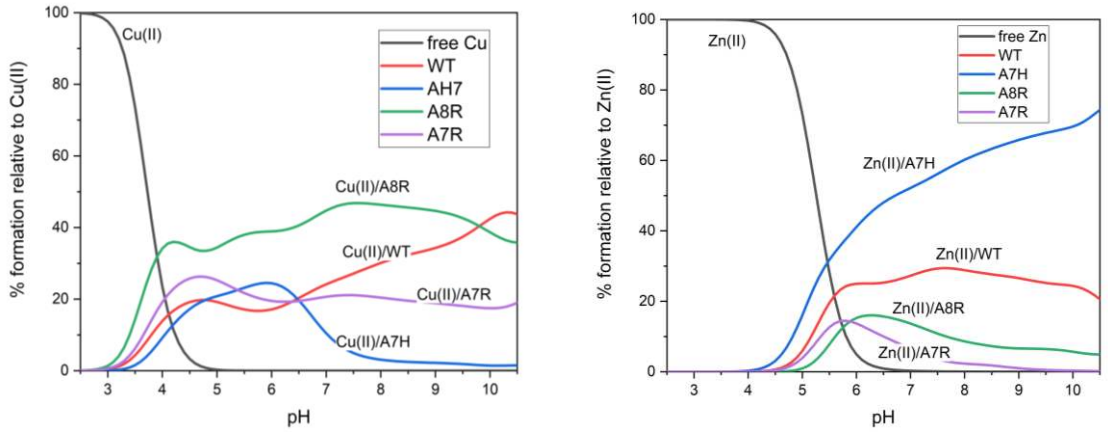


**Figure 7.3** - Competition plots for a solution containing equimolar concentrations ($1 \cdot 10^{-3}$ M) of metal ion, WT calcitermin, A7R, A8R and A7H. (a) Cu(II); (b) Zn(II).

To investigate the effect of specific amino acid substitutions on calcitermin stability, the degradation profile of the three derivatives have been compared to WT calcitermin. The substitution of alanine at position 7 with either arginine (A7R) or histidine (A7H) did not improve calcitermin stability. Both peptides have a half-life similar to that of WT (~16 minutes).[8] This suggests that position 7 is not crucial for protecting against proteolytic degradation. In contrast, the substitution of alanine with arginine at position 8 (A8R) significantly increased the peptide resistance to degradation, nearly doubling its half-life to 33 minutes (same value of calcitermin metal complex seen in Chapter 4). Arginine residue at position 8 may exert a "protective effect" on the adjacent metal-binding site. This protection could physically hinder proteolytic enzymes, such as a coordinated metal ion would. This suggests a potential analogy where the presence of the arginine residue mimics the stabilizing effect of a metal complex, a phenomenon not observed with the substitution at position 7, which is located on the opposite side of the peptide backbone.

All compounds were tested for their antimicrobial activity against the following chosen pathogenic organisms: the Gram-negative *Escherichia coli*, the Gram-positive *Enterococcus faecalis* and the fungi *Candida albicans*. The results indicate that the tested peptides exhibit a certain degree of antimicrobial activity, especially after 3 hours of contact and at the highest concentration of 0.128 mg/ml. A7R shows activity against *E. coli* (up to -30% CFU reduction) and *E. faecalis* (up to -15%). However, it displayed no antifungal effect against *C. albicans* within 3 hours. A8R demonstrated broader activity, since it displayed up to -40% CFU reduction with both *E. coli* and *E. faecalis.* It also showed a slight antifungal action (up to -17%) against *C. albicans.* A7H was most effective against *E. faecalis* (up to -31%). It also had some activity against *C. albicans* (up to -20%) and the least against *E. coli* (-7 %).

Generally, the peptide antimicrobial activity is significantly enhanced by the presence of bivalent metal ions, Zn(II) and Cu(II), which themselves possess antimicrobial properties. Therefore, a synergistic effect between the peptide and the metal ions is likely. The effect is more evident in most of the cases with Zn(II). Finally, the antimicrobial activity of the new derivatives and WT calcitermin has been compared. The new derivatives showed higher antibacterial activity against Gram-positive and Gram-negative bacteria than wild-type calcitermin, especially at pH 5.4, which confirms the positive effect of introducing charged residues. This activity was further enhanced by zinc and copper ions. However, WT calcitermin remained a more effective antifungal agent against *C. albicans*.

In order to better understand the mechanism of actions of these antimicrobial peptide, many different factors have to be considered, as the metal binding mode, the peptide charge or its structure. In this context, far-UV CD measurements in water revealed a disordered structure for all the systems (ligand and their complexes), while they adopt a helical-like structure in the presence of membrane-mimicking SDS (**Figure 7.4**). This ability to transition from an unstructured state in water to a partially helical conformation in a membrane-mimicking environment is significant. Peptide with helical structure generally exhibit stronger membrane activity and toxicity. The potential of this “smart” structural transition is a promising strategy for the development of drugs that are more selective toward pathogen membranes, which could potentially reduce toxicity to host cells.[15]

a) b)

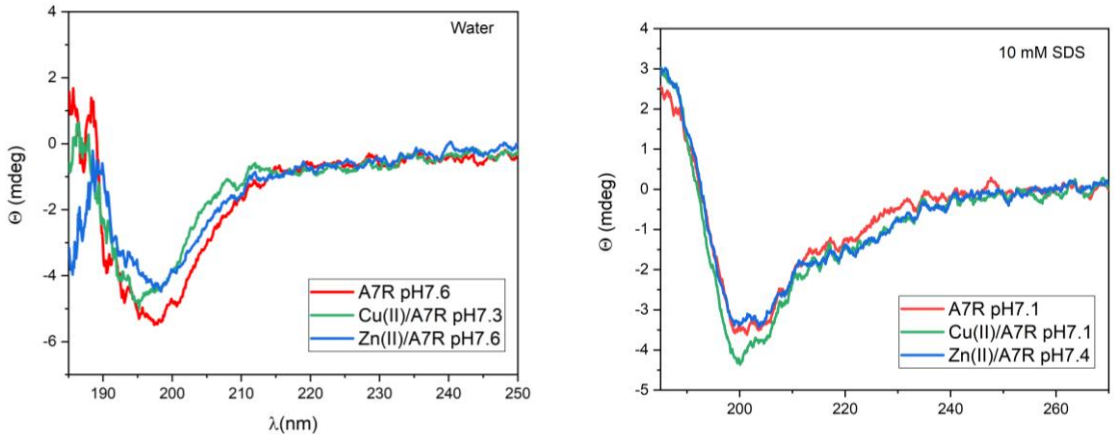

**Figure 7.4** - CD spectra of peptide A7R and its Cu(II) and Zn(II) complexes at *T*=298 K, in (a) aqueous solution and (b) 10mM SDS solution, M:L ratio 1:0.8, $C_M=0.08\cdot10^{-3}$ M, optical path 0.01 cm.

## 7.4 Conclusions

In the present work we characterized three different calcitermin derivatives presenting higher number of positively charged residues: A7R, A8R and A7H. The investigation of the thermodynamic properties highlights that the two derivatives containing arginine residues exhibit the same coordination modes as wild-type calcitermin. On the contrary, A7H peptide demonstrated a different behavior, particularly with zinc ion, as it formed more stable complexes due to the coordination of a fourth histidine residue or to the formation of a polymorphic binding states.

The structural characterization of the peptides revealed their ability to transition from an unfolded system in aqueous solution to an α-helical structure in a bacterial membrane-mimicking solvent. This offers a potential strategy to design peptides with enhanced selectivity for bacterial membranes and reduced toxicity towards host cells.

Based on the study of their stability in human plasma, the substitution of alanine at position 8 with an arginine residue was the only modification that enhanced the peptide resistance to degradation, extending its half-life to approximately 33 minutes. This finding is consistence with the results obtained for calcitermin metal complexes (see Chapter 4), suggesting that an arginine residue adjacent to the metal-binding site can confer a protective effect against proteolytic enzymes.

Finally, antimicrobial studies highlighted how the introduction of charged residue was an efficient method to boost antimicrobial activity of the peptide against Gram-positive and Gram-negative bacteria. This activity was further enhanced by zinc and copper ions. However, WT calcitermin remained a more effective antifungal agent against *C. albicans*.

This research work includes the publication "S. Leveraro, M. D'Accolti, E. Marzola, E. Caselli, R. Guerrini, M. Rowińska-Żyrek, M. Remelli, D. Bellotti, *Journal of Inorganic Biochemistry* 2025, 262, 112761".

## 7.5 References


[1] Chrom, C. L., Renn, L. M. & Caputo, G. A., *Antibiotics (Basel, Switzerland)*, **2019,** *8*.

[2] Satchanska, G., Davidova, S. & Gergova, A. (2024) Diversity and Mechanisms of Action of Plant, Animal, and Human Antimicrobial Peptides in *Antibiotics*

[3] Svenson, J., Karstad, R., Flaten, G. E., Brandsdal, B. O., Brandl, M. & Svendsen, J. S., *Molecular pharmaceutics*, **2009,** *6*, 996-1005.

[4] Cutrona, K. J., Kaufman, B. A., Figueroa, D. M. & Elmore, D. E., *FEBS letters*, **2015,** *589*, 3915-20.

[5] Schmidt, N. W., Tai, K. P., Kamdar, K., Mishra, A., Lai, G. H., Zhao, K., Ouellette, A. J. & Wong, G. C., *The Journal of biological chemistry*, **2012,** *287*, 21866-72.

[6] Huang, Y., Huang, J. & Chen, Y., *Protein & cell*, **2010,** *1*, 143-52.

[7] Leveraro, S., D'Accolti, M., Marzola, E., Caselli, E., Guerrini, R., Rowinska-Zyrek, M., Remelli, M. & Bellotti, D., *Journal of Inorganic Biochemistry*, **2025,** *262*, 112761.
[8] D'Accolti, M., Bellotti, D., Dzień, E., Leonetti, C., Leveraro, S., Albanese, V., Marzola, E., Guerrini, R., Caselli, E., Rowińska-Żyrek, M. & Remelli, M., *Scientific Reports*, **2023,** *13*, 18228.
[9] Leveraro, S., Garstka, K., Śliwka, P., Janek, T., Rowińska-Żyrek, M., Remelli, M. & Bellotti, D., *Dalton Transactions*, **2024**.
[10] Sigel, H. & Martin, R. B., *Chemical Reviews*, **1982,** *82*, 385-426.
[11] Prenesti, E., Daniele, P. G., Prencipe, M. & Ostacoli, G., *Polyhedron*, **1999,** *18*, 3233-3241.
[12] Székely, E., Csire, G., Balogh, B. D., Erdei, J. Z., Király, J. M., Kocsi, J., Pinkóczy, J. & Várnagy, K. (2022) The Role of Side Chains in the Fine-Tuning of the Metal-Binding Ability of Multihistidine Peptides in *Molecules*
[13] Bellotti, D., Leveraro, S., Hecel, A. & Remelli, M., *Analytical Biochemistry*, **2023,** *680*, 115315.
[14] Bellotti, D., Łoboda, D., Rowińska-Żyrek, M. & Remelli, M., *New Journal of Chemistry*, **2018,** *42*, 8123-8130.
[15] Xiong, M., Han, Z., Song, Z., Yu, J., Ying, H., Yin, L. & Cheng, J., *Angewandte Chemie (International ed in English)*, **2017,** *56*, 10826-10829.

# 8. Chapter Eight: Unveiling the antiviral properties of calcitermin and its Cu(II), Zn(II) and Ni(II) complexes

## 8.1 Outline of the work

Antimicrobial peptides, despite their name, can explicate their activity against many other pathogens rather than bacteria, such as fungi, and certain viruses.[1] Therefore they represent a promising drugs also for the treatment of viral diseases. They can prevent viral entry intro host cells, inhibit viral uncoating, or interfering with various intracellular stages of viral life cycle. Certain AMPs can internalize into host cells and inhibit viral replication by targeting essential viral enzymes or interfering with the synthesis of viral nucleic acids (DNA/RNA) or proteins. Moreover, as for the antibacterial and antifungal activity seen in the previous chapters, the antiviral activity can be enhanced by metal ions and formation of metal complexes.[2-4] We decided to extend the investigation of the calcitermin-metal complex formation behaviour also to nickel ion. Since calcitermin presents three histidine residues and the free terminal amino and carboxyl groups, it is a good candidate for the binding of divalent nickel ions. Nickel plays a significant role in bioinorganic chemistry, particularly since the discovery of its presence in the enzyme urease. Nickel complexes have demonstrated a wide spectrum of activity against pathogens, likely by disrupting enzyme function after penetrating the cells. While nickel is recognized for its toxic potential, causing metabolic alterations, oxidative stress and cell death through non-specific interactions with biomolecules and the generation of reactive oxygen species, it is also an essential element for a variety of organisms, including bacteria and plants. The antimicrobial and antiviral properties of nickel complexes are well documented in literature.[5-11]

Once investigated the thermodynamic properties of Ni(II) complexes, we tested the antiviral potential of calcitermin and its Cu(II), Zn(II) and Ni(II) complexes against the virus *Herpes simplex* type I (HSV1). Despite the availability of different antiviral drugs to tackle this virus, it is developing resistance mechanisms, making its eradication challenging.

## 8.2 Experimental procedure

Analyses performed on the above mentioned peptide follow the scheme:

- Potentiometric determination of Ni(II) complex-formation constants.
- Mass spectrometric analysis to evaluate the stoichiometry of the formed Ni(II) complexes.
- Spectrophotometric (UV-Vis and CD) analyses of the Ni(II) complexes.
- Far-UV CD spectroscopy to investigate the structural conformations of apo-peptides and Ni(II) complexes.

The employed experimental conditions, instruments and materials are reported in details in Caproni *et al.,* 2025. [12]

## 8.3 Results and discussion

The overall stability constants (log$\beta$) and acid dissociation constants (p$K_a$) for the formed metal complexes are reported in **Table 8.1** together with the proposed coordination mode for each species. The formation of only mononuclear species has been confirmed by the analyses of MS spectra.

From the potentiometric data analyses, we can affirm that the nickel complexes formation behaviour is consistent with that of Cu(II) complexes formation of the calcitermin derivatives discusses in the previous chapters. The complexation starts around pH 4.5, with the first species in which two histidine residues are already deprotonated and bound to the metal ion. In the complexation, also the carboxyl groups of the glutamic acid could participate, enabling the interconversion among different coordination modes in an octahedral environment.[13, 14] Subsequently, increasing the alkalinity of the solution the deprotonation of the terminal amino group, three backbone amides, the phenolic group of tyrosine and the amino group of the two lysines occurs. Tyrosine and lysines are not involved in the complexation, while the terminal amino group can partially interact with Ni(II). The progressively binding of the three backbone amides to Ni(II) are confirmed by the spectroscopic data (UV-Vis and CD, **Figure 8.1**). Indeed, in the UV-Vis spectra from pH 8.5-11.0 we recorded $\lambda_{max}$ = 465-445 nm, while in the CD spectra it is visible a band near 250 nm corresponding to the $N^-$ → Ni(II) transition.[15-18]

a) b)

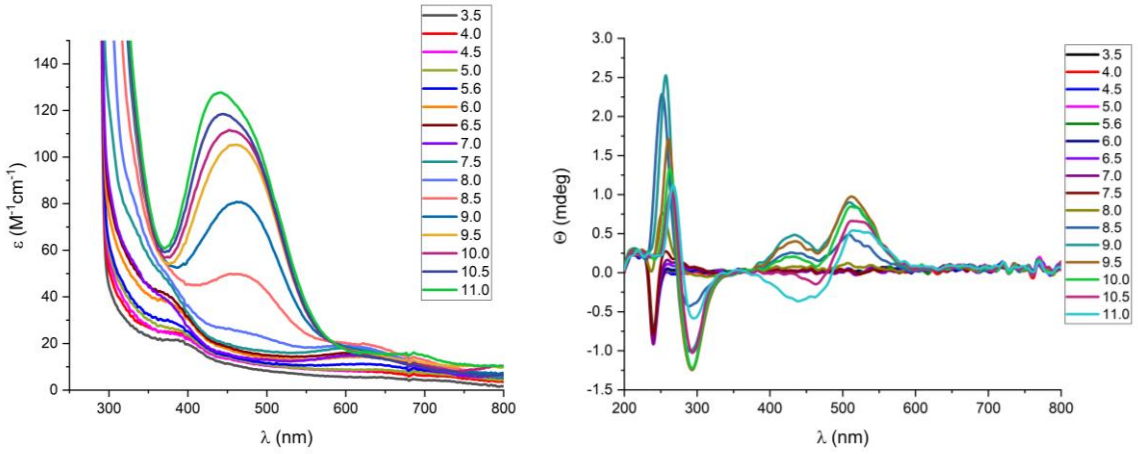


**Figure 8.1** – (a) Vis absorption spectra, (b) CD spectra of Ni(II)/WT calcitermin; M:L ratio = 0.8:1; $C_M = 0.4 \cdot 10^{-3}$ M, optical path 1 cm.

**Table 8.1** – Equilibrium constants and proposed coordination modes for Ni(II) complexes at $T$ = 298 K and $I$ = 0.1 (KCl). Values in parentheses are standard deviations on the last significant figure.

| Species | logβ | p$K_a$ | Coord. |
|---|---|---|---|
| | **WT** | | |
| $[NiH_5L]^{4+}$ | 49.5(1) | 6.0 | $2N_{Im}$, $COO^-$ |
| $[NiH_4L]^{3+}$ | 43.51(6) | 7.14 | $3N_{Im}$ |
| $[NiH_3L]^{2+}$ | 36.37(9) | 8.2 | $3N_{Im}/3N_{Im}$,$NH_2$ |
| $[NiH_2L]^{+}$ | 28.1(1) | 8.9 | $2N_{Im}$,$N^-$ |
| [NiHL] | 19.2(1) | 9.2 | $2N_{Im}$, $2N^-$ |
| $[NiL]^-$ | 10.0(1) | 9.7 | $N_{Im}$, $3N^-$ |
| $[NiH_{-1}L]^{2-}$ | 0.3(1) | - | $N_{Im}$, $3N^-$ |
| $[NiH_{-3}L]^{4-}$ | -20.6(1) | - | $N_{Im}$, $3N^-$ |

FAR-UV CD measurements revealed that the secondary structure of the wild-type calcitermin remains a random coil conformation after coordinating with Ni(II) ions, there are no significant changes in the spectra shape, which show a negative band around 198 nm (**Figure 8.2**).[19, 20] The dominance of a random coil structure is particularly relevant to its potential antiviral function. Many peptides that inhibit viral adhesion and into cells are known to have a higher content of random coil secondary structure. [21]

a) b)

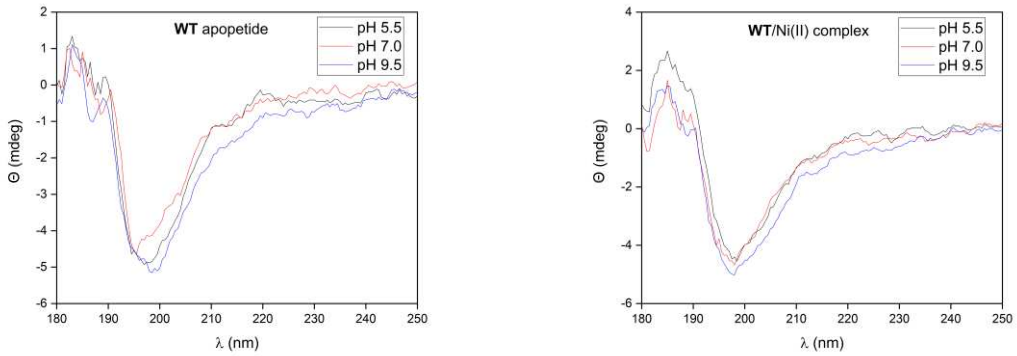


**Figure 8.2** - FAR-UV CD spectra of (a) WT calcitemin and (b) its Ni(II) complexes at $T$=298 K, in aqueous solution at different pH values, M:L ratio 1:0.8, $C_M$=0.08·10$^{-3}$ M, optical path 0.01 cm.

Once determined the thermodynamic constants of Ni(II)-calcitermin complexes, a comparison with Cu(II) and Zn(II) complexes is needed. The competition plot shows that Cu(II) complexes are consistently more stable than those formed with Ni(II) and Zn(II) across the entire pH. In particular, the ability of WT calcitermin to bind Zn(II) and Ni(II) is comparable. These findings are in perfect agreement with the Irving-Williams series, which

predicts the stability of complexes formed by transition metal ions based on their electronic configuration. This series establishes higher stability for copper and then nickel and zinc.[22]

a) b)

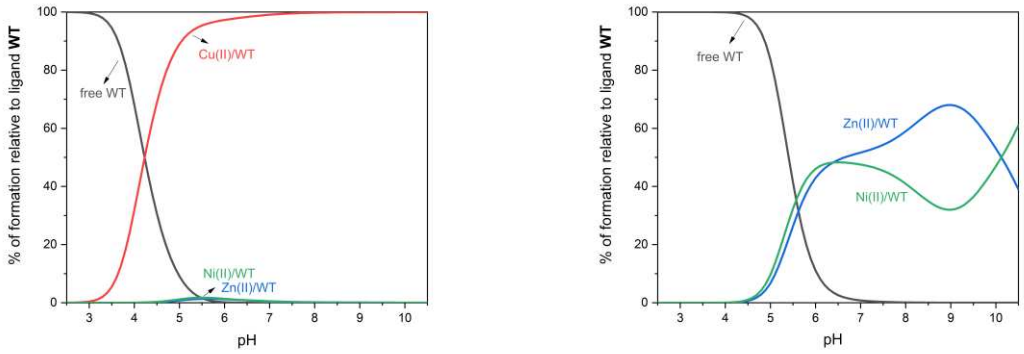


**Figure 8.3** - Competition plots for simulated solutions containing equimolar concentrations (1 mM) of (a) Cu(II), Zn(II) and Ni(II) wild-type calcitermin complexes; and (b) Zn(II) and Ni(II) wild-type calcitermin complexes.

The in vitro anti-HSV-1 activity of nickel chloride ($NiCl_2$), zinc chloride ($ZnCl_2$), copper chloride ($CuCl_2$) and calcitermin (WT) was assessed through a plaque reduction assay, both individually and in combination. There were two distinct types of assays: in the first case, the formulation was administered to cells prior to viral infection, called "pre-treatment" (**Figure 8.4a)**. In the second case, the formulation was added to the infected cell after viral removal, called "post-infection" (**Figure 8.4b**). Plaque reduction plot of cells pre-treated with metal salts, the peptide, or the metal-peptide complex formulations, shows that $NiCl_2$ alone (45%), WT calcitermin alone (67%), or the $NiCl_2$WT complex (50%), led to the biggest reductions. Notably, the results show that metal-peptide complex formulations tend to induce a lower plaque reduction than that obtained with the formulations alone, suggesting that the combination of the two exerts a slower but more prolonged effect. In the second protocol with the cell treatment after 1 h of infection, higher plaque reduction has been obtained with $NiCl_2$, WT and $NiCl_2$-WT.

From the conducted studies, the virucidal effects of the wild-type calcitermin metal complexes are comparable to those of the raw metal salts.

a) b)

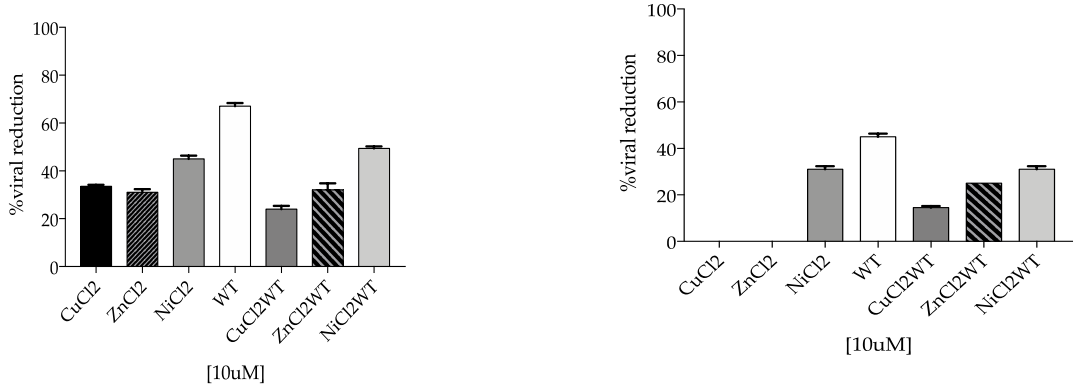

**Figure 8.4** - Virucidal effect of $NiCl_2$, $ZnCl_2$ and $CuCl_2$ alone or in combination with calcitermin, against HSV-1 Kos strain 1 (1x105 pfu/ml). Vero cells were treated with the formulations before (a) and after infection (b).

## 8.4 Conclusions

The present work is an implementation in the description of the thermodynamics, structure, coordination chemistry and antiviral activity of the studied peptide calcitermin. Together with the previous studies, we could be able to comprehend the coordination chemistry of calcitermin and its different derivatives with copper and zinc metal ions. We expanded the study to a diverse divalent metal ion, which is nickel, aiming at testing also its antiviral activity. The nickel metal complexes exhibit a coordination mode that is strikingly similar to that of the copper ion, as evidenced by the thermodynamic studies. Nevertheless, this resulted in the formation of complexes that were significantly less stable than the copper ion but very similar to the zinc ion. The nickel complexes seem to present random coil conformation, not affected by the pH changes. Such flexibility allows them to interact with different targets as required to exert the virucidal action.

The findings from the pre-treatment assay suggest that the anti-HSV-1 mechanism of the formulations, particularly when combined with WT calcitermin, likely involves interference with the initial viral absorption and cellular penetration steps. This mechanism is plausible because metal complexes can interact with lipids and proteins on the cell membrane, thereby altering its permeability and structure, which impedes the virus ability to enter the cell.

Although the virucidal effects of the wild-type calcitermin metal complexes are comparable to those of the raw metal salts, the complexes present significant pharmaceutical advantages. These advantages, which address the limitations (such as toxicity, poor solubility and undefined distribution) of raw metal salts, include increased solubility, reduced toxicity and targeted delivery. These characteristics make calcitermin and its complexes promising candidates for further research as potential therapeutic agents, although a more thorough investigation is needed to fully elucidate their complex mechanism of action.

## 8.5 References


[1] Datta, S. & Roy, A., *International Journal of Peptide Research and Therapeutics*, **2021,** *27*, 555-577.
[2] Hutchinson, D. W., *Antiviral Research*, **1985,** *5*, 193-205.
[3] Pinkham, A. M., Yu, Z. & Cowan, J. A., *Journal of Medicinal Chemistry*, **2018,** *61*, 980-988.
[4] Abate, C., Carnamucio, F., Giuffrè, O. & Foti, C., *Biomolecules*, **2022,** *12*.
[5] Houston, D. M. J., Bugert, J. J., Denyer, S. P. & Heard, C. M., *PLOS ONE*, **2017,** *12*, e0188609.
[6] Ahmad, R. & Choudhary, M., *New Journal of Chemistry*, **2024,** *48*, 15053-15076.
[7] Das, A., Rajeev, A., Bhunia, S., Arunkumar, M., Chari, N. & Sankaralingam, M., *Inorganica Chimica Acta*, **2021,** *526*, 120515.

[8] Hunter, T. M., McNae, I. W., Simpson, D. P., Smith, A. M., Moggach, S., White, F., Walkinshaw, M. D., Parsons, S. & Sadler, P. J., *Chemistry – A European Journal*, **2007,** *13*, 40-50.
[9] Graham, R. D. & Williams, D. R., *Journal of Inorganic and Nuclear Chemistry*, **1979,** *41*, 1245-1249.
[10] Atasever Arslan, B., Kaya, B., Şahin, O., Baday, S., Saylan, C. C. & Ülküseven, B., *Journal of Molecular Structure*, **2021,** *1246*, 131166.
[11] Sari, N., *The Journal of Socio-Economics*, **2013,** *43*, 60-67.
[12] Caproni, A., Leveraro, S., Szarszoń, K., Nordi, C., Fontana, R., Buratto, M., Marconi, P., Remelli, M., Sicurella, M. & Bellotti, D., *Anal Biochem*, **2025,** *700*, 115784.
[13] Rowińska-Żyrek, M. & Kozłowski, H. (2017) Nickel Binding Sites – Coordination Modes and Thermodynamics in *The Biological Chemistry of Nickel* (Zamble, D., Rowińska-Żyrek, M. & Kozlowski, H., eds) pp. 0, The Royal Society of Chemistry.
[14] Bal, W., Kozlowski, H., Robbins, R. & Pettit, L. D., *Inorganica Chimica Acta*, **1995,** *231*, 7-12.
[15] Garstka, K., Bellotti, D., Wątły, J., Kozłowski, H., Remelli, M. & Rowińska-Żyrek, M., *Dalton Transactions*, **2023,** *52*, 16140-16150.
[16] Ősz, K., Bóka, B., Várnagy, K., Sóvágó, I., Kurtán, T. & Antus, S., *Polyhedron*, **2002,** *21*, 2149-2159.
[17] Bal, W., Lukszo, J., Jezowska-Bojczuk, M. & Kasprzak, K. S., *Chemical Research in Toxicology*, **1995,** *8*, 683-692.
[18] Bellotti, D., Rowińska-Żyrek, M. & Remelli, M., *Dalton Transactions*, **2020,** *49*, 9393-9403.
[19] Bakshi, K., Liyanage, M. R., Volkin, D. B. & Middaugh, C. R. (2014) Circular Dichroism of Peptides in *Therapeutic Peptides: Methods and Protocols* (Nixon, A. E., ed) pp. 247-253, Humana Press, Totowa, NJ.
[20] Johnson Jr, W. C., *Proteins: Structure, Function, and Bioinformatics*, **1990,** *7*, 205-214.
[21] Urmi, U. L., Vijay, A. K., Kuppusamy, R., Islam, S. & Willcox, M. D. P., *Peptides*, **2023,** *166*, 171024.
[22] Irving, H. & Williams, R. J. P., *Journal of the Chemical Society (Resumed)*, **1953**, 3192-3210.

# 9. Chapter Nine: Spectrophotometric approach to study the formation of reactive oxygen species (ROS) catalyzed by Cu(II)-calcitermin complexes

## 9.1 Outline of the work

Copper redox activity can be exploited to favor the formation of reactive oxygen species (ROS) which can be useful in pathogen elimination and in killing cancer cells.[1] ROS are highly reactive molecules resulting from the incomplete reduction of dioxygen to superoxide ($O_2^{\bullet-}$), hydrogen peroxide ($H_2O_2$), and hydroxyl radical (•OH), fueled by a physiological reductant such as ascorbate.[2-4] These species can damage biomolecules (such as lipids, proteins and nucleic acids) and thus affect cellular function. Copper plays a crucial role in the generation of these reactive species due to its ability to participate in redox reactions. In fact, copper can easily alternate between two oxidation states: Cu(II) and Cu(I). This ability makes it a powerful agent for oxidation-reduction (redox) reactions in biology, with both physiological and pathological implications. One of the main reactions that copper can undergo are the Fenton and Haber-Weiss reactions, a metal-catalyzed cycle that converts less reactive oxygen species ($O_2^{\bullet-}$, $H_2O_2$) into the highly damaging hydroxyl radical •OH.[5] These reactions are classically described with iron, but also copper can participate in an equivalent, or Fenton and Haber-Weiss-like reactions, due to its ability to cycle between reduced Cu(I) and oxidized Cu(II) states. The overall process is divided into two main steps that regenerate the copper catalyst:

1. The Haber-Weiss step: the oxidized copper ion Cu(II) reacts with the superoxide anion ($O_2^{\bullet-}$), reducing the copper to Cu(I).
2. The Fenton-like reaction: the reduced copper ion Cu(I) reacts with hydrogen peroxide ($H_2O_2$) to produce the hydroxyl radical •OH, and simultaneously converts the copper back to its oxidized state Cu(II).

The net reaction shows that the cycle consumes superoxide and hydrogen peroxide to produce the hydroxyl radical. The continuous cycling of copper between its two oxidation states Cu(I)/Cu(II) in the presence of $O_2^{\bullet-}$ and $H_2O_2$ creates a persistent source of the highly reactive hydroxyl radical, which causes widespread damage to cellular components (lipids, proteins, DNA).

$$Cu(II) + O_2^{\bullet-} \rightarrow Cu(I) + O_2$$

(Haber-Weiss)

$$Cu(I) + H_2O_2 \rightarrow Cu(II) + OH^{\bullet} + OH^-$$

(Fenton reaction)

---

$$O_2^{\bullet-} + H_2O_2 \xrightarrow{Cu(I)/Cu(II)} O_2 + OH^{\bullet} + OH^-$$

(sum reaction)

**Figure 9.1 –** Copper-mediated increase of oxidative stress. Copper can participate in Fenton and Haber-Weiss reactions, which lead to the formation of the highly reactive hydroxyl radical intermediate.

Given the metallo-chelating properties of the antimicrobial peptide calcitermin, we decided to evaluate its ability to favor the production of ROS species, both as a free peptide and as a complex with Cu(II). This information can contribute to clarify the potential mechanisms of action of this AMP and, in particular, to assess the potential involvement of ROS species in its microbicidal activity. Indeed, as already underlined above, calcitermin demonstrated enhanced antimicrobial activity in the presence of Cu(II) ion. This preliminary analysis has been performed using a spectrophotometric method reported in literature.[6]

## 9.2 Experimental method

A stock solution of 100 mM HEPES buffer (sodium salt of 2-[4-(2-hydroxyethyl)piperazin-1-yl]ethanesulfonic acid) has been prepared and its pH has been adjusted to 7.3 using concentrated sodium hydroxide.

The ROS production has been determined using an ascorbate consumption assay monitored *via* UV-Vis spectrophotometry. The decrease in the absorption band at $\lambda_{max}$ = 265 nm of the ascorbate has been plotted as a function of time. The samples have been prepared from stock solutions at the concentration of 1 mM and mixed *in situ* in the UV-Vis cuvette at a final concentration of 12 μM for the peptide and 10 μM for Cu(II) in HEPES at pH 7.3. The final volume has been adjusted with buffer solution to 2 mL. After 180 seconds, ascorbate has been introduced in the UV-Vis cuvette to obtain a final concentration of 100 μM.

## 9.3 Results and discussion

As widely discussed in the previous chapters, calcitermin has demonstrated to stably coordinate Cu(II) ion mainly through the histidine residues of its peptide sequence. Knowing the speciation model of the Cu(II)/calcitermin system, it is possible to simulate the metal-binding behavior of the peptide under the experimental conditions used in these experiments (pH 7.3, $T$ = 298 K, $C_{calcitermin}$ = 12 μM and $C_{Cu(II)}$ = 10 μM). Using the HYSS software and the thermodynamic and spectroscopic data present in the literature,[7] it has been possible to determine that, in the studied solutions, calcitermin forms distorted octahedral complexes, with a coordination sphere in which three imidazole nitrogens of the histidines and the terminal amine or an amide of the peptide backbone are involved. No free Cu(II) is present in solution under the studied experimental conditions.

Solutions containing either the peptide, a Cu(II) salt or the Cu(II)/calcitermin complex mixture have been tested in the buffer solution of HEPES at pH 7.3 and $T$ = 298 K, in the presence of ascorbate; ascorbate consumption has been monitored as a function of reaction time (**Figure 9.2**). Ascorbate is readily oxidized by the metal ion (red curve) and this is correlated to ROS production. The occurrence of a catalytic reaction is exclusively observed in the presence of copper, as both free Cu(II) ion and complexed with calcitermin. No

evidence of ascorbate degradation has been recorded in the solution containing only calcitermin peptide. Ascorbate acts as a reducing agent, forming Cu(I) and the ascorbate radical. However, in the presence of oxygen, Cu(I) is re-oxidized to Cu(II), forming the superoxide radical capable of dismutation into $H_2O_2$ and $O_2$. In the presence of ascorbate, the metal Cu(II) can be restored to its reduced form, which will catalyze the formation of highly reactive hydroxyl radicals (•OH) from $H_2O_2$ in a classic Fenton reaction. Therefore, the ascorbate degradation is a signal of ROS production.

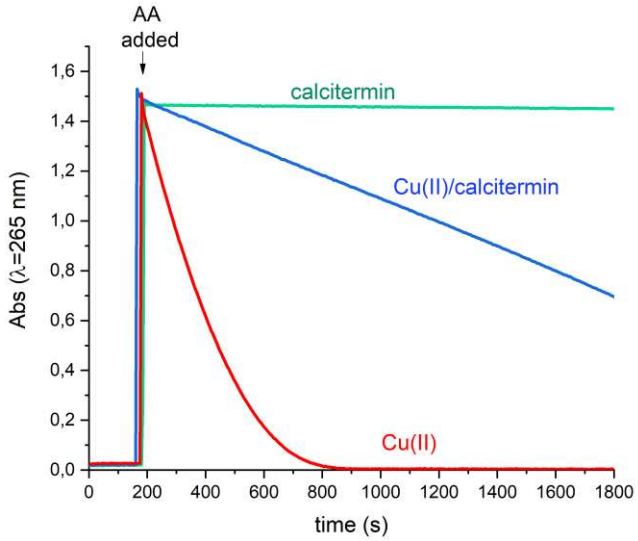


**Figure 9.2** – Bleaching of the characteristic ascorbate absorption band ($\lambda_{max}$ = 265 nm) as a function of time, at $T$ = 298 K, in buffer solution (HEPES 100 mM). The tested solutions contain ascorbic acid 100 µM and calcitermin 12 µM (green curve); ascorbic acid 100 µM and $CuCl_2$ 10 µM (red curve); ascorbic acid 100 µM, calcitermin 12 µM and Cu(II) 10 µM (L:M=1:0.84) (blue curve).

## 9.4 Conclusions

The investigation reported in the present chapter was aimed at clarifying the ability of the antimicrobial peptide calcitermin and its copper(II) complexes to generate reactive oxygen species. The obtained data show that the free peptide is not involved in ROS production; however, it demonstrates a certain capacity to modulate ROS production when complexed with Cu(II), which remains the catalytic metal center. Two possible scenarios can be hypothesized: (a) the metal-peptide complexes are indeed able to promote the formation of hydroxyl radicals; (b) the reduction step of the metal ion to Cu(I) decreases the affinity of the ligand for the metal, which would return in the form of free, uncomplexed ion, able to trigger the Fenton reaction.

In order to shed light on the latter mechanism, the complex-formation equilibria in the Cu(I)/calcitermin system could be investigated, and the possible presence of an excess of free Cu(I) ion, under the used experimental conditions, measured, for example through potentiometric titrations.

In principle, copper complexes with a strong affinity for both Cu(I) and Cu(II) would be effective catalysts, allowing for a rapid and efficient redox cycle (both oxidation states should be accessible and the barrier between them should be small); chelators that stabilize only one oxidation state too much are generally not very redox-active. Moreover, in the biological environment, the metal complex should be sufficiently stable to resist to competition due to other endogenous ligands (like albumin, Cu-chaperones, etc.) but rather support the antimicrobial activity of the peptide, by promoting the production of ROS.

The results of this work are in agreement with data reported in the literature, under similar experimental conditions, for Cu(II) complexes with metallo-chelating peptides such as kanamycin A,[8] piscidin 1, 2 and 3,[9] and beta-amyloid peptide (Aβ)[6] and others.[5, 10, 11] The present results highlight the possible involvement of the Cu(II)-calcitermin complex in ROS production, although further investigation is needed to fully clarify these aspects, especially from the point of view of its antimicrobial potential.

## 9.5 References


[1] Łoboda, D., Kozłowski, H. & Rowińska-Żyrek, M., *New Journal of Chemistry*, **2018,** *42*, 7560-7568.

[2] Cheignon, C., Tomas, M., Bonnefont-Rousselot, D., Faller, P., Hureau, C. & Collin, F., *Redox biology*, **2018,** *14*, 450-464.

[3] Tassone, G., Kola, A., Valensin, D. & Pozzi, C., *Life (Basel, Switzerland)*, **2021,** *11*.

[4] Hureau, C. (2022) Role of Metal Ions in Alzheimer's Disease: Mechanistic Aspects Contributing to Neurotoxicity in *Alzheimer's Disease: Recent Findings in Pathophysiology, Diagnostic and Therapeutic Modalities* (Thimmaiah, G., ed) pp. 170-192, Royal Society of Chemistry, Cambridge.

[5] Stokowa-Sołtys, K., Kierpiec, K. & Wieczorek, R., *Dalton Transactions*, **2022,** *51*, 7040-7052.

[6] Lefèvre, M., Malikidogo, K. P., Esmieu, C. & Hureau, C. (2022) Sequence–Activity Relationship of ATCUN Peptides in the Context of Alzheimer's Disease in *Molecules*

[7] Bellotti, D., Toniolo, M., Dudek, D., Mikołajczyk, A., Guerrini, R., Matera-Witkiewicz, A., Remelli, M. & Rowińska-Żyrek, M., *Dalton Transactions*, **2019,** *48*, 13740-13752.

[8] Szczepanik, W., Kaczmarek, P., Sobczak, J., Bal, W., Gatner, K. & Jeżowska-Bojczuk, M., *New Journal of Chemistry*, **2002,** *26*, 1507-1514.

[9] Adriana, M., Aleksandra, M., Denise, B., Kinga, G., Joanna, W., Aleksandra, H., Robert, W., Agnieszka, M.-W. & Magdalena, R.-Ż., *Inorganic Chemistry*, **2024,** *63*, 12958-12968.

[10] Szarszoń, K., Baran, N., Śliwka, P., Wiloch, M., Janek, T. & Wątły, J., *Inorg Chem*, **2024,** *63*, 19105-19116.

[11] Faller, P. & Hureau, C., *Dalton Transactions*, **2009**, 1080-1094.

# 10. Chapter Ten: Effect of D-amino acids substitution on activity and stability of calcitermin

## 10.1 Outline of the work

This work aims to explore strategies to increase the calcitermin efficacy through an extension of its half-life, which is approximately 18 minutes. Several strategies can be employed to improve peptide resistance towards proteolytic enzymes, including replacing L-amino acids with their corresponding D-series counterparts. This substitution would prevent the amino acids recognition from proteolytic enzymes such as endo- and exo-peptidases. An additional advantage of this strategy is that D-amino acids contribute to the reduction in the immunogenicity of the therapeutic peptides.[1-3] In particular, we decided to focus on the degradation process carried out by exo-peptidades such as aminopeptidases, dipeptidyl-peptidases and carboxypeptidases. Aminopeptidases act on the amino terminal end of a peptide, where the amino group is free and they typically cleave one single amino acid residue at a time. Dipeptidyl-peptidases is a specialized type of aminopeptidase, they systematically remove dipeptides from the N-terminus of a peptide chain. Carboxypeptidases act on the carboxyl-terminal end of a peptide chain, where the carboxyl group is free, by cleaving one single amino acid residue at a time.[4] For that reason, we decided to substitute L-amino acids with their D-series at the terminal ends of calcitermin peptide using different combinations. The studied peptides are (where the D-amino acids are reported with low-case letters): vAIALKAAHYHTHKE (L1), VaIALKAAHYHTHKE (L2), vaIALKAAHYHTHKE (L3), vAIALKAAHYHTHKe (L4), vaIALKAAHYHTHke (L5). The analysis of the effect of D-amino acids substitution has been conducted by means of different experimental techniques.

## 10.2 Experimental procedure

Analyses performed on the above mentioned peptides follow the scheme:

- Potentiometric determination of ligand protonation and Zn(II) and Cu(II) complex-formation constants.
- Mass spectrometric analysis to evaluate ligand purity and the stoichiometry of the formed complexes.
- Spectrophotometric (UV-Vis and CD) analyses of the Cu(II) complexes.
- Far-UV CD spectroscopy to investigate the structural conformations of apo-peptides, Cu(II) and Zn(II) complexes.
- Peptide stability in human plasma.

The employed experimental conditions, instruments and materials are reported in details, in Leveraro *et al*., 2025.[5] Peptides have been purchased and used without further purification.

## 10.3 Results and discussion

Under the experimental conditions here employed, only variously protonated, mononuclear complexes with metal/ligand stoichiometry 1:1 have been detected by potentiometry and mass spectrometry. The overall protonation constants of the free ligands are shown in **Table 10.1**; the complex-formation constants (log$\beta$) and the corresponding acid dissociation constants (p$K_a$) of protonated complexes are instead reported in **Table 10.2**. In ESI-MS experiments, the only detected *m/z* signals correspond to equimolar Cu(II) and Zn(II) complexes with different protonation states. Potassium and/or sodium adducts are also formed. The most intense signals (*m/z* = 563.64, *z* = +3) correspond to the free peptide, confirming its purity. Signals observed in metal containing solutions (*m/z* = 583.94, *z* = +3, and *m/z*= 875.89, *z* = +2) (**Figure 10.1b, 10.2b)** correspond to the species $[CuH_4L]^{3+}$ and $[ZnH_3L]^{2+}$ respectively.

a)

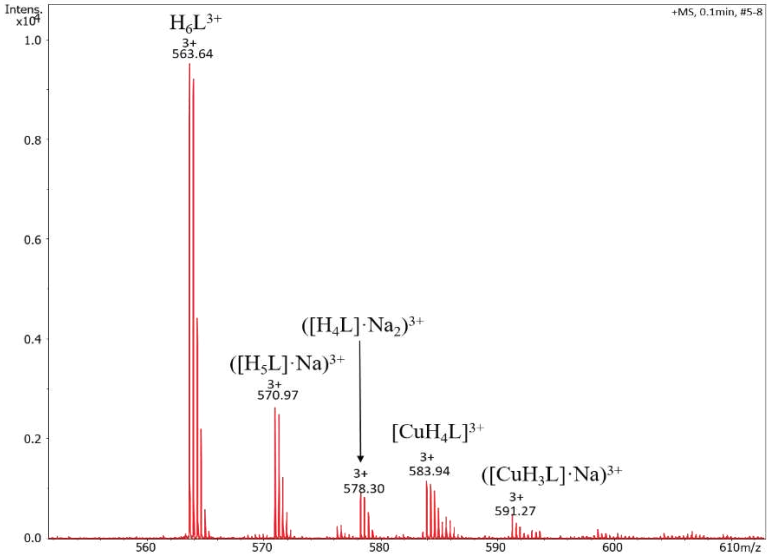


b)

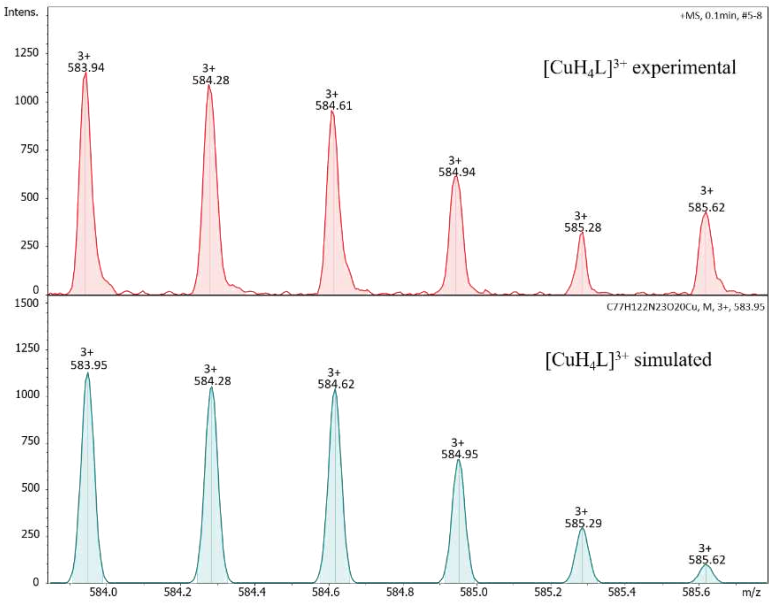

**Figure 10.1-** ESI-MS spectrum for (a) Cu(II)/L1 system at L:M molar ratio = 1:0.9 in MeOH:$H_2O$ (1:1) mixture solution, and (b) comparison between the experimental and simulated isotopic patterns of chosen metal complex $[CuH_4L]^{3+}$.

a)

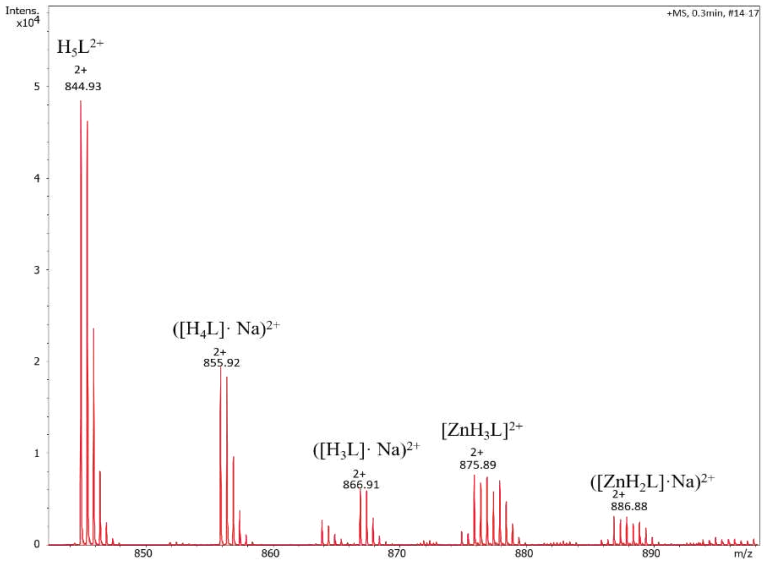


b)

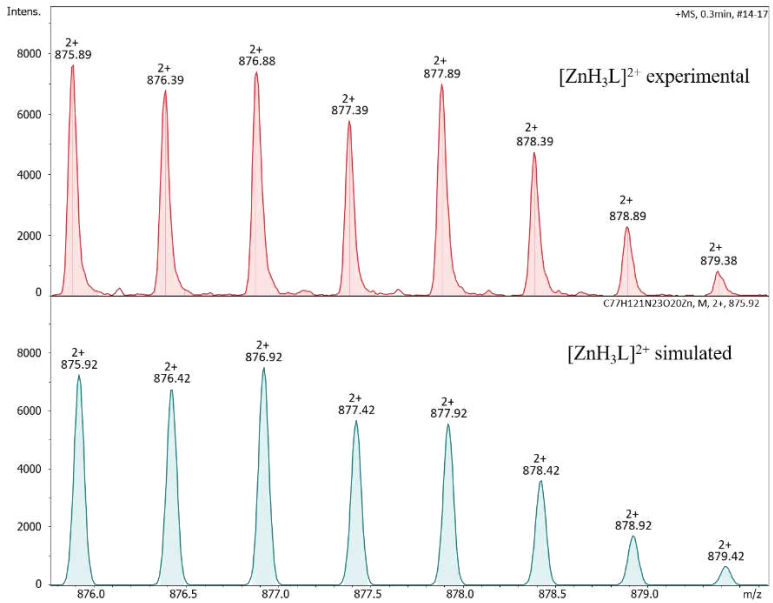


**Figure 10.2 -** ESI-MS spectrum for (a) Zn(II)/L1 system at L:M molar ratio = 1:0.9 in MeOH:$H_2O$ (1:1) mixture solution, and (b) comparison between the experimental and simulated isotopic patterns of chosen metal complex $[ZnH_3L]^{2+}$.

The investigated peptides L1, L2, L3, L4 and L5 are unprotected fragments and thus their acid-base behavior depends on both the amino acids side chains and their amino and carboxyl termini. The investigated peptides, once completely deprotonated, bear a triple negative charge ($L^{3-}$). The obtained protonation constants are in good agreement with literature values for similar systems [6, 7] and show reasonable similarities among the considered peptides. Nine different species have been detected in solution. The most acidic

moiety is the terminal carboxyl group with a log*K* varying from 2.55 to 2.82. The glutamic acid side chain, with comparable log*K* values in all mutants (4.24, 3.92, 3.98, 4.07 and 3.99), follows it. Histidines residues are characterized by log*K* values ranging from 5.50 to 6.91: the acidity of imidazole groups increases with the positive charge of the peptide, as expected. Then, all the five ligands show very similar log*K* values for their terminal amino groups (7.62, 7.76, 7.71, 7.70 and 7.83). Under alkaline conditions, the log*K* values of the phenolic group of tyrosine residues fall in the range 9.34 - 9.60. Finally, the deprotonation of the most basic residues, lysines, occurs; although their log*K* values are rather high, they could be measured under the considered experimental conditions (pH range 2.5-10.5).

**Table 10.1** – Protonation constants for all the investigated ligands at $T$ = 298 K and $I$ = 0.1 M (KCl). Values in parentheses are standard deviations on the last significant figure.

| **Species** | **log*β*** | **log*K*** | **Residue** | **log*β*** | **log*K*** | **Residue** |
|---|---|---|---|---|---|---|
| | **vAIALKAAHYHTHKE (L1)** | | | **VaIALKAAHYHTHKE (L2)** | | |
| $HL^{2-}$ | 10.77(9) | 10.77 | Lys | 10.84(6) | 10.84 | Lys |
| $H_2L^{-}$ | 20.96(5) | 10.19 | Lys | 21.07(4) | 10.23 | Lys |
| $H_3L$ | 30.30(7) | 9.34 | Tyr | 30.67(5) | 9.60 | Tyr |
| $H_4L^{+}$ | 37.93(7) | 7.62 | $N_{term}$ | 38.43(5) | 7.76 | $N_{term}$ |
| $H_5L^{2+}$ | 44.77(7) | 6.85 | His | 45.28(5) | 6.85 | His |
| $H_6L^{3+}$ | 50.97(7) | 6.19 | His | 51.58(5) | 6.30 | His |
| $H_7L^{4+}$ | 56.54(7) | 5.58 | His | 57.08(5) | 5.50 | His |
| $H_8L^{5+}$ | 60.78(7) | 4.24 | Glu | 61.00(5) | 3.92 | Glu |
| $H_9L^{6+}$ | 63.50(7) | 2.72 | $C_{term}$ | 63.55(5) | 2.55 | $C_{term}$ |
| | **vaIALKAAHYHTHKE (L3)** | | | **vAILAKAAHYHTHKe (L4)** | | |
| $HL^{2-}$ | 10.94(8) | 10.94 | Lys | 10.87(8) | 10.87 | Lys |
| $H_2L^{-}$ | 21.13(5) | 10.19 | Lys | 21.23(4) | 10.36 | Lys |
| $H_3L$ | 30.57(7) | 9.44 | Tyr | 30.67(6) | 9.44 | Tyr |
| $H_4L^{+}$ | 38.28(7) | 7.71 | $N_{term}$ | 38.37(6) | 7.70 | $N_{term}$ |
| $H_5L^{2+}$ | 45.09(7) | 6.81 | His | 45.27(6) | 6.91 | His |
| $H_6L^{3+}$ | 51.35(7) | 6.27 | His | 51.57(6) | 6.29 | His |
| $H_7L^{4+}$ | 56.86(7) | 5.51 | His | 57.19(6) | 5.62 | His |
| $H_8L^{5+}$ | 60.84(8) | 3.98 | Glu | 61.26(6) | 4.07 | Glu |
| $H_9L^{6+}$ | 63.65(8) | 2.82 | $C_{term}$ | 64.06(6) | 2.80 | $C_{term}$ |
| | **vaIALKAAHYHTHke (L5)** | | | | | |
| $HL^{2-}$ | 10.87(8) | 10.87 | Lys | | | |
| $H_2L^{-}$ | 21.22(4) | 10.34 | Lys | | | |
| $H_3L$ | 30.80(6) | 9.58 | Tyr | | | |
| $H_4L^{+}$ | 38.63(6) | 7.83 | $N_{term}$ | | | |
| $H_5L^{2+}$ | 45.50(6) | 6.87 | His | | | |
| $H_6L^{3+}$ | 51.81(6) | 6.31 | His | | | |
| $H_7L^{4+}$ | 57.32(6) | 5.51 | His | | | |
| $H_8L^{5+}$ | 61.32(7) | 3.99 | Glu | | | |
| $H_9L^{6+}$ | 63.89(7) | 2.57 | $C_{term}$ | | | |

**Table 10.2** – Equilibrium constants and proposed coordination modes for Cu(II) and Zn(II) complexes at $T$ = 298 K and $I$ = 0.1 M (KCl). Values in parentheses are standard deviations on the last significant figure.

| Species | log$\beta$ | p$K_a$ | Coord. | log$\beta$ | p$K_a$ | Coord. |
|---|---|---|---|---|---|---|
| | **vAIALKAAHYHTHKE (L1)** | | | **VaIALKAAHYHTHKE (L2)** | | |
| $[CuH_6L]^{5+}$ | 55.6(1) | 4.2 | $N_{Im}$,$COO^-$ | 55.7(1) | 3.99 | $N_{Im}$,$COO^-$ |
| $[CuH_5L]^{4+}$ | 51.44(4) | 5.10 | $2N_{Im}$,$COO^-$ | 51.74(2) | 5.20 | $2N_{Im}$,$COO^-$ |
| $[CuH_4L]^{3+}$ | 46.33(5) | 5.96 | $3N_{Im}$ | 46.54(3) | 6.40 | $3N_{Im}$ |
| $[CuH_3L]^{2+}$ | 40.38(5) | 7.00 | $2N_{Im}$,$N^-$ | 40.14(4) | 6.93 | $2N_{Im}$,$N^-$ |
| $[CuH_2L]^{+}$ | 33.37(7) | 7.33 | $2N_{Im}$,$N^-$,$NH_2$ | 33.21(4) | 7.90 | $2N_{Im}$,$N^-$,$NH_2$ |
| [CuHL] | 26.04(6) | 9.23 | $2N_{Im}$,$2N^-$ | 25.31(4) | 9.76 | $2N_{Im}$,$2N^-$ |
| $[CuL]^-$ | 16.82(9) | 9.55 | $2N_{Im}$,$2N^-$ | 15.55(5) | 10.38 | $2N_{Im}$,$2N^-$ |
| $[CuH_{-1}L]^{2-}$ | 7.26(7) | - | $N_{Im}$,$3N^-$ | 5.17(5) | - | $N_{Im}$,$3N^-$ |
| $[CuH_{-3}L]^{4-}$ | -13.89(7) | - | $N_{Im}$,$3N^-$ | -17.2(2) | - | $N_{Im}$,$3N^-$ |
| | **vaIALKAAHYHTHKE (L3)** | | | **vAIALKAAHYHTHKe (L4)** | | |
| $[CuH_6L]^{5+}$ | - | - | - | 56.1(1) | 4.2 | $N_{Im}$,$COO^-$ |
| $[CuH_5L]^{4+}$ | 51.48(4) | 5.22 | $2N_{Im}$,$COO^-$ | 51.91(3) | 5.10 | $2N_{Im}$,$COO^-$ |
| $[CuH_4L]^{3+}$ | 46.26(5) | 6.18 | $3N_{Im}$ | 46.81(4) | 6.13 | $3N_{Im}$ |
| $[CuH_3L]^{2+}$ | 40.08(7) | 6.96 | $2N_{Im}$,$N^-$ | 40.68(4) | 7.03 | $2N_{Im}$,$N^-$ |
| $[CuH_2L]^{+}$ | 33.12(7) | 7.77 | $2N_{Im}$,$N^-$,$NH_2$ | 33.65(5) | 7.45 | $2N_{Im}$,$N^-$,$NH_2$ |
| [CuHL] | 25.35(7) | 9.40 | $2N_{Im}$,$2N^-$ | 26.19(5) | 9.33 | $2N_{Im}$,$2N^-$ |
| $[CuL]^-$ | 15.94(9) | 10.06 | $2N_{Im}$,$2N^-$ | 16.87(7) | 9.76 | $2N_{Im}$,$2N^-$ |
| $[CuH_{-1}L]^{2-}$ | 5.88(9) | - | $N_{Im}$,$3N^-$ | 7.11(6) | - | $N_{Im}$,$3N^-$ |
| $[CuH_{-3}L]^{4-}$ | -15.1(1) | - | $N_{Im}$,$3N^-$ | -13.85(6) | - | $N_{Im}$,$3N^-$ |
| | **vaIALKAAHYHTHke (L5)** | | | | | |
| $[CuH_5L]^{4+}$ | 52.11(3) | 5.28 | $2N_{Im}$,$COO^-$ | | | |
| $[CuH_4L]^{3+}$ | 46.84(4) | 6.13 | $3N_{Im}$ | | | |
| $[CuH_3L]^{2+}$ | 40.70(5) | 6.97 | $2N_{Im}$,$N^-$ | | | |
| $[CuH_2L]^{+}$ | 33.74(6) | 7.51 | $2N_{Im}$,$N^-$,$NH_2$ | | | |
| [CuHL] | 26.22(6) | 9.54 | $2N_{Im}$,$2N^-$ | | | |
| $[CuL]^-$ | 16.68(9) | 9.59 | $2N_{Im}$,$2N^-$ | | | |
| $[CuH_{-1}L]^{2-}$ | 7.09(7) | - | $N_{Im}$,$3N^-$ | | | |
| $[CuH_{-3}L]^{4-}$ | -14.64(8) | | $N_{Im}$,$3N^-$ | | | |
| | **vAIALKAAHYHTHKE (L1)** | | | **VaIALKAAHYHTHKE (L2)** | | |
| $[ZnH_5L]^{4+}$ | 48.5(1) | 5.4 | $2N_{Im}$,$COO^-$ | 48.8(1) | 5.5 | $2N_{Im}$,$COO^-$ |
| $[ZnH_4L]^{3+}$ | 43.08(3) | 7.11 | $3N_{Im}$ | 43.37(3) | 7.26 | $3N_{Im}$ |

| | | | | | | |
|---|---|---|---|---|---|---|
| $[ZnH_3L]^{2+}$ | 35.97(5) | 7.53 | $3N_{Im},OH^-$ | 36.11(5) | 7.61 | $3N_{Im},OH^-$ |
| $[ZnH_2L]^{+}$ | 28.44(4) | 8.51 | $3N_{Im},2OH^-$ | 28.50(3) | 8.83 | $3N_{Im},2OH^-$ |
| [ZnHL] | 19.93(5) | 9.43 | $3N_{Im},2OH^-$ | 19.67(5) | 9.59 | $3N_{Im},2OH^-$ |
| $[ZnL]^-$ | 10.50(5) | - | $3N_{Im},2OH^-$ | 10.08(4) | - | $3N_{Im},2OH^-$ |
| $[ZnH_{-2}L]^{3-}$ | -9.82(5) | - | $3N_{Im},2OH^-$ | -11.17(6) | - | $3N_{Im},2OH^-$ |

| | **VaIALKAAHYHTHKE (L3)** | | | **vAIALKAAHYHTHKe (L4)** | | |
|---|---|---|---|---|---|---|
| $[ZnH_5L]^{4+}$ | 48.72(7) | 5.49 | $2\ N_{Im},COO^-$ | 49.0(1) | 5.5 | $2\ N_{Im},COO^-$ |
| $[ZnH_4L]^{3+}$ | 43.23(2) | 7.08 | $3N_{Im}$ | 43.48(3) | 7.21 | $3N_{Im}$ |
| $[ZnH_3L]^{2+}$ | 36.15(3) | 7.69 | $3N_{Im},OH^-$ | 36.27(6) | 7.66 | $3N_{Im},OH^-$ |
| $[ZnH_2L]^{+}$ | 28.46(3) | 8.53 | $3N_{Im},OH^-$ | 28.61(4) | 8.55 | $3N_{Im},OH^-$ |
| [ZnHL] | 19.92(3) | 9.58 | $3N_{Im},2OH^-$ | 20.06(5) | 9.42 | $3N_{Im},2OH^-$ |
| $[ZnL]^-$ | 10.34(4) | 10.24 | $3N_{Im},2OH^-$ | 10.64(5) | - | $3N_{Im},2OH^-$ |
| $[ZnH_{-1}L]^{2-}$ | 0.10(5) | 10.81 | $3N_{Im},2OH^-$ | - | - | $3N_{Im},2OH^-$ |
| $[ZnH_{-2}L]^{3-}$ | -10.72(7) | - | $3N_{Im},2OH^-$ | -10.00(6) | - | $3N_{Im},2OH^-$ |

| | **vaIALKAAHYHTHke (L5)** | | |
|---|---|---|---|
| $[ZnH_5L]^{4+}$ | 49.38(7) | 5.43 | $2\ N_{Im},COO^-$ |
| $[ZnH_4L]^{3+}$ | 43.95(2) | 7.30 | $3N_{Im}$ |
| $[ZnH_3L]^{2+}$ | 36.64(3) | 7.89 | $3N_{Im},OH^-$ |
| $[ZnH_2L]^{+}$ | 28.76(3) | 8.62 | $3N_{Im},OH^-$ |
| [ZnHL] | 20.14(3) | 9.52 | $3N_{Im},2OH^-$ |
| $[ZnL]^-$ | 10.62(3) | - | $3N_{Im},2OH^-$ |
| $[ZnH_{-2}L]^{3-}$ | -10.19(5) | - | $3N_{Im},2OH^-$ |

a)

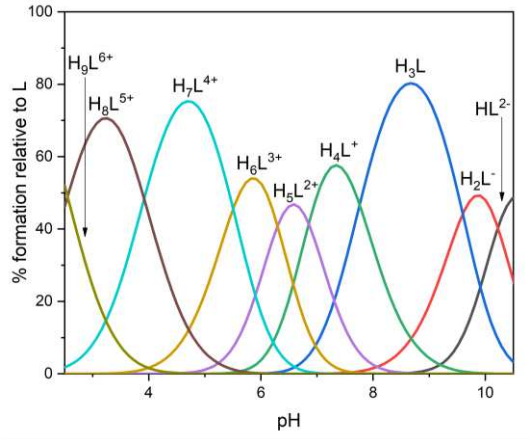


b)

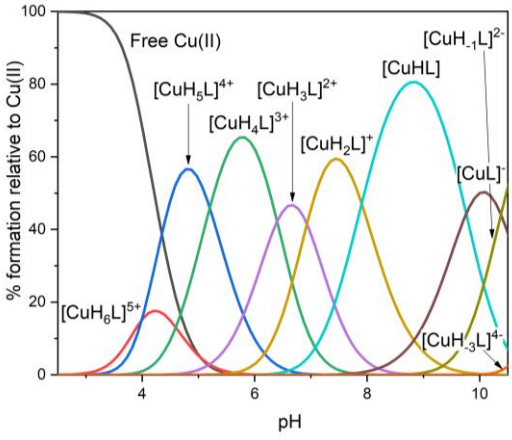

c)

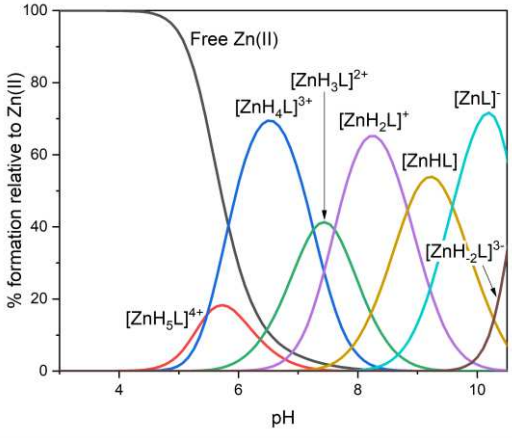


**Figure 10.3** – Representative species distribution diagrams for (a) ligand L2 and complex-formation of L2 with (b) Cu(II), (c) Zn(II), at $T = 298$ K and $I = 0.1$ M (KCl). $C_L = 5 \cdot 10^{-3}$ M and (b,c) M/L molar ratio 0.8:1.

a)

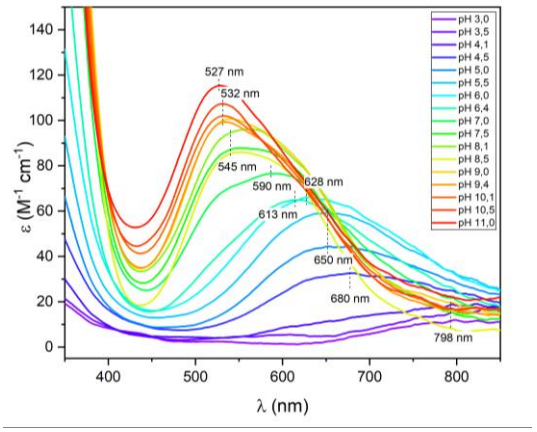


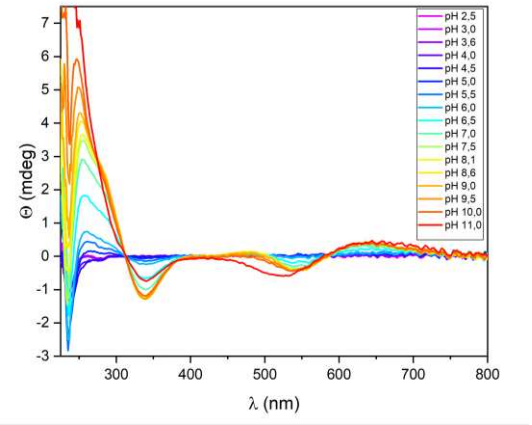


b)

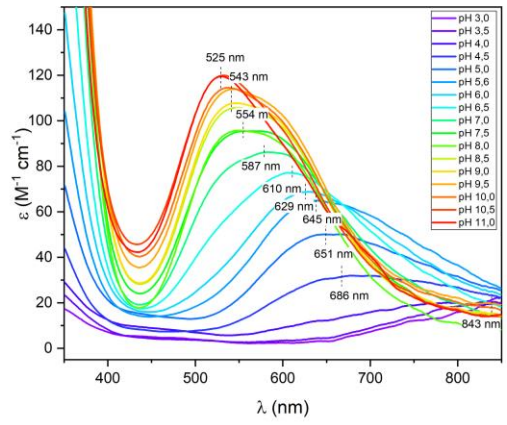


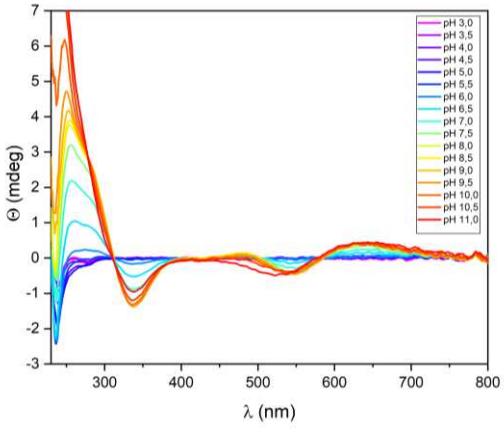

c)

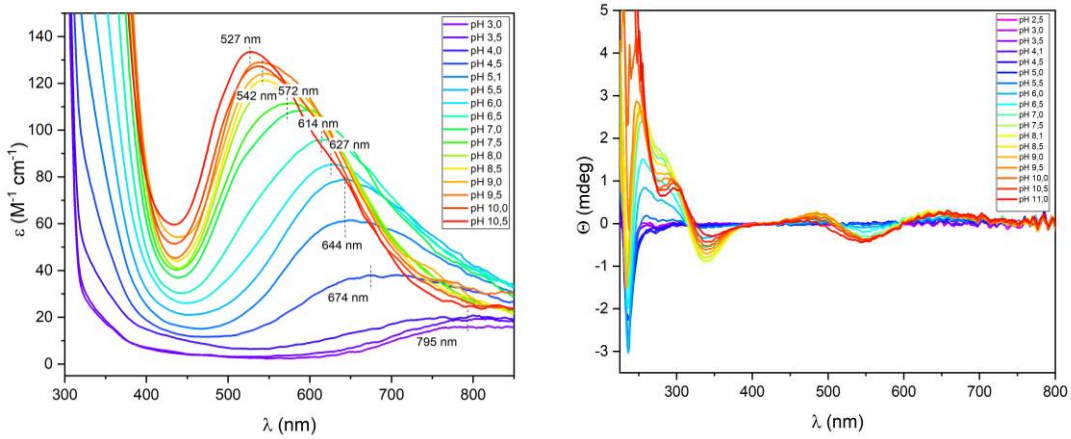


d)

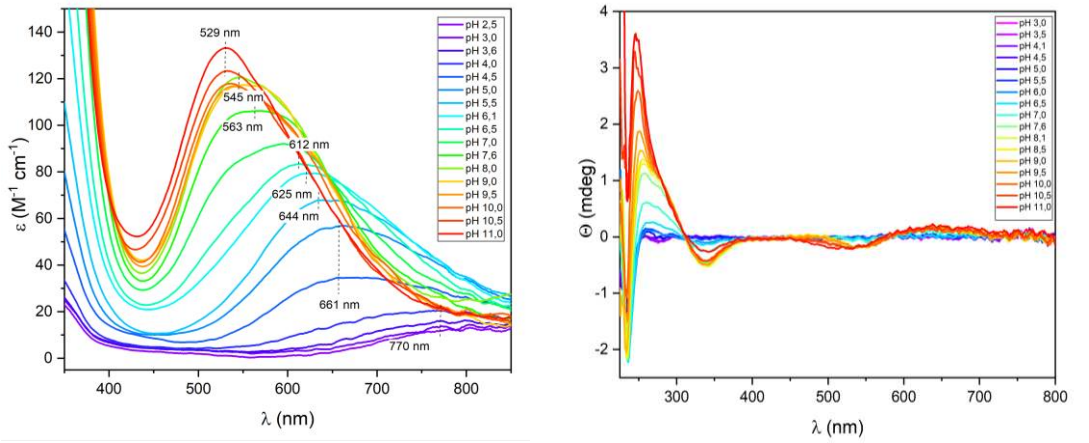


e)

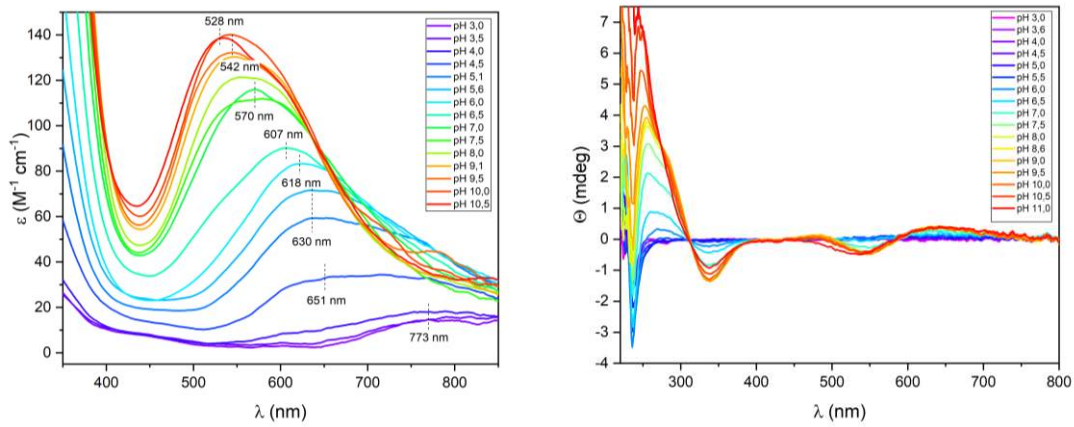


**Figure 10.4 –** Vis absorption (left) and CD spectra (right) of (a) Cu(II)/L1, (b) Cu(II)/L2, (c) Cu(II)/L3, (d) Cu(II)/L4 and (e) Cu(II)/L5 systems; M:L ratio = 0.8:1; $C_M = 0.4 \cdot 10^{-3}$ M, optical path 1 cm.

The formation of Cu(II) complexes in solution begins around pH 3 for all the studied ligands. The first complex detected by potentiometry is $[CuH_6L]^{5+}$ for L1, L2 and L4, and $[CuH_5L]^{4+}$ for L3 and L5. The stoichiometry of the two species suggests that one or two histidine

residues are involved in the coordination sphere, respectively. In the complexation, also one of the carboxyl groups of the C-terminal glutamic acid may participate, with the formation of a macrocycle. Increasing the pH values, the $[CuH_5L]^{4+}$ is rapidly substituted by the $[CuH_4L]^{3+}$ species, in which the interaction between Cu(II) and the ligands has led to the release of the proton of the third histidine (p$K_a$ = 5.10 for L1 and L4, 5.20 for L2, 5.22 for L3 and 5.28 for L5). The $[CuH_4L]^{3+}$ species ($3N_{Im}$ coordination) reaches its maximum of formation around pH 5.5-5.8 in all the studied ligands. The obtained wavelengths of maximum absorption at those pH range from $\lambda_{max}$ = 625 nm to $\lambda_{max}$ = 630 nm and agree with the expected $\lambda_{max}$ value of 627 nm[8] for a species with a $3N_{Im}$ coordination mode. Subsequently, the next two deprotonation steps lead to the formation of $[CuH_2L]^{+}$ species with a proposed coordination mode ($2N_{Im}$, $N^-$, $NH_2$) forming a 4N complex. The proposed coordination is supported by the UV-Vis and CD spectra (**Figure 10.4**). The coordination of the first backbone amide is clearly shown by the CD spectra. Specifically, the appearance of more intense CD bands above pH 6-6.5 confirms the binding of this amide to the copper ion. This stronger CD absorption is a common spectroscopic characteristic when a metal-binding event involves a nitrogen atom near the peptide-backbone chiral α-carbon. Additionally, the terminal amino group coordination is in accordance with the significantly lower deprotonation values acquired in the presence of the copper ion in comparison to those obtained in its absence. At higher pH, the formation of the [CuHL] species suggests the deprotonation and coordination of a second backbone amide, which most likely substitutes the terminal amino group in the equatorial plane of the complex, giving rise to a ($2N_{Im}$, $2N^-$) coordination mode. This species reaches its maximum of formation around pH 8.5, which is characterized by a $\lambda_{max}$ ranging from 542 to 545 nm, in good agreement with the expected[8] value of 539 nm for a species characterized by a ($2N_{Im}$, $2N^-$) coordination mode. No UV-Vis changes are visible in all the spectra until pH 10, indicating no changes in the coordination modes. In fact, the next deprotonation step is attributable to the release of a proton from the phenolic group of the tyrosine residue, which would not participate in the copper coordination sphere. At pH higher than 10, the $[CuH_{-1}L]^-$ species becomes predominant in solution. This corresponds to the deprotonation and binding of a third backbone amide to the copper ion. This change is spectroscopically confirmed by a remarkable shift in the UV-Vis spectra above pH 10, where the $\lambda_{max}$ reaches approximately 522 nm. This final value is indicative of a ($N_{Im}$, $3N^-$) coordination mode.[8] Finally, no additional changes are observed in the UV-Vis or CD spectra at higher pH values, suggesting no further changes in the complex coordination mode. In fact, the spontaneous release of protons from the lysine residues would occur without affecting the binding environment of copper ion.

In the case of zinc, the complexation starts around pH 4 with the first detected species $[ZnH_5L]^{4+}$, in which two histidine residues are already deprotonated and bound to the metal ion; one carboxyl group of the glutamic acid can take part in metal complexation. Increasing the pH value of the solution, zinc ion facilitates the deprotonation and the subsequent binding of the third histidine residue, leading to the formation of a ($3N_{Im}$, $COO^-$) or ($3N_{Im}$) species, with a tetrahedral geometry. Subsequently, one of the coordinated water molecules releases a proton, with p$K_a$ values ranging from 7.08 to 7.30, leading to a suggested coordination mode ($3N_{Im}$, $OH^-$). In the most alkaline pH range, we observed the deprotonation of four additional basic sites of the ligand, in the order: the terminal amino group (p$K_a$ ranging from 7.53 to 7.89), the tyrosine (p$K_a$ ranging from 9.42 to 9.59) and the two lysine residues. The

release of a proton from a second coordinated water molecule has also been detected, thus suggesting a change in geometry to a trigonal bipyramid.

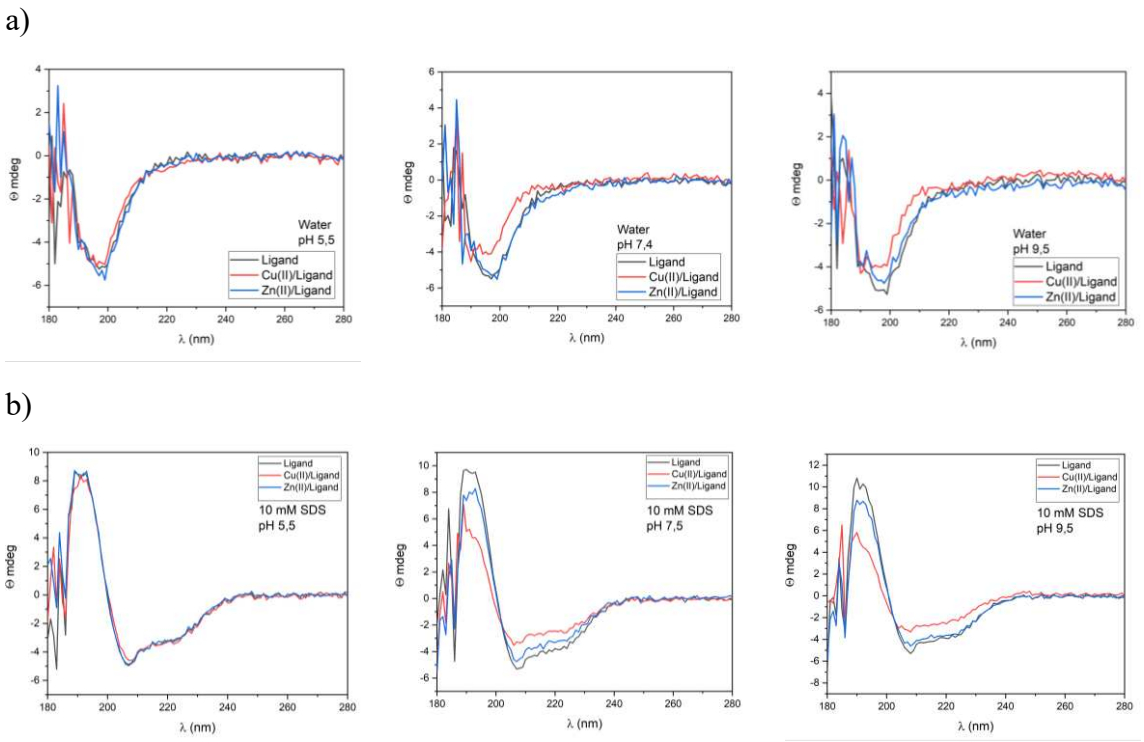


**Figure 10.5** – FAR-UV CD spectra of L4 derivative and its Cu(II) and Zn(II) complexes at $T$ = 298 K, in (a) aqueous solution and (b) SDS solution at different pH values; M:L ratio 1:0.8, $C_M = 0.08 \cdot 10^{-3}$ M, optical path 0.01 cm.

The second step of the present study was the investigation of the secondary structure of the apo-peptides and their metal-complexes, both in aqueous solution and in membrane-mimicking solvent (SDS), at different pH values. All derivatives behave in the same way, and the results obtained for L4 are reported here as an example (**Figure 10.5**). The spectra show that the peptide and its metal complexes present random coil conformation in aqueous solution at the all investigated pH values; in fact, the spectra are characterized by a negative ellipticity at a minimum of 195 nm. On the other hand, the peptide and its metal complexes are able to assume an α-helix conformation in a membrane-mimicking solvent (SDS), characterized by CD spectra with a positive ellipticity at a maximum of 193 nm and negative ellipticity at the double minimum of 208 and 222 nm. These results are in perfect agreement with those obtained for wild-type calcitermin, under the same experimental conditions.[7] The fact that, after the D-amino acid substitution at its termini, the peptide retained the α-helix structure in the SDS solution, has already been documented in literature with similar systems. [9]

Finally, we have evaluated the impact of D-amino acid substitutions on the peptide stability in human plasma, in comparison with the susceptibility of wild-type calcitermin (WT). When added to human plasma, the concentration of all peptides decreases with an approximately exponential decay and the following half-lives ($t_{1/2}$): WT 18 min, L1 144 min, L2 167 min, L3 144 min, L4 77 min and L5 462 min (**Figure 10.6**). D-amino acid substitution at the peptide termini is an effective strategy for boosting the resistance against

proteolytic degradation; in fact, all the peptidomimetics presents longer half-life compared to wild-type calcitermin. The single or double D-amino acid substitution at the N-terminal end increased the half-life by approximatively 8-fold, preventing the cleavage by aminopeptidases or dipeptidylaminopeptidases. The most efficient modification, however, involves the simultaneous substitution of the first two (N-terminal) and the last two (C-terminal) amino acids (L5 derivative), increasing dramatically the half-life by 26-fold. This result suggests that the substitution at the C-terminus effectively prevents carboxypeptidase activity. Most likely, replacing the lysine residue at the C-terminus with its corresponding D-isomer is sufficient to inhibit the activity of carboxypeptidase N, which typically cleaves basic amino acids like arginine and lysine.[10]

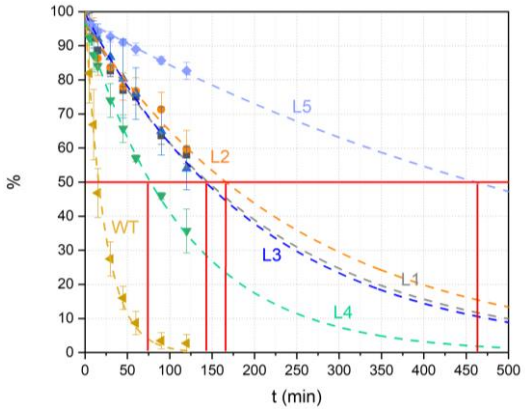


**Figure 10.6** – Stability of wild-type calcitermin (WT) and its derivatives vAIALKAAHYHTHKE (L1), VaIALKAAHYHTHKE (L2), vaIALKAAHYHTHKE (L3), vAIALKAAHYHTHKe (L4) and vaIALKAAHYHTHke (L5) in human plasma.

## 10.4 Conclusions

In conclusion, the strategic substitution of L-amino acids with their D-isomers at the peptide N- and/or C-terminus proved highly effective for increasing resistance to exo-peptidases (such as aminopeptidases and carboxylpeptidases). This modification substantially enhanced the peptide half-life, with improvements ranging from a 4-fold increase in the least favorable case to a remarkable 26-fold increase in the best one. However, from a thermodynamic perspective, the D-substitutions resulted in only a slight difference in overall complex stability towards Cu(II) (**Figure 10.7**). Specifically, the derivatives VaIALKAAHYHTHKE (L2) and vaIALKAAHYHTHKE (L3) exhibited the lowest metal binding affinity toward Cu(II), particularly under highly alkaline pH conditions. This diminished affinity is consistent with the observed higher deprotonations constants for the third amide nitrogen. Most likely, the D-substitutions on those specific positions, induce a small conformational change in the peptide, which increase the distance between the Cu(II) ion and the third amide nitrogen, making its deprotonation and subsequent binding energetically and sterically more difficult.[11]

Also in the case of the Zn(II) metal ion, the binding affinities of the D-peptidomimetics and wild-type calcitermin are comparable. The different percentage of formation between the peptides can be considered negligible.

a) b)

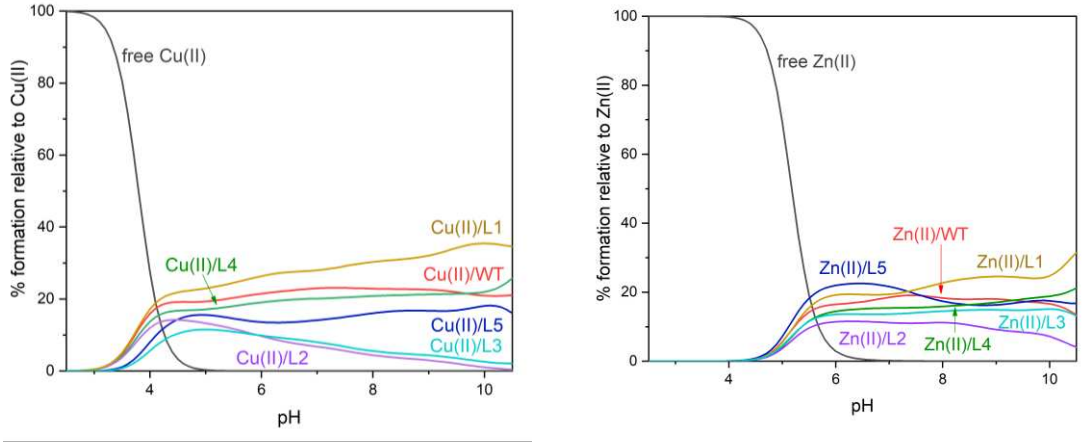


**Figure 10.7** – Competition plots for a solution containing equimolar concentrations ($1 \cdot 10^{-3}$ M) of metal ion, WT calcitermin, L1, L2, L3, L4 and L5. (a) Cu(II); (b) Zn(II).

The present study could be completed with the measurements of the antimicrobial activity of these calcitermin derivatives and the consequent comparison with other model peptides already reported in the literature.[9]

## 10.5 References


[1] Gill, T. J., Gould, H. J. & Doty, P., *Nature*, **1963,** *197*, 746-747.

[2] Bessalle, R., Kapitkovsky, A., Gorea, A., Shalit, I. & Fridkin, M., *FEBS letters*, **1990,** *274*, 151-155.

[3] Duarte, C. A., Cabrales, A., Echevarría, R., Paneque, T., Ramírez, A. C., Casillas, D., Sobrino-Iglesias, X., Garay, H., Besada, V. & Fernández-Ortega, C., *Biotechnology and applied biochemistry*, **2025,** *72*, 187-195.

[4] Lai, X., Tang, J. & ElSayed, M. E. H., *Expert Opinion on Drug Discovery*, **2021,** *16*, 1467-1482.

[5] Leveraro, S., D'Accolti, M., Marzola, E., Caselli, E., Guerrini, R., Rowinska-Zyrek, M., Remelli, M. & Bellotti, D., *Journal of Inorganic Biochemistry*, **2025,** *262*, 112761.

[6] D'Accolti, M., Bellotti, D., Dzień, E., Leonetti, C., Leveraro, S., Albanese, V., Marzola, E., Guerrini, R., Caselli, E., Rowińska-Żyrek, M. & Remelli, M., *Scientific Reports*, **2023,** *13*, 18228.

[7] Bellotti, D., Toniolo, M., Dudek, D., Mikołajczyk, A., Guerrini, R., Matera-Witkiewicz, A., Remelli, M. & Rowińska-Żyrek, M., *Dalton Transactions*, **2019,** *48*, 13740-13752.

[8] Sigel, H. & Martin, R. B., *Chemical Reviews*, **1982,** *82*, 385-426.

[9] Hong, S. Y., Oh, J. E. & Lee, K.-H., *Biochemical Pharmacology*, **1999,** *58*, 1775-1780.

[10] van der Velden, V. H. & Hulsmann, A. R., *Clinical and experimental allergy : journal of the British Society for Allergy and Clinical Immunology*, **1999,** *29*, 445-56.

[11] Wątły, J., Szarszoń, K., Sabieraj, M., Kola, A., Wieczorek, R., Janek, T. & Valensin, D., *Inorganic Chemistry*, **2025,** *64*, 6365-6377.

# 11. Chapter Eleven: Microplusin: a strong copper(II) chelator

## 11.1 Outline of the work

Microplusin is an antimicrobial peptide isolated from the cattle thick *Rhipicephalus microplus*. Structurally, microplusin consists of five α-helices with disordered N- and C-termini. It contains six cysteine residues forming three disulfide bonds and a histidine-rich region in both the N- and C-terminal domain.[1] This peptide shows a broad spectrum of activity, being effective against Gram-positive and Gram-negative bacteria, fungi and yeast at micromolar and submicromolar concentrations.[2] Different studies indicate that, while microplusin does not disrupt bacterial membranes, it acts as a potent chelator of copper ions, by implementing the nutritional immunity mechanism. Furthermore, microplusin has been shown to negatively affect cellular respiration in *Micrococcus luteus*, most likely through the removal of copper ions from heme-copper terminal oxidases.[3]

The peptide is initially expressed as a precursor, with a 20 amino acid-long N-terminal signal sequence. After reaching its final target, the signal sequence is cut and the mature peptide is obtained. In this work, we decided to study some short peptide fragments of this mature protein, corresponding to the N-terminal (HHQEL) and the C-terminal (DPEAHHEHDH) domains. Both terminal sequences are unfolded and rich in histidine residues and lie on the same side of the three-dimensional structure. Previous NMR studies suggest a preferred binding site in the N-terminus, however an unequivocal determination of the binding residues has not been obtained and the bioinorganic chemistry of microplusin still remains unraveled.

In the present investigation, we decided to study two distinct derivatives of the N-terminal domain. The first derivative, HHQEL-$NH_2$ (L1), incorporates the C-terminal amidation to emulate the mature peptide. The second derivative, Ac-HHQEL-$NH_2$ (L2), includes both C-terminal amidation and N-terminal acetylation. The acetylation has been introduced to mimic the presence of the signal sequence found in the precursor protein. The analysis of this acetylated derivative will allow us to assess the precursor potential for copper ion binding and determine its inherent antimicrobial activity prior to its processing into the mature peptide. In addition, we also studied the acetylated C-terminal domain, Ac-DPEAHHEHDH (L3), which mimics the mature peptide, as well.

## 11.2 Experimental procedure

Analyses performed on the above mentioned peptides follow the scheme:

- Potentiometric determination of the ligand protonation and Cu(II) complex-formation constants.
- Mass spectrometry analysis to evaluate ligand purity and the stoichiometry of the formed Cu(II) complexes.

- Spectrophotometric (UV-Vis and CD) analyses of Cu(II) complexes.
- FAR-UV CD spectroscopy to investigate the structural conformation of apo-peptides and Cu(II) complexes.

The employed experimental conditions, instruments and materials are reported in details in Leveraro *et al.*, 2025.[4] Peptides have been purchased and used without further purification.

## 11.3 Results and discussion

Speciation models for the studied peptides and their Cu(II) complexes have been obtained by potentiometric titrations. The protonation constants are reported in **Table 11.1**, while the complex-formation constants are reported in **Table 11.2** together with the suggested coordination environment for the formed species.

**Table 11.1** – Protonation constants for all the investigated ligands at $T$ = 298 K and $I$ = 0.1 M (KCl). Values in parentheses are standard deviations on the last significant figure.

| **Species** | **log*β*** | **log*K*** | **Residue** | **log*β*** | **log*K*** | **Residue** |
|---|---|---|---|---|---|---|
| | **HHQEL-NH$_2$ (L1)** | | | **Ac-HHQEL-NH$_2$ (L2)** | | |
| HL | 7.57(4) | 7.57 | $N_{term}$ | 6.86(5) | 6.86 | His |
| $H_2L^{+}$ | 13.77(4) | 6.21 | His | 12.83(5) | 5.98 | His |
| $H_3L^{2+}$ | 18.64(5) | 4.87 | His | 16.95(6) | 4.11 | Glu |
| $H_4L^{3+}$ | 21.69(5) | 3.04 | Glu | - | - | |
| | **Ac-DPEAHHEHDH (L3)** | | | | | |
| $HL^{4-}$ | 7.71(8) | 7.71 | His | | | |
| $H_2L^{3-}$ | 14.94(6) | 7.23 | His | | | |
| $H_3L^{2-}$ | 21.54(7) | 6.60 | His | | | |
| $H_4L^{-}$ | 27.21(7) | 5.67 | His | | | |
| $H_5L$ | 31.55(9) | 4.34 | Glu | | | |
| $H_6L^{+}$ | 35.41(9) | 3.86 | Glu | | | |
| $H_7L^{2+}$ | 38.70(9) | 3.29 | Asp | | | |
| $H_8L^{3+}$ | 41.1(1) | 2.4 | Asp | | | |
| $H_9L^{4+}$ | 43.1(1) | 2.0 | $C_{term}$ | | | |

**Table 11.2 –** Equilibrium constants and proposed coordination modes for Cu(II) complexes at $T$ = 298 K and $I$ = 0.1 M (KCl). Values in parentheses are standard deviations on the last significant figure.

| **Species** | **logβ** | **p*K*$_a$** | **Coord.** | **logβ** | **p*K*$_a$** | **Coord.** |
|---|---|---|---|---|---|---|
| | **HHQEL-NH$_2$ (L1)** | | | **Ac-HHQEL-NH$_2$ (L2)** | | |
| $[CuHL]^{2+}$ | 15.31(8) | 3.62 | $2N_{Im}$,$(COO^-)$/ $N_{Im}$,$NH_2$ | 11.26(9) | 4.97 | $N_{Im}$,$(COO^-)$ |
| $[CuL]^{+}$ | 11.69(5) | 5.80 | $2N_{Im}$,$NH_2$,$(COO^-)$ | 6.30(4) | 6.54 | $2N_{Im}$,$(COO^-)$ |

| | | | | | | |
|---|---|---|---|---|---|---|
| $[CuH_{-1}L]$ | 5.89(9) | 9.20 | $N_{Im},NH_2,N^-$ | -0.25(6) | 7.56 | $2N_{Im},N^-$ |
| $[CuH_{-2}L]$ | -3.3(1) | 10.4 | $N_{Im},2N^-$ | -7.80(6) | 8.61 | $N_{Im},2N^-,(N_{Im(ax)})$ |
| $[CuH_{-3}L]^{4-}$ | -13.7(1) | - | $3N^-$ $(N_{Im(ax)})$ | -16.41(7) | - | $3N^-$ $(N_{Im(ax)})$ |

| **Ac-DPEAHHEHDH (L3)** | | | |
|---|---|---|---|
| $[CuH_3L]$ | 26.14(7) | 4.60 | $N_{Im},COO^-$ |
| $[CuH_2L]^-$ | 21.54(4) | 5.36 | $2N_{Im}$ |
| $[CuHL]^{2-}$ | 16.19(4) | 6.17 | $3N_{Im}$ |
| $[CuL]^{3-}$ | 10.02(4) | 8.07 | $3\text{-}4N_{Im}$ |
| $[CuH_{-1}L]^{4-}$ | 1.95(7) | 8.68 | $3N_{Im},N^-,(N_{Im(ax)})$ |
| $[CuH_{-2}L]^{5-}$ | -6.72(6) | 9.06 | $3N_{Im},2N^-,(N_{Im(ax)})$ |
| $[CuH_{-3}L]^{3-}$ | -15.78(6) | - | $N_{Im},3N^-,(N_{Im(ax)})$ |

The speciation model obtained by potentiometry is supported by MS results: the formation, in solution, of 1:1 metal:ligand complexes, variously protonated, was observed, under the employed experimental conditions. Signals corresponding to different sodium or potassium adducts, together with the differently protonated free ligand and metal complexes have been detected. The most intense signals (*m/z* = 662.34, 704.35, z= +1 for the ligands L1 and L2, respectively; *m/z* = 633.25, z = +2 for L3) correspond to the free peptides, confirming their purity. Signals from the metal-containing solutions (*m/z* = 723.25, 765.26, z= +1, in the case of L1 and L2, respectively; *m/z* = 663.71, z= +2 for L3) correspond to the species $[CuL]^+$ (L1 and L2) and $[CuH_5L]^{2+}$. No poly-nuclear complexes or bis-complexes have been identified.

L1 and L2 differ only for the protection of the amino terminal group and thus the coordination processes are similar. The first detected species is $[CuHL]^{2+}$: its stoichiometry suggests that one histidine residue is already bound to the metal ion (L2). The already-deprotonated carboxyl group of glutamic acid could participate in the coordination sphere. In the case of L1, two different coordination modes are conceivable: in the first case two histidine residues are already bound to the metal ion (2 $N_{Im}$, $COO^-$); while in the second, the free amino terminal group and one histidine residue are involved in the coordination sphere, resulting in a ($N_{Im}$, $NH_2$) donor set, typical in case of histamine-like binding site ($NH_2$-Hxx). When pH is increased, copper ion promotes the release of a proton from the histidine or the free terminal amino group of the L1 derivative with a p*K*a of 3.62. Increasing the alkalinity of the solution, the progressive deprotonation and subsequent coordination of up to three backbone amide groups occur. This stepwise process of deprotonation and binding ultimately induces a conformational change of the complex, causing one histidine residue to move to an axial position relatively to the copper center. The coordination of an axial group in copper complexes generally causes a shift of the wavelength of maximum absorption towards lower energies (red-shift), which would justify the experimental $\lambda_{max}$ obtained (577 nm for L1 and 573 nm for L2, **Figure 11.2a**, **11.4a**) compared to the expected value of 563 nm for a ($3N^-$) complex.[5] The progressive binding of backbone amide is supported by the increasing intensity of CD bands at alkaline pH (**Figure 11.2b** and **Figure 11.4b**).

a) b)

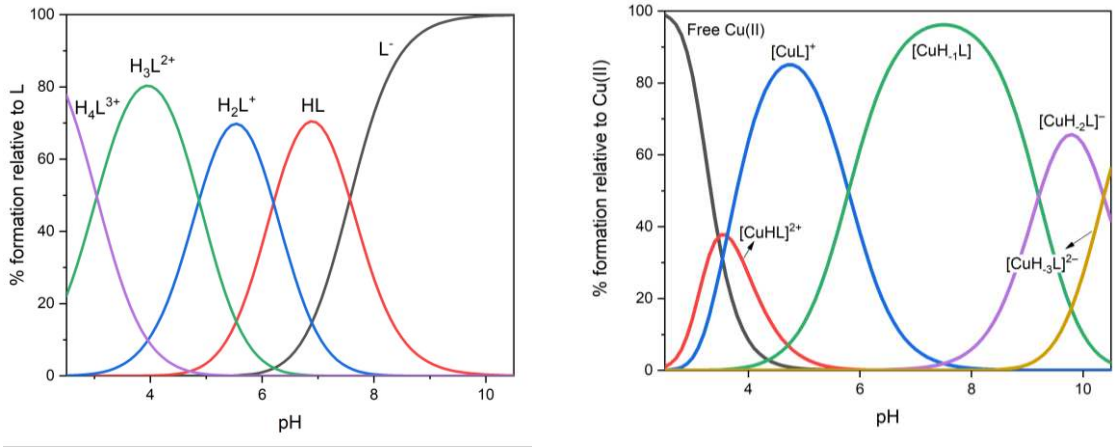


**Figure 11.1 –** Representative distribution diagram for the formation of (a) ligand species and (b) Cu(II) complexes with HHQEL-$NH_2$ at $T$= 298 K and $I$= 0.1 M (KCl); M:L molar ratio = 0.8:1.

a) b)

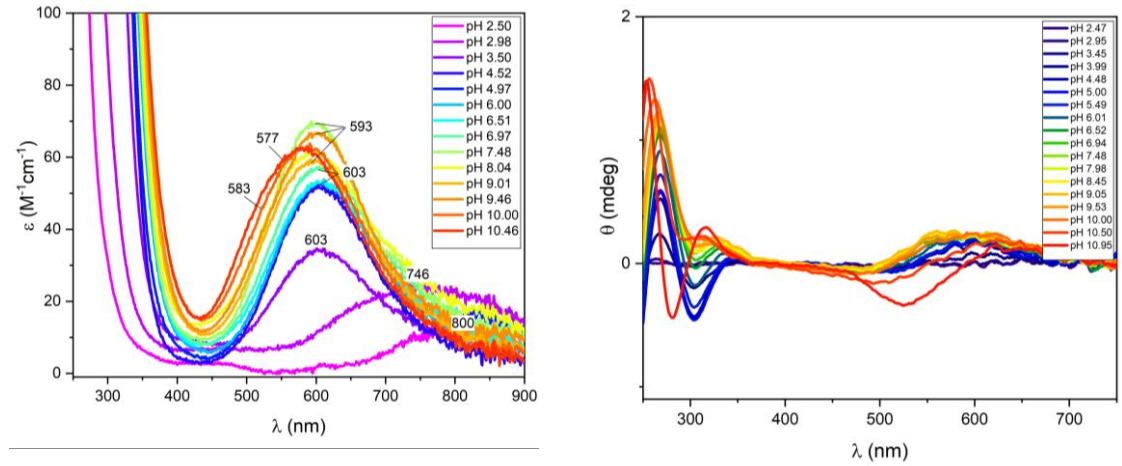


**Figure 11.2** – (a) Vis absorption spectra, (b) CD spectra of Cu(II)/HHQEL-$NH_2$ system; M:L ratio 0.8:1. $C_M = 0.4 \cdot 10^{-3}$ M, optical path 1 cm.

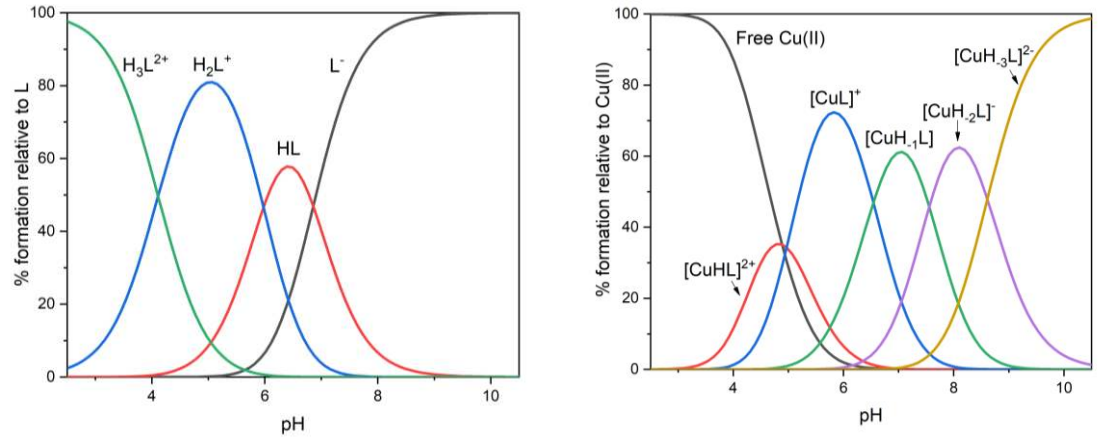

**Figure 11.3 –** Representative distribution diagram for the formation of (a) ligand species and (b) Cu(II) complexes with Ac-HHQEL-$NH_2$ at $T$= 298 K and $I$= 0.1 M (KCl); M:L molar ratio = 0.8:1.

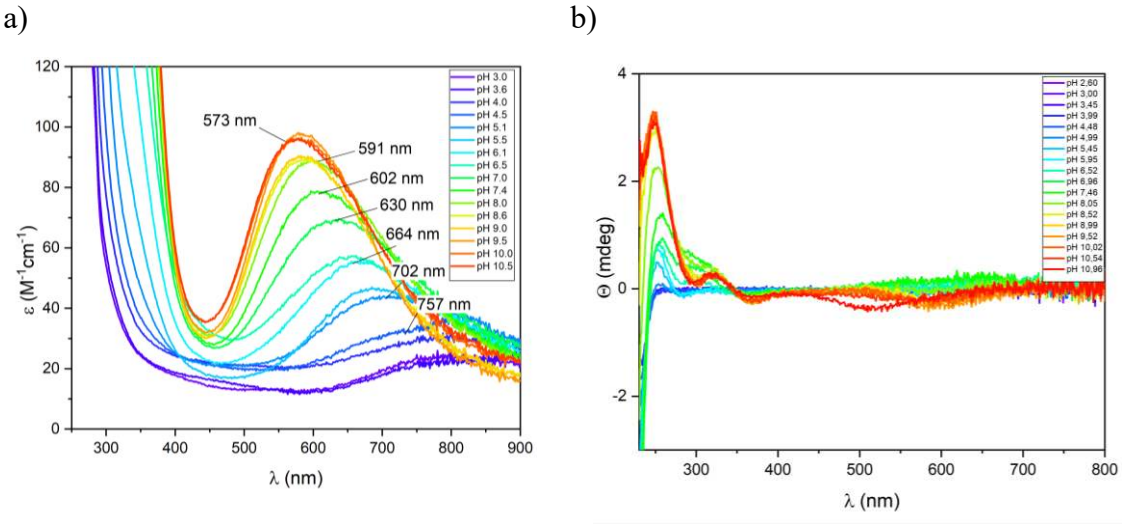


**Figure 11.4** – (a) Vis absorption spectra, (b) CD spectra of Cu(II)/Ac-HHQEL-$NH_2$ system; M:L ratio 0.8:1. $C_M = 0.4 \cdot 10^{-3}$ M, optical path 1 cm.

L3 corresponds to the C-terminal sequence of the mature microplusin. The copper complexation starts around pH 3.5, with the complex [$CuH_3L$]. According to its stoichiometry, the ligand has already lost six acidic protons from its fully protonated form, which should correspond to its most acidic residues (the terminal carboxyl group, two aspartic acid and two glutamic acid side chains, and one histidine residue). Therefore, the suggested coordination is ($1N_{Im}$, $n$$COO^-$), where one histidine residue and one (or more) carboxyl group(s) are bound to the metal ion. Increasing the solution pH, the complexation proceeds with the coordination of additional histidine residues. The species $[CuL]^{3-}$ is the most abundant in solution from pH 6 to pH 8. The UV-Vis absorption spectra recorded across this pH interval are characterized by a $\lambda_{max}$ that shifts from 629 nm to 564 nm. Those values suggests the coexistence in solution of two distinct coordination modes for the copper center. The ($3N_{Im}$) coordination mode involves the coordination of three imidazole nitrogens atoms from the histidine residues in the equatorial plane of the complex. The expected $\lambda_{max}$ for a ($3N_{Im}$) complex is 627 nm[5]. The second coordination mode is $4N_{Im}$ in which four imidazole nitrogen atoms are involved in the complexation in the equatorial plane of the complex (expected $\lambda_{max}$ for a ($4N_{Im}$) complex is 576 nm[5]). It cannot be excluded that the forth histidine binds to the metal centre in axial position. Finally, in more alkaline conditions, the deprotonation and binding of three backbone amides to copper ion occurs, which gradually substitute histidine residues in the equatorial plane of the complex. One histidine residue could be shifted to the axial position, justifying the recording of red shift in the UV-Vis spectra in the interested pH range (**Figure 11.6a**). From the recorded CD spectra (**Figure 11.6b**) is clearly visible the enhancement of the square planar geometry of the copper complexes as the nitrogen atoms coordinate to the copper ion.[6]

a) b)

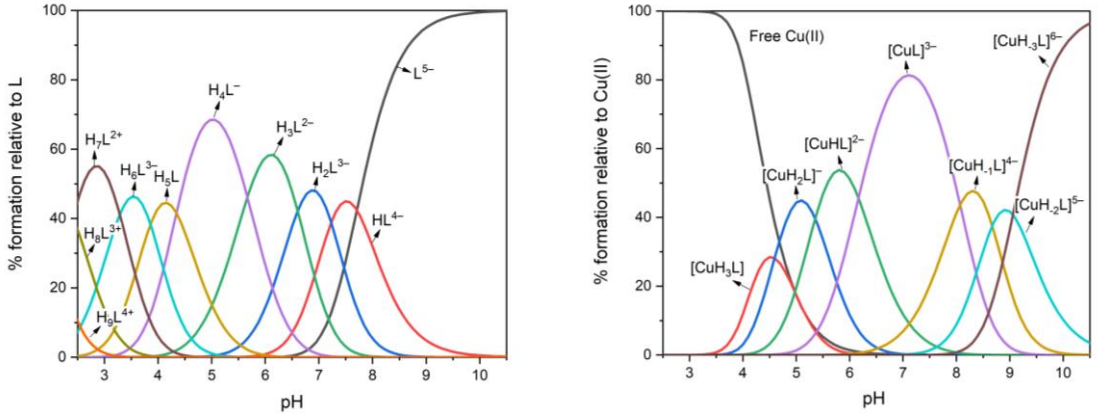


**Figure 11.5 –** Representative distribution diagram for the formation of (a) ligand species and (b) Cu(II) complexes with Ac-DPEAHHEHDH at *T*= 298 K and *I*= 0.1 M (KCl); M:L molar ratio = 0.8:1.

a) b)

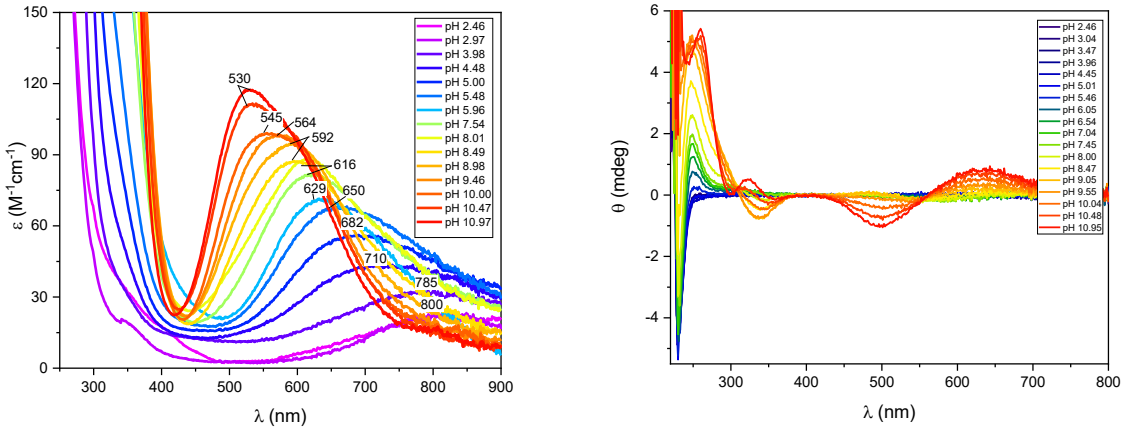


**Figure 11.6** – (a) Vis absorption spectra, (b) CD spectra of Cu(II)/Ac-DPEAHHEHDH system; M:L ratio 0.8:1. $C_M = 0.4 \cdot 10^{-3}$ M, optical path 1 cm.

FAR-UV CD measurements in aqueous solution and SDS solution of the apo-peptides and the copper complexes conducted at different pH values, revealed the presence of only random coil conformations, confirming the unstructured model of the N-and C-terminal domain (**Figure 11.7**).

a)

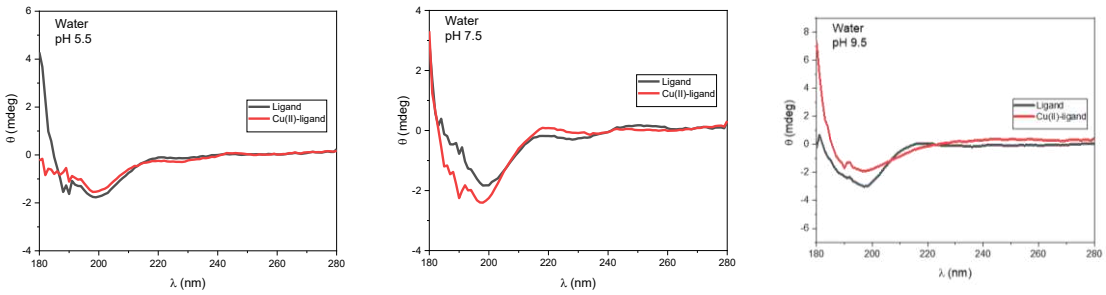

b)

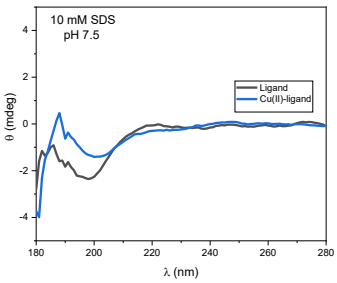


**Figure 11.7** – (a) Far-UV CD spectra of HHQEL-$NH_2$ (L1) and its copper complexes in aqueous solution at different pH values. (b) Far-UV CD spectra of HHQEL-$NH_2$ (L1) and its copper complexes in SDS solution at pH 7.5.M:L ratio 1:0.8, $C_M=0.1\cdot10^{-3}$ M, optical path 0.01 cm.

## 11.4 Conclusions

Microplusin is a natural antimicrobial peptide able to chelate Cu(II) metal ions and then also to induce pathogen starvation, thanks to the nutritional immunity mechanism. Previous studies suggest a preferred Cu(II) binding-site at the N-terminus although all the possible coordination modes of copper to the peptide were poorly defined.

All the peptides studied here proved to be efficient ligands for Cu(II) ions, although with different binding affinities. According to the competition diagram (**Figure 11.8**), the N-terminal domain of the mature peptide (L1: HHQEL-$NH_2$) exhibits by far the highest metal-binding affinity, with respect to the C-terminal domain and the N-terminal end of the precursor (L2: Ac-HHQEL-$NH_2$). This behavior can be ascribed to the differences in terms of coordination modes of the three derivatives: ($1N_{Im}$,$1N^-$,$1NH_2$) for HHQEL-$NH_2$, ($2N_{Im}$,$1N^-$) for Ac-HHQEL-$NH_2$ and (3-$4N_{Im}$) for Ac-DPEAHHEHDH, around pH 7.4. Notably, the N terminal mature peptide (L1) is the only one having the free amino terminal group, suggesting its significant impact on the stability of the complex. Although the precursor protein is able to coordinate copper ion in the same domain (HHQEL), the lower metal affinity suggests also a lower antimicrobial activity, compared to the mature peptide, with the mechanism of nutritional immunity.

The metal binding behavior of the microplusin fragments is fully consistent with the previously formulated hypotheses about the peptide biological role. The high efficacy of HHQEL in metal chelation is in line with the necessity to recover and stabilize as much micronutrients as possible from the medium, acting as a primary metal scavenger. The C-terminal domain is instead not the major ligand for Cu(II) ions, although it contains several histidine residues. It might modulate interactions with other targets (e.g. DNA, cell surfaces), by analogy to other histidine-rich peptides and to the structural similarity with the C-terminal domain of the α-subunit of bacterial RNA polymerase,[1] or it might be still involved in the process of copper acquisition by temporarily interact with the metal ion, supporting the primary binding-site and increasing the local concentration of copper, since both the N- and C-terminal tails lies on the same side of the peptide 3D-structure.

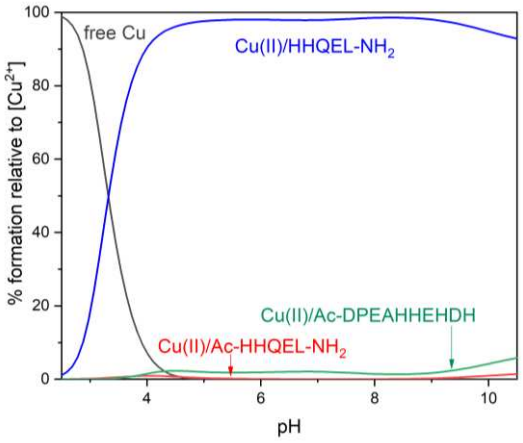


**Figure 11.8** – Competition plot for a solution containing equimolar concentrations ($1 \cdot 10^{-3}$ M) of HHQEL-$NH_2$, Ac-HHQEL-$NH_2$, Ac-DPEAHHEHDH and Cu(II).

## 11.5 References


[1] Silva, F. D., Rezende, C. A., Rossi, D. C., Esteves, E., Dyszy, F. H., Schreier, S., Gueiros-Filho, F., Campos, C. B., Pires, J. R. & Daffre, S., *The Journal of biological chemistry*, **2009,** *284*, 34735-46.

[2] Alexander, J. L., Thompson, Z. & Cowan, J. A., *ACS Chemical Biology*, **2018,** *13*, 844-853.

[3] Libardo, M. D. J. & Angeles-Boza, A. M., *Comments on Inorganic Chemistry*, **2014,** *34*, 42-58.

[4] Leveraro, S., D'Accolti, M., Marzola, E., Caselli, E., Guerrini, R., Rowinska-Zyrek, M., Remelli, M. & Bellotti, D., *Journal of Inorganic Biochemistry*, **2025,** *262*, 112761.

[5] Sigel, H. & Martin, R. B., *Chemical Reviews*, **1982,** *82*, 385-426.

[6] Stanyon, H. F., Cong, X., Chen, Y., Shahidullah, N., Rossetti, G., Dreyer, J., Papamokos, G., Carloni, P. & Viles, J. H., *The FEBS journal*, **2014,** *281*, 3945-54.

# 12. Chapter Twelve: Final conclusions/Future perspectives

Antimicrobial resistance (AMR) poses a growing and critical threat to global public health, severely challenging the successful prevention and treatment of persistent diseases. Despite numerous measures implemented over recent decades, this dangerous global trend continues unchecked, underscoring the urgent need for new antimicrobial drugs. In this context, naturally occurring antimicrobial peptides (AMPs) – widely distributed across the plant and animal kingdoms – hold great promise as novel therapeutics.

Unfortunately, AMPs present some significant drawbacks which hinder their clinical application, primarily due to decreased biological activity *in vivo* and high susceptibility to both human and pathogen proteolytic enzymes. This enzymatic activity transforms the active peptides into lower-molecular-weight oligopeptides, often leading to their inactivation. A widely accepted approach to overcome these drawbacks is to produce mutants with structural modifications with respect to the naturals AMPs. The resulting peptides, known as peptidomimetics, are designed to possess improved characteristics, such as enhanced resistance to degradation and longer half-lives. Common strategies for peptidomimetics design include terminal modifications (like N-acylation and/or C-amidation), cyclization or the substitution or incorporation of non-proteinogenic amino acids. The introduction of these non-canonical amino acids (e.g, D-amino acids, N-methyl-α-amino acids, β- and γ-amino acids or α-alkylated amino acids) is particularly effective as they are not typically recognized by natural enzymes. Considering these principles, our study has been focused on modifying the natural antimicrobial peptide calcitermin, present in the human airways, in order to improve its enzymatic stability and, as a consequence, its microbicidal activity. We achieved longer peptide half-lives by applying terminal protections and, in a separate case, substituting the L-amino acids at its termini with their D-isomer counterparts.

A key supplementary characteristic of antimicrobial peptides (AMPs) is their ability to chelate metal ions. These micronutrients are essential for pathogen growth and virulence, meaning that AMPs sequestration of these ions can induce pathogen starvation and death. Consequently, an effective strategy to boost a peptide microbicidal activity is to enhance its sequestering ability or modulate its structure and charge to optimize metal interaction. Following this strategy, we introduced several amino acid substitutions in the calcitermin sequence. The alanine-to-serine substitution has been adopted since serine residues can stabilize copper complexes through an electronic effect. Furthermore, we substituted alanine with either arginine or histidine: alanine-to-arginine replacement aims to increase the net positive charge of the peptide, and the alanine-to-histidine substitution has been performed to extend the functional metal-binding site within the peptide sequence.

To conclude the work, we decided to compare the thermodynamic stability of the best obtained calcitermin derivatives for each class of introduced substitutions. We choose the best obtained ligands for copper (VAIALKA<u>S</u>HYHTHKE, VAIALKA<u>R</u>HYHTHKE, <u>v</u>AIALKAAHYHTHKE and <u>Ac</u>-VAIALKAAHYHTHKE) and the best ligands obtained for

zinc (VAIALKSAHYHTHKE, VAIALKHAHYHTHKE, vAIALKAAHYHTHKE and Ac-VAIALKAAHYHTHKE) and we compared them with the wild-type calcitermin.

In case of copper ion binding (**Figure 12.1**), we observed the wild-type calcitermin (WT), the A8S derivative and the D-valine derivative exhibit comparable metal binding affinities. Interestingly, these three derivatives share an identical coordination behavior across the entire investigated pH range. On the other hand, the acetylated calcitermin showed a different coordination mode, resulting from the modification of the free N-terminal amino group, and, at the same time, it demonstrated the weakest metal binding affinity. The latter result strongly suggest the crucial role of the free N-terminus in determining the stability of the copper complexes. This observation is consistent with results on microplusin systems (see Chapter 11). Conversely, the A8R derivative presented a higher metal binding affinity across almost all the pH range. This enhanced performance is due to the substitution of an alanine with an arginine residue in position 8, which is hypothesized to exert a stabilizing effect through electrostatic interactions or even hydrogen bonding with the terminal carboxyl group, or weak interactions with coordinated solvent molecules.

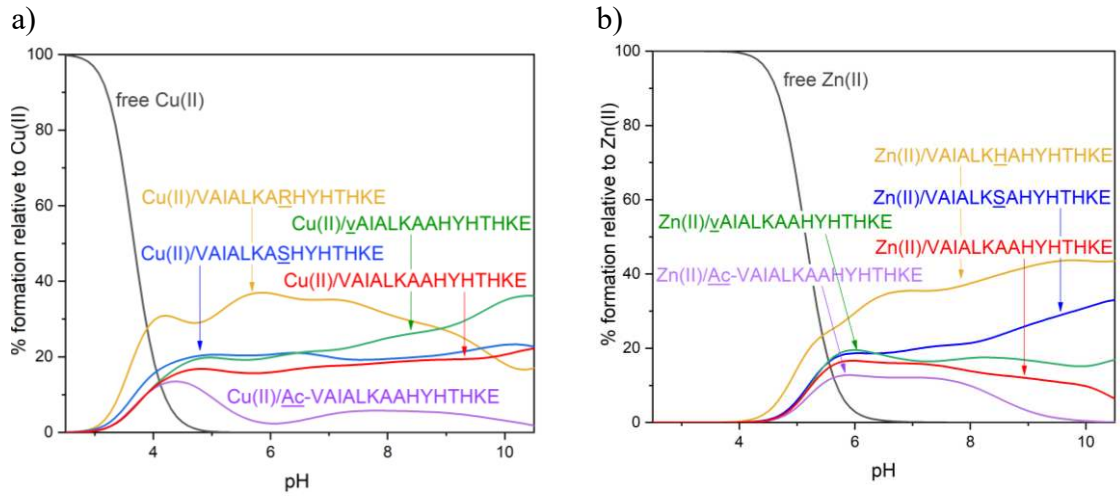


**Figure 12.1**- Competition plots for a solution containing equimolar concentrations ($1 \cdot 10^{-3}$ M) of (a) metal ion Cu(II), WT calcitermin, VAIALKASHYHTHKE (A8S), VAIALKARHYHTHKE (A8R), Ac-VAIALKAAHYHTHKE and vAIALKAAHYHTHKE; (b) metal ion Zn(II), WT calcitermin, Ac-VAIALKAAHYHTHKE, VAIALKHAHYHTHKE (A7H), VAIALKSAHYHTHKE (A7S) and vAIALKAAHYHTHKE.

In the case of the zinc ion binding, most derivatives displayed a very similar coordination behavior, which consistently involved three histidine residues and coordinated water molecules. The only derivative deviating from this pattern is A7H. This derivative exhibits the highest metal affinity across the entire pH range. The presence of a fourth histidine residue in the A7H sequence significantly enhanced its zinc-binding affinity, a result attributed to higher metal complex stability and the formation of a polymorphic binding state.

To conclude and provide an overview of the bioinorganic chemistry of copper coordination with peptides containing histidine residues, we compared the metal binding affinity of the natural peptides studied in this PhD thesis (calcitermin and microplusin) and the studied peptides with some natural ones from the literature. Calcitermin and microplusin, the two

peptides present different His patterns: WT calcitermin possesses three alternated histidines (-HxHxH-), while the microplusin C-terminal end contains four histidines with the following pattern, -HHxHxH-. As shown in **Figure 12.2a**, acetylated calcitermin and the microplusin C-terminal domain exhibit comparable metal binding affinities in the acidic pH range. The affinity is exactly equal at around pH 7, where the two peptides adopt the same coordination mode ($3N_{Im}$). At alkaline pH, in the case of microplusin, the coordination of the fourth histidine occurs, most likely to an axial position, slightly destabilizing the complex and hindering the coordination of the amide nitrogens which is shifted to significantly higher pH values, compared to calcitermin. This can be the explanation why the presence of the three-alternating-histidine-residues pattern (-HxHxH-) is a preferred structural motif for achieving optimal Cu(II) binding behavior and stability at alkaline pH, with the respect to the pattern (-HHxHxH-) (**Figure 12.2a**).

Furthermore, we extended our comparative analysis to five peptides, including WT calcitermin, the N-terminal end of microplusin (HHQEL-$NH_2$), the N-terminal domain of the Hpn protein secreted by *Helicobacter pylori* which bears the well-known ATCUN motif (MAHHEQHG-$NH_2$),[1] and two fragments of the human salivary peptide mucin7 (HHHQSPK[2] and HPDK[3]). The competition diagram (**Figure 12.2b**) shows that HHHQSPK is the best ligand across the entire pH range, due to the simultaneous presence of two highly favorable structural motifs: the canonical ATCUN motif ($NH_2$-xxH) and the histamine-like binding site ($NH_2$-Hxx). Also the coordination of HHQEL-$NH_2$ at acidic pH is very efficient, since it involves both the amino group and imidazole nitrogen of terminal histidine (histamine-like coordination), along with the second histidine residue and the first amide nitrogen. However, the subsequent coordination of the remaining two amide nitrogens only occurs at very alkaline pH values. In fact, among the other peptides, HHQEL-$NH_2$ exhibits the strongest binding affinity in acidic conditions, while MAHHEEQHG-$NH_2$ is the most effective ligand in alkaline conditions. The "pure" ATCUN peptide (MAHHEEQHG-$NH_2$), exhibits the best binding affinity above pH 7 compared to WT calcitermin, HPDK and HHQEL-$NH_2$. Finally, WT calcitermin and HPDK display the lowest overall ligand affinity for the Cu(II) ion across the entire pH range, suggesting that not only the number but, above all, the position of His residues in the peptide sequence rule its metal-binding affinity.

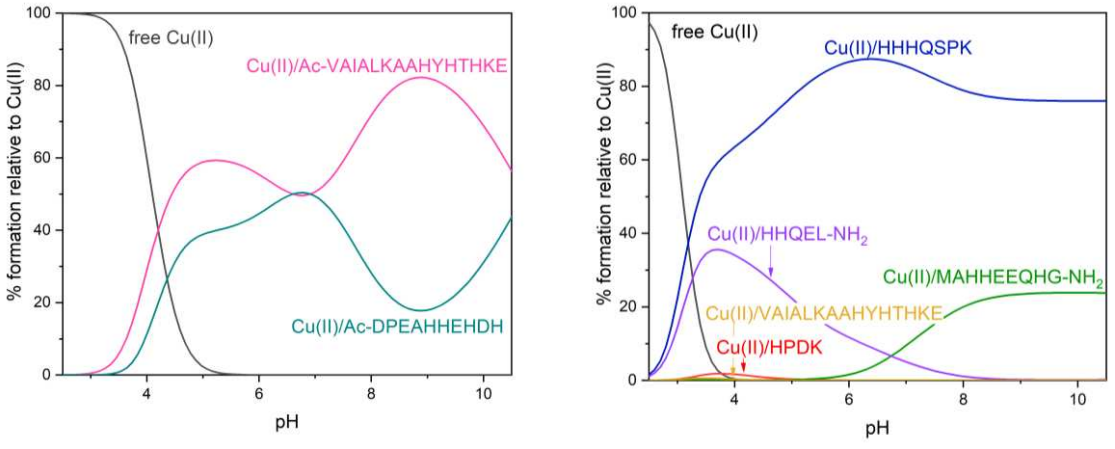


**Figure 12.2 -** Competition plots for a solution containing equimolar concentrations ($1 \cdot 10^{-3}$ M) of (a) metal ion Cu(II), WT calcitermin (VAIALKAAHYHTHKE) and the C-terminal

end of microplusin Ac-DPEAHHEHDH; (b) metal ion Cu(II), WT calcitermin (VAIALKAAHYHTHKE), HHHQSPK, HHQEL-$NH_2$ (microplusin), HPDK, MAHHEEQHG-$NH_2$.

Antimicrobial peptides (AMPs) represent a crucial resource for pharmacological innovation, offering a promising alternative to the development of traditional antimicrobial agents. Their distinguishing characteristics include a broad spectrum of activity, different mechanisms of action and low toxicity. The multi-way nature of their action significantly reduces the propensity of pathogens to develop resistance mechanisms. Of particular interest is the ability of many AMPs to coordinate metal ions, triggering the mechanism of nutritional immunity. In fact, the sequestration of essential micronutrients, such as copper Cu(II) or Zn(II), is fundamental for inhibiting pathogen growth.

Overall, we can affirm that this research project, aimed at the design and synthesis of peptidomimetics of the natural calcitermin, successfully achieved the goal of improving its thermodynamic and biological properties. We obtained some peptidomimetics with improved binding affinities for copper and zinc ions, which can translate into a stronger antimicrobial activity through to the nutritional immunity mechanism. Moreover, the adopted modification strategies led to proteolytically more stable derivatives, ensuring a greater *in vivo* half-life and extending the useful time for the therapeutic action to be exerted.

The most promising candidates for future pharmacological applications are listed below:

- Ac-VAIALKAAHYHTHKE, the calcitermin derivative acetylate at the N-terminus, exhibits a longer half-life compared to the wild-type calcitermin, and a great antimicrobial and antifungal activity, especially in the presence of the zinc metal ion.
- VAIALKARHYHTHKE (A8R) is more resistant to proteases than wild-type calcitermin, with a better binding affinity for the copper ion, and a greater antimicrobial activity against Gram-positive and Gram-negative bacteria in the presence of metal ions. The introduction of an additional positive charge (arginine) improves the peptide ability to exploit the bacterial membrane permeability.
- vaIALKAAHYHTHke (D-substitution): two L-amino acids have been substituted with their D-isomers at both the N- and C-termini thus improving the resistance to exo-peptidases. This peptidomimetic exhibits the same coordination modes as the native peptide. The expected antimicrobial results should not differ significantly from the wild-type, consistent with literature data that predict a limited impact for a very low number of amino acid substitutions.[4]

As for the antimicrobial activity of the investigated peptides, the results confirm a synergistic effect between the peptide and the metal, with, in some cases, a better performance of the metal complex itself. The great performance in the presence of Cu(II) ions support the hypothesis of an additional mechanism of action, based on the potential formation of hydroxyl radicals. This ability opens opportunities for applications not only in the antimicrobial field but also in oncology. Lastly, considering that the wild-type calcitermin peptide was previously successfully formulated into a topical gel for the treatment of *Candida albicans*,[5] the same formulation could be extended to selected peptidomimetics and/or their metal complexes aiming at a superior performance and further clinical developments.

## 12.1 References


[1] Bellotti, D., Sinigaglia, A., Guerrini, R., Marzola, E., Rowińska-Żyrek, M. & Remelli, M., *Journal of Inorganic Biochemistry*, **2021,** *214*, 111304.

[2] Szarszoń, K., Andrä, S., Janek, T. & Wątły, J., *Inorganic Chemistry*, **2024,** *63*, 11616-11627.

[3] Gawłowski, J., Ślusarczyk, A., Szarszoń, K., Zobi, F., Janek, T. & Wątły, J., *Dalton Transactions*, **2025,** *54*, 13257-13270.

[4] Hong, S. Y., Oh, J. E. & Lee, K.-H., *Biochemical Pharmacology*, **1999,** *58*, 1775-1780.

[5] Bellotti, D., D'Accolti, M., Pula, W., Huang, N., Simeliere, F., Caselli, E., Esposito, E. & Remelli, M., *Gels (Basel, Switzerland)*, **2023,** *9*.

# Annexes

The full version of the published journal articles are reported as annexes.

Inorganic Chemistry

pubs.acs.org/IC Article

# Metal-Induced Amide Deprotonation and Binding Typical for Cu(II), Not Possible for Zn(II) and Fe(II)

Silvia Leveraro, Valentyn Dzyhovskyi, Kinga Garstka, Agnieszka Szebesczyk, Fabio Zobi, Denise Bellotti,* Kamila Stokowa-Sołtys,* Maurizio Remelli,* and Magdalena Rowińska-Żyrek*

Cite This: https://doi.org/10.1021/acs.inorgchem.5c00672 Read Online

ACCESS | Metrics & More | Article Recommendations | Supporting Information

**ABSTRACT:** Amide groups of the peptide backbone are very weak acids. In fact, their deprotonation in water solution is not a phenomenon usually observed in the measuring range of a glass electrode unless the proton is displaced by a metal such as Cu(II) or Ni(II). Other metals are not usually expected to deprotonate and bind to amide nitrogens, although, lately, some controversies have started to arise in the literature, suggesting that Zn(II) and Fe(II) may be capable of doing so. In order to clarify this phenomenon, we chose to study simple metal−peptide systems with Ala-to-Pro mutations, which excluded further amides from binding. A comparison of the metal-binding modes of Ac-AAAHAAA-$NH_2$, Ac-AAPHAAA-$NH_2$, and Ac-AAPHPAA-$NH_2$ complexes with Cu(II), Zn(II), and Fe(II) is a simple and elegant way of showing that neither Zn(II) nor Fe(II) is able to deprotonate and bind to amide nitrogens.

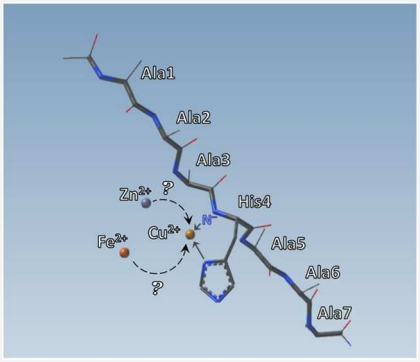


## INTRODUCTION

Metal−protein interactions are an intensively studied field and can be regarded as one of the main pillars of bioinorganic chemistry. In particular, the knowledge of the peculiarities of Zn(II) and Cu(II) binding to proteins and peptides is a topic that has been expanding for several decades,[1−7] while the studies on the thermodynamics of Fe(II) to peptide binding have only recently gained some attention, and the data available on Fe(II)−peptide interactions is very sparse.[8−11]

The amide dissociation constant ($pK_a$) depends on its chemical environment, usually reaching values in the range of 15−18.[12] Cu(II) and Ni(II) ions are known to lower the amide $pK_a$: in fact, these metal ions can displace the amide proton and bind the amide nitrogen at a relatively low pH value (usually pH > 6.0 for Cu(II) and >9.5 for Ni(II) complexes).[13−15] Typically, the metal ion anchors on a histidine imidazole ring in the acidic pH range; at a higher pH, it deprotonates and binds the nitrogen atom of the amide group that belongs to the same histidine, i.e., the amide group preceding the His residue in the N-terminal direction. At higher pH, further preceding amide groups can be involved in complexation, forming thermodynamically stable five-membered and six-membered fused chelate rings.[16−18]

Proline is the only natural amino acid having a secondary amino nitrogen: proline is technically an imino acid. Its presence in the peptide chain results in a peptide bond that does not contain a replaceable amide proton. As a consequence, the introduction of proline in the peptide sequence serves as a so-called "breaking point", making the typical stepwise coordination of consecutive amide nitrogens impossible.[19] It is worth noting that, in the presence of a "breaking proline" before histidine, i.e., in the N-terminal direction, the deprotonation/coordination of amide nitrogens by the metal ion can proceed in the opposite (C-terminal) direction, as it happens for the Prion protein,[20] although the formed metal chelates have reduced stability.

In recent years, contradictory opinions have started to emerge about the capability of other divalent metal ions to bind amide nitrogens. Intrigued by several literature discussions on the possibility of Zn(II)-induced amide deprotonation and binding[21−23] and by our own preliminary findings on the possible Fe(II)−amide binding,[8,9] we wanted to understand if Zn(II) and/or Fe(II) are indeed able to deprotonate amide nitrogens. We decided to study metal complexes of a simple model system based on an N-terminally and C-terminally protected ligand with one histidine only (AHA, (Ac-AAAHAAA-$NH_2$)). We substituted the neighboring alanines with prolines (PHA (Ac-AAPHAAA-$NH_2$) and PHP (Ac-AAPHPAA-$NH_2$)) in order to make sure that amide coordination will not proceed in the N-terminal or C-terminal direction.

Received: February 12, 2025
Revised: March 2, 2025
Accepted: March 7, 2025

## RESULTS AND DISCUSSION

Under the experimental conditions employed here, only variously protonated mononuclear complexes with a metal/ligand stoichiometry of 1:1 have been detected by potentiometry and mass spectrometry. Precipitation of copper hydroxide has been observed only in the case of copper with the PHP peptide around pH 7.5, while precipitation of iron hydroxide has been observed with all three peptides around pH 9.5.

**Ligand Protonation.** For each peptide, the obtained protonation *macro*-constants are reported in Table 1; the complete set of thermodynamic parameters, obtained by potentiometry and calorimetry, is shown in Table S1. The L symbol indicates the ligand in its unprotonated form, i.e., when all its dissociable protons (in the explored pH range) have been released. The investigated peptides **AHA** (Ac-AAAHAAA-$NH_2$), **PHA** (Ac-AAPHAAA-$NH_2$), and **PHP** (Ac-AAPHPAA-$NH_2$) have the N- and C-terminal ends modified through acetylation and amidation, respectively. Each of them presents only one deprotonable site, represented by the histidine residue. Once completely deprotonated, the ligands are neutral (L). All of the thermodynamic parameters concerning ligand protonation equilibria are in good agreement with literature values for similar systems[24] and show reasonable similarities among the considered peptides.

**Table 1. Protonation Constant ($K$) for the Investigated Ligands (AHA, PHA, and PHP) at $T$ = 298 K and $I$ = 0.1 M (NaCl)[a]**

| | species | log $K$ | residue |
|---|---|---|---|
| Ac-AAAHAAA-$NH_2$ (**AHA**) | $\mathbf{HL^+}$ | 6.47(1) | His |
| Ac-AAPHAAA-$NH_2$ (**PHA**) | $\mathbf{HL^+}$ | 6.43(1) | His |
| Ac-AAPHPAA-$NH_2$ (**PHP**) | $\mathbf{HL^+}$ | 6.56(2) | His |

[a]Standard deviations on the last significant digit are listed in parentheses.

**Cu(II) Complexes.** The investigated systems are able to form Cu(II) complexes in a stoichiometric ratio of 1:1 under the employed experimental conditions (Tables 2 and S1 in SI). The identified MS signals align closely with equimolar Cu(II) complexes ($m/z$ = 343.12, 356.13, and 369.14, $z$ = 2+ for the AHA, PHA, and PHP ligands, respectively); the experimental signals were compared with the corresponding simulated isotopic patterns, showing perfect alignment (Figures S1−S3 in SI). Furthermore, all measured mass spectra displayed signals corresponding to the ligands and their sodium or potassium adducts.

The formation of copper complexes in solution begins around pH 4 for all of the studied ligands (see distribution diagrams reported in Figures S4−S6 in SI). The first complex detected by potentiometry is always $[CuL]^{2+}$: the stoichiometry of this species indicates that histidine is already deprotonated and thus coordinated to copper. This species is 1N ($N_{Im}$), with the other coordination positions of the metal ion being saturated by water molecules. The complex $[CuL]^{2+}$ reaches its maximum of formation around pH 5.8 with **AHA** and pH 6.3 with **PHA** and **PHP**. The experimental wavelengths of maximum absorption ($\lambda_{max}$ = 767 nm for **AHA** at pH 5.0, $\lambda_{max}$ = 766 nm for **PHA** at pH 6.0, and $\lambda_{max}$ = 762 nm for **PHP** at pH 6.0; Figure 1) are in good agreement with the expected value for a coordination ($1N_{Im}$) (expected $\lambda_{max}$ = 760 nm).[12] Increasing the pH value, in the case of **AHA**, the first and the second amide deprotonate and coordinate copper almost simultaneously: the complex $[CuH_{-1}L]^+$ is quickly substituted with the $[CuH_{-2}L]$ species, which is, by far, the most abundant complex in a solution with pH of 6.3 up to 8.3. These two steps ($pK_a$ = 6.08 and $pK_a$ = 6.13; Table 2) are accompanied by a shift in the visible absorption spectra toward shorter wavelengths, thus indicating an increase in the number of coordinated nitrogen atoms around Cu(II) (Figure 1A). The experimental wavelength of the maximum absorption at pH 8 is 602 nm, only a little bit higher than the predicted value for a ($N_{Im}$, $2N^-$) coordination mode (583 nm).[12,25] Finally, the last detected complex is $[CuH_{-3}L]^-$, which is characterized by $pK_a$ = 8.68. The visible spectra in the alkaline pH range suggest the coordination of a third amide. The formation of that species causes a clear blue-shift of the vis-absorption band to $\lambda_{max}$ = 517 nm, which almost perfectly agrees with the expected literature value (522 nm)[12] for the ($N_{Im}$, $3N^-$) coordination mode with a square planar geometry. Moreover, the shape and intensity of the CD signal in the pH range 9.0−11.0 (Figure 2A) show a negative Cotton effect at 490 nm and a positive Cotton effect at 624 nm, along with, in the UV region, a positive band at 314 nm (distinctive of a $N_{amide}^- \rightarrow$ Cu(II) charge transfer[26]), consistent with the suggested ($N_{Im}$, $3N^-$) coordination mode. In addition, the 4N binding mode for $[CuH_{-3}L]^-$ is also confirmed by electron paramagnetic resonance (EPR) results at pH 10 ($g_{II}$ = 2.19, $A_{II}$ = 197; (Figure 3A and Table S2 in SI).[27] The coordination path described above and the corresponding donor-atom sets are also supported by complex-formation enthalpies (Table S1 in SI), which, in turn, are in excellent agreement with literature

**Table 2. Equilibrium Constants and the Proposed Coordination Modes for Cu(II) Complexes at $T$ = 298 K and $I$ = 0.1 (NaCl)[a]**

| | species | log $\beta$ | $pK_a$ | equatorial coordination |
|---|---|---|---|---|
| Ac-AAAHAAA-$NH_2$ (**AHA**) | $\mathbf{[CuL]^{2+}}$ | 3.44(6) | 6.07 | $N_{Im}$ |
| | $\mathbf{[CuH_{-1}L]^+}$ | −2.63(3) | 6.14 | $N_{Im}$, $N^-$ |
| | $\mathbf{[CuH_{-2}L]}$ | −8.77(1) | 8.68 | $N_{Im}$, $2N^-$ |
| | $\mathbf{[CuH_{-3}L]^-}$ | −17.45(2) | | $N_{Im}$, $3N^-$ |
| Ac-AAPHAAA-$NH_2$ (**PHA**) | $\mathbf{[CuL]^{2+}}$ | 3.56(4) | | $N_{Im}$ |
| | $\mathbf{[CuH_{-2}L]}$ | −9.65(2) | 9.73 | $2N^-$ |
| | $\mathbf{[CuH_{-3}L]^-}$ | −19.38(2) | | $3N^-$ |
| Ac-AAPHPAA-$NH_2$ (**PHP**) | $\mathbf{[CuL]^{2+}}$ | 3.81(5) | | $N_{Im}$ |
| | $\mathbf{[CuH_{-2}L]}$ | −9.66(3) | | $N_{Im}$, $N^-$, $OH^-$ |

[a]Values in parentheses are standard deviations on the last significant digit.


https://doi.org/10.1021/acs.inorgchem.5c00672
Inorg. Chem. XXXX, XXX, XXX−XXX

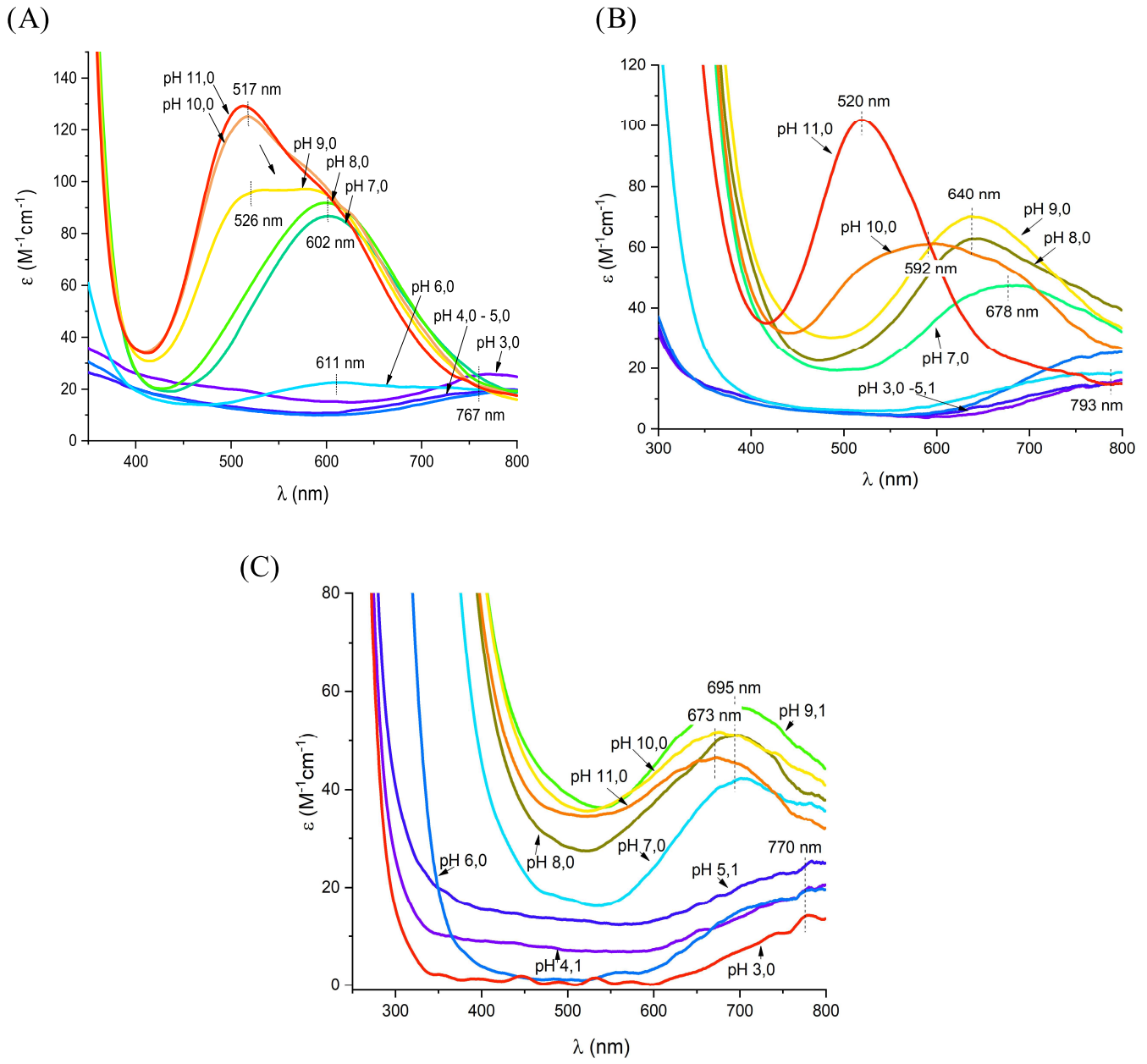


**Figure 1.** UV−vis absorption spectra of Cu(II) complexes with (A) **AHA**, (B) **PHA**, and (C) **PHP** at different pH values: M:L 0.9:1, $C_M$ = 0.45 × $10^{-3}$ M, optical path 1 cm. The wavelength of the maximum absorption is reported for each vis-absorption spectrum.

data for analogous peptides.[28] Lastly, on the basis of the wide available literature on Cu(II)/peptide complexes,[20,29−32] although in the absence of direct evidence, we can reasonably suggest that the progressive amide coordination proceeds in the N-terminal direction, starting from the His anchoring site.

In the case of **PHA**, the $[CuH_{-1}L]^+$ species has not been detected by potentiometry, while the formation of the $[CuH_{-2}L]$ complex was observed, starting from pH 6 and involving almost all of the Cu(II) ions around pH 8. The stoichiometry of this species implies the deprotonation/coordination of two amide nitrogens, necessarily in the C-terminal direction (starting from the His residue to which the metal ion is anchored), due to the presence of proline before His. Indeed, the value of $\lambda_{max} \approx 640$ nm suggests a ($2N^-$) coordination mode in the equatorial plane of the complex (expected $\lambda_{max}$ value: 633 nm);[12] the imidazole nitrogen, already bound to the metal ion should be shifted to an axial position of the distorted octahedron, justifying the observed red-shift between the experimental and expected $\lambda_{max}$ values.[12] Two water molecules complete the equatorial coordination. Finally, at alkaline pH values, a last deprotonation step has been observed with a $pK_a$ = 9.73; all of the spectroscopic parameters suggest the coordination of a further amide nitrogen (available in the C-terminal direction). In addition, the $\Delta H°$ value for the formation of the $[CuH_{-3}L]^-$ species (76 kJ/mol; Table S1 in SI) is practically identical to the corresponding one of AHA (73 kJ/mol; Table S1 in SI), suggesting the same donor-atom set, most likely with the imidazole in the axial position.

As for the last peptide, **PHP**, potentiometric and calorimetric measurements have been performed only up to pH 7.5 due to copper hydroxide precipitation. In this case, the


https://doi.org/10.1021/acs.inorgchem.5c00672
Inorg. Chem. XXXX, XXX, XXX−XXX

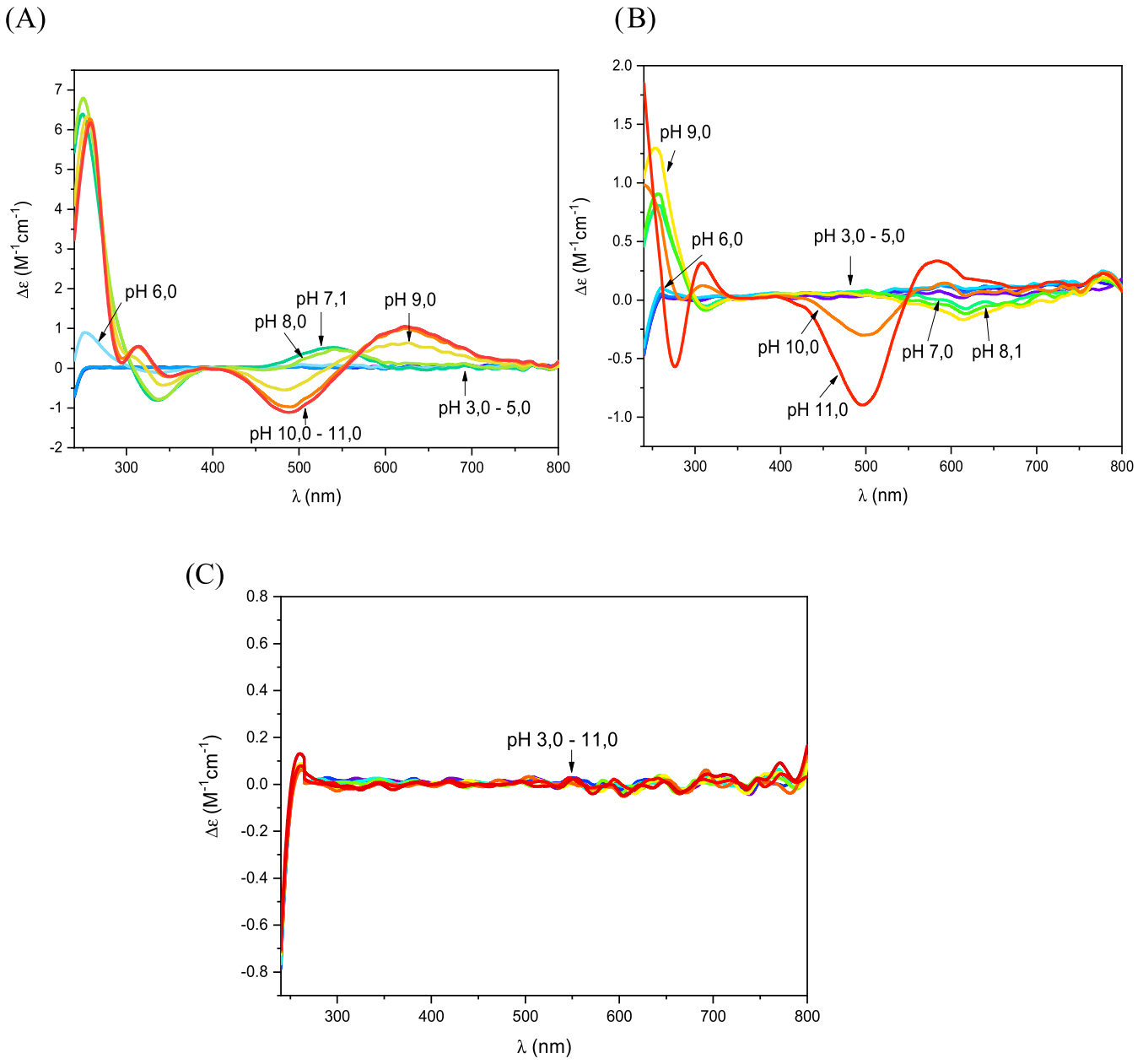


**Figure 2.** CD spectra of Cu(II) complexes with (A) **AHA**, (B) **PHA**, and (C) **PHP** at different pH values: M:L ratio 0.9:1, $C_M = 0.44 \times 10^{-3}$ M, optical path 1 cm.

two alanines adjacent to the histidine (positions 3 and 5) have been replaced with prolines, and only one backbone amide is available next to the coordinated histidine in the N-terminal direction. As in the previous peptide, after the coordination of imidazole nitrogen with the formation of the $[CuL]^{2+}$ complex, the expected deprotonation and coordination of the amide nitrogen were not detectable by potentiometry. The species $[CuH_{-2}L]$ was instead found to form, derived from the deprotonation of a water molecule and starting from a pH value of 6, with likely coordination ($1N_{Im}$, $N^-$, $OH^-$). The experimental value of $\lambda_{max}$ at pH 8 (≈658 nm) is in good agreement with the expected value for the suggested coordination mode (expected $\lambda_{max}$ = 660 nm).[12] The 2N binding mode is also confirmed by EPR results (Figure 3C and Table S2 in SI).[27] The CD spectra (Figure 2C) remain unchanged throughout the entire explored pH range: no signal of the coordinated nitrogens could be detected, but this is not unusual when only one backbone amide is bound to copper. In conclusion, the presence of two proline residues around the metal-binding site provides great structural rigidity, thus hindering the binding of other backbone amides far from the His anchoring site.

**Zn(II) Complexes.** The investigated peptides are able to form Zn(II) complexes in a stoichiometric ratio of 1:1 under the employed experimental conditions. The identified MS signals align closely with equimolar Zn(II) complexes ($m/z$ = 343.12, 356.13, and 369.14, $z$ = 2+ for the **AHA**, **PHA**, and **PHP** ligands, respectively; Figures S1−S3 in SI), and they are almost perfectly superimposable to the corresponding simulated isotopic patterns.

Potentiometric results, reported in Table 3 and plotted in the distribution diagrams of Figures S7−S9, show that the three ligands behave in a very similar way toward the Zn(II) ion. In fact, for all of the studied systems, at the most acidic pH


https://doi.org/10.1021/acs.inorgchem.5c00672
Inorg. Chem. XXXX, XXX, XXX−XXX

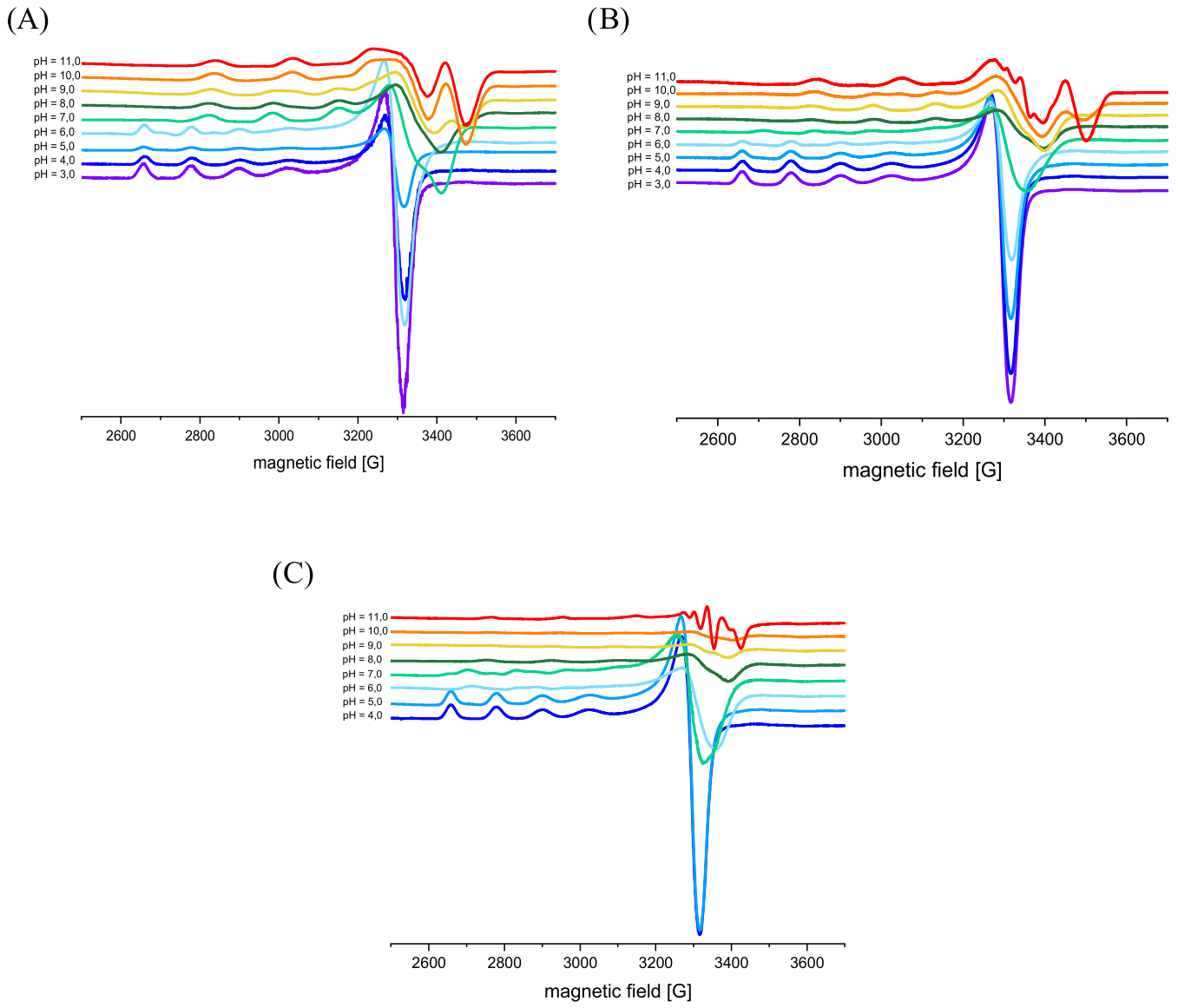


**Figure 3.** X-band EPR spectra of frozen solution (77 K) of Cu(II) complexes with (A) **AHA**, (B) **PHA**, and (C) **PHP** at different pH values: $I$ = 0.1 M (NaCl), M:L ratio 0.9:1, $C_M = 2 \times 10^{-3}$ M.

**Table 3. Equilibrium Constants and the Proposed Coordination Modes for Zn(II) Complexes at $T$ = 298 K and $I$ = 0.1 (NaCl)**[a]

| | species | log $\beta$ | p$K_a$ | coordination mode |
|---|---|---|---|---|
| Ac-AAAHAAA-$NH_2$ (**AHA**) | $[\mathbf{ZnL}]^{2+}$ | 3.70(6) | | $N_{Im}$ |
| | $[\mathbf{ZnH_{-2}L}]$ | −12.27(6) | 8.02 | $N_{Im}$, $2OH^-$ |
| | $[\mathbf{ZnH_{-3}L}]^-$ | −20.29(4) | | $N_{Im}$, $3OH^-$ |
| Ac-AAPHAAA-$NH_2$ (**PHA**) | $[\mathbf{ZnL}]^{2+}$ | 3.60(1) | | $N_{Im}$ |
| | $[\mathbf{ZnH_{-2}L}]$ | −12.00(1) | 8.01 | $N_{Im}$, $2OH^-$ |
| | $[\mathbf{ZnH_{-3}L}]^-$ | −20.01(8) | | $N_{Im}$, $3OH^-$ |
| Ac-AAPHPAA-$NH_2$ (**PHP**) | $[\mathbf{ZnL}]^{2+}$ | 3.70(6) | | $N_{Im}$ |
| | $[\mathbf{ZnH_{-2}L}]$ | −12.13(6) | 8.06 | $N_{Im}$, $2OH^-$ |
| | $[\mathbf{ZnH_{-3}L}]^-$ | −20.19(4) | | $N_{Im}$, $3OH^-$ |

[a]Values in parentheses are standard deviations on the last significant digit.

values, the free metal ion is prevalent and Zn(II) complexes begin to form only above pH 4. The first detected species is $[ZnL]^{2+}$, in which the histidine residue is deprotonated and bound to the metal ion. Its complex geometry can be tetrahedral,[18,33,34] where three water molecules complete the Zn(II) coordination sphere. When the pH value is increased, two complexes are formed, $[ZnH_{-2}L]$ and $[ZnH_{-3}L]^-$, most likely derived from the $[ZnL]^{2+}$ complex through the simple release of protons from the coordinated water molecules. All of the thermodynamic results unequivocally demonstrate that the


https://doi.org/10.1021/acs.inorgchem.5c00672
Inorg. Chem. XXXX, XXX, XXX−XXX

Table 4. Equilibrium Constants and the Proposed Coordination Modes for Fe(II) Complexes at $T$ = 298 K and $I$ = 0.1 M (NaCl)[a]

| | species | log $\beta$ | p$K_a$ | coordination mode |
|---|---|---|---|---|
| Ac-AAAHAAA-$NH_2$ (**AHA**) | $[FeL]^{2+}$ | 3.41(6) | 7.75 | $N_{Im}$ |
| | $[FeH_{-1}L]^{+}$ | −4.34(3) | | $N_{Im}$, $OH^-$ |
| | $[FeH_{-3}L]^{-}$ | −22.28(3) | 10.25 | $N_{Im}$, $3OH^-$ |
| | $[FeH_{-4}L]^{2-}$ | −32.53(3) | | $N_{Im}$, $4OH^-$ |
| Ac-AAPHAAA-$NH_2$ (**PHA**) | $[FeL]^{2+}$ | 3.15(6) | 7.64 | $N_{Im}$ |
| | $[FeH_{-1}L]^{+}$ | −4.49(3) | | $N_{Im}$, $OH^-$ |
| | $[FeH_{-3}L]^{-}$ | −21.98(3) | 9.66 | $N_{Im}$, $3OH^-$ |
| | $[FeH_{-4}L]^{2-}$ | −31.64(4) | | $N_{Im}$, $4OH^-$ |
| Ac-AAPHPAA-$NH_2$ (**PHP**) | $[FeL]^{2+}$ | 3.30(5) | 7.79 | $N_{Im}$ |
| | $[FeH_{-1}L]^{+}$ | −4.49(3) | | $N_{Im}$, $OH^-$ |
| | $[FeH_{-3}L]^{-}$ | −22.28(2) | 10.05 | $N_{Im}$, $3OH^-$ |
| | $[FeH_{-4}L]^{2-}$ | −32.33(3) | | $N_{Im}$, $4OH^-$ |

[a]Values in parentheses are standard deviations of the last significant figure.

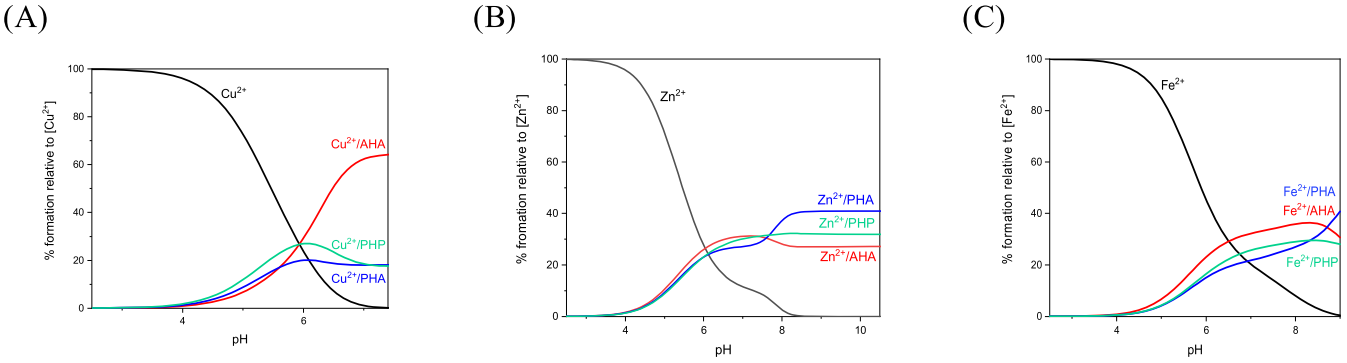


**Figure 4.** Competition plots for a simulated solution containing equimolar concentrations of (A) Cu(II), (B) Zn(II), (C) Fe(II), and **AHA**, **PHA**, and **PHP**. The diagrams are calculated from the overall stability constants of the binary complexes and simulate a situation in which equimolar concentrations of all of the chosen ligands and metals are present in a solution.

availability or not of backbone amide nitrogens near the His anchoring site makes no difference in the complexing behavior of Zn(II) ion, and the only binding site always is the imidazole side group of histidine. Of particular relevance is the result concerning the formation enthalpy values of the $[ZnH_{-3}L]^{-}$ species, formed by the three peptides, which are almost identical, taking into account the standard deviations of 107 kJ/mol for AHA, 103 kJ/mol for PHA, and 106 kJ/mol for PHP (Table S1 in SI). In fact, this is the species formed in the most alkaline pH range; thus, the complex is potentially more prone to involve amide nitrogens in metal coordination.

**Fe(II) Complexes.** Also, the systems containing the Fe(II) ion have been investigated by potentiometry (Table 4 and Figures S10−S12) with the support of mass spectrometry for a confirmation of the stoichiometry of the formed complexes (Figures S1−S3 in SI.) Once again, only mononuclear 1:1 species have been detected, with a degree of protonation depending on the solution pH. Iron hydroxide precipitation was observed at a pH higher than 9.5.

For all of the studied systems, Fe(II) complexes begin to form above pH 4, as in the case of Zn(II). The first detected species is $[FeL]^{2+}$, where the histidine residue is unprotonated and bound to the metal ion. With the increasing pH, four water molecules, which complete the Fe(II) coordination sphere, undergo stepwise deprotonation, resulting in $[FeH_{-1}L]^{+}$, $[FeH_{-3}L]^{-}$, and $[FeH_{-4}L]^{2-}$ complexes. The almost perfect correspondence between the speciation models of the three Fe(II)/peptide systems, especially in the case of the two ligands **AHA** and **PHP**, leads to the conclusion that after the anchoring of the metal ion to the His residue, no additional interaction with peptide ligands (and then with backbone amides) takes place.

**Comparison of Metal Chelating Abilities.** In an attempt to better understand the binding ability of the investigated ligands toward Cu(II), Zn(II), and Fe(II) ions, competition plots have been built up (Figures 4 and S13). These diagrams are calculated from the overall stability constants of the binary complexes and simulate a situation in which equimolar concentrations of all of the chosen ligands and metals are present in a solution; such competition diagrams are a powerful way to compare the complexing affinity of **AHA**, **PHA**, and **PHP** peptides toward the Cu(II), Zn(II), and Fe(II) ions for the whole explored pH range.

From the competition plot of copper complexes with the three peptides (Figure 4A), it is possible to notice how **AHA** leads to the formation of copper complexes with much higher stability than that of the other two peptides, especially at an alkaline pH. The substitution of one or two alanines adjacent to the metal-binding site with one or two prolines reduces the number of available amides of the peptide backbone for the complexation of the copper ion. In fact, the results reported above show that the copper ion can coordinate up to four nitrogens with the peptide **AHA**, while with **PHA** and **PHP**, the coordination stops at two or three nitrogens. The competition curve for the Cu(II)−PHP system has been stopped at pH 7.5 due to precipitation.


https://doi.org/10.1021/acs.inorgchem.5c00672
Inorg. Chem. XXXX, XXX, XXX−XXX

What is even more striking is the fact that the stabilities of the Zn(II) complexes are almost identical (Figure 4B). This proves that the coordination mode in the native AHA peptide does not differ from that of its Ala-substituted analogues, clearly indicating that the coordination modes do not involve amide nitrogens.

The same situation is observed for Fe(II) complexes of our model systems: their stabilities are fairly similar; therefore, amide binding in the case of the AHA peptide can be excluded.

**Density Functional Theory (DFT) Studies Confirm (Lack of) Amide Coordinating Abilities.** Finally, in order to support the experimental results, we investigated computationally the relative energies of the mononuclear 1:1 metal−peptide $MH_{-x}L$ species formed as a function of the deprotonation degree with the increasing solution pH. In all cases, the relative energies of the complexes were evaluated for the $OH^-$ vs the corresponding amide-deprotonated structures (Figure 5). For the peptide, stepwise amide deprotonation was evaluated as Ac-$A^3A^2A^1$HAAA-$NH_2$, where for $A^{\#}$, # indicates the sequence of deprotonated alanines.

In the case of the Cu(II) ion, the computational data are in agreement with the experimental results in that in all cases, with increasing pH value, amide deprotonation and coordination to copper(II) lead to more stable ($N_{Im}$, $nN^-$) complexes as compared to the corresponding hydroxy ($N_{Im}$, $n$$OH^-$) complexes ensuing from coordinated water deprotonation.

Considering that the Zn(II) ion binds to AHA in a 1:1 molar ratio, the computational data suggest that amide ($N_{Im}$, $nN^-$) complexes are unlikely to form in solution due to the very high strain imposed on the tetrahedral geometry of the ion and because of the fact that $[ZnH_{-x}L]$ complexes generated via the simple release of protons from the coordinated water molecules are the most likely species to be formed. Indeed, despite our efforts, amide-deprotonated $[ZnH_{-2}L]$ and $[ZnH_{-3}L]^-$ species never converged in the calculations.

Finally, the Fe(II) ion case proved to be the most challenging and more difficult to interpret. In its low-spin state, DFT calculations indicate that for $[FeH_{-1}L]^+$ and $[FeH_{-3}L]^-$ species, both amide ($N_{Im}$, $nN^-$) and hydroxy ($N_{Im}$, $n$$OH^-$) complexes are very close in energy (only ca. 0.5 kcal/mol $\Delta E$), while at high pH, $[FeH_{-4}L]^{2-}$, in which four coordinated water molecules are deprotonated, is far more stable than the corresponding ($N_{Im}$, 3N, $1OH^-$) complex. Overall, considering both theoretical and experimental evidence, we conclude that although theoretically possible, it is highly unlikely that backbone amide deprotonation is the metal-anchoring site for the Fe(II) ion under experimental conditions.

## ■ CONCLUSIONS

In the present study, for the first time, precise details of the formation equilibria and metal coordination modes of Cu(II), Zn(II), and Fe(II) complexes with the model peptide Ac-AAAHAAA-$NH_2$ and two mutants have been deeply investigated in order to obtain a clear answer of the capability of Zn(II) and Fe(II) to displace backbone amide protons and bind amide nitrogens, as Cu(II) notoriously does. Both experimental and computational results clearly show that the metal-induced amide deprotonation and binding are not likely for the model Ac-AAAHAAA-$NH_2$ peptide in the case of both Zn(II) and Fe(II) ions. As a matter of fact, the complex-formation behavior of Ac-AAAHAAA-$NH_2$ toward Zn(II) and Fe(II) is nearly identical to that of its Ala-to-Pro substituted analogues, Ac-AAPHAAA-$NH_2$ and Ac-AAPHPAA-$NH_2$, where the tertiary nitrogen atoms of backbone amides belonging to proline residues around the histidine, the metal-anchoring site, cannot bind metal ions. This simple model

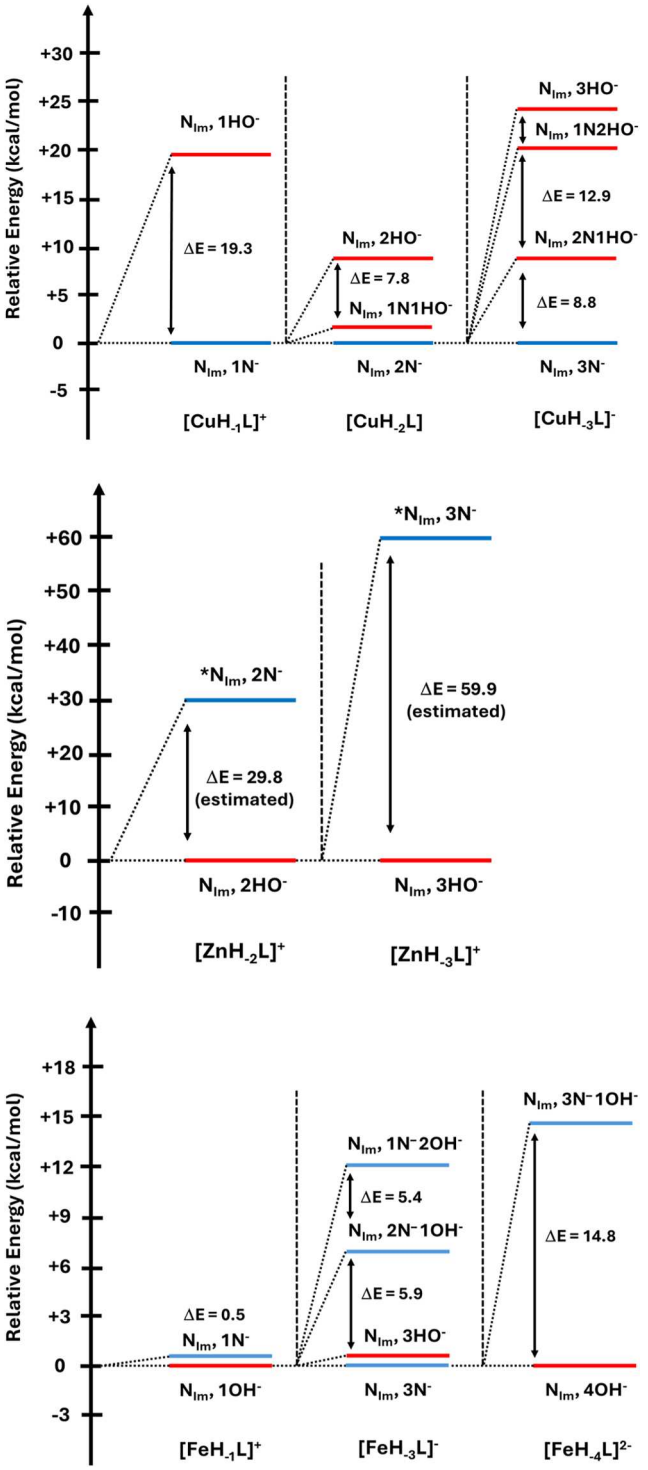


**Figure 5.** Correlative energies of mononuclear 1:1 metal−peptide $MH_{-x}L$ species formed as a function of the deprotonation degree with the increasing solution pH. In all cases, the relative energies of the complexes were evaluated for the $OH^-$ versus the corresponding amide-deprotonated structures. The * indicates a nonconvergent structure whose energy was estimated by its lowest computed point on the potential energy surface.


https://doi.org/10.1021/acs.inorgchem.5c00672
Inorg. Chem. XXXX, XXX, XXX−XXX

study clarifies the lately ongoing discussion about possible Zn(II)- and Fe(II)-amide binding and constitutes a valuable contribution to the very sparse literature data on iron−peptide complexes.

## EXPERIMENTAL SECTION

**Materials and Methods.** The peptides (Ac-AAAHAAA-$NH_2$, Ac-AAPHAAA-$NH_2$, and Ac-AAPHPAA-$NH_2$) were purchased from KareBio and used as received. Copper(II), zinc(II) chloride, and ammonium iron(II) sulfate were extra pure products (Sigma-Aldrich). The carbonate-free stock solution of 0.1 M NaOH (Sigma-Aldrich) was potentiometrically standardized with potassium hydrogen phthalate (Sigma-Aldrich). In the case of iron(II), the concentration of Fe(II) ions was determined using UV−vis spectroscopy of the Fe(II)−phenanthroline complex, as published before.[9]

**Mass Spectrometry.** High-resolution mass spectra were obtained on a Bruker ESI-Q-TOF spectrometer (Bruker Daltonics, Germany). The mass spectrometer was operated in positive- and negative-ion modes. The instrumental parameters were as follows: scan range was $m/z$ 50−3000, dry gas was nitrogen, temperature was 180 °C, and ion energy was 5 eV. The capillary voltage was optimized to the highest S/N ratio, and it was 3500 V. The samples ($[L]_{tot} = 1 \times 10^{-4}$ M and M:L molar ratio = 0.9:1) were prepared in a 1:1 methanol−water mixture, and the initial pH was set to 7.4. The sample was infused at a flow rate of 180 $\mu$L $min^{-1}$. The instrument was calibrated externally with a Low Concentration Tuning Mix ESI-FOF instrument (Agilent Technologies (SD ≤ 1 ppm) and sodium formate clusters (SD ≤ 1 ppm)). Data were processed using the Bruker Compass DataAnalysis 4.2 program. The mass accuracy for the calibration was >5 ppm, enabling, together with the true isotopic pattern, an unambiguous confirmation of the elemental composition of the obtained complex.

**Potentiometric Measurements.** The stability constants for ligand protonation and metal complex formation were calculated from potentiometric titration curves carried out over the pH range of 2.0−11.0 at $T$ = 298 K. The total volume of the solution was 3 mL in the case of Cu(II) and Zn(II) complexes and 1.5 mL in the case of Fe(II) complexes. The pH-metric titrations were performed with a Metrohm 809 Titrando pH-meter titrator provided with a Mettler-Toledo glass body, microcombination pH electrode. The titration cell was equipped with a magnetic stirring system, a microburet delivery tube, and an inlet−outlet tube for high-purity grade argon in order to maintain an inert atmosphere. Solutions were titrated with 0.1 M carbonate-free NaOH. The electrode was calibrated daily for hydrogen ion concentration by titrating HCl with NaOH in the same experimental conditions as above. Purities and the exact concentrations of the ligand solutions were determined by the Gran method.[35] The ligand concentration was 0.5 mM, and the metal-to-ligand ratio was 0.9:1. Due to the high susceptibility of Fe(II) ions to oxidation, all of the experiments were carried out in degassed solvents and under anaerobic conditions according to the procedure described in our previous paper.[9] Argon provides an inert atmosphere and prevents the oxidation and diffusion of $CO_2$ to the solution. It is worth noting that during the experiment, no color changes of the test sample or iron hydroxide precipitation were observed until pH 9.5. Access to the atmospheric oxygen resulted in the sample color turning yellow, followed by the precipitation of a brown-yellow Fe(III) hydroxide. The standard potential and the slope of the electrode couple were computed by means of the Glee program.[36] The HYPERQUAD2013 program was used for calculating the stability constants.[37] The constants for hydrolytic of Cu(II), Zn(II), and Fe(II) species were used in these calculations and taken from the literature.[38,39] The speciation and competition diagrams were computed with the HySS program[40] and drawn in the OriginPro 2016 program.

**Calorimetric Measurements.** Protonation and metal complex-formation enthalpy ($\Delta H°$) values were determined for the three peptides and their Cu(II) and Zn(II) complexes by titration calorimetry, with a Tronac model 450 isoperibol calorimeter, equipped with a 3 mL reaction vessel. The corresponding data for the Fe(II) complexes cannot be determined with this system, since it is not possible to avoid contact with the atmosphere during the experiments. The calorimetric measurements were carried out by titrating aliquots of samples of the same composition as in potentiometry with a standard solution of HCl. The reaction heats—corrected for nonchemical contributions[41] and for the dilution heats determined through specific experiments—were calculated by considering the calories as equivalent to 4.187 J. The protonation and complex-formation enthalpies and entropies were computed from experimental calorimetric titration by means of the computer program Hyp$\Delta H$.[42]

**Spectroscopic Measurements.** The absorption spectra of Cu(II) containing solutions were recorded on a Varian Cary50 Probe spectrophotometer in the range 200−800 nm, using a quartz cuvette with an optical path of 1 cm. In order to obtain information on the structure of the most abundant species in the solution, the observed wavelength of the maximum absorption at a given pH was compared with the expected $\lambda_{max}$ value obtained from the literature.[12,21,25,43,44] Circular dichroism (CD) spectra were recorded on a Jasco J-1500 spectropolarimeter in the 240−800 nm range. Electron paramagnetic resonance (EPR) spectra were recorded in liquid nitrogen on a Bruker ELEXSYS E500 CW-EPR spectrometer at X-band frequency (9.6 GHz) and equipped with an ER 036TM NMR teslameter and an E41 FC frequency counter. Ethylene glycol (30%) was used as a cryoprotectant. The EPR parameters were analyzed by computer simulation of the experimental spectra using WIN-EPR SIMFONIA software, version 1.2 (Bruker, Billerica, MA).

**DFT Calculations.** All computations were performed with Gaussian 09 programs. Geometry optimizations and frequency calculations were performed in the water. The B3LYP functional was used in combination with the standard 6-31G(d,p) basis sets. The spin state of the Cu(II) and Fe(II) ions were set, respectively, as doublet and singlet. The default spin formalism was followed in the calculations, and default Gaussian 09 values were adopted for the numerical integration grids, self-consistent-field (SCF), and geometry optimization convergence criteria. Geometries were optimized without symmetry restrictions. The nature of the stationary points was checked by computing the vibrational frequencies to verify true minima. The analysis also provided all thermochemical quantities used to calculate the relative energy of the different M(II)-AHA species at different deprotonation states. No imaginary frequencies were observed in any of the computed species, except for the amide-deprotonated $[ZnH_{-2}L]$ and $[ZnH_{-3}L]^-$ species, which never converged.

To calculate the relative energies of the $OH^-$ vs the corresponding amide-deprotonated M(II)−AHA structures, the stoichiometry was kept constant where possible.[45] Alternatively, the relative energy of the deprotonated M(II)−AHA complexes was calculated considering the thermochemical data of the Gaussian output by adopting the free energies of reaction changes ($\Delta_r G°$) according to[46]

$$\Delta_r G°(298.15\ \mathrm{K}) = \sum (\varepsilon_o + G_{corr})_{products} - \sum (\varepsilon_o + G_{corr})_{reactants}$$

where $\varepsilon_o$ = total energy of the molecule and $G_{corr}$ = Gibbs free energy correction, for the following general reaction, considering the entropy increase of the liberated water molecules:

$$[MH_{-n}L]^x(N_{Im}, n OH^-) \rightarrow [MH_{-n}L]^x(N_{Im}, n N^-_{amide}) + n H_2O$$

In the above reaction, $nOH^-$ and $nN_{amide}^-$ are the number of deprotonated water molecules and the number of deprotonated amides, respectively, directly coordinated to the metal ion M. All energies are given in kcal/mol calculated according to E = Hartrees * 627.5095.

## ASSOCIATED CONTENT

### Supporting Information

The Supporting Information is available free of charge at https://pubs.acs.org/doi/10.1021/acs.inorgchem.5c00672.



https://doi.org/10.1021/acs.inorgchem.5c00672
Inorg. Chem. XXXX, XXX, XXX−XXX

ESI-MS spectra, species distribution diagrams, thermodynamic parameters of protonation, and metal complex formation for all studied complexes; EPR parameters for Cu(II) complexes; and competition plots (PDF)

## AUTHOR INFORMATION


### Corresponding Authors

**Denise Bellotti** − *Department of Chemistry, Fribourg University, 1700 Fribourg, Switzerland*; Email: blldns@unife.it

**Kamila Stokowa-Sołtys** − *Faculty of Chemistry, University of Wroclaw, 50-383 Wroclaw, Poland*; Email: kamila.stokowa-soltys@uwr.edu.pl

**Maurizio Remelli** − *Department of Chemistry, Fribourg University, 1700 Fribourg, Switzerland*; Email: rmm@unife.it

**Magdalena Rowińska-Żyrek** − *Faculty of Chemistry, University of Wroclaw, 50-383 Wroclaw, Poland*; orcid.org/0000-0002-0425-1128; Email: magdalena.rowinska-zyrek@uwr.edu.pl

### Authors

**Silvia Leveraro** − *Faculty of Chemistry, University of Wroclaw, 50-383 Wroclaw, Poland; Department of Chemical, Pharmaceutical and Agricultural Sciences, University of Ferrara, 44121 Ferrara, Italy*

**Valentyn Dzyhovskyi** − *Faculty of Chemistry, University of Wroclaw, 50-383 Wroclaw, Poland*

**Kinga Garstka** − *Faculty of Chemistry, University of Wroclaw, 50-383 Wroclaw, Poland*

**Agnieszka Szebeszczyk** − *Institute of Health Sciences, University of Opole, 45-060 Opole, Poland*; orcid.org/0000-0003-3533-1988

**Fabio Zobi** − *Department of Chemistry, Fribourg University, 1700 Fribourg, Switzerland*; orcid.org/0000-0002-9077-7184

Complete contact information is available at: https://pubs.acs.org/10.1021/acs.inorgchem.5c00672


### Author Contributions

The manuscript was written through contributions of all authors. All authors have given approval to the final version of the manuscript.


### Funding

The financial support by the National Science Centre (Grants 2023/51/B/ST5/01098 and 2018/31/D/ST4/02574) is gratefully acknowledged.


### Notes

The authors declare no competing financial interest.

## REFERENCES


(1) Kozłowski, H.; Kowalik-Jankowska, T.; Jezowska-Bojczuk, M. Chemical and Biological Aspects of Cu2+ Interactions with Peptides and Aminoglycosides. *Coord. Chem. Rev.* **2005**, *249* (21−22), 2323−2334.

(2) Faller, P.; Hureau, C. Bioinorganic Chemistry of Copper and Zinc Ions Coordinated to Amyloid-$\beta$ Peptide. *Dalton Trans.* **2009**, *7*, 1080−1094.

(3) Millhauser, G. L. The Rich Chemistry of the Copper and Zinc Sites in PrPC. *Prions Prion Dis.* **2023**, 25−43.

(4) Grenács, Á.; Sóvágó, I. Copper(II), Nickel(II) and Zinc(II) Comp lexes of the N-Terminal Nonapeptide Fragment of Amyloid-$\beta$ and Its Derivatives. *J. Inorg. Biochem.* **2014**, *139*, 49−56.

(5) Zawisza, I.; Rózga, M.; Bal, W. Affinity of Copper and Zinc Ions to Proteins and Peptides Related to Neurodegenerative Conditions (A$\beta$, APP, $\alpha$-Synuclein, PrP). *Coord. Chem. Rev.* **2012**, *256* (19−20), 2297−2307.

(6) Raics, M.; Sanna, D.; Sóvágó, I.; Kállay, C. Copper(II), Nickel(II) and Zinc(II) Complexes of Hexapeptides Containing Separate Aspartyl and Histidyl Residues. *Inorg. Chim. Acta* **2015**, *426*, 99−106.

(7) Bellotti, D.; Rowińska-Żyrek, M.; Remelli, M. Novel Insights into the Metal Binding Ability of ZinT Periplasmic Protein from *Escherichia coli* and Salmonella Enterica. *Dalton Trans.* **2020**, *49* (27), 9393−9403.

(8) Garstka, K.; Dzyhovskyi, V.; Watły, J.; Stokowa-Sołtys, K.; Światek-Kozłowska, J.; Kozłowski, H.; Barceló-Oliver, M.; Bellotti, D.; Rowińska-Żyrek, M. CH vs. HC—Promiscuous Metal Sponges in Antimicrobial Peptides and Metallophores. *Molecules* **2023**, *28* (10), 3985.

(9) Dzyhovskyi, V.; Stokowa-Sołtys, K. Divalent Metal Ion Binding to Staphylococcus Aureus FeoB Transporter Regions. *J. Inorg. Biochem.* **2023**, *244*, No. 112203.

(10) Dzyhovskyi, V.; Remelli, M.; Stokowa-Sołtys, K. Exploring Divalent Metal Ion Coordination. Unraveling Binding Modes in *Staphylococcus aureus* MntH Fragments. *J. Inorg. Biochem.* **2025**, *263*, No. 112769.

(11) Orzel, B.; Pelucelli, A.; Ostrowska, M.; Potocki, S.; Kozlowski, H.; Peana, M.; Gumienna-Kontecka, E. Fe(II), Mn(II), and Zn(II) Binding to the C-Terminal Region of FeoB Protein: An Insight into the Coordination Chemistry and Specificity of the *Escherichia coli* Fe(II) Transporter. *Inorg. Chem.* **2023**, *62* (45), 18607−18624.

(12) Sigel, H.; Martin, R. B. Coordinating Properties of the Amide Bond. Stability and Structure of Metal Ion Complexes of Peptides and Related Ligands. *Chem. Rev.* **1982**, *82* (4), 385−426.

(13) Farkas, E.; Enyedy, É. A.; Micera, G.; Garribba, E. Coordination Modes of Hydroxamic Acids in Copper(II), Nickel(II) and Zinc(II) Mixed-Ligand Complexes in Aqueous Solution. *Polyhedron* **2000**, *19* (14), 1727−1736.

(14) Remelli, M.; Brasili, D.; Guerrini, R.; Pontecchiani, F.; Potocki, S.; Rowinska-Zyrek, M.; Watly, J.; Kozlowski, H. Zn(II) and Ni(II) Complexes with Poly-Histidyl Peptides Derived from a Snake Venom. *Inorg. Chim. Acta* **2018**, *472*, 149−156, DOI: 10.1016/j.ica.2017.05.070.

(15) Bellotti, D.; Sinigaglia, A.; Guerrini, R.; Marzola, E.; Rowińska-Żyrek, M.; Remelli, M. The N-Terminal Domain of Helicobacter Pylori's Hpn Protein: The Role of Multiple Histidine Residues. *J. Inorg. Biochem.* **2021**, *214*, No. 111304.

(16) Kozłowski, H.; Bal, W.; Dyba, M.; Kowalik-Jankowska, T. Specific Structure−Stability Relations in Metallopeptides. *Coord. Chem. Rev.* **1999**, *184* (1), 319−346.

(17) Bellotti, D.; Łoboda, D.; Rowinska-Zyrek, M.; Remelli, M. Investigation on the Metal Binding Sites of a Putative Zn(II) Transporter in Opportunistic Yeast Species Candida Albicans. *New J. Chem.* **2018**, *42* (10), 8123−8130.

(18) Kastal, Z.; Balabán, A.; Vida, S.; Kállay, C.; Nagy, L.; Várnagy, K.; Sóvágó, I. Copper(II), Nickel(II) and Zinc(II) Complexes of Peptide Fragments of Tau Protein. *Molecules* **2024**, *29* (10), 2171.

(19) Formicka-Kozlowska, G.; Kozlowska, H.; Siemion, I. Z.; Sobczyk, K.; Nawrocka, E. Copper (II) Interaction with Proline-Containing Tetrapeptides. *J. Inorg. Biochem.* **1981**, *15* (3), 201−212.

(20) Gralka, E.; Valensin, D.; Porciatti, E.; Gajda, C.; Gaggelli, E.; Valensin, G.; Kamysz, W.; Nadolny, R.; Guerrini, R.; Bacco, D.; Remelli, M.; Kozlowski, H. CuII Binding Sites Located at His-96 and His-111 of the Human Prion Protein: Thermodynamic and Spectroscopic Studies on Model Peptides. *Dalton Trans.* **2008**, *38*, 5207−5219.

(21) Székely, E.; Csire, G.; Balogh, B. D.; Erdei, J. Z.; Király, J. M.; Kocsi, J.; Pinkóczy, J.; Várnagy, K. The Role of Side Chains in the Fine-Tuning of the Metal-Binding Ability of Multihistidine Peptides. *Molecules* **2022**, *27* (11), 3435.




https://doi.org/10.1021/acs.inorgchem.5c00672
*Inorg. Chem.* XXXX, XXX, XXX−XXX

(22) Grasso, G.; Magrì, A.; Bellia, F.; Pietropaolo, A.; La Mendola, D.; Rizzarelli, E. The Copper(II) and Zinc(II) Coordination Mode of HExxH and HxxEH Motif in Small Peptides: The Role of Carboxylate Location and Hydrogen Bonding Network. *J. Inorg. Biochem.* **2014**, *130*, 92−102.
(23) Kállay, C.; Ősz, K.; Dávid, A.; Valastyán, Z.; Malandrinos, G.; Hadjiliadis, N.; Sóvágó, I. Zinc(II) Binding Ability of Tri-, Tetra- and Penta-Peptides Containing Two or Three Histidyl Residues. *Dalton Trans.* **2007**, *36*, 4040.
(24) The IUPAC Stability Constants Database, SC-Database and mini-SCDatabase, 2024. https://search.worldcat.org/title/The-IUPAC-stability-constants-database-SC-database-and-mini-SCDatabase/oclc/855867134.
(25) Prenesti, E.; Daniele, P. G.; Prencipe, M.; Ostacoli, G. Spectrum−Structure Correlation for Visible Absorption Spectra of Copper(II) Complexes in Aqueous Solution. *Polyhedron* **1999**, *18* (25), 3233−3241.
(26) Daniele, P. G.; Prenesti, E.; Ostacoli, G. Ultraviolet-Circular Dichroism Spectra for Structural Analysis of Copper(II) Complexes with Aliphatic and Aromatic Ligands in Aqueous Solution. *J. Chem. Soc., Dalton Trans.*. **1996**, *15*, 3269−3275.
(27) Peisach, J.; Blumberg, W. E. Structural Implications Derived from the Analysis of Electron Paramagnetic Resonance Spectra of Natural and Artificial Copper Proteins. *Arch. Biochem. Biophys.* **1974**, *165* (2), 691−708.
(28) Łuczkowski, M.; Kozłowski, H.; Łęgowska, A.; Rolka, K.; Remelli, M. The Possible Role of Gly Residues in the Prion Octarepeat Region in the Coordination of Cu2+ Ions. *Dalton Trans.* **2003**, *3* (4), 619−624.
(29) Bellotti, D.; D'Accolti, M.; Pula, W.; Huang, N.; Simeliere, F.; Caselli, E.; Esposito, E.; Remelli, M. Calcitermin-Loaded Smart Gels Activity against Candida Albicans: A Preliminary In Vitro Study. *Gels* **2023**, *9* (2), 165.
(30) Bal, W.; Dyba, M.; Kozłowski, H. The Impact of the Amino-Acid Sequence on the Specificity of Copper(II) Interactions with Peptides Having Nonco-Ordinating Side-Chains. *Acta Biochim. Pol.* **1997**, *44* (3), 467−476.
(31) Mlynarz, P.; Valensin, D.; Kociolek, K.; Zabrocki, J.; Olejnik, J.; Kozlowski, H. Impact of the Peptide Sequence on the Coordination Abilities of Albumin-like Tripeptides towards Cu2+, Ni2+ and Zn2+ Ions. Potential Albumin-like Peptide Chelators. *New J. Chem.* **2002**, *26* (2), 264−268.
(32) Witkowska, D.; Politano, R.; Rowinska-Zyrek, M.; Guerrini, R.; Remelli, M.; Kozlowski, H. The Coordination of Ni(II) and Cu(II) Ions to the Polyhistidyl Motif of Hpn Protein: Is It as Strong as We Think? *Chem. - Eur. J.* **2012**, *18* (35), 11088−11099.
(33) Kállay, C.; Várnagy, K.; Malandrinos, G.; Hadjiliadis, N.; Sanna, D.; Sóvágó, I. Thermodynamic and Structural Characterization of the Macrochelates Formed in the Reactions of Copper(II) and Zinc(II) Ions with Peptides of Histidine. *Inorg. Chim. Acta* **2009**, *362* (3), 935−945.
(34) Hecel, A.; Kola, A.; Valensin, D.; Kozlowski, H.; Rowinska-Zyrek, M. Metal Complexes of Two Specific Regions of ZnuA, a Periplasmic Zinc(II) Transporter from *Escherichia coli*. *Inorg. Chem.* **2020**, *59* (3), 1947−1958.
(35) Gran, G.; Dahlenborg, H.; Laurell, S.; Rottenberg, M. Determination of the Equivalent Point in Potentiometric Titrations. *Acta Chem. Scand.* **1950**, *4*, 559−577.
(36) Gans, P.; O'Sullivan, B. GLEE, a New Computer Program for Glass Electrode Calibration. *Talanta* **2000**, *51* (1), 33−37.
(37) Gans, P.; Sabatini, A.; Vacca, A. Investigation of Equilibria in Solution. Determination of Equilibrium Constants with the HYPERQUAD Suite of Programs. *Talanta* **1996**, *43* (10), 1739−1753.
(38) Arena, G.; Cali, R.; Rizzarelli, E.; Sammartano, S. Thermodynamic Study on the Formation of the Cupric Ion Hydrolytic Species. *Thermochim. Acta* **1976**, *16* (3), 315−321.
(39) *Hydrolysis of Metal Ions*; Brown, P. L.; Ekberg, C., Eds.; Wiley-VCH Verlag GmbH & Co. KGaA, 2016.
(40) Alderighi, L.; Gans, P.; Ienco, A.; Peters, D.; Sabatini, A.; Vacca, A. Hyperquad Simulation and Speciation (HySS): A Utility Program for the Investigation of Equilibria Involving Soluble and Partially Soluble Species. *Coord. Chem. Rev.* **1999**, *184* (1), 311−318.
(41) Hansen, L. D.; Jensen, T. E.; Mayne, S.; Eatough, D. J.; Izatt, R. M.; Christensen, J. J. Heat-Loss Corrections for Small Isoperibol-Calorimeter Reaction Vessels. *J. Chem. Thermodyn.* **1975**, *7* (10), 919−926.
(42) Gans, P.; Sabatini, A.; Vacca, A. Simultaneous Calculation of Equilibrium Constants and Standard Formation Enthalpies from Calorimetric Data for Systems with Multiple Equilibria in Solution. *J. Solution Chem.* **2008**, *37* (4), 467−476.
(43) Perinelli, M.; Guerrini, R.; Albanese, V.; Marchetti, N.; Bellotti, D.; Gentili, S.; Tegoni, M.; Remelli, M. Cu(II) Coordination to His-Containing Linear Peptides and Related Branched Ones: Equalities and Diversities. *J. Inorg. Biochem.* **2020**, *205*, No. 110980.
(44) Rowińska-Żyrek, M.; Kozłowski, H. Nickel Binding Sites—Coordination Modes and Thermodynamics. In *The Biological Chemistry of Nickel*; The Royal Society of Chemistry, 2017; pp 43−59.
(45) Dunbar, R. C.; Martens, J.; Berden, G.; Oomens, J. Complexes of Ni(II) and Cu(II) with Small Peptides: Deciding Whether to Deprotonate. *Phys. Chem. Chem. Phys.* **2016**, *18* (38), 26923−26932.
(46) Ochterski, J. W.; et al. *Thermochemistry in Gaussian*; Gaussian Inc.: Wallingford, CT, 2000.


https://doi.org/10.1021/acs.inorgchem.5c00672
*Inorg. Chem.* XXXX, XXX, XXX−XXX

scientific reports

Check for updates

OPEN

# Impact of *C*- and *N*-terminal protection on the stability, metal chelation and antimicrobial properties of calcitermin

Maria D'Accolti[1], Denise Bellotti[1,2]✉, Emilia Dzień[2], Carlotta Leonetti[1], Silvia Leveraro[1], Valentina Albanese[3], Erika Marzola[1], Remo Guerrini[1], Elisabetta Caselli[1], Magdalena Rowińska-Żyrek[2] & Maurizio Remelli[1]

**The main limitation to the use of antimicrobial peptides (AMPs) as regular drugs, against antibiotic and antifungal resistance, mainly relates to their rapid degradation by proteolytic enzymes. The introduction of suitable structural changes in the peptide chain can make the peptide less susceptible to the action of proteases, thus overcoming this problem. To improve the plasma stability of calcitermin, a metal-chelating AMP present in the human respiratory tract and investigated in the present study, *C*- and/or *N*- terminal modifications have been introduced in the native sequence. Evaluation of peptide stability has been performed to determine the half-life times in human plasma of both native calcitermin and its derivatives. However, the protection of the peptide termini can also affect its metal coordination behaviour. Thus, the characterization of $Zn^{2+}$ and $Cu^{2+}$ complexes has been performed by means of several techniques, including potentiometry, high-resolution mass spectrometry, UV–Vis, circular dichroism and EPR. On the basis of the obtained results, it was possible to compare the biological activity of the studied systems, taking into account both the metal-binding ability and the peptide stability to search for a link among them. A significant result of this study is that the *N*-terminal protection increases the calcitermin half-life over seven times and the formation of metal complexes confers resistance towards degradation almost doubling its half-life.**

Antimicrobial resistance (AMR) is one of the most important health challenges of the twenty-first century. Among several novel approaches aimed at overcoming the global drug-resistance crisis, the use of antimicrobial peptides (AMPs) represents a promising strategy for the design of new drugs[1]. They exhibit a broad spectrum of activity, being effective against a wide variety of pathogens, like Gram-positive[2] and Gram-negative bacteria[3], fungi[4], viruses[5] and even cancer cells[5] and are present in all living organisms (invertebrates, vertebrates, plants, prokaryotes)[6]. However, these extraordinary candidate molecules present some drawbacks, the major one being the fact that they are metabolically unstable. The AMPs activity level is subject to modulation or degradation by both human and pathogenic proteolytic enzymes. In fact, many endo- and exo-peptidases act to transform high molecular weight peptides into shorter oligopeptides, making them inactive. This problem translates into short half-lives (usually less than 30 min) and scarce bioavailability[7]. Therefore, in order to improve the therapeutic potential of these molecules, a rational design of new AMP analogues is required with the aim of optimizing their chemical properties and the engineering of delivery systems[8].

Calcitermin is a 15-mer peptide (VAIALKAAHYHTHKE, **WT**) corresponding to the *C*-terminal domain of calgranulin C, a pro-inflammatory protein of the S100 family. It contains an effective metal-binding domain with three alternated histidine residues in position 9, 11 and 13, and the free terminal amino and carboxyl groups[9]. The complex-formation equilibria of this natural peptide with $Zn^{2+}$ and $Cu^{2+}$ ions have been recently studied by our research group to obtain information on stoichiometry and structure of complex species formed throughout a wide pH range[9]. Moreover, calcitermin proved to adopt a helical conformation in membranes, and $Zn^{2+}$ and

[1]Department of Chemical, Pharmaceutical and Agricultural Sciences, University of Ferrara, L. Borsari 46, 44121 Ferrara, Italy. [2]Faculty of Chemistry, University of Wrocław, F. Joliot-Curie 14, 50-383 Wrocław, Poland. [3]Department of Environmental and Prevention Sciences, University of Ferrara, L. Borsari 46, 44121 Ferrara, Italy. ✉email: blldns@unife.it

$Cu^{2+}$ ions are able to enhance its antimicrobial activity against *C. albicans* and common bacteria like *S. aureus* and *E. faecalis*[9–11].

In order to improve the microbicide activity of calcitermin, different strategies can be employed: *(i)* extending its life-time, i.e. its resistance to proteases; *(ii)* enhancing its sequestering ability towards the metal micronutrients (necessary for the survival and virulence of pathogens), thus hampering the microbe growth; *(iii)* changing the peptide charge and structure before and/or after the metal interaction[12,13]. It is worth to note that three calcitermin His-to-Ala mutants – H9A, H11A and H13A, where one histidine residue is replaced with alanine—exhibit promising antimicrobial activity according to the estimated minimal inhibitory concentrations (MIC) in vitro[9]. These calcitermin mutants indeed represent an outstanding example of how different metal coordination modes (obtained by means of His-to-Ala substitution) result in significant changes of their antimicrobial properties. This type of information can be obtained through a detailed investigation on thermodynamics and coordination chemistry of the metal-peptide interaction, which can lay the foundations for a deeper insight into the way of action of metal chelating AMPs, in order to design new effective antibiotic therapies.

Considering the above results, this work is aimed at finding calcitermin derivatives where the peptide structure and, consequently, its physico-chemical properties are modified in order to achieve, first of all, a longer half-life and a lower proteolytic susceptibility, without losing its antimicrobial properties. Several strategies to improve the stability of peptides have been explored in the last forty years[14]. To increase the resistance towards exo-peptidases one common strategy is based on the chemical modification of one or both the peptide ends (*e.g.* by *N*-acylation, *C*-amidation, cyclization, binding to polyethyleneglycol)[8]. The degradation by endo-peptidases can be instead prevented by replacing one or more residues with non-proteinogenic amino acids which are normally not recognized by enzymes, like D-amino acids[15], *N*-methyl-α-amino acids[16], β- and γ- amino acids[17–19], α-alkylated amino acids[20], *N*-substituted glycines[21].

Given the importance of the peptide termini in the degradation processes carried out by exopeptidases—enzymes that catalyze the cleavage of the terminal peptide bonds—we protected the amino- and carboxyl-termini of calcitermin by acetylation and amidation respectively[22], obtaining the following derivatives: Ac-VAIALKAAHYHTHKE (**L1**), Ac-VAIALKAAHYHTHKE-$NH_2$ (**L2**) and VAIALKAAHYHTHKE-$NH_2$ (**L3**). The terminal protection should confer higher proteolytic stability and preserve the principal metal binding site of calcitermin, corresponding to the histidine motif -HxHxH-. Moreover, the study of the protected peptides will elucidate the role of the terminal groups in calcitermin antimicrobial and metal-chelating properties. An in-depth investigation on the complex-formation equilibria of these derivatives with $Zn^{2+}$ and $Cu^{2+}$ ions, together with their stability and activity, will provide further information on their way of action.

## Results and discussion

Under the experimental conditions here employed, only variously protonated mononuclear complexes, with metal/ligand stoichiometry of 1:1, have been detected by potentiometry and mass spectrometry. No precipitation has been observed over the explored pH range (2.5–10.5). The overall complex-formation constants (log$\beta$) and corresponding acid dissociation constants (p$K_a$) are reported in Tables 1, 2 and Tables S1, S2, and the calculated species distribution diagrams for each system are shown in Figs. S1–S8. Spectroscopic results, including Vis absorption spectra, CD spectra and EPR spectra, recorded at different pH values, are shown in Figs. S9–S20.

| | Ac-VAIALKAAHYHTHKE (L1) | | | Ac-VAIALKAAHYHTHKE-$NH_2$ (L2) | | |
|---|---|---|---|---|---|---|
| **Species** | **log$\beta$** | **p$K_a$** | **Coordination** | **log$\beta$** | **p$K_a$** | **Coordination** |
| $[CuH_2L]^{4+}$ | 18.21(3) | 4.40 | $N_{Im}$, $COO^-$ | 23.06(4) | 5.49 | $2N_{Im}$ |
| $[CuHL]^{3+}$ | 13.81(2) | 5.38 | $2N_{Im}$, $COO^-$ | 17.57(5) | 6.30 | $3N_{Im}$ |
| $[CuL]^{2+}$ | 8.43(2) | 6.59 | $3N_{Im}$ | 11.27(7) | 6.70 | $3N_{Im}$, $N^-$ |
| $[CuH_{-1}L]^{+}$ | 1.84(3) | 6.88 | $3N_{Im}$, $N^-$ | 4.57(6) | 9.44 | $2N_{Im}$, $2N^-$ |
| $[CuH_{-2}L]$ | −5.04(3) | – | $2N_{Im}$, $2N^-$ | −4.87(9) | 9.91 | $2N_{Im}$, $2N^-$ |
| $[CuH_{-3}L]^{-}$ | – | – | – | −14.78(7) | – | $N_{Im}$, $3N^-$ |
| | VAIALKAAHYHTHKE-$NH_2$ (L3) | | | | | |
| **Species** | **log$\beta$** | **p$K_a$** | **Coordination** | | | |
| $[CuH_5L]^{5+}$ | 51.38(2) | 5.16 | $2N_{Im}$ | | | |
| $[CuH_4L]^{4+}$ | 46.21(2) | 6.21 | $3N_{Im}$ | | | |
| $[CuH_3L]^{3+}$ | 40.00(3) | 6.90 | $2N_{Im}$, $NH_2$ | | | |
| $[CuH_2L]^{2+}$ | 33.11(2) | 7.75 | $2N_{Im}$, $NH_2$, $N^-$ | | | |
| $[CuHL]^{+}$ | 25.36(3) | 9.53 | $2N_{Im}$, $2N^-$ | | | |
| $[CuL]$ | 15.83(5) | 10.01 | $2N_{Im}$, $2N^-$ | | | |
| $[CuH_{-1}L]^{-}$ | 5.82(4) | – | $N_{Im}$, $3N^-$ | | | |
| $[CuH_{-3}L]^{3-}$ | −15.03(9) | – | $N_{Im}$, $3N^-$ | | | |

**Table 1.** Equilibrium constants and proposed coordination modes for $Cu^{2+}$ complexes at $T = 298$ K and $I = 0.1$ M (KCl). Values in parentheses are standard deviations on the last significant figure.

| Species | Ac-VAIALKAAHYHTHKE (L1) | | | Ac-VAIALKAAHYHTHKE-$NH_2$ (L2) | | |
|---|---|---|---|---|---|---|
| | log$\beta$ | p$K_a$ | Coordination | log$\beta$ | p$K_a$ | Coordination |
| $[ZnH_2L]^{4+}$ | – | – | – | 20.29(6) | 6.14 | $2N_{Im}$ |
| $[ZnHL]^{3+}$ | 11.00(5) | 5.80 | $2N_{Im}$ | 14.15(4) | 7.63 | $3N_{Im}$ |
| $[ZnL]^{2+}$ | 5.21(2) | 7.33 | $3N_{Im}$ | 6.52(5) | 8.93 | $3N_{Im}$, $OH^-$ |
| $[ZnH_{-1}L]^{+}$ | −2.12(3) | – | $3N_{Im}$, $OH^-$ | −2.41(7) | 9.44 | $3N_{Im}$, $2OH^-$ |
| $[ZnH_{-2}L]$ | | | | −11.85(3) | – | $3N_{Im}$, $2OH^-$ |
| Species | VAIALKAAHYHTHKE-$NH_2$ (L3) | | | | | |
| | log$\beta$ | p$K_a$ | Coordination | | | |
| $[ZnH_5L]^{5+}$ | 48.7(1) | 5.6 | $2N_{Im}$ | | | |
| $[ZnH_4L]^{4+}$ | 43.07(3) | 7.32 | $3N_{Im}$ | | | |
| $[ZnH_3L]^{3+}$ | 35.75(6) | 7.69 | $3N_{Im}$, $OH^-$ | | | |
| $[ZnH_2L]^{2+}$ | 28.06(4) | 8.65 | $3N_{Im}$, $OH^-$ | | | |
| $[ZnHL]^{+}$ | 19.40(5) | 9.47 | $3N_{Im}$, $2OH^-$ | | | |
| [ZnL] | 9.94(4) | – | $3N_{Im}$, $2OH^-$ | | | |
| $[ZnH_{-2}L]^{2-}$ | −10.70(7) | – | $3N_{Im}$, $2OH^-$ | | | |

**Table 2.** Equilibrium constants and proposed coordination modes for $Zn^{2+}$ complexes at $T = 298$ K and $I = 0.1$ M (KCl). Values in parentheses are standard deviations on the last significant figure.

## Formation of copper complexes with L1, L2 and L3

ESI–MS results are reported in Table S4 and Figs. S21–S23: the only detected *m/z* signals correspond to equimolar $Cu^{2+}$ complexes with different protonation states. Potassium and/or sodium adducts are also formed. The formation of copper complexes in solution begins around pH 3–3.5. The first detected species, however, display different coordination modes depending on the system.

**L1** is the only ligand with the free carboxyl terminus, and its first formed species, $[CuH_2L]^{4+}$, is likely characterized by a coordination mode ($N_{Im}$, $COO^-$). In this case, besides the histidine residue, one or both the carboxyl groups of *C*-terminal glutamic acid can participate in the complexation, forming a macrocycle. The wavelength of maximum absorption measured at pH 4, at least partly imputable to the species $[CuH_2L]^{4+}$ (760 nm, Fig. S9), is in fair agreement with the expected value for a coordination ($N_{Im}$, $COO^-$)[23], taking into account that at this pH most of the copper is still present as a hexa-aquo complex. The complex $[CuH_2L]^{4+}$ is rapidly substituted in solution by the species $[CuHL]^{3+}$, where a second histidine interacts with the metal center ($pK_a = 4.40$) giving a ($2N_{Im}$, $COO^-$) complex (experimental $\lambda_{max} = 655$ nm, Fig. S9; predicted $\lambda_{max} = 663$ nm[23]). In the case of amidated peptides (**L2** and **L3**), the stoichiometry of the complex species formed at the most acidic pH values ($[CuH_2L]^{4+}$ and $[CuH_5L]^{5+}$, respectively) suggests that two histidines are already deprotonated. In other words, the protection of the *C*-terminus likely favors the initial formation of a 2N complex where $Cu^{2+}$ interacts with two imidazole groups of the histidine side chains. Indeed, the 2N species are predominant in solution in the pH range 4–5.5. EPR spectra registered at pH 5.5 confirm the presence of 2N complexes (**L1**: $A_{//} = 174$; $g_{//} = 2.28$; $g_{\perp} = 2.02$; **L2**: $A_{//} = 157$; $g_{//} = 2.31$; $g_{\perp} = 2.02$; **L3**: $A_{//} = 163$; $g_{//} = 2.28$; $g_{\perp} = 2.02$; Table S3)[24]. Increasing the pH value, the $Cu^{2+}$ ion can displace the acidic proton from a third histidine, and it coordinates three imidazoles forming a ($3N_{Im}$) species, which is prevalent in solution at around pH 6 in all the systems. The obtained wavelengths of maximum absorption at pH 6.0 range from $\lambda_{max} = 626$ nm to $\lambda_{max} = 635$ nm and agree with the proposed coordination mode (expected $\lambda_{max} = 627$ nm)[23].

In the alkaline pH range, we can distinguish two situations depending on the considered system. In the case of acetylated peptides, **L1** and **L2**, the next deprotonation step involves an amide group of the peptide backbone, while in **L3**, the free terminal amino group can deprotonate and interact with the metal ion. The EPR results confirm the formation of 4N species, since the spectra above pH 7 show the same superhyperfine structure and the following EPR parameters: $A_{//} = 182$–$198$; $g_{//} = 2.20$–$2.21$; $g_{\perp} = 2.02$–$2.05$ (Table S3), that agree with the expected literature values[24].

Examining in details the systems **L1** and **L2**, starting from pH 5.5, we can observe the formation of $[CuH_{-1}L]^{+}$ (for **L1**) and $[CuL]^{2+}$ (for **L2**) (Figs. S3, S4) with $pK_a = 6.59$ and 6.30, respectively. The experimental values of $\lambda_{max}$ for solutions where these complexes reach their maximum of formation is 557 nm (Figs. S9, S12), exactly the value expected for a coordination ($3N_{Im}$, $N^-$)[23]. Circular dichroism spectra recorded at pH above 6 (Figs. S10, S13) also show the appearance of intense signals in the visible spectral region, which can be attributed to the coordination of the amide nitrogen (it is closer to the chiral α-carbon of the peptide backbone and therefore can produce a stronger CD absorption when the metal binding occurs). Increasing the pH value the intensity of CD bands increases suggesting the binding of a second amide that replaces a histidine in the equatorial plane of the complex, forming a ($2N_{Im}$, $2N^-$) species and increasing the square-planar character of the corresponding complexes, $[CuH_{-2}L]$ (for **L1**) and $[CuH_{-1}L]^{+}$ (for **L2**)[25,26]. For $Cu^{2+}$/**L2** system, increasing the pH two further species were detected $[CuH_{-2}L]$ and $[CuH_{-3}L]^{-}$. The former one is obtained with a $pK_a = 9.44$, likely corresponding to the deprotonation of the phenolic group of tyrosine, which does not participate in the metal complexation, while the latter one is formed under the most alkaline conditions and can be ascribed to the displacement of a

third amide proton, giving rise to the ($N_{Im}$, $3N^-$) species ($\lambda_{max}$ = 525 nm) (Fig. 1a). The employed experimental techniques however do not allow to establish which His residues or backbone amides mainly participate in the complex formation.

As mentioned above, **L3** behaves differently than the acetylated analogues. Close to neutral pH, we observe the formation of the $[CuH_3L]^{3+}$ species, which dominates around pH 6.5. The Vis spectra show a clear blue-shift between pH 5.5 (where $[CuH_4L]^{4+}$ complex is predominant) and pH 6.5, but the wavelength of maximum absorption does not drop below 600 nm, as expected for 4N-type $Cu^{2+}$ complexes (*i.e.* with four equatorially bound nitrogen atoms). Therefore, it can be assumed that the increase of pH favors the coordination of the terminal amine that replaces an imidazole donor group in the metal coordination sphere (Fig. 1b). The prevailing complex at physiological pH is $[CuH_2L]^{2+}$: the wavelength of maximum absorption significantly decreases, and the value recorded at pH 7.5 (553 nm) is very close to both those expected for a coordination ($3N_{Im}$, $N^-$) (557 nm) and ($2N_{Im}$, $NH_2$, $N^-$) (549 nm). It cannot be excluded that both complexes are present in solution, or that it may exist a continuous and rapid "interconversion" between them, given the lability of the coordination bonds with the $Cu^{2+}$ ion. Above pH 7.5, once again we observed the gradual coordination of three backbone amides, forming ($2N_{Im}$, $2N^-$) and ($N_{Im}$, $3N^-$) species, which dominate under alkaline conditions. The tyrosine and the two lysine residues simply lose their proton without participating in the complexation.

## Formation of zinc complexes with L1, L2 and L3

Only mononuclear zinc complexes have been identified under the employed experimental conditions. MS spectra confirm the presence of different $Zn^{2+}$ complexes with various protonation states: $[ZnHL]^{3+}$ (**L1**, $m/z$ = 599.3), $[ZnL]^{2+}$ (**L2**, $m/z$ = 898.4), $[ZnH_3L]^{3+}$ (**L3**, $m/z$ = 584.6) and $[ZnH_2L \cdot K]^{3+}$ (**L3**, $m/z$ = 597.3) (Table S4). For all the systems, the stoichiometry of the first identified species indicates that only one histidine residue is protonated and therefore the $Zn^{2+}$ ion should coordinate two imidazole nitrogens, with a geometry that can be reasonably assumed to be tetrahedral[28]. The terminal Glu residue (or at least one of its carboxylate moieties in **L1**) can also bind the metal replacing a water molecule, as already reported for wild-type calcitermin[9]. When pH is increased, an acidic proton is released from the third histidine with a p$K_a$ of 5.80 (**L1**), 6.14 (**L2**) and 5.6 (**L3**), forming the species ($3N_{Im}$) where the third His can replace the carboxylate group (if coordinated) in the set of donor groups. A further deprotonation step leads to the formation of complexes $[ZnH_{-1}L]^+$ (**L1**, p$K_a$ = 7.33), $[ZnL]^{2+}$ (**L2**, p$K_a$ = 7.63) and $[ZnH_3L]^{3+}$ (**L3**, p$K_a$ = 7.32). In these cases, the release of the proton is attributable to the ionization of a coordinated water molecule. Increasing the pH, the complex-formation pattern and the geometry of the formed complexes with the acetylated peptides, **L1** and **L2**, are practically the same, with the only difference that, in the case of **L2**, we observe the deprotonation of the Tyr residue (p$K_a$ = 9.44) without metal coordination. The formed zinc species with **L1** and **L2** are most likely tetrahedral complexes with two or three coordinated histidines (Fig. 2), while water molecules saturate the coordination sphere. Instead, in the case of **L3**, after the formation of $[ZnH_3L]^{3+}$, we observe the mere deprotonation of the four basic sites of the ligand, in the order: the terminal amine (p$K_a$ = 7.69), the phenolic oxygen of tyrosine (p$K_a$ = 9.47), and the two ε-amino groups of lysines. In the end, above pH 9 and in the case of the amidated peptides, the formation of $[ZnHL]^+$ (for **L3**) and $[ZnH_{-1}L]^+$ (for **L2**) may be due to the release of an acidic proton from a second water molecule, which occupies a coordination position in a trigonal bipyramidal complex.

## Comparison of metal chelating abilities

Competition diagrams (Fig. S24) allow to compare the overall capacity of the studied ligands to coordinate $Zn^{2+}$ or $Cu^{2+}$ ions. Although they can be used only for a qualitative comparison of the binding affinities, the stability of

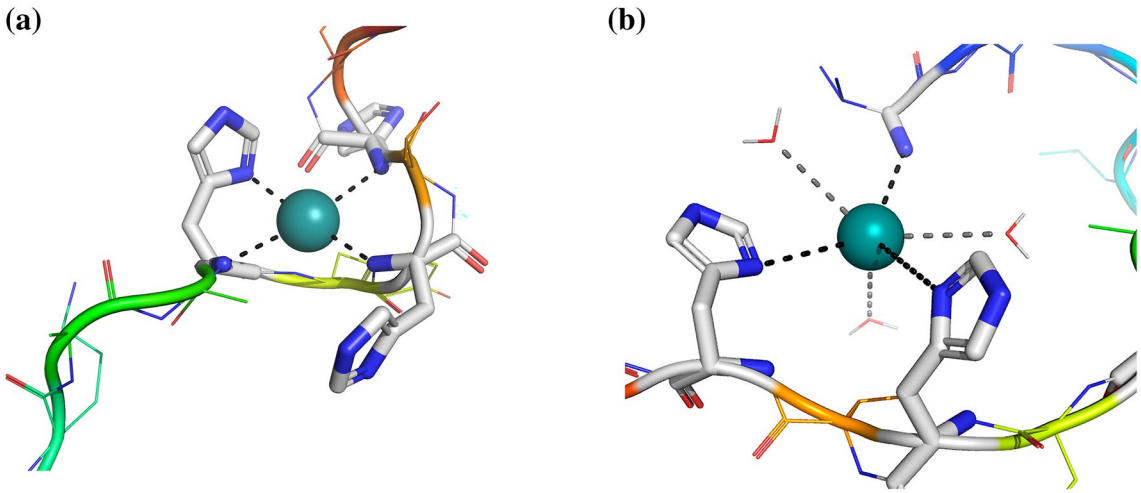


**Figure 1.** (**a**) Coordination hypothesis ($N_{Im}$, $3N^-$) for $[CuH_{-3}L]^-$ species of peptide **L2**. (**b**) Coordination hypothesis ($2N_{Im}$, $NH_2$) for the $[CuH_3L]^{3+}$ species of peptide **L3**. Molecular structure generated with PyMol[27].

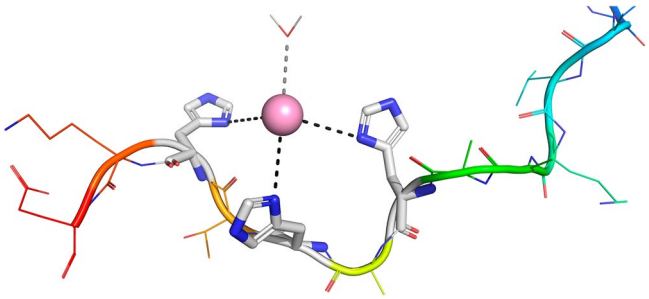

**Figure 2.** Coordination hypothesis for the ($3N_{Im}$) $Zn^{2+}$ complexes. Molecular structure generated with PyMol[27].

the formed complexes in the entire explored pH range, regardless of stoichiometry and structure of the formed species, can be evaluated.

In Fig. S24a the affinity for copper of the wild-type calcitermin is compared to that of its protected derivatives. The metal chelating ability of **WT** and **L1** is the same under acidic conditions. The presence of the terminal carboxylic group moderately enhances the stability of the formed complexes. Above pH 4.5, **WT** exhibits the best copper binding ability. Both the free terminal amine and carboxylate contribute to thermodynamically favour the formed complexes, thanks to the presence of a higher number of donor sites. On the other hand, the metal binding ability of the protected analogues above pH 5 is comparable. This is in accordance with the speciation models that indicate a similar coordination behaviour for these systems, with the progressive binding of the three histidines, followed by the terminal amino group and the backbone amides.

In the case of zinc (Fig. S24b), **WT** is a slightly better ligand in the entire pH range. The protected analogues behave similarly up to pH 6, after which the greater stability is shown by the complexes formed by the *N*-acetylated peptide, **L1**. This trend can confirm that the terminal amine is not involved in zinc complexation. On the contrary, the *C*-terminal carboxyl group seems to stabilize the formation of the complexes; suggesting that Glu residue takes part in the coordination by means of its side chain and/or terminal COOH, as in the case of WT[9].

## Peptide stability in plasma

The stability of the investigated peptides in human plasma is reported in Fig. 3a and is compared with the proteolytic susceptibility of wild-type calcitermin (**WT**). The concentration of all the peptides decreases with an approximately exponential decay and a half-life period ($t_{1/2}$) of about 20 min for **L3**, 68 min for **L2** and more than two hours (135 min predicted with an exponential regression) in the case of **L1**. The degradation profile of **L3** follows that of the native peptide, with a $t_{1/2}$ comparable to the value obtained for **WT** ($t_{1/2} = 18 \pm 3$ min). On the contrary the acetylated peptides, **L1** and **L2**, showed an improved resistance to degradation, with **L1** displaying the highest persistence in the human plasma. This result highlights the efficacy of the *N*-terminus protection as a general method to increase the resistance to proteolytic degradation of antimicrobial peptides[8]. The amidation of the *C*-terminus, instead, seems to affect less the resistance of calcitermin toward the activity of peptidases.

The effect of metal complex formation on the peptide stability has been evaluated for **WT** and **L1**—the least and most stable peptides, respectively. The complexation of $Cu^{2+}$ and $Zn^{2+}$ increases the half-life of **WT** from

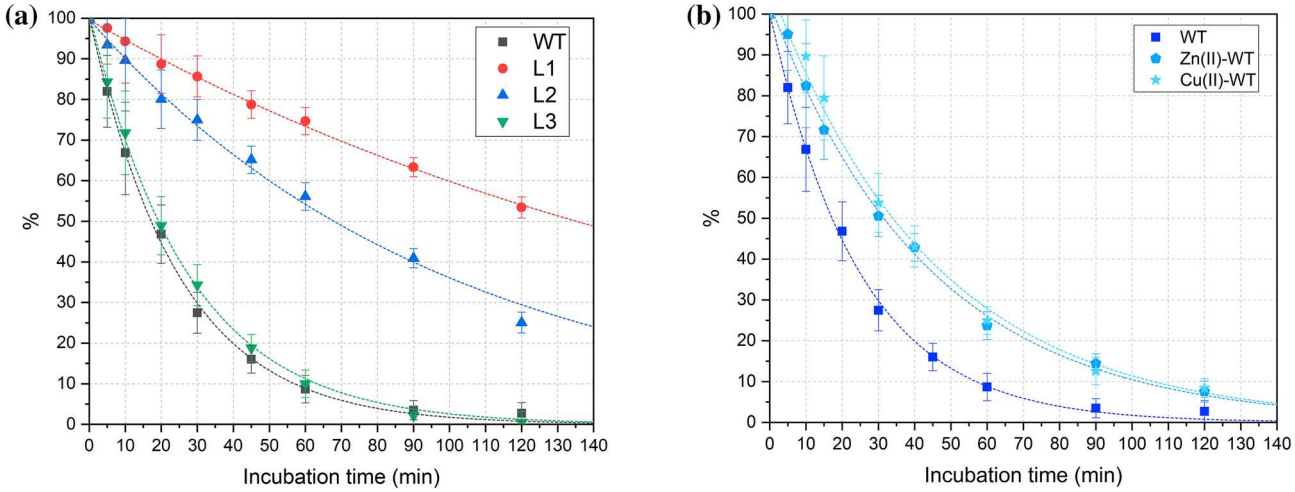


**Figure 3.** Stability in human plasma of wild-type calcitermin (**WT**) and its (**a**) *N*- and/or *C*-terminal protected analogues (**L1**, **L2**, **L3**); or (**b**) $Zn^{2+}$ and $Cu^{2+}$ complexes.

18 min to about 33 min (Fig. 3b), while the $t_{1/2}$ rises from 135 min to ≈150 min ($Zn^{2+}$) or ≈160 min ($Cu^{2+}$) in the case of **L1** (Fig. S25).

## Antimicrobial activity

The antimicrobial activity of **WT** calcitermin and its protected derivatives (**L1, L2, L3**) was assessed on *C. albicans*, *S. aureus*, and *E. coli*, respectively representative of human pathogens of fungal and bacterial origin.

Regarding *C. albicans* (Fig. 4), the results showed a remarkable CFU reduction of the yeast in the presence of **WT** compared to untreated controls. The reduction was already evident after 3 h (Fig. 4A), with all used concentrations, despite a true dose-dependence was not observable (− 67%, − 67%, and − 73%, for 0.032–0.064 and 0.128 mg/mL respectively, $p < 0.05$). A significant reduction was also observed with 0.128 mg/mL **WT** in the presence of $ZnCl_2$ (− 49%, $p < 0.05$), whereas no significant reduction was observed for the $Cu^{2+}$/**WT** complex. After 24 h of contact, the reduction was maintained and remarkably increased by $ZnCl_2$ presence, especially at 0.128 mg/mL (− 96%, $p < 0.0001$) (Fig. 4B). Instead, at 3 h, the **L1** derivative exhibited some antifungal action only at 0.128 mg/mL (Fig. 4C). At 24 h, limited yet significant CFU reduction was observed with **L1** alone (− 18%, − 17%, and − 23%, for 0.032, 0.064, and 0.128 mg/mL, respectively; $p < 0.05$), and increased activity was detected with the addition of $ZnCl_2$ (− 26% and − 88%, for 0.064 mg/mL and 0.128 mg/mL, $p < 0.05$ and $p < 0.001$, respectively). Some CFU decrease was also observed with **L1** + $CuCl_2$ (− 12%, − 28% and − 34% for 0.032, 0.064, and 0.128 mg/mL, respectively; $p < 0.05$) (Fig. 4C,D). Similarly, at 3 h, the **L2** derivative was significantly active only at 0.128 mg/mL in the presence of $ZnCl_2$ (− 74%, $p < 0.01$), while at 24 h a significant CFU reduction was observed at 0.064 and 0.128 mg/mL plus $ZnCl_2$ (respectively − 46%, $p < 0.0001$; and − 97%, $p < 0.0001$) and plus $CuCl_2$ (− 17% and − 23%, respectively; $p < 0.01$) (Fig. 4E,F). Comparable results were observed for **L3**, which at 3 h was active only at 0.128 mg/mL in the presence of $ZnCl_2$ (− 51%, $p < 0.01$), and at 24 h exhibited antifungal activity at 0.064 and 0.128 mg/mL in the presence of $ZnCl_2$ (respectively − 37%, $p < 0.05$; and − 76%, $p < 0.01$) (Fig. 4G,H). $ZnCl_2$ alone, included as a control, exhibited a significant antifungal activity in all performed assays, reducing *C. albicans* CFU number up to 64.9% at 3 h and to 94% at 24 h ($p < 0.0001$). By contrast, negligible or no CFU reduction was observed in all conditions with $CuCl_2$ alone, which significantly reduced *C. albicans* CFU number only at 24 h, in one out of the total performed assays (Table S5).

Summarizing, the results on *C. albicans* confirmed the antifungal activity of **WT** calcitermin, even at low concentrations, at both 3 and 24 h. The **WT**/zinc complex was quite effective against *C. albicans* at 24 h, at 0.128 mg/mL, although only a slightly lower activity was found for $ZnCl_2$ itself at the same concentration. On the other hand, no activity was shown by $CuCl_2$ alone and its presence did not significantly affect the **WT** activity, although $Cu^{2+}$ can form stable complexes with calcitermin even at pH 5.4. Of note, previous studies showed that both $Zn^{2+}$ and $Cu^{2+}$ ions possess antifungal activity per se at concentrations consistent with those used in our study, showing similar minimal inhibitory concentrations, although $Zn^{2+}$ was generally proven to be more effective compared to $Cu^{2+}$[29–31]. Our results confirmed the $Zn^{2+}$ anti-*C. albicans* activity, whereas a marked antifungal activity by $Cu^{2+}$ ion was not evidenced. This might be due to: the different type of assay performed in our study compared to those previously reported; the different metal ion formulations tested (Zn/Cu chloride vs. Zn/Cu oxide), the absence in our study of a nanoparticle delivery system[32,33]; the suboptimal concentrations of ions used in our assays, which may have induced some yeast tolerance to metal ions. Further studies would be needed to address these points. The amidation of the carboxyl terminal (peptides **L2** and **L3**) did not improve the antifungal activity of **WT**, also in the presence of zinc. Some effect due to acetylation of the *N*-terminus of calcitermin (**L1** and **L2** peptides) was observed in the presence of $CuCl_2$, after 24 h; in particular, $Cu^{2+}$ complexes with a concentration of 0.128 mg/mL were significantly more active than both the corresponding controls and the calcitermin complexes.

The antimicrobial action of calcitermin and its derivatives was also tested on bacteria, including the Gram-negative bacillus *E. coli* and the Gram-positive coccus *S. aureus*. Regarding *E. coli,* the results showed that **WT** was active essentially in the presence of $ZnCl_2$ or $CuCl_2$ (Fig. 5A,B). At 3 h, the CFU number decreased to − 38% ($p < 0.05$), − 55% ($p < 0.01$), and − 91% ($p < 0.001$) with respect to controls, using 0.032, 0.064, and 0.128 mg/mL of peptide + $ZnCl_2$, respectively. With the addition of $CuCl_2$, the CFU decrease corresponded to − 38% ($p < 0.01$), − 56% ($p < 0.05$), and − 91% ($p < 0.001$) for 0.032, 0.064, and 0.128 mg/mL of peptide, respectively. At 24 h, no significant CFU reduction was observed with **WT** with or without $ZnCl_2$, whereas a − 82% decrease of CFU number was detected with 0.128 mg/mL of calcitermin in the presence of $CuCl_2$ ($p < 0.0001$).

Differently from **WT**, the **L1** derivative induced a dose-dependent CFU decrease at 3 h (− 28%, − 39%, and − 40%, for 0.032, 0.064, and 0.128 mg/mL, respectively; $p < 0.05$). The reduction was increased in the presence of $ZnCl_2$ (− 67%, − 81%, and − 96%, respectively; $p < 0.001$), and $CuCl_2$ (− 65%, − 63%, and − 85% for 0.032, 0.064, and 0.128 mg/mL, respectively; $p < 0.01$). At 24 h, **L1** was active only at 0.128 mg/mL, alone (− 19%, $p < 0.05$) or in the presence of $CuCl_2$, which significantly increased **L1** action (− 67% and − 90% for 0.064 and 0.128 mg/mL, respectively; $p < 0.001$) (Fig. 5C,D).

A similar trend was observed for **L2**, which at 3 h reduced *E. coli* CFUs only in the presence of $ZnCl_2$ (− 64%, − 76%, and − 96% at 0.032, 0.064 and 0.128 mg/mL, respectively; $p < 0.001$) or $CuCl_2$ (− 55%, − 65%, and − 82%, respectively; $p < 0.01$). At 24 h, no significant CFU reduction was observed except for 0.032 and 0.064 mg/mL in the presence of $ZnCl_2$ (Fig. 5E,F). The activity of the **L3** derivative was essentially detectable only at 3 h in the presence of $ZnCl_2$ and $CuCl_2$, inducing a significant CFU decrease at 0.032, 0.064 and 0.128 mg/mL (for $ZnCl_2$, − 58%, − 79%, and − 94%, respectively, $p < 0.001$; for $CuCl_2$, − 51%, − 81%, and − 82%, respectively, $p < 0.001$). After 24 h, no significant reduction was observed at any L3 concentration, except for 0.128 mg/mL in the presence of $CuCl_2$ (− 41%, $p < 0.01$) (Fig. 5G,H).

As also observed in the antifungal assays, $ZnCl_2$ exhibited an anti-*E. coli* activity per se, reducing the CFU number up to − 95% at 3 h ($p < 0.0001$), although it was not anymore active at 24 h, showing a − 30% reduction

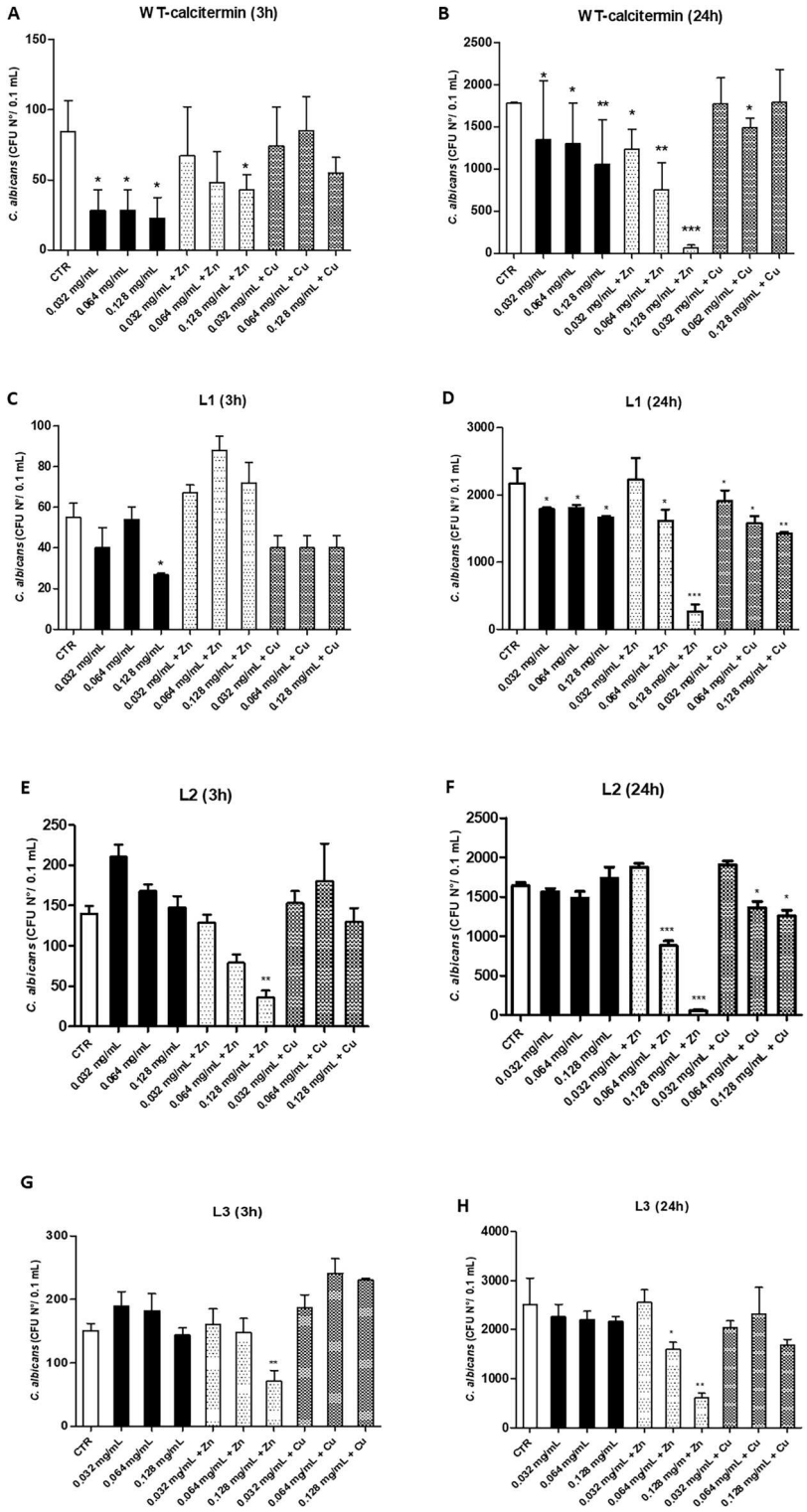


**Figure 4.** In vitro antifungal activity of **WT** and **L1, L2, L3** derivatives. All assays were performed in the presence or absence of $ZnCl_2$, or $CuCl_2$ in aqueous buffer (5.4 pH). (**A**,**B**) WT-calcitermin action at 3 and 24 h-incubation; (**C**,**D**) L1 action at 3 and 24 h-incubation; (**E**,**F**) L2 action at 3 and 24 h-incubation; (**G**,**H**) L3 action at 3 and 24 h-incubation. Results are expressed ad mean value of CFUs ± SD obtained in triplicate samples from two independent experiments; *$p \leq 0.05$; **$p \leq 0.01$; ***$p \leq 0.001$.

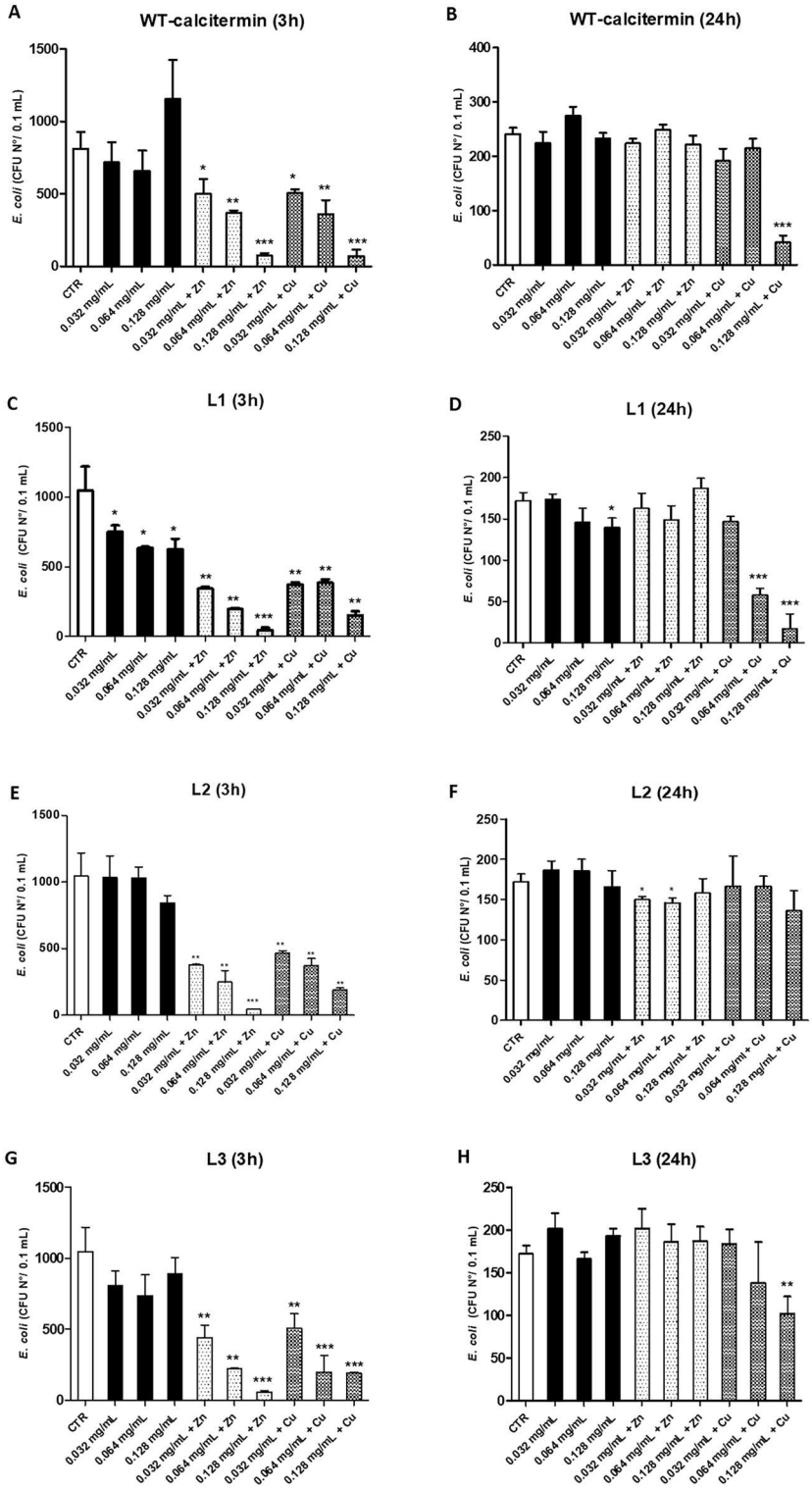


**Figure 5.** In vitro anti-*E. coli* activity of **WT** and **L1, L2, L3** derivatives. All assays were performed in the presence or absence of $ZnCl_2$, or $CuCl_2$ in aqueous buffer (5.4 pH). (**A**,**B**) WT-calcitermin action at 3 and 24 h-incubation; (**C**,**D**) L1 action at 3 and 24 h-incubation; (**E**,**F**) L2 action at 3 and 24 h-incubation; (**G**,**H**) L3 action at 3 and 24 h-incubation. Results are expressed ad mean value of CFUs ± SD obtained in triplicate samples from two independent experiments; *$p \leq 0.05$; **$p \leq 0.01$; ***$p \leq 0.001$.

only in one of the performed assays ($p < 0.05$). Also $CuCl_2$ displayed a high antibacterial activity, inducing an up to 96% reduction at both 3 and 24 h of incubation ($p < 0.0001$) (Table S6). In conclusion, only the derivative **L1** showed a significant anti-*E. coli* activity in the absence of metals, especially after 3 h. Interestingly, **L1** was also the least sensitive peptide of the series towards the proteolytic enzymes. Copper and zinc exhibited antimicrobial activity against *E. coli* at 3 h, both in their free and complexed form; this behaviour was very similar for all peptides, regardless of the protection of the terminals. However, at 24 h, only copper (and its complexes) showed some activity, especially in the case of **L1**, whose complexes with $Cu^{2+}$ were already active at the concentration of 0.064 mg/ml.

Regarding *S. aureus*, the assays were performed only at 3 h, since at 24 h of incubation in aqueous buffer at pH 5.4 no viable bacteria were detectable even in untreated controls. At 3 h, the data showed that **WT** was significantly active only at 0.128 mg/mL in the presence of $ZnCl_2$ (− 41%, $p < 0.05$) (Fig. 6A).

Similarly, both **L1** and **L2** derivatives induced a significant CFU decrease only at 0.128 mg/mL in presence of $ZnCl_2$ (− 46%, $p < 0.05$; − 54%, $p < 0.01$, respectively for **L1** and **L2**) (Fig. 6B,C). **L3** action was instead more evident, inducing a CFU decrease corresponding to -28% ($p$ = n.s.), − 43% ($p < 0.05$), and − 49% ($p < 0.05$) at 0.032, 0.064, and 0.128 mg/mL concentration, respectively. Moreover, the action of 0.128 mg/mL of **L3** was increased by the addition of $ZnCl_2$ (− 73% CFU decrease, $p < 0.001$) (Fig. 6D), and by the presence of $CuCl_2$ (− 47%, $p < 0.01$) (Fig. 6).

Likewise, $ZnCl_2$ alone showed a clear antimicrobial activity toward *S. aureus*, inducing an up to 77% CFU reduction, compared to controls (Table S7). Regarding *S. aureus*, in conclusion, **WT** calcitermin showed no effect, but a significant antimicrobial activity was observed for **L3**. $Zn^{2+}$ complexes of all peptides were active at higher concentrations, especially when the terminals were protected. Among the $Cu^{2+}$ complexes, only the one with **L3**

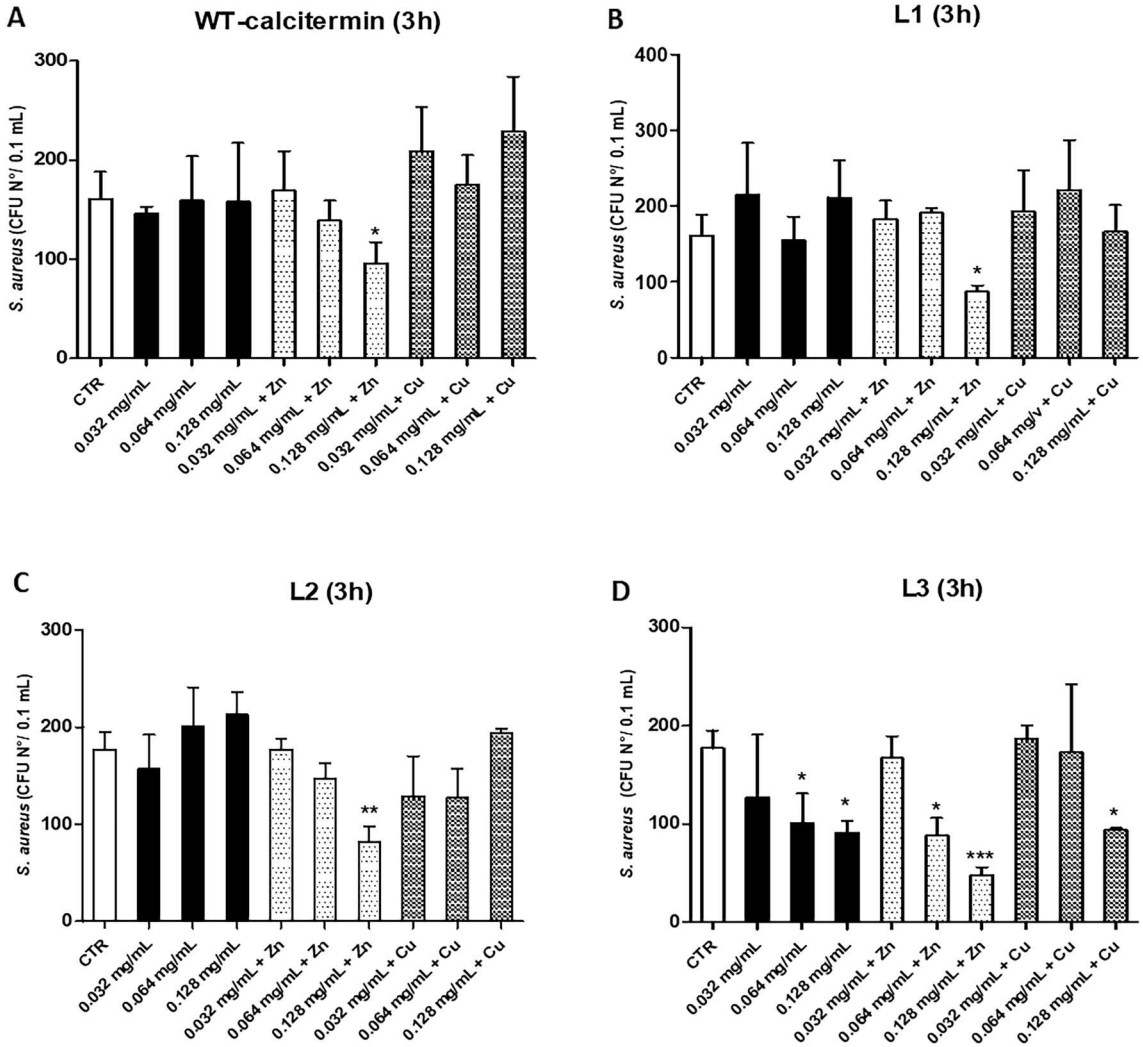


**Figure 6.** In vitro anti-*S. aureus* activity of **WT** and **L1, L2, L3** derivatives. All assays were performed for 3 h-incubation time in the presence or absence of $ZnCl_2$ or $CuCl_2$ in aqueous buffer (pH 5.4). (**A**) WT-calcitermin action; (**B**) L1 action; (**C**) L2 action; (**D**) L3 action. Results are expressed ad mean value of CFUs ± SD obtained in triplicate samples from two independent experiments; *p ≤ 0.05; **p ≤ 0.01; ***p ≤ 0.001.

showed a detectable action, at a concentration of 0.128 mg/ml, although this was comparable to that shown by the same peptide in the absence of metals.

## Concluding remarks

Although calcitermin and its antimicrobial activity have been known for over twenty years, this peptide is still sparsely studied as a potential new drug. The studies of Cole and coworkers[10] first showed that bivalent endogenous metals, such as zinc and copper, can modulate the antimicrobial activity of calcitermin; later on, our research group investigated its metal binding properties. Then, a systematic study on calcitermin derivatives has begun, modifying the amino acid sequence in an opportune manner, with a view to improving interaction with cell membranes, to increasing stability towards proteolytic enzymes and/or to improving the sequestering ability towards metal ions to promote nutritional immunity. The encouraging previous results have led us to study the new calcitermin derivatives reported in this paper, where the native peptide has been protected at one or both of its termini. This is one of the ways, already known in the literature, to increase the resistance to proteolytic degradation of a peptide[34–37]. However, since any variation in the structure of the peptide can affect both its ability to form metal complexes and its antimicrobial properties, we have carried out a thorough study, both from the chemical and microbiological point of view, to shed light on the behaviour of the modified peptides. The formation of metal complexes with calcitermin is driven by the presence of its three histidine residues. This coordination site is preserved in all peptides studied here, and stable complexes with all ligands have always been observed. According to Pearson's classification, in fact, the imidazole side chain of histidine is a good binding site (borderline basic character) for $Cu^{2+}$ and $Zn^{2+}$ ions (borderline Lewis acids)[38] and, on the basis of their electronic configuration, the Irving-Williams series also predicts a higher binding affinity for $Cu^{2+}$ than $Zn^{2+}$[39].

The metal coordination did not affect the peptide structure, and for all the systems a prevalence of random coil conformation was observed (Figs. S16–S18). However, the contribution to the complex-formation by the amino and carboxyl termini, although secondary, is evident: both with copper and zinc, the most stable complexes are always those formed by the native calcitermin, throughout the explored pH range. Noteworthy, the metal complexed forms of the studied peptides display higher resistance to degradation. Indeed, the formation of both copper and zinc complexes with calcitermin almost doubled its half-life in human plasma, suggesting that the interaction with metal ions can be a fruitful strategy to increase the peptide stability in biological fluids. Whether this correlates with the slightly better antimicrobial activity of the studied metal complexes is not easy to judge, and further investigation is required. Similarly, it is not straightforward to link the antimicrobial activity of the studied peptides with their stability in plasma.

Acetylation of the *N*-terminal confers a much longer half-life with respect to peptides with free amino terminus. This is an important indication for the design of calcitermin derivatives (as well as other AMP derivatives)[35–37] that may persist in the body long enough to perform their microbicidal action. Indeed, the study of peptide degradation will be deepened trying to identify the responsible enzymes and the most vulnerable peptide bonds, also extending the investigation to other biological fluids, such as saliva and gastric juices. Moreover, a preliminary investigation on peptide interaction with albumin (one of the major proteins in plasma) has been carried out to evaluate the protein-peptide binding, which may affect the decrease of peptide concentration detected after incubation in plasma. We observed a variation in the α-helical content of albumin structure when the studied peptides are added to the solution (Fig. S26). The mechanism and effect of such interaction will require further specific investigations; however, all the investigated peptides, even in their metal complexed form, behave in the same way and decrease the same extent the α-helix structure of the protein. Therefore, the interaction with albumin does not affect the relative stability of calcitermin and its derivative systems.

Lastly, although the new calcitermin derivatives studied here were not particularly promising as commercial antimicrobials against fungi such as *C. albicans* or against Gram-positive or Gram-negative bacteria, encouraging results have been obtained for their metal (especially $Zn^{2+}$) complexes. The investigation will be therefore extended to other derivatives, other microorganisms and other experimental conditions. In conclusion, calcitermin and its derivatives remain a promising class of peptides of great interest as new generation of metal-enhanced antimicrobials.

## Methods

### Potentiometry

Stability constants for proton and metal complexes were obtained from pH-metric titration curves registered at $T = 298$ K and ionic strength 0.1 M (KCl). The potentiometric apparatus was previously described[40]. Solutions were titrated with 0.1 M carbonate-free KOH. The electrode was daily calibrated for hydrogen ion concentration by titrating $HNO_3$ with the standard base solution, under the same experimental conditions as above. The asymmetry potential and the slope of the electrode couple were computed by means of SUPERQUAD[41] and Glee[42] programs. The purities and exact concentrations of the ligand solutions were determined by the Gran method[43]. The HYPERQUAD[44] program was employed for the overall formation constant ($\beta$) calculations, referred to the following equilibrium equation: $pM + qL + rH \leftrightarrows M_pL_qH_r$ (charges omitted; p is 0 in the case of ligand protonation; r can be negative). The computed standard deviations (referring to random errors only) were given by the program itself and are shown in parentheses as uncertainties on the last significant figure. Hydrolysis constants for metal ions were taken from the literature[45,46]. The distribution and competition diagrams were computed using the HYSS program[47].

### Mass spectrometry

High-resolution mass spectra were obtained on the LCMS-9030 qTOF Shimadzu (Shimadzu, Kyoto, Japan), equipped with a standard ESI source and the Nexera X2 system. The instrumental parameters were as follows:

positive ion mode, scan range *m*/*z* 100–3000, dry gas nitrogen, temperature 170 °C, and ion energy 5 eV. The capillary voltage was optimized to the highest S/N ratio and it was 4500 V. The small changes in voltage (± 500 V) did not significantly affect the optimized spectra. The samples ($[L]_{tot} = 1{\cdot}10^{-4}$ M and M:L molar ratio = 1:1) were prepared in a 1:1 methanol–water mixture at pH 5.2 and 7.4. They were directly infused at a flow rate of 3 µl/min. The instrument was externally calibrated with a Tunemix™ mixture (Bruker Daltonik, Germany) in quadratic regression mode. Data were processed using the Bruker Compass DataAnalysis 4.2 program. The mass accuracy for the calibration was > 5 ppm, enabling together with the true isotopic pattern (using SigmaFit) an unambiguous confirmation of the elemental composition of the obtained complex.

## Spectroscopic measurements

The absorption spectra of $Cu^{2+}$ containing solutions were recorded on a Varian Cary50 Probe spectrophotometer, in the range 350–900 nm, using a quartz cuvette with an optical path of 1 cm. To describe the species present in solution, the observed wavelength of maximum absorption at a given pH was compared with the expected $\lambda_{max}$ value obtained from literature[23,48–50]. Circular dichroism (CD) spectra were recorded on a Jasco J-1500 spectropolarimeter in the 180–800 nm range, using a quartz cuvette with an optical path of 1 cm in the visible and near-UV range, and 0.01 cm in the 180–250 nm range. Electron paramagnetic resonance (EPR) spectra were recorded in liquid nitrogen on a Bruker ELEXSYS E500 CW-EPR spectrometer at X-band frequency (9.5 GHz) and equipped with an ER 036TM NMR teslameter and an E41 FC frequency counter. Ethylene glycol (30%) was used as a cryoprotectant. The EPR parameters were analyzed by computer simulation of the experimental spectra using WIN-EPR SIMFONIA software, version 1.2 (Bruker, Billerica, MA, USA).

## Peptide stability in plasma

The persistence of calcitermin and its analogues and metal complexes in human plasma has been studied in vitro by means of the following procedure[51]. Each peptide ($C = 1{\cdot}10^{-4}$ M) and metal complex (metal:ligand ratio 1:1) was incubated in a sample containing 1 ml of human plasma (obtained as a pool of 40 individuals from the University Hospital of Ferrara) and 1 ml of ammonium acetate buffer (pH 7.4) at 37 °C. L-phenylalaninol is added as internal standard. At regular time intervals, 200 µl aliquots were taken and enzymatic reaction was blocked by adding 300 µl of $HClO_4$ 0.5 M. The sample was then centrifugated for 6 min at 14,000 × *g*. The supernatant was then filtered and analysed by HPLC. The analytical column was an Agilent Poroshell 120 SB-C18 (4.6 × 100 mm, 2.7 µm, pore size 120 Å). Flow rate = 0.5 ml/min, mobile phase $H_2O$ + 0.1% v/v TFA, linear gradient from 0 to 60% of acetonitrile + 0.1% v/v TFA over 30 min for the elution of peptides, temperature 25 °C, detection wavelength 210 nm. The results on calcitermin are the mean of three independent measurements while only one test was performed with the three protected peptides; in the latter cases, the errors have been estimated on the basis of those obtained for the wild-type calcitermin. Informed consent was obtained from all subjects and/or their legal guardian(s) prior to the donation of blood samples. All experimental protocols were approved by the National Research and Research Transversal Processes boards at University of Ferrara. All methods were carried out in accordance with relevant guidelines and regulations.

## Biological tests

The potential antimicrobial activity of wild-type calcitermin and *N*- and *C*- terminally protected derivatives was investigated by using the yeast *C. albicans* (ATCC 10231), the Gram-positive *S. aureus* (ATCC 25293), and the Gram-negative *E. coli* (ATCC 25922) (all from American Type Culture Collection, ATCC, Thermo Scientific, Milan, Italy). All microbes were grown at 37 °C in Tryptic Soy Broth (TSB; Biolife, Milan, Italy) or Tryptic Soy Agar plates (TSA, Biolife, Milan, Italy). Peptides were tested at a final concentration C = 0.128, 0.064, 0.032 mg/mL, in the presence or absence of $ZnCl_2$ or $CuCl_2$, at a M:L molar ratio 0.9:1. Briefly, all the microbes were expanded in TSB at 37 °C under agitation for 12 h and then sub-cultured by 1:10 dilution in TSB under the same conditions until reaching $OD_{600nm} = 0.3–0.4$, as measured by spectrophotometric reading using a GENESYS 10S UV–Vis spectrophotometer (Thermo Scientific, Milan, Italy), corresponding to $0.9–1.2 \times 10^7$ colony forming units (CFU) per mL, $1.5–2 \times 10^8$ CFU/mL and $2.4–3.2 \times 10^8$ CFU/mL, for *C. albicans, S. aureus* and *E. coli* respectively. The cultures were then centrifuged at 4500 rpm for 10 min in a SL 8 centrifuge (TX-150 Rotor) (Thermo Scientific, Milan, Italy), and the cellular pellets were washed with PBS pH 5.4. Pelletized cultures were then suspended in 10 mL of PBS pH 5.4, then the suspensions were diluted to a final concentration of $10^4$ CFU/mL. Aliquots of 100 µl (corresponding to $10^3$ CFU) were seeded in each well of a 96-wells plate. 3 µl of TSB at pH 5.4 were added to each well to obtain a final 1.5% TSB concentration in the culture medium. Peptides were serially diluted in PBS pH 5.4 to C = 0.257, 0.128, and 0.064 mg/mL. $ZnCl_2$ and $CuCl_2$ solutions were added where requested to obtain a M:L ratio 0.9:1. 100 µl of the prepared peptides ± $ZnCl_2$/$CuCl_2$ solutions were then added to each well, obtaining the final 0.128, 0.064 and 0.032 mg/mL peptide concentrations in a total 0.2 mL volume. PBS alone and PBS + $ZnCl_2$/$CuCl_2$ solutions were included as controls. The plates were incubated at 37 °C on a platform rocker with slow stirring for 3 and 24 h. At the end of the incubation times, 100 µl aliquots were taken from each sample and diluted in PBS pH 5.4 to be seeded on TSA plates. Specifically, aliquots were diluted 1:10 at 3 h, and 1:200, 1:100,000 and 1:10 at 24 h, for *C. albicans*, *E. coli*, and *S. aureus* respectively. After incubation for 24 h at 37 °C, grown CFUs were enumerated. Samples were assayed in triplicate in two independent experiments. Student's *t*-test was used for the evaluation of significance in biological tests; a $p$ value ≤ 0.05 was considered significant.

## Data availability

The datasets used in the current study is available from the corresponding author upon request.

Received: 4 August 2023; Accepted: 19 October 2023
Published online: 25 October 2023

## References


1. Steckbeck, J. D., Deslouches, B. & Montelaro, R. C. Antimicrobial peptides: New drugs for bad bugs?. *Expert Opin. Biol. Ther.* **14**, 11–14. https://doi.org/10.1517/14712598.2013.844227 (2014).
2. Malanovic, N. & Lohner, K. Antimicrobial peptides targeting gram-positive bacteria. *Pharmaceuticals (Basel)* **9**, 59. https://doi.org/10.3390/ph9030059 (2016).
3. Vishnepolsky, B. *et al.* De novo design and in vitro testing of antimicrobial peptides against gram-negative bacteria. *Pharmaceuticals (Basel)* **12**, 82. https://doi.org/10.3390/ph12020082 (2019).
4. Lugardon, K. *et al.* Antibacterial and antifungal activities of vasostatin-1, the N-terminal fragment of chromogranin A. *J. Biol. Chem.* **275**, 10745–10753. https://doi.org/10.1074/jbc.275.15.10745 (2000).
5. Chernysh, S. *et al.* Antiviral and antitumor peptides from insects. *Proc. Natl. Acad. Sci. U. S. A.* **99**, 12628. https://doi.org/10.1073/pnas.192301899 (2002).
6. Wang, G., Li, X. & Wang, Z. APD3: The antimicrobial peptide database as a tool for research and education. *Nucleic Acids Res.* **44**, 1087–1093. https://doi.org/10.1093/nar/gkv1278 (2016).
7. Gülseren, İ & Vahapoglu, B. The stability of food bioactive peptides in blood: An overview. *Int. J. Pept. Res. Ther.* **28**, 2. https://doi.org/10.1007/s10989-021-10321-w (2021).
8. Bellotti, D. & Remelli, M. Lights and shadows on the therapeutic use of antimicrobial peptides. *Molecules* **27**, 4584. https://doi.org/10.3390/molecules27144584 (2022).
9. Bellotti, D. *et al.* Bioinorganic chemistry of calcitermin—The picklock of its antimicrobial activity. *Dalton Trans.* **48**, 13740–13752. https://doi.org/10.1039/c9dt02869b (2019).
10. Cole, A. M. *et al.* Calcitermin, a novel antimicrobial peptide isolated from human airway secretions. *FEBS Lett.* **504**, 5–10. https://doi.org/10.1016/S0014-5793(01)02731-4 (2001).
11. Bellotti, D. *et al.* Calcitermin-loaded smart gels activity against Candida albicans: A preliminary in vitro study. *Gels* **9**, 165 (2023).
12. Jiang, H. *et al.* A branched tripeptide with an anion-binding motif as a new delivery carrier for efficient gene transfection. *ChemBioChem* **20**, 1410–1416. https://doi.org/10.1002/cbic.201800728 (2019).
13. Alexander, J. L., Thompson, Z. & Cowan, J. A. Antimicrobial metallopeptides. *ACS Chem. Biol.* **13**, 844–853. https://doi.org/10.1021/acschembio.7b00989 (2018).
14. Lenci, E. & Trabocchi, A. Peptidomimetic toolbox for drug discovery. *Chem. Soc. Rev.* **49**, 3262–3277. https://doi.org/10.1039/D0CS00102C (2020).
15. Mutter, M. & Tuchscherer, G. Non-native architectures in protein design and mimicry. *Cell. Mol. Life Sci.* **53**, 851–863. https://doi.org/10.1007/s000180050105 (1997).
16. Sandberg, B. E. B., Lee, C. M., Hanley, M. R. & Iversen, L. L. Synthesis and biological properties of enzyme-resistant analogs of substance-P. *Eur. J. Biochem.* **114**, 329–337. https://doi.org/10.1111/j.1432-1033.1981.tb05152.x (1981).
17. Porter, E. A., Weisblum, B. & Gellman, S. H. Mimicry of host-defense peptides by unnatural oligomers: Antimicrobial β-peptides. *J. Am. Chem. Soc.* **124**, 7324–7330. https://doi.org/10.1021/ja0260871 (2002).
18. Cabrele, C., Martinek, T. A., Reiser, O. & Berlicki, Ł. Peptides containing β-amino acid patterns: Challenges and successes in medicinal chemistry. *J. Med. Chem.* **57**, 9718–9739. https://doi.org/10.1021/jm5010896 (2014).
19. Robinson, J. A. Folded synthetic peptides and other molecules targeting outer membrane protein complexes in gram-negative bacteria. *Front. Chem.* **7**, 1–11. https://doi.org/10.3389/fchem.2019.00045 (2019).
20. Degenkolb, T. & Brückner, H. Peptaibiomics: Towards a myriad of bioactive peptides containing Cα-dialkylamino acids?. *Chem. Biodivers.* **5**, 1817–1843. https://doi.org/10.1002/cbdv.200890171 (2008).
21. Dancs, Á. *et al.* Tuning the coordination properties of multi-histidine peptides by using a tripodal scaffold: Solution chemical study and catechol oxidase mimicking. *NJCh* **41**, 808–823. https://doi.org/10.1039/c6nj03126a (2017).
22. Shi, S. M. & Di, L. In *Peptide Therapeutics: Fundamentals of Design, Development, and Delivery* (ed. Jois, S. D.) 163–182 (Springer International Publishing, 2022).
23. Sigel, H. & Martin, R. B. Coordinating properties of the amide bond. Stability and structure of metal ion complexes of peptides and related ligands. *Chem. Rev.* **82**, 385–426. https://doi.org/10.1021/cr00050a003 (1982).
24. Peisach, J. & Blumberg, W. E. Structural implications derived from the analysis of electron paramagnetic resonance spectra of natural and artificial copper proteins. *Arch. Biochem. Biophys.* **165**, 691–708. https://doi.org/10.1016/0003-9861(74)90298-7 (1974).
25. Stanyon, H. F. *et al.* Developing predictive rules for coordination geometry from visible circular dichroism of copper(II) and nickel(II) ions in histidine and amide main-chain complexes. *FEBS J.* **281**, 3945–3954. https://doi.org/10.1111/febs.12934 (2014).
26. Daniele, P. G., Prenesti, E. & Ostacoli, G. Ultraviolet–circular dichroism spectra for structural analysis of copper(II) complexes with aliphatic and aromatic ligands in aqueous solution. *Dalton Trans.* **15**, 3269–3275 (1996).
27. The PyMOL Molecular Graphics System, V. r. p., Schrödinger, LLC.
28. Alberts, I. L., Nadassy, K. & Wodak, S. J. Analysis of zinc binding sites in protein crystal structures. *Protein Sci.* **7**, 1700–1716. https://doi.org/10.1002/pro.5560070805 (1998).
29. Djearamane, S. *et al.* Antifungal properties of zinc oxide nanoparticles on Candida albicans. *Coatings* **12**, 1864 (2022).
30. Pasquet, J. *et al.* The contribution of zinc ions to the antimicrobial activity of zinc oxide. *Colloids Surf. Physicochem. Eng. Aspects* **457**, 263–274. https://doi.org/10.1016/j.colsurfa.2014.05.057 (2014).
31. Karimiyan, A., Najafzadeh, H., Ghorbanpour, M. & Hekmati-Moghaddam, S. H. Antifungal effect of magnesium oxide, zinc oxide, silicon oxide and copper oxide nanoparticles against Candida albicans. *Zahedan J. Res. Med. Sci.* **17**, e2179. https://doi.org/10.17795/zjrms-2179 (2015).
32. Vincent, M., Duval, R. E., Hartemann, P. & Engels-Deutsch, M. Contact killing and antimicrobial properties of copper. *J. Appl. Microbiol.* **124**, 1032–1046. https://doi.org/10.1111/jam.13681%JJournalofAppliedMicrobiology (2018).
33. Martínez, A. *et al.* Dual antifungal activity against Candida albicans of copper metallic nanostructures and hierarchical copper oxide marigold-like nanostructures grown in situ in the culture medium. *J. Appl. Microbiol.* **130**, 1883–1892. https://doi.org/10.1111/jam.14859%JJournalofAppliedMicrobiology (2021).
34. Powell, M. F. In *Annual Reports in Medicinal Chemistry* Vol. 28 (ed. Bristol, J. A.) 285–294 (Academic Press, 1993).
35. Li, D. *et al.* N-terminal acetylation of antimicrobial peptide L163 improves its stability against protease degradation. *J. Pept. Sci.* **27**, e3337. https://doi.org/10.1002/psc.3337 (2021).
36. He, Z., Yuan, C., Zhang, L. & Yousef, A. E. N-terminal acetylation in paenibacillin, a novel lantibiotic. *FEBS Lett.* **582**, 2787–2792. https://doi.org/10.1016/j.febslet.2008.07.008 (2008).
37. Krishnakumari, V. & Nagaraj, R. N-terminal fatty acylation of peptides spanning the cationic C-terminal segment of bovine β-defensin-2 results in salt-resistant antibacterial activity. *Biophys. Chem.* **199**, 25–33. https://doi.org/10.1016/j.bpc.2015.02.005 (2015).
38. Pearson, R. G. Hard and soft acids and bases. *J. Am. Chem. Soc.* **85**, 3533–3539. https://doi.org/10.1021/ja00905a001 (1963).
39. Irving, H. & Williams, R. J. P. 637. The stability of transition-metal complexes. *J. Chem. Soc. (Resumed)* https://doi.org/10.1039/JR9530003192 (1953).

40. Bellotti, D., Tocchio, C., Guerrini, R., Rowińska-Żyrek, M. & Remelli, M. Thermodynamic and spectroscopic study of Cu(ii) and Zn(ii) complexes with the (148–156) peptide fragment of C4YJH2, a putative metal transporter of Candida albicans. *Metallomics* **11**, 1988–1998. https://doi.org/10.1039/c9mt00251k (2019).
41. Gans, P., Sabatini, A. & Vacca, A. SUPERQUAD: An improved general program for computation of formation constants from potentiometric data. *Dalton Trans.* **6**, 1195–1200 (1985).
42. Gans, P. & O'Sullivan, B. GLEE, a new computer program for glass electrode calibration. *Talanta* **51**, 33–37. https://doi.org/10.1016/s0039-9140(99)00245-3 (2000).
43. Gran, G. Determination of the equivalent point in potentiometric titrations. *Acta Chem. Scand.* **4**, 559–577. https://doi.org/10.3891/acta.chem.scand.04-0559 (1950).
44. Gans, P., Sabatini, A. & Vacca, A. Investigation of equilibria in solution. Determination of equilibrium constants with the HYPERQUAD suite of programs. *Talanta* **43**, 1739–1753 (1996).
45. Brown, P. L. & Ekberg, C. *Hydrolysis of Metal Ions* 499–716 (Wiley, 2016).
46. Arena, G., Cali, R., Rizzarelli, E. & Sammartano, S. Thermodynamic study on the formation of the cupric ion hydrolytic species. *Therm. Acta* **16**, 315–321. https://doi.org/10.1016/0040-6031(76)80024-X (1976).
47. Alderighi, L. *et al.* Hyperquad simulation and speciation (HySS): A utility program for the investigation of equilibria involving soluble and partially soluble species. *Coord. Chem. Rev.* **184**, 311–318 (1999).
48. Berto, S. *et al.* Oxovanadium(IV) coordination compounds with Kojic acid derivatives in aqueous solution. *Molecules* **24**, 3768. https://doi.org/10.3390/molecules24203768 (2019).
49. Prenesti, E., Daniele, P. G., Prencipe, M. & Ostacoli, G. Spectrum-structure correlation for visible absorption spectra of copper(II) complexes in aqueous solution. *Polyhedron* **18**, 3233–3241. https://doi.org/10.1016/S0277-5387(99)00279-X (1999).
50. Billo, E. J. Copper(II) chromosomes and the rule of average environment. *Inorg. Nuclear Chem. Lett.* **10**, 613–617. https://doi.org/10.1016/0020-1650(74)80002-4 (1974).
51. Benovitz, D. E. & Spatola, A. F. Enkephalin pseudopeptides: Resistance to in vitro proteolytic degradation afforded by amide bond replacements extends to remote sites. *Peptides* **6**, 257–261. https://doi.org/10.1016/0196-9781(85)90049-X (1985).


## Acknowledgements

This research was funded by the Polish National Science Centre (UMO-2020/37/N/ST4/03165-D.B.). Staff exchange was possible due to COST Action CA18202, NECTAR—Network for Equilibria and Chemical Thermodynamics Advanced Research, supported by COST (European Cooperation in Science and Technology). M.R. and E.C. are supported by University of Ferrara (FAR 2021, FIRD 2022).

## Author contributions

D.B., M.D.A., M.R., E.C. and M.R.-Z. conceived and planned the experiments. D.B., M.D.A., E.D., C.L., S.L., V.A. and E.M. conducted the experiments. D.B., M.D.A., M.R., E.C., R.G. and M.R.-Z. analysed the results. D.B., M.D.A., M.R., E.C. and M.R.-Z. wrote the main manuscript. All authors reviewed the manuscript.

## Competing interests

The authors declare no competing interests.

## Additional information

**Supplementary Information** The online version contains supplementary material available at https://doi.org/10.1038/s41598-023-45437-0.

**Correspondence** and requests for materials should be addressed to D.B.

**Reprints and permissions information** is available at www.nature.com/reprints.

**Publisher's note** Springer Nature remains neutral with regard to jurisdictional claims in published maps and institutional affiliations.

View Article Online
DOI: 10.1039/D4DT01514B

ARTICLE

# Metal coordination governs the antimicrobial efficacy of calcitermin derivatives

Received 00th January 20xx,
Accepted 00th January 20xx

DOI: 10.1039/x0xx00000x

Silvia Leveraro,[a] Kinga Garstka,[b] Paulina Śliwka,[c] Tomasz Janek,[c] Magdalena Rowińska-Żyrek,[b] Maurizio Remelli,[a] Denise Bellotti *[a]

Antimicrobial peptides are promising alternatives to classical antibiotics. Their microbicidal activity can arise from different mechanisms, one of which is known as nutritional immunity and has metal micronutrients and metal-binding biomolecules as its main players. Calcitermin is an antimicrobial peptide and an effective metal-chelator. Its properties as antibacterial and anti-Candida agent have been recently studied both as free peptide and in presence of zinc and copper ions, with which it forms stable complexes. Calcitermin derivatives have also gained attractiveness thanks to the possibility of improving their properties, like metal-binding affinity and/or stability in biological fluids, through ad-hoc modifications of the native peptide sequence. In this work, the Ala-to-Ser substitutions close to the coordination site of calcitermin have been introduced to study the impact on the biological activity and metal-binding properties. Our results show that the metal coordination has a clear impact on the bioactivity of the studied compounds, to the point that also the truncated fragment of calcitermin, solely containing the main metal-binding residues, shows antimicrobial activity.

## Introduction

One of the most important advances in modern medicine is the discovery of antibiotics. Besides their use against infections, they are essential for many medical procedures, like chemotherapy, organ transplant and surgery. Overuse and misuse of these drugs is, however, a major problem of the 21st century, that translates into an increase in the phenomenon of antimicrobial resistance (AMR) and into a decrease of the effectiveness of existing antibiotics. AMR prevents the successful treatment of infectious diseases and leads to the use of last-resort classes of drugs which are not always readily available in developing countries, are expensive, and induce various side-effects. [1, 2] Official reports estimate that by 2050, AMR will cause 10 million deaths worldwide, every year.[2,3] Another major factor contributing to the antibiotic crisis is that the development of new antimicrobial drugs has considerably slowed down, due to a decrease in investments. In fact, the permanence of antibiotics on the market is uncertain since they are usually used for short-term treatments and can develop antimicrobial resistance.[4] Hence the need of innovative pharmacological therapies to overcome the clinical and financial burden of the AMR. Antimicrobial peptides (AMPs) represent a promising base for developing new drugs, since they can exert different mechanisms of action to perform their overall antimicrobial activity. AMPs are biomolecules of great interest, having a broad-spectrum activity against many type of pathogens, including Gram positive[5] and Gram-negative bacteria,[6] fungi,[7] viruses[8] and even cancer cells.[8] Furthermore, they act through multiple distinct mechanisms and pathways, thus increasing their antimicrobial efficacy and reducing the risk of resistance development. The main mechanisms of action of AMPs are: (i) disruption of bacterial cell membranes,[9] (ii) inhibition of intracellular functions,[10] (iii) demolition of biofilm,[10] (iv) immunomodulatory activity[9] and (v) nutritional immunity (Table 1).[11] Going deeper into the last-mentioned mechanism, i.e. nutritional immunity, AMPs act as mediators of the immune defence of the host organism through the sequestration of metallic nutrients such as $Zn^{2+}$, $Cu^{2+}$, $Mn^{2+}$ or $Ca^{2+}$, interfering with the homeostasis of pathogenic cells. In other words, microorganisms cannot assimilate enough nutrients crucial for their life and virulence.[11] Moreover, in addition to the role of biologically relevant metal ions in nutritional immunity, they have a further effect on the activity of antimicrobial peptides: the antimicrobial activity of AMPs can be enhanced by metal interaction, for example affecting the AMP charge and/or structure.[11]

In this context, calcitermin is of particular interest. It is a well-studied 15-mer AMP (VAIALKAAHYHTHKE, WT) corresponding to the C-terminal domain of calgranulin C, a pro-inflammatory protein of the S100 family. The presence of three alternated histidine residue (His9, His11 and His13) and the free terminal amino and carboxyl groups makes it able to bind metal ions like $Zn^{2+}$ and $Cu^{2+}$,[12] which also enhance its antimicrobial activity against *Candida albicans*,[13] and common bacteria like

[a] Department of Chemical, Pharmaceutical and Agricultural Sciences, University of Ferrara, Via L. Borsari 46, 44121 Ferrara, Italy.
[b] Faculty of Chemistry, University of Wrocław, F. Joliot-Curie 14, 50-383 Wrocław, Poland.
[c] Department of Biotechnology and Food Microbiology, Wrocław University of Environmental and Life Sciences, Chełmońskiego 37, 51-630 Wrocław, Poland.
* Corresponding author.
† Footnotes relating to the title and/or authors should appear here.
Electronic Supplementary Information (ESI) available: [details of any supplementary information available should be included here]. See DOI: 10.1039/x0xx00000x

*Staphylococcus aureus* and *Enterococcus faecalis* at acidic pH, a typical condition in case of inflammation.[14] It also has the potential to adopt helical conformation in membranes.[13] The lowering of the pH value contributes to the protonation of the three histidine residues, thus favouring the interaction of calcitermin with the negatively charged groups present on the surface of bacterial cells.[12, 14, 15]

**Table 1**. Main mechanisms of action of AMPs.

| | |
|---|---|
| **Disruption of the bacterial cell membrane** | Most AMPs have a net positive charge that allows an electrostatic interaction with the anionic charges present on the bacterial membrane. When the interaction is stabilized, a subsequent insertion of the antimicrobial peptide inside the membrane occurs and pores form. There is therefore a loss of membrane integrity and metabolites, and the consequent death of the bacterial cell. |
| **Inhibition of intracellular functions** | Some peptides cross the membrane and interfere with processes essential for the survival of the pathogen. They can act in various ways including inhibition of DNA replication, inhibition of protein synthesis, interference with the biosynthesis of nucleic acids, interference with metabolism or cell division. |
| **Action on biofilm** | The mechanism by which AMPs act on biofilm is uncertain, but the ability to prevent the occurrence of different stages of the biofilm formation has been recognized. Thanks to biofilm, bacteria are able to tolerate high concentrations of antimicrobials while being totally sensitive to them in planktonic conditions. |
| **Immunomodulatory activity** | AMPs are able to regulate immunomodulatory mechanisms by exerting a chemotactic action on leukocytes, increasing leukocyte/monocyte activity, and the expression of proinflammatory cytokines. |
| **Nutritional immunity** | Through the uptake and coordination of metal ions from the surrounding environment, such as zinc, iron and copper, AMPs can deprive the pathogen of micronutrients essential for its survival. |

A systematic study was undertaken on calcitermin derivatives obtained by introducing modifications in the amino acid sequence of the native peptide, with the aim of studying their impact on the stability in plasma, metal coordination and antimicrobial activity of the peptide. Previous studies carried out on metal-chelating peptides have highlighted that the presence of serine residues in the proximity of coordinated histidines favours the binding of the backbone N-amides by copper ion, affecting the complex formation ability of the investigated systems and generally increasing the $Cu^{2+}$ binding affinity.[16-18] We therefore introduced Ala-to-Ser substitutions close to the coordination site of calcitermin, -HYHTH-, obtaining the following derivatives: VAIALKSAHYHTHKE (**A7S**), VAIALKASHYHTHKE (**A8S**) and VAIALKSSHYHTHKE (**A7S/A8S**), where the alanine residues in position 7 and/or 8 have been replaced by serines. Ala-to-Ser substitutions are introduced with the aim of verifying their impact on metal coordination, and if this can affect the antimicrobial activity of calcitermin.[19-24] Metal coordination and antimicrobial properties have also been investigated for the calcitermin variant truncated between position 7 and 8 and protected at the amino and carboxyl termini (Ac-AHYHTHKE-$NH_2$, **WT(8-15)**). Compared to wild-type calcitermin, in **WT(8-15)** the more lipophilic portion of the molecule, not directly involved in metal coordination, was excluded in order to clarify whether the coordination site -HYHTH- is enough to form $Cu^{2+}$ and $Zn^{2+}$ complexes with microbicidal activity.

## Results and discussion

Under the experimental conditions here employed, only variously protonated mononuclear complexes with metal/ligand stoichiometry of 1:1, have been detected by potentiometry and mass spectrometry. No precipitation has been observed over the explored pH range (2.5-10.5). The overall protonation and complex-formation constants (log$\beta$) and the corresponding acid dissociation constants (p$K_a$) are reported in Tables 2-4, and Tables S1-S2. The corresponding species distribution diagrams, calculated from the experimental thermodynamic constants, are shown in Figures S1-S3 and Figure S5-S7. Spectroscopic results, including Vis absorption spectra, CD spectra and EPR spectra, recorded at different pH values, are shown in Figures S9-S17. ESI-MS results are reported in Figures S21-S23 and Table S4: the only detected *m/z* signals correspond to equimolar $Cu^{2+}$ and $Zn^{2+}$ complexes with different protonation states. Potassium and/or sodium adducts are also formed. The obtained experimental data were comparatively analysed, and the structure of the complexes inferred by means of combined experimental techniques and comparison with literature data on similar systems.

### Ligand protonation

For each peptide, the obtained protonation macro-constants reported in Table 2 have been compared with literature data in order to assign each protonation step to the corresponding functional group. The symbol L here indicates the ligand in its unprotonated form, i.e. when all the dissociable protons (in the explored pH range) have been released. The investigated peptides **A7S, A8S** and **A7S/A8S** are unprotected fragments and

View Article Online
DOI: 10.1039/D4DT01514B

thus their acid-base behaviour depends both on the amino acids side chains, and on their amino and carboxyl termini.

spontaneously release their protons in the pH range explored by potentiometry, since they are very weak acids (p$K_a$ ≈ 15).[26]

**Table 2**. Overall ($\beta$) and step ($K$) protonation constants for the investigated ligands at $T$ = 298 K and $I$ = 0.1 M (KCl). Values in parentheses are standard deviations on the last significant figure.

| | VAIALKSAHYHTHKE (**A7S**) | | | VAIALKASHYHTHKE (**A8S**) | | |
|---|---|---|---|---|---|---|
| **Species** | **log$\beta$** | **log$K$** | **Group/Residue** | **log$\beta$** | **log$K$** | **Group/Residue** |
| $HL^{2-}$ | 10.5(1) | 10.5 | Lys | 10.77(4) | 10.77 | Lys |
| $H_2L^{-}$ | 20.97(5) | 10.44 | Lys | 21.01(2) | 10.24 | Lys |
| $H_3L$ | 30.34(6) | 9.37 | Tyr | 30.26(4) | 9.25 | Tyr |
| $H_4L^{+}$ | 37.97(6) | 7.64 | $NH_2$ | 37.81(4) | 7.54 | $NH_2$ |
| $H_5L^{2+}$ | 44.80(6) | 6.83 | His | 44.58(4) | 6.77 | His |
| $H_6L^{3+}$ | 51.06(6) | 6.25 | His | 50.81(4) | 6.23 | His |
| $H_7L^{4+}$ | 56.57(6) | 5.51 | His | 56.25(4) | 5.44 | His |
| $H_8L^{5+}$ | 60.56(6) | 3.99 | Glu | 60.32(4) | 4.07 | Glu |
| $H_9L^{6+}$ | 63.41(6) | 2.85 | $COO^{-}$ | 62.83(4) | 2.51 | $COO^{-}$ |
| | VAIALKSSHYHTHKE (**A7S/A8S**) | | | | | |
| **Species** | **log$\beta$** | **log$K$** | **Group/Residue** | | | |
| $HL^{2-}$ | 10.81(7) | 10.81 | Lys | | | |
| $H_2L^{-}$ | 21.11(3) | 10.30 | Lys | | | |
| $H_3L$ | 30.42(4) | 9.31 | Tyr | | | |
| $H_4L^{+}$ | 38.01(4) | 7.59 | $NH_2$ | | | |
| $H_5L^{2+}$ | 44.87(4) | 6.86 | His | | | |
| $H_6L^{3+}$ | 51.10(4) | 6.23 | His | | | |
| $H_7L^{4+}$ | 56.72(4) | 5.62 | His | | | |
| $H_8L^{5+}$ | 60.94(4) | 4.22 | Glu | | | |
| $H_9L^{6+}$ | 64.03(4) | 3.09 | $COO^{-}$ | | | |

All the investigated peptides, once completely deprotonated, bear a triple negative charge ($L^{3-}$). The obtained protonation constants are in good agreement with literature values for similar systems[25] and show reasonable similarities among the considered peptides. Nine different species have been always detected in solution, arising from the protonation of the following sites: three histidines, the phenolic group of tyrosine, the glutamic acid, two lysines and the terminal amino and carboxyl groups. The most acidic moiety is the terminal carboxyl group with a log$K$ varying from 2.51 to 3.09. It is followed by the glutamic acid side chain, with comparable log$K$ values in all mutants (3.99, 4.07, and 4.22). Histidine residues are characterized by log$K$ values ranging from 5.44 to 6.86, in good agreement with the expectation based on literature data.[25] Then, the three ligands show very similar log$K$ values for their terminal amino groups (7.64, 7.54, and 7.59). Under alkaline conditions, the spontaneously release of the phenolic proton by tyrosine side chains occurs with log$K$ values varying from 9.25 to 9.37. Finally, the deprotonation of the most basic residues, lysines, occurred with log$K$ values ranging from 10.24 to 10.81. The backbone amidic groups of the peptide cannot

**Formation of $Cu^{2+}$ complexes with A7S, A8S and A7S/A8S**

The formation of $Cu^{2+}$ complexes in solution begins around pH 3–3.5 for all the studied ligands. **A7S** and **A8S** peptides interact with copper ion in a very similar way, forming the same nine species in solution. The first complex detected by potentiometry is $[CuH_6L]^{5+}$: the stoichiometry of this species indicates that three acid-base sites are already deprotonated. It is conceivable that the coordination mode involves the imidazole nitrogen of one histidine residue ($N_{Im}$) and one of the carboxylic groups of the C-terminal glutamic acid, with the formation of a macrocycle. The complex reaches its maximum of formation around pH 4 with both **A7S** and **A8S**, where free $Cu^{2+}$ is still present as the major species; the experimental wavelength of maximum absorption ($\lambda_{max}$ = 737 nm for **A7S** and 741 nm for **A8S**; Figure S9 and S12) is in good agreement with the expected value for a coordination ($1N_{Im}$, $COO^{-}$) (expected $\lambda_{max}$ = 731 nm).[26] The complex $[CuH_6L]^{5+}$ is rapidly substituted in solution by the species $[CuH_5L]^{4+}$, where a second histidine interacts with the metal giving a ($2N_{Im}$ , $COO^{-}$) complex (experimental $\lambda_{max}$ = 664 nm for **A7S**, and $\lambda_{max}$ = 660 nm for **A8S**;

View Article Online
DOI: 10.1039/D4DT01514B

**Table 3**. Equilibrium constants and proposed coordination modes for $Cu^{2+}$ complexes at $T$ = 298 K and $I$ = 0.1 M (KCl). Values in parentheses are standard deviations on the last significant figure.

| | VAIALKSAHYHTHKE (**A7S**) | | | VAIALKASHYHTHKE (**A8S**) | | |
|---|---|---|---|---|---|---|
| **Species** | **log*β*** | **p$K_a$** | **Coordination** | **log*β*** | **p$K_a$** | **Coordination** |
| $[CuH_6L]^{5+}$ | 55.3(1) | 4.00 | $N_{Im}$, $COO^-$ | 55.4(1) | 4.4 | $N_{Im}$, $COO^-$ |
| $[CuH_5L]^{4+}$ | 51.27(4) | 5.02 | $2N_{Im}$, $COO^-$ | 51.04(6) | 4.84 | $2N_{Im}$, $COO^-$ |
| $[CuH_4L]^{3+}$ | 46.25(4) | 6.13 | $3N_{Im}$ | 46.19(5) | 5.98 | $3N_{Im}$ |
| $[CuH_3L]^{2+}$ | 40.12(5) | 7.05 | $2N_{Im}$, $N^-$ | 40.21(6) | 7.02 | $2N_{Im}$, $N^-$ |
| $[CuH_2L]^{+}$ | 33.07(6) | 7.45 | $2N_{Im}$, $N^-$, $NH_2$ | 33.19(8) | 7.36 | $2N_{Im}$, $N^-$, $NH_2$ |
| [CuHL] | 25.62(5) | 9.33 | $2N_{Im}$, $2N^-$ | 25.83(7) | 9.16 (Y) | $2N_{Im}$, $2N^-$ |
| $[CuL]^-$ | 16.29(8) | 9.83 | $2N_{Im}$, $2N^-$ | 16.7(1) | 9.7 | $2N_{Im}$, $2N^-$ |
| $[CuH_{-1}L]^{2-}$ | 6.46(6) | - | $N_{Im}$, $3N^-$ | 6.99(8) | - | $N_{Im}$, $3N^-$ |
| $[CuH_{-3}L]^{4-}$ | -14.80(8) | - | $N_{Im}$, $3N^-$ | -14.20(9) | - | $N_{Im}$, $3N^-$ |
| | VAIALKSSHYHTHKE (**A7S/A8S**) | | | | | |
| **Species** | **log*β*** | **p$K_a$** | **Coordination** | | | |
| $[CuH_5L]^{4+}$ | 51.35(2) | 5.42 | $2N_{Im}$, $COO^-$ | | | |
| $[CuH_4L]^{3+}$ | 45.93(3) | 6.36 | $3N_{Im}$ | | | |
| $[CuH_3L]^{2+}$ | 39.57(5) | 7.17 | $2N_{Im}$, $N^-$ | | | |
| $[CuH_2L]^{+}$ | 32.40(5) | 7.83 | $2N_{Im}$, $N^-$, $NH_2$ | | | |
| [CuHL] | 24.58(6) | 9.21 | $2N_{Im}$, $2N^-$ | | | |
| $[CuL]^-$ | 15.37(7) | - | $2N_{Im}$, $2N^-$ | | | |
| $[CuH_{-2}L]^{3-}$ | -4.98(8) | - | $2N_{Im}$, $2N^-$ | | | |

**Table 4.** Equilibrium constants and proposed coordination modes for $Zn^{2+}$ complexes at $T$ = 298 K and $I$ = 0.1 M (KCl). Values in parentheses are standard deviations on the last significant figure.

| | VAIALKSAHYHTHKE (**A7S**) | | | VAIALKASHYHTHKE (**A8S**) | | |
|---|---|---|---|---|---|---|
| **Species** | **log*β*** | **p$K_a$** | **Coordination** | **log*β*** | **p$K_a$** | **Coordination** |
| $[ZnH_5L]^{4+}$ | 48.6(1) | 5.5 | $2N_{Im}$, $COO^-$ | 48.1(2) | 5.3 | $2N_{Im}$, $COO^-$ |
| $[ZnH_4L]^{3+}$ | 43.07(3) | 6.84 | $3N_{Im}$ | 42.74(4) | 7.18 | $3N_{Im}$ |
| $[ZnH_3L]^{2+}$ | 36.24(5) | 7.74 | $3N_{Im}$, $OH^-$ | 35.57(8) | 7.52 | $3N_{Im}$, $OH^-$ |
| $[ZnH_2L]^{+}$ | 28.49(5) | 8.28 | $3N_{Im}$, $2OH^-$ | 28.04(6) | 8.55 | $3N_{Im}$, $2OH^-$ |
| [ZnHL] | 20.21(5) | 9.32 | $3N_{Im}$, $2OH^-$ | 19.49(7) | 9.33 | $3N_{Im}$, $2OH^-$ |
| $[ZnL]^-$ | 10.89(5) | - | $3N_{Im}$, $2OH^-$ | 10.16(7) | - | $3N_{Im}$, $2OH^-$ |
| $[ZnH_{-2}L]^{3-}$ | -9.57(5) | - | $3N_{Im}$, $2OH^-$ | -11.15(8) | - | $3N_{Im}$, $2OH^-$ |
| | VAIALKSSHYHTHKE (**A7S/A8S**) | | | | | |
| **Species** | **log*β*** | **p$K_a$** | **Coordination** | | | |
| $[ZnH_4L]^{3+}$ | 43.10(2) | 7.06 | $3N_{Im}$ | | | |
| $[ZnH_3L]^{2+}$ | 36.04(4) | 7.64 | $3N_{Im}$, $OH^-$ | | | |
| $[ZnH_2L]^{+}$ | 28.40(4) | 8.29 | $3N_{Im}$, $OH^-$ | | | |
| [ZnHL] | 20.11(4) | 9.30 | $3N_{Im}$, $2OH^-$ | | | |
| $[ZnL]^-$ | 10.81(4) | - | $3N_{Im}$, $2OH^-$ | | | |
| $[ZnH_{-2}L]^{3-}$ | -9.54(5) | - | $3N_{Im}$, $2OH^-$ | | | |

View Article Online
DOI: 10.1039/D4DT01514B

predicted $\lambda_{max}$ = 663 nm[26]) (Figure S9 and S12). EPR spectra registered at pH 4.5 confirm the presence of 2N complexes as major species (**A7S**: $g_{//}$=2.30, $A_{//}$=164 G; **A8S**: $g_{//}$=2.29, $A_{//}$=173 G; Table S3).[27, 28] Increasing the pH value, the interaction between $Cu^{2+}$ and the ligands favours the release of the proton of the third histidine (p$K_a$ = 5.02 (for **A7S**) and p$K_a$ = 4.84 (for **A8S**)). This leads to the formation of $[CuH_4L]^{3+}$ species ($3N_{Im}$ coordination), which is prevalent in solution at around pH 6 (Figure 1a). The obtained wavelengths of maximum absorption at pH 6.0 range from $\lambda_{max}$ = 622 nm to $\lambda_{max}$ = 634 nm and agree with the proposed coordination mode (expected $\lambda_{max}$ = 627 nm);[26] moreover, the EPR parameters at pH 6.5 undergoes a remarkable decrease of $g_{//}$ value, and a slightly increase of $A_{//}$ value (Table S3), as expected for the binding of a third nitrogen atom.[29, 30] It should be noted that the EPR parameters listed in Table S3 provide only a qualitative evaluation and a formal description of the complexes in solution. In fact, in the pH range where more species with different number and type of ligands coexist, the superposition of two or more individual spectra occurs. The two next deprotonation steps most likely involve a backbone N-amide and the terminal amine, which coordinate the metal ion in equatorial position, forming a 4N complex ($2N_{Im}$, $N^-$, $NH_2$). The proposed coordination is supported by the UV-Vis and CD data (Figure S9 and S12). The binding of the amide is confirmed by CD spectra recorded at pH above 6 (Figure S10 and S13), where a significant change in the visible region is observed. Indeed, the coordination of the amide nitrogen, close to the chiral α-carbon of the peptide backbone, produces a stronger CD absorption when the metal binding occurs.[31, 32]

Afterward, the formation of the species [CuHL] is consistent with the coordination of a second amide nitrogen (p$K_a$ = 7.45 for **A7S**, p$K_a$ = 7.36 for **A8S**), which most likely replace the amine group in the equatorial plane of the complex, giving a ($2N_{Im}$, $2N^-$) coordination (Figure 1b). The next detected species ($[CuL]^-$) derives from the deprotonation of the complex [CuHL]. No changes occur in the spectroscopic data between pH 8.5 and 9.5, thus the coordination mode is still ($2N_{Im}$, $2N^-$) (experimental $\lambda_{max}$ = 540 nm). This strongly suggests that the proton released with p$K_a$ = 9.33 (**A7S**) and 9.16 (**A8S**) belongs to the non-coordinating tyrosine residue. At pH higher than 10, for $Cu^{2+}$/**A7S** and $Cu^{2+}$/**A8S** systems, the complex $[CuH_{-1}L]^{2-}$ predominates in solution: a third N-amide of the peptide backbone deprotonates and most likely coordinates $Cu^{2+}$ replacing one histidine donor group. Indeed, the remarkable change in UV-Vis spectra supports the hypothesis of a variation in the coordination mode to ($N_{Im}$, $3N^-$). Finally, increasing the pH value, no changes in the Vis, CD and EPR spectroscopic data are observed (Figures S9-S14) and the species $[CuH_{-3}L]^{4-}$ is formed, therefore two lysine residues likely deprotonate without participating in the $Cu^{2+}$ coordination.

In the case of **A7S/A8S** ligand, seven $Cu^{2+}$ complexes with various protonation degrees have been identified. The first detected species is $[CuH_5L]^{4+}$ in which the stoichiometry suggests that the terminal carboxylic group, the glutamic acid and the two histidines are already deprotonated and likely participate in the complexation. The 2N species is predominant

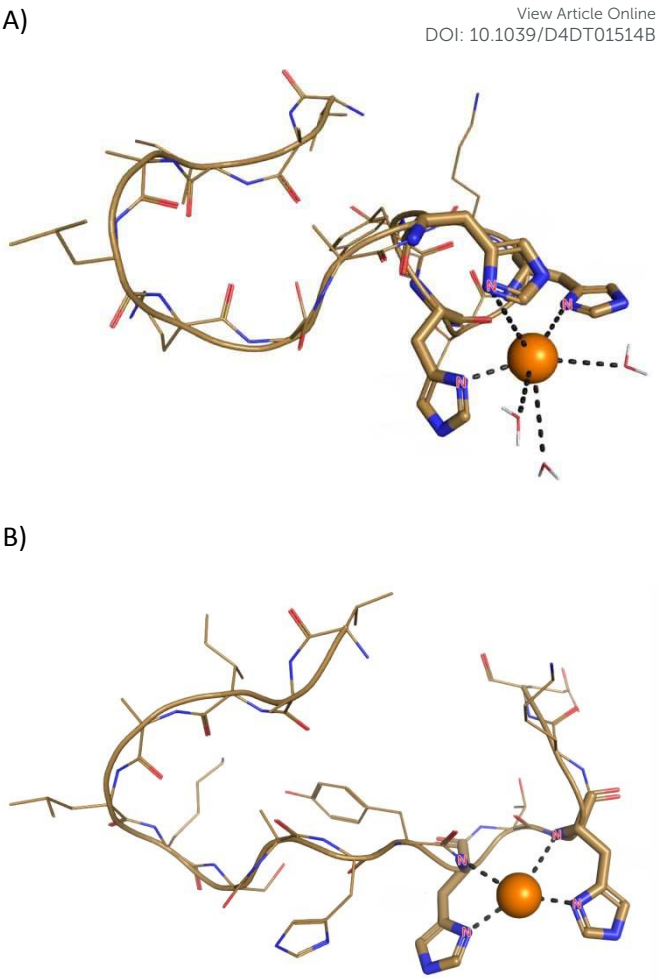


**Figure 1**. Proposed coordination for $Cu^{2+}$ complexes with **A7S** at (A) acidic pH ($3N_{Im}$), and (B) alkaline pH ($2N_{Im}$, $2N^-$).[14] Atom colour code: carbon=gold; nitrogen=blue; oxygen=red; hydrogen=white; copper=orange. Molecular structure generated with Pymol.

in solution in the pH range 4-5, as confirmed by the obtained EPR parameters ($g_{//}$=2.31, $A_{//}$=160 G; Table S3).[29] The release of a proton with p$K_a$ = 5.42 gives rise to the $[CuH_4L]^{3+}$ species, where the metal coordinates three histidine residues with a distorted octahedral geometry. The observed $\lambda_{max}$ at pH 6.0, where this complex is the most abundant in solution, confirms the ($3N_{Im}$) coordination hypothesis (experimental $\lambda_{max}$=622 nm, expected $\lambda_{max}$=627 nm).[26] Similarly to the previous described systems, also for **A7S/A8S** the release of three further protons to form $[CuH_3L]^{2+}$, $[CuH_2L]^+$ and [CuHL] involves the equatorial coordination of the terminal amine group, and two backbone N-amides. The blue-shift observed in the UV-Vis spectra above pH 6.5 (Figure S15) confirms the formation of 4N complexes with an increased square-planar character. The presence of four equatorial nitrogen atoms is also suggested by the EPR parameters obtained above pH 8.5 ($g_{//}$=2.20, $A_{//}$=194 G; Figure S17). At higher pH, the species $[CuL]^-$ and $[CuH_{-2}L]^{3-}$ are formed by the spontaneous deprotonation of tyrosine and of two lysine residues, respectively. The coordination mode remains unchanged with two imidazole nitrogens and two amide groups bound to the metal ion ($2N_{Im}$, $2N^-$).

View Article Online
DOI: 10.1039/D4DT01514B





**Formation of $Zn^{2+}$ complexes with A7S, A8S and A7S/A8S**

Only mononuclear $Zn^{2+}$ complexes have been identified under the employed experimental conditions, as confirmed by MS spectra (Figures S21-S23). In the case of **A7S** and **A8S**, $Zn^{2+}$ complexes begin to form around pH 4.0 (Figures S5-S6). The first observed $Zn^{2+}$ species is $[ZnH_5L]^{4+}$, where the metal ion likely interacts with two imidazole nitrogens and a carboxylic group of the glutamic acid or C-terminus. The coordination geometry can be reasonably assumed to be tetrahedral, as already reported for wild-type calcitermin and similar peptides.[14, 33] Increasing the pH value, the release of one proton with a p$K_a$ of 5.5 (**A7S**) and 5.3 (**A8S**) leads to the formation of the $[ZnH_4L]^{3+}$ species. The coordination likely involves an additional histidyl residue that replaces the carboxyl group (if coordinated) in the set of donors. The obtained ($3N_{Im}$) species dominates in solution until pH 7 (Figure 2). Analogously, in the case of **A7S/A8S** system, the $[ZnH_4L]^{3+}$ complex is the most abundant in solution up to pH 7 and it also corresponds to the first identified species (Figure S7). For all the investigated ligands, increasing the pH the $[ZnH_3L]^{2+}$ species forms due to the ionization of a coordinated water molecule. We further observed the mere deprotonation of a basic site of the ligand (**A7S** p$K_a$ =7.74, **A8S** p$K_a$ =7.52 and **A7S/A8S** p$K_a$ =7.64) corresponding to the free terminal amino group which is not involved in the coordination. It may follow the deprotonation of a second water molecule which leads to the formation of [ZnHL] species and the remaining two complexes $[ZnL]^-$, $[ZnH_{-2}L]^{3-}$ are related to the deprotonations of the tyrosine and two lysine residues which are not involved in the coordination.

**Comparison of metal chelating abilities**

To better understand the capacity of the investigated peptides to stably coordinate metal ions, it is useful to compare their metal-binding ability with that of wild-type calcitermin (WT), here taken as a reference. Such evaluation can be obtained by competition diagrams (Figure 3), which are based on the determined thermodynamic constants and describe the formation of the binary metal complexes with each ligand at different pH values. The diagrams reported in Figure 3 show the hypothetical situation of a solution containing equimolar concentration of metal ion, **WT**, **A7S**, **A8S** and **A7S/A8S**.

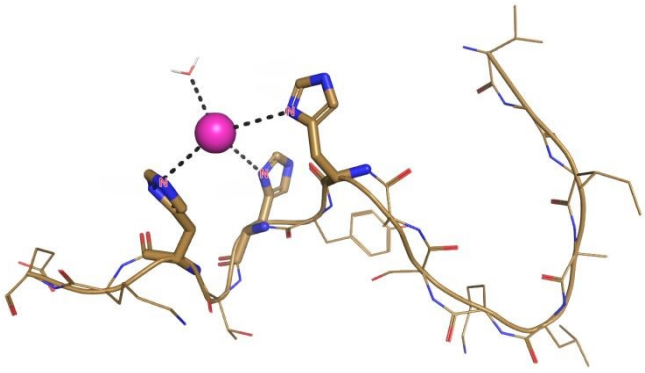

**Figure 2**. Proposed coordination ($3N_{Im}$) for $Zn^{2+}$ complex with **A7S**.[14] Atom colour code: carbon=gold; nitrogen=blue; oxygen=red; hydrogen=white; zinc=purple. Molecular structure generated with Pymol.

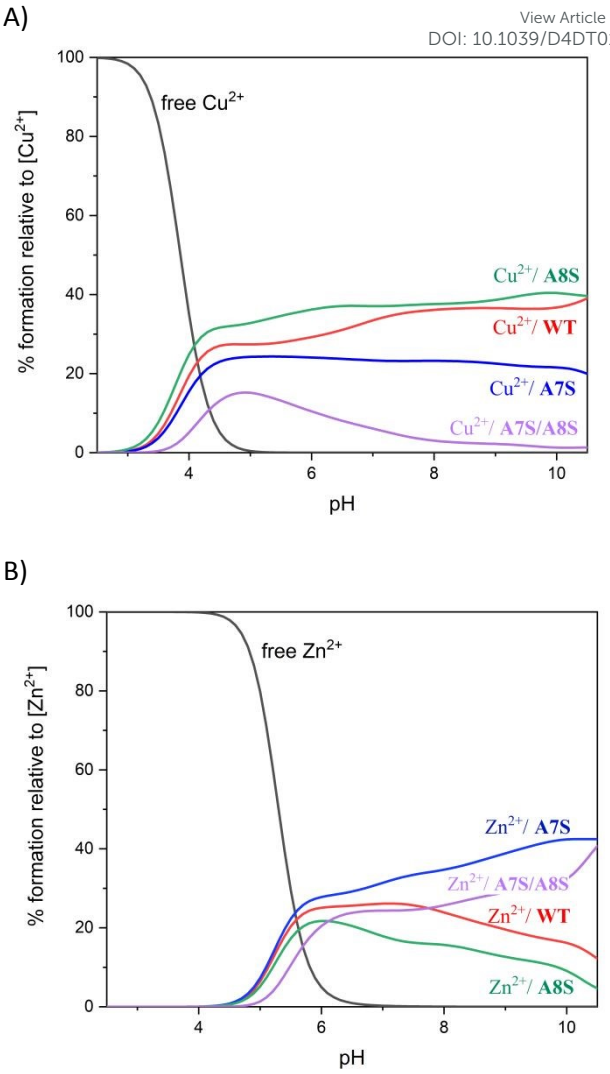


**Figure 3**. Competition plots for a simulated solution containing equimolar concentrations of (A) $Cu^{2+}$, (B) $Zn^{2+}$, and **WT**,[13] **A7S**, **A8S** and **A7S/A8S**.

According to the calculated plots, the $Cu^{2+}$ chelating ability of **A8S** is comparable to that of **WT**. Interestingly, $Cu^{2+}$ complexes of **A8S** are more stable than those of **A7S**, suggesting that the effect exerted by serine depends on the spatial proximity to the coordinated histidines. Furthermore, in the case of **A7S/A8S** the presence of two consecutive serine residues makes the interaction of the amides with $Cu^{2+}$ more difficult. In fact, the plot shows that the binding capacity of **A7S/A8S** rapidly decreases above pH 5, when amides start to coordinate the metal ion. This also can explain why, under the most alkaline conditions, the binding of a third amide is prevented in the case of **A7S/A8S** (see above).

The relatively low stability of $Cu^{2+}$-**A7S/A8S** complexes induced us to investigate the possible degradation of this peptide under alkaline conditions, as reported for square-planar $Ni^{2+}$ complexes with peptides containing a general sequence $R_1$-(Ser/Thr)-Xaa-His-Zaa-$R_2$.[24] No noticeable hydrolysis phenomenon was observed in our case, after 3 hours in water solution at T=25°C and pH 8.4 (Figure S25), thus suggesting that

the affinity of **A7S/A8S** for $Cu^{2+}$ is affected by a steric and/or electronic effects due to the two consecutive serine residues.
A different behaviour is observed in the case of $Zn^{2+}$ complexes. The four peptides behave similarly up to neutral pH, after which an improved stability is shown by the complexes formed by the two peptides containing the substitution A7S. This behaviour is not easily rationalizable, and it would require further investigation. Actually, the effect of the Ala-to-Ser substitution on the stability of $Zn^{2+}$-peptide complexes is still a controversial issue in the literature.[16-18]

**Peptide stability in human plasma**

The resistance towards degradation of the investigated peptides in human plasma is reported in Figure 4 and is compared with the proteolytic susceptibility of WT calcitermin (18 min).[13] The degradation profile of the three Ala-to-Ser derivatives follows that of the native peptide and the concentration exponentially decreases with a half-life period ($t_{1/2}$) of 19 ± 4 min for **A7S/A8S**, 21 ± 4 min for **A7S** and 22 ± 4 min for **A8S**. According to the experimental data, the Ala-to-Ser substitutions in position 7 and 8 do not significantly enhance the resistance of calcitermin in human plasma. This is not surprising, considering that most L-amino acid peptides that are not N-terminally modified are easily degraded by aminopeptidases or dipeptidylaminopeptidases.[34] Indeed, chemical modification of one or both the peptide termini is a common strategy to increase the peptide stability (e.g. by cyclization, carboxyl-terminus amidation, amino-terminus acylation, binding to polyethyleneglycol). Aiming at higher resistance towards endopeptidases, instead, the substitution of one or more residues with non-proteinogenic amino acids which are normally not recognized by enzymes can be sought (e.g. D-amino acids, N-methyl-α-amino acids, β- and γ- amino acids, α-alkylated amino acids, N-substituted glycines).[35-37]

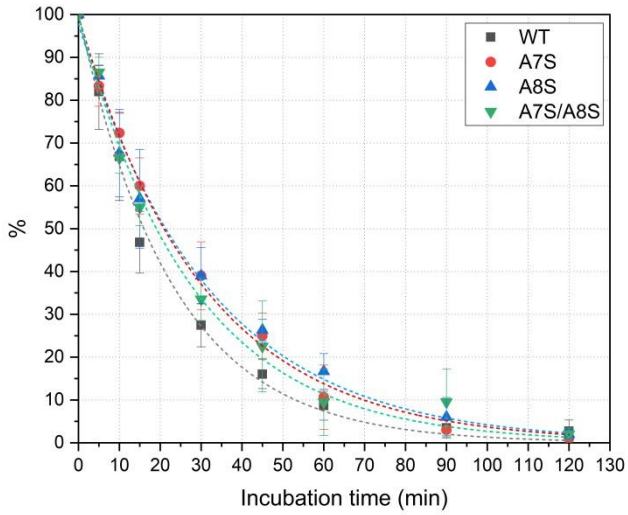


**Figure 4**. Stability of wild-type calcitermin (**WT**)[13] and its derivatives (**A7S**, **A8S**, **A7S/A8S**) in human plasma.

**Antimicrobial activity**

All peptides and their metal complexes were tested for their antimicrobial activity against a representative panel of microbial pathogens: *Staphylococcus aureus* ATCC 25923, *Staphylococcus epidermidis* KCTC 1917, *Enterococcus faecalis* ATCC 29212, *Pseudomonas aeruginosa* ATCC 15422, *Escherichia coli* ATCC 25922, *Klebsiella rhinoscleromatis* 13884, *Klebsiella pneumoniae* 13882, *Klebsiella ozaenae* 11298, *Proteus mirabilis* ATCC 21100, *Candida albicans* 10231. The minimal inhibitory concentration (MIC) has been determined for all active compounds and their metal complexes (Table 5). The results showed that $Zn^{2+}$ and $Cu^{2+}$ did not have antibacterial activity against Gram-positive, Gram-negative bacteria and *C. albicans* strains at concentrations used in the peptide complexes, range of 0.1 to 12 μg/ml (data not shown).
Comparing the antimicrobial results with those of **WT**, a first observation is that **A7S/A8S** and **WT(8-15)** mutants show activity against *E. faecalis* and *P. aeruginosa*, not observed for **WT**. In particular, the metal complexes exhibit an enhanced capacity to kill these bacteria with respect to the free peptide.
Similarly, the system **A7S/A8S** is the only mutant being active towards *S. aureus*, with MIC values comparable to those of **WT** (MIC=128 μg/ml for the metal complexes). It is noteworthy the efficacy of **A7S/A8S**-$Cu^{2+}$ against *K. pneumoniae*, which shows a clear enhancement of the antimicrobial power (MIC = 4 μg/ml) with respect to both **WT** and the other mutants. All the calcitermin mutants and their complexes are active against *K. rhinoscleromatis*, especially in the case of **WT(8-15)**-$Zn^{2+}$ (MIC = 8 μg/ml), free **WT(8-15)** and **A7S**-$Cu^{2+}$. In the case of *K. ozaenae*, activity has been observed for **A8S**, **WT(8-15)** and **A7S/A8S,** the latter being the best, as both free peptide and $Cu^{2+}$ complexes (MIC = 4 μg/ml). Only **A7S** and **A7S**-$Zn^{2+}$ exhibit antimicrobial power against *P. mirabilis* (MIC=32 μg/ml).
Activity against *S. epidermidis* has been detected by all the systems (except **A7S/A8S** free peptide); **WT(8-15)** proved to be the best antimicrobial agent against this Gram-positive bacterium, especially in the presence of metal ions. No activity has been detected against *E. coli* for all the investigated peptides and metal complexes. We also tested the antifungal activity of our compounds using *C. albicans* as reference organism. As previously reported for WT calcitermin and its protected derivatives,[13] the antifungal power is enhanced by the presence of metal ions. The same occurs for **A7S**, **A8S**, **A7S/A8S** and **WT(8-15)**, although **WT** showed the best anti-*Candida* performance (Table 5). Several antibacterial and antifungal peptides require $Cu^{2+}$ and $Zn^{2+}$ for their antimicrobial activity.[38] Often, the presence of metal ions or their coordination trigger various metal–ligand–cell interactions that may lead to activating cell wall bound autolytic enzymes and permeabilization of the cell membrane.[39] Given the comparison with **WT** antimicrobial activity (Table 5), in our opinion, Ala-to-Ser substitutions close to the coordination site of calcitermin, -HYHTH-, can improve the peptide and/or complex interaction with the cell membrane of microorganisms, and possibly cause the cell lysis or the formation of transient pores and the transport of peptides and metal-peptide complexes inside the cell; this property enables them to interact with intracellular

View Article Online
DOI: 10.1039/D4DT01514B

**Table 5**. *In vitro* antimicrobial activity expressed as minimal inhibitory concentration (MIC) at pH=5.4. MIC [μg/ml]. For *E. coli* ATCC 25922, no MIC was determined for all peptides and their metal complexes at the maximum concentration tested. The results represent the averages of triplicate experiments ± SD. Reduced MIC values of peptide/metal system with respect to peptide (higher antimicrobial activity) are marked in green; increased MIC values of peptide/metal system with respect to peptide (lower antimicrobial activity) are marked in red.

| Strain | A7S | | | A8S | | | A7S/A8S | | | WT(8-15) | | | WT | | |
|---|---|---|---|---|---|---|---|---|---|---|---|---|---|---|---|
| | L | $LZn^{2+}$ | $LCu^{2+}$ | L | $LZn^{2+}$ | $LCu^{2+}$ | L | $LZn^{2+}$ | $LCu^{2+}$ | L | $LZn^{2+}$ | $LCu^{2+}$ | L | $LZn^{2+}$ | $LCu^{2+}$ |
| *S. aureus* ATCC 25923 | >256 | >256 | >256 | >256 | >256 | >256 | 256±1 | 128±1 | 128±3 | >256 | >256 | >256 | 128±4 | >256 | 128±4 |
| *S. epidermidis* KCTC 1917 | 128±3 | 32±2 | 32±1 | 128±3 | 32±1 | 64±2 | >256 | 128±1 | 128±1 | 32±1 | 16±1 | 8±2 | >256 | 256±2 | 256±2 |
| *E. faecalis* ATCC 29212 | >256 | >256 | 128±2 | >256 | >256 | 128±4 | 256±2 | 128±3 | 128±2 | >256 | 128±2 | 128±2 | >256 | >256 | >256 |
| *P. aeruginosa* ATCC 15422 | >256 | >256 | >256 | >256 | >256 | >256 | >256 | 128±2 | 128±2 | >256 | 128±3 | 256±3 | >256 | >256 | >256 |
| *K. rhinoscleromatis* ATCC 13884 | 128±1 | 256±3 | 16±1 | 64±2 | 128±2 | 32±1 | 128±4 | 32±2 | 32±1 | 16±1 | 8±1 | 32±2 | 128±2 | 256±4 | 128±4 |
| *K. pneumoniae* ATCC 13882 | 128±2 | >256 | 256±3 | >256 | >256 | >256 | 128±3 | >256 | 4±1 | >256 | >256 | >256 | 128±2 | >256 | >256 |
| *K. ozaenae* ATCC 11298 | >256 | >256 | >256 | 32±1 | >256 | 16±1 | 4±1 | >256 | 4±1 | 128±2 | >256 | 32±3 | 256±3 | >256 | 128±2 |
| *P. mirabilis* ATCC 21100 | 32±1 | 32±1 | >256 | >256 | >256 | >256 | >256 | >256 | >256 | >256 | >256 | >256 | >256 | >256 | >256 |
| *C. albicans* ATCC 10231 | >256 | 128±1 | 128±2 | >256 | 256±4 | 256±2 | 256±4 | 256±5 | 128±1 | >256 | 256±4 | 128±4 | >256 | 4±1 | 4±1 |

**Table 6.** Cell viability assay. NHDF cells were plated in a 96-well titre plate with 256 μg/ml of peptides and $Cu^{2+}$ and $Zn^{2+}$ complexes and incubated for 24 h. Percentage of viable cells were determined by MTT assay. The results represent the averages of triplicate experiments ± SD.

| Compounds | % of viable cells |
|---|---|
| A7S | 97±1 |
| A7S/$Zn^{2+}$ | 96±1 |
| A7S/$Cu^{2+}$ | 97±1 |
| A8S | 96±1 |
| A8S/$Zn^{2+}$ | 94±1 |
| A8S/$Cu^{2+}$ | 94±1 |
| A7S/A8S | 96±1 |
| A7S/A8S/$Zn^{2+}$ | 96±1 |
| A7S/A8S/$Cu^{2+}$ | 95±1 |
| WT(8-15) | 98±1 |
| WT(8-15)/$Zn^{2+}$ | 98±1 |
| WT(8-15)/$Cu^{2+}$ | 98±1 |
| WT | 98±1 |
| WT/$Zn^{2+}$ | 96±1 |
| WT/$Cu^{2+}$ | 96±1 |

targets and enhance the antimicrobial activity. A synergistic effect between metals and peptides, not strictly related to the formation of a complex, is also conceivable, since under the tested most diluted conditions the metal complexes tend to dissociate.

In this research, all peptides and their $Cu^{2+}$ and $Zn^{2+}$ complexes were used to determine the *in vitro* antiproliferative/cytotoxic activity on normal human dermal fibroblasts (NHDF) cells. Cell survival was evaluated using a standard 24 h incubation with the peptides and their metal complexes. In general, all peptides (**WT(8-15)**, **A7S/A8S**, **A8S** and **A7S**) and their $Cu^{2+}$ and $Zn^{2+}$ complexes at concentration 256 μg/ml (highest concentration tested in the antimicrobial activity assays) were had no toxic effect against NHDF cells (Table 6). Despite of the potential cytotoxicity of $Cu^{2+}$, due to its ability to generate hydroxyl radical (which is toxic to the human cells),[40] in our experiments **WT(8-15)**/$Cu^{2+}$, **A7S/A8S**/$Cu^{2+}$, **A8S**/$Cu^{2+}$ and **A7S**/$Cu^{2+}$ complexes did not exhibit notable cytotoxic effects at concentration 256 μg/ml after 24 h exposure. The results of this studies show that all peptides and their $Cu^{2+}$ and $Zn^{2+}$ complexes, appear be a new promising antimicrobial metal-peptide complexes, and should be considered for further biological assays.

## Conclusions

The present investigation was aimed at studying the impact of different Ala-to Ser substitutions in the calcitermin peptide on its coordination and antimicrobial properties. New derivatives of calcitermin were synthesized and analysed, in which the two alanine residues, the closest to the metal coordination site, were replaced by serines. First of all, the stability of these calcitermin derivatives was tested in human plasma: no significant enhancement in the resistance to proteolysis was detected, with respect to wild-type calcitermin. On the other hand, previous studies highlighted that the presence of one or more serine residues close to coordinated histidines affects the stability of $Cu^{2+}$ complexes and this effect was associated to metal interaction with the amides of the peptide backbone.[16-18, 41]

The comparison of the stabilities of metal complexes with Ala-to-Ser substituted mutants of calcitermin shows two interesting facts: (i) the presence of two consecutive serines close to the metal binding site decreases the thermodynamic stability of the $Cu^{2+}$ complex; the difference becomes largest at basic pH, which is a consequence of the third amide not being bound to the central $Cu^{2+}$; (ii) $Zn^{2+}$ complexes with all serine mutants have a

comparable affinity towards $Zn^{2+}$ at around physiological pH (both at pH 5.4 and 7.4); some differences are observed at basic pH, in which the A8S mutant has the lowest affinity towards $Zn^{2+}$.

As a general remark, the antimicrobial properties of our compounds are clearly enhanced in the presence of $Zn^{2+}$ or $Cu^{2+}$, and this phenomenon is most visible for $Cu^{2+}$. This agrees with previously reported data on calcitermin activity, suggesting a possible synergistic effect between peptide and metal or a better performance of the metal complex itself. The obtained better performances in the presence of $Cu^{2+}$ open also the way to the hypothesis of hydroxyl radicals formation, which could exert a membrane damaging activity. This can be an option which deserve further in-depth studies, as reported for other antimicrobial peptides and their complexes.[42-45]

More in details, a higher activity in the presence of metal ions with respect to the ligand itself (Table 5) is more evident for **A7S/A8S** and **WT(8-15)**. The only exceptions are against the microorganism *P. mirabilis*, for which neither the peptide, nor the metal/peptide systems are effective, and *K. ozaenae* for which the presence of $Zn^{2+}$ seems to decrease the antimicrobial activity. This also occurs for all the investigated peptides, suggesting that $Zn^{2+}$ may inhibit the activity of the peptides against *K. ozaenae*. It is also noteworthy that the enhancement of the microbicidal activity for metal/peptide systems is generally confirmed in the case of Gram-positive bacteria and *C. albicans*; by contrast, this effect is less pronounced in the case of Gram-negative bacteria, in particular *Klebsiella* species.

The investigation of the bioactivity of **WT(8-15)** also allows to estimate the antimicrobial potential of the minimum metal-binding sequence of calcitermin, which corresponds to the three alternated histidine residues. Interestingly, it not only exhibits a bioactivity comparable to the other peptides, but it is also the best antimicrobial agent against *S. epidermidis* (**WT(8-15)** MIC = 32 μg/ml; **WT(8-15)**-$Zn^{2+}$ MIC = 16 μg/ml; **WT(8-15)**-$Cu^{2+}$ MIC = 8 μg/ml) and *K. rhinoscleromatis* (**WT(8-15)** MIC = 16 μg/ml; **WT(8-15)**-$Zn^{2+}$ MIC = 8 μg/ml; **WT(8-15)**-$Cu^{2+}$ MIC = 32 μg/ml). The obtained results, therefore, show that the lipophilic portion of calcitermin is not strictly essential to exert antimicrobial activity. This further supports the importance of the interaction with the metal ion in describing the microbicidal power of calcitermin and paves the way for the engineering of the peptide to effectively improve its proteolytic stability.

## Experimental

### Materials

$ZnCl_2$ and $CuCl_2$ were extra pure products (Sigma-Aldrich); the concentrations of their stock solutions were standardized by EDTA titration and periodically checked via ICP-MS. The carbonate-free stock solutions of 0.1 M KOH were prepared by diluting concentrated KOH (Sigma-Aldrich) and then potentiometrically standardized with potassium hydrogen phthalate (99.9% purity), as primary standard. All sample solutions were prepared with fresh Milli-Q® water. The HCl stock solutions was prepared by diluting concentrated HCl and then standardized with standard KOH. The ionic strength was adjusted to 0.1 M by adding KCl (Sigma-Aldrich). Sample solutions of metal-peptide complexes were prepared with metal:ligand ratio 0.8:1. Grade A glassware was always employed.

### Peptide synthesis and purification

Wild-type calcitermin (VAIALKSAHYHTHKE, **WT**) and its derivatives (VAIALKSAHYHTHKE, **A7S**; VAIALKASHYHTHKE, **A8S**; VAIALKSSHYHTHKE, **A7S/A8S** and Ac-AHYHTHKE-$NH_2$, **WT(8-15)**) were synthesized according to published methods[46] using Fmoc/t-butyl chemistry with a Syro XP multiple peptide synthesizer (MultiSynTech GmbH, Written Germany). Wang resin preloaded with Fmoc-Glu(OtBU) was used as a solid support for the synthesis of the three peptides. Fmoc-amino acids (4-fold excess) were sequentially coupled to the growing peptide chain using DIPCDI/HOBt (N,N'-diisopropylcarbodiimide/1-hydroxybenzotriazole) (4-fold excess) as activating mixture for 1 h at room temperature. Cycles of deprotection of Fmoc (40% piperidine/N,N-dimethylformamide) and coupling with the subsequent amino acids were repeated until the desired peptide-bound resin was completed. N-terminal acetylation has been performed with acetic anhydride (0.5 M) with the presence of N-methylmorpholine (0.25 M) (3:1 v/v; 2 ml/0.2 g of resin) as the last synthetic step. The protected peptide-resin was treated with trifluoroacetic acid (TFA)/$H_2O$/triisopropylsilane 90:5:5; v/v; 10 mL per 0.2 g of resin[47] for 1.5 h at room temperature. After filtration of the resin, the solvent was concentrated *in vacuo* and the resin triturated with ethyl ether. Crude peptides were purified by preparative reversed-phase HPLC using a Water Delta Prep 3000 system with a Jupiter column C18(250 × 30 mm, 300 A, 15 μm spherical particle size). The column was perfused at a flow rate of 20 ml/min with a mobile phase containing solvent A (water in 0.1% TFA), and a linear gradient from 0 to 80% of solvent B (60% v/v, acetonitrile in 0.1% TFA) over 35 min for the elution of peptides. Analytical HPLC analyses were performed on Beckman 116 liquid chromatograph equipped with a Beckman 166 diode array detector. Analytical purity of the peptides was assessed using a Zorbax C18 column (4.6 ×150 mm, 3 μm particle size) with the above solvent system (solvents A and B) programmed at a flow rate of 0.7 ml $min^{-1}$ using a linear gradient from 0% to 100% B over 30 min. All analogues showed ≥ 95% purity when monitored at 220 nm. Molecular weight of final compounds was determined by a mass spectrometer ESI Micromass ZMD-2000.

### Potentiometry

Stability constants for proton and metal complexes were obtained from pH-metric titration curves registered at $T$ = 298 K and ionic strength 0.1 M (KCl). The potentiometric apparatus was previously described.[17] Solutions of peptides ($[L]_{tot}$ = $5 \cdot 10^{-4}$ M) and metal complexes ($[L]_{tot}$ = $5 \cdot 10^{-4}$ M and M:L molar ratio 0.8:1) were titrated with 0.1 M carbonate-free KOH. The

electrode was daily calibrated for hydrogen ion concentration by titrating HCl with the standard base solution, under the same experimental conditions as above. The asymmetry potential and the slope of the electrode couple were computed by means of SUPERQUAD[48] and Glee[49] programs. The purities and exact concentrations of the ligand solutions were determined by the Gran method.[50] The HYPERQUAD[51] program was employed for the overall formation constant ($\beta$) calculations, referred to the following equilibrium equation: $pM+qL+rH \leftrightarrows M_pL_qH_r$ (charges omitted; p is 0 in the case of ligand protonation; r can be negative). The computed standard deviations (referring to random errors only) were given by the program itself and are shown in parentheses as uncertainties on the last significant figure. Hydrolysis constants for metal ions were taken from the literature.[52, 53] The distribution and competition diagrams were computed using the HYSS program.[54]

**Mass Spectrometry**

High-resolution mass spectra were obtained on the Bruker ESI-Q-TOF spectrometer (Bruker Daltonics, Germany). The instrumental parameters were as follows: positive ion mode, scan range *m/z* 50–3000, dry gas nitrogen, temperature 180°C and ion energy 5 eV. The capillary voltage was optimized to the highest S/N ratio and it was 3500 V. The samples ($[L]_{tot} = 2 \cdot 10^{-4}$ M and M:L molar ratio = 0.8:1) were prepared in a 1:1 methanol-water mixture at pH about 7.4. They were directly infused at a flow rate of 180 µl/min. The instrument was calibrated externally with the Low Concentration Tuning Mix ESI-TOF (Agilent Technologies (SD ≤ 1 ppm) and sodium formate clusters (SD ≤ 1 ppm)). Data were processed using the Bruker Compass DataAnalysis 4.2 program. The mass accuracy for the calibration was > 5 ppm, enabling together with the true isotopic pattern an unambiguous confirmation of the elemental composition of the obtained complex.

**Spectroscopic measurements**

The absorption spectra of $Cu^{2+}$ containing solutions were recorded on a Varian Cary50 Probe spectrophotometer, in the range 350–850 nm, using a quartz cuvette with an optical path of 1 cm. Circular dichroism (CD) spectra were recorded on a Jasco J-1500 spectropolarimeter in the 180-700 nm range, using a quartz cuvette with an optical path of 1 cm in the UV-visible, and 0.01 cm in the 180-250 nm range. Electron paramagnetic resonance (EPR) spectra were recorded in liquid nitrogen on a Bruker ELEXSYS E500 CW-EPR spectrometer at X-band frequency (9.6 GHz) and equipped with an ER 036TM NMR teslameter and an E41 FC frequency counter. Ethylene glycol (30%) was used as a cryoprotectant. The EPR parameters were analysed by computer simulation of the experimental spectra using WIN-EPR SIMFONIA software, version 1.2 (Bruker, Billerica, MA, USA). To describe the species present in solution, the observed spectroscopic parameters at a given pH were compared with the expected values obtained from literature.[26,55, 56] The pH values where each species is predominant in solution were chosen for spectroscopic analysis. By means of the parameters of the average environment (Billo's method)[26,55, 56] the wavelengths of maximum absorption ($\lambda_{max}$) are attributed to the presence of characteristic donor groups.

**Peptide stability in human plasma**

The persistence of **A7S**, **A8S** and **A7/8S** peptides in human plasma has been studied *in vitro* by means of the following procedure.[57] Each peptide ($C=1 \cdot 10^{-4}$ M) was incubated in a sample containing 1 ml of human plasma (obtained as a pool of 40 individuals from the University Hospital of Ferrara) and 1 ml of ammonium acetate buffer (pH 7.4) at 37 °C. L-phenylalaninol is added as internal standard. At regular time intervals, 200 µl aliquots were taken and enzymatic reaction was blocked by adding 300 µl of $HClO_4$ 0.5 M. The sample was then centrifugated for 6 min at 14000 x g. The supernatant was then filtered and analysed by HPLC. The analytical column was an Agilent Poroshell 120 SB-C18 (4.6 x 100 mm, 2.7 µm, pore size 120 Å). Flow rate = 0.5 ml/min, mobile phase $H_2O$: acetonitrile = 83:17 + 0.1% v/v TFA, isocratic elution, temperature 25 °C, detection wavelength 214 nm. The reported results are the mean of three independent measurements. Informed consent was obtained from all subjects and/or their legal guardian(s) prior to the donation of blood samples. All methods were carried out in accordance with relevant guidelines and regulations.

***In vitro* antimicrobial activity**

The antimicrobial properties of four peptides/complexes were tested against human pathogenic strains. Eight reference bacteria strains from American Type Culture Collection (ATCC), namely *Staphylococcus aureus* 25923, *Enterococcus faecalis* 29212, *Pseudomonas aeruginosa* 15442, *Escherichia coli* 10536, *Klebsiella rhinoscleromatis* 13884, *Klebsiella pneumoniae* 13882, *Klebsiella ozaenae* 11298, *Proteus mirabilis* 21100, and one from Korean Collection for Type Cultures (KCTC), namely *Streptococcus epidermidis* 1917 were grown at 37 °C in Tryptone Soy Broth (TSB) medium (Merck Millipore, Darmstadt, Germany) buffered with 25 mM 2-(N-morpholino)ethanesulfonic acid (MES buffer, Merck Millipore, Darmstadt, Germany), pH 5.4.[12] *Candida albicans* ATCC 10231 was grown aerobically at 37°C on Yeast Peptone Dextrose (YPD) broth (A&A Biotechnology, Gdańsk, Poland) buffered with 25 mM 2-(N-morpholino)ethanesulfonic acid (MES buffer, Merck Millipore, Darmstadt, Germany), pH 5.4.

**Bacterial susceptibility assay**

The peptides and metal complexes minimal inhibitory concentrations (MICs) were determined using the serial broth microdilution method.[58] The final concentration of each peptide and metal complex was ranged from 4 to 256 µg/ml. Stock solutions ($1 \cdot 10^{-3}$ M) of peptides (**A7S**; **A8S**; **A7S/A8S**; **WT(8-15)** and **WT**) and metal complexes (molar ratio 1:1) were prepared

in appropriate medium (TSB for bacterial and YPD for *C. albicans* strains buffered with $25 \cdot 10^{-3}$ M MES). Portions of 100 µL volumes of peptides and their metal complexes (4 to 256 µg/ml) were dispensed into the wells of the microplate. Bacteria incubated with $Zn^{2+}$ and $Cu^{2+}$ (range of 0.1 to 12 µg/ml; concentrations used in the complexes) were used as additional controls. In each test hole, 1 µl of microorganisms suspension at an optical density ($OD_{600}$) of 1.0 corresponding to $1\text{-}5 \times 10^8$ CFU/ml was added. The plates were incubated at 37℃ for 24 h. After incubation, 20 µl of 2,3,5-triphenyltetrazolium chloride (TTC, Merck Millipore, Darmstadt, Germany) solution 0.125% (w/v) was added into each well, and the plates were incubated again for 2 h. After the incubation, visual readings were performed in microplate reader (Spark®, Tecan Trading AG., Switzerland) at 540 nm. The MIC was defined as the lowest concentration of the tested compounds that completely inhibited visible bacterial and *C. albicans* growth. All assays were performed in triplicate.

**Cell Culture Conditions**

The Normal Human Dermal Fibroblasts (NHDF) (Lonza, Basel, Switzerland) were cultured in α-Minimum Essential Medium (α-MEM, Institute of Immunology and Experimental Therapy (IITD), Poland) containing 10% foetal bovine serum (FBS), $2 \cdot 10^{-3}$ M glutamine and antibiotics (100 U/ml penicillin, 100 µg/ml streptomycin). Cells were cultured in 25 $cm^2$ tissue culture flasks (Sarstedt, Nümbrecht, Germany) at 37℃ with 5% $CO_2$ in humidified air. Cells were routinely passaged twice a week using 0.25% trypsin/0.05% EDTA solution.

**Cell Proliferation (MTT Assay)**

The NHDF cells were seeded onto 96-well plates at a density of $3 \times 10^3$ cells per well. The cells were incubated for 24 h with 256 µg/ml of peptides and their $Zn^{2+}$ and $Cu^{2+}$ complexes (molar ratio 1:1). The cell proliferation rate was determined with the standard MTT (3-(4,5-dimethylthiazol-2-yl)-2,5-diphenyltetrazoliumbromide) (Sigma, St Louis, MO, USA) assay procedure.[59] Measurements were made in three independent experiments, each performed in triplicate.

## Author Contributions

D.B., M.R., and M.R.-Z. conceived and planned the experiments. S.L., D.B., K.G. and P.S. conducted the experiments. D.B., T.J., M.R., and M.R.-Z. analysed the results. D.B., S.L., T.J., M.R. and M.R.-Z. wrote the main manuscript. All authors reviewed the manuscript.

## Conflicts of interest

There are no conflicts to declare.

## Acknowledgements

This research was funded by the Polish National Science Centre (UMO-2020/37/N/ST4/03165-D.B.). Staff exchange was possible due to Erasmus+ programme. D.B. is also supported by the National Recovery and Resilience Plan (NRRP), Mission 04 Component 2 Investment 1.5 – NextGenerationEU, Call for tender n. 3277 dated 30/12/2021; Award Number: 0001052 dated 23/06/2022.

## Notes and references

1. M. I. Hutchings, A. W. Truman and B. Wilkinson, *Curr. Opin. Microbiol.*, 2019, **51**, 72-80.
2. P. Dadgostar, *Infection and drug resistance*, 2019, **12**, 3903-3910.
3. R. Laxminarayan, A. Duse, C. Wattal, A. K. Zaidi, H. F. Wertheim, N. Sumpradit, E. Vlieghe, G. L. Hara, I. M. Gould, H. Goossens, C. Greko, A. D. So, M. Bigdeli, G. Tomson, W. Woodhouse, E. Ombaka, A. Q. Peralta, F. N. Qamar, F. Mir, S. Kariuki, Z. A. Bhutta, A. Coates, R. Bergstrom, G. D. Wright, E. D. Brown and O. Cars, *Lancet Infect. Dis.*, 2013, **13**, 1057-1098.
4. D. M. P. De Oliveira, B. M. Forde, T. J. Kidd, P. N. A. Harris, M. A. Schembri, S. A. Beatson, D. L. Paterson and M. J. Walker, *Clin. Microbiol. Rev.*, 2020, **33**, 181.
5. N. Malanovic and K. Lohner, *Pharmaceuticals (Basel, Switzerland)*, 2016, **9**.
6. B. Vishnepolsky, G. Zaalishvili, M. Karapetian, T. Nasrashvili, N. Kuljanishvili, A. Gabrielian, A. Rosenthal, D. E. Hurt, M. Tartakovsky, M. Grigolava and M. Pirtskhalava, *Pharmaceuticals (Basel, Switzerland)*, 2019, **12**.
7. K. Lugardon, R. Raffner, Y. Goumon, A. Corti, A. Delmas, P. Bulet, D. Aunis and M.-H. Metz-Boutigue, *J. Biol. Chem.*, 2000, **275**, 10745-10753.
8. S. Chernysh, S. I. Kim, G. Bekker, V. A. Pleskach, N. A. Filatova, V. B. Anikin, V. G. Platonov and P. Bulet, *Proceedings of the National Academy of Sciences of the United States of America*, 2002, **99**, 12628-12632.
9. K. Browne, S. Chakraborty, R. Chen, M. D. Willcox, D. S. Black, W. R. Walsh and N. Kumar, *Int. J. Mol. Sci.*, 2020, **21**.
10. M. Rima, M. Rima, Z. Fajloun, J. M. Sabatier, B. Bechinger and T. Naas, *Antibiotics (Basel, Switzerland)*, 2021, **10**.
11. D. Dudek, H. Kozlowski and M. Rowinska-Zyrek, *NJCh*, 2018, **42**.
12. A. M. Cole, Y. H. Kim, S. Tahk, T. Hong, P. Weis, A. J. Waring and T. Ganz, *FEBS Lett.*, 2001, **504**, 5-10.
13. M. D'Accolti, D. Bellotti, E. Dzień, C. Leonetti, S. Leveraro, V. Albanese, E. Marzola, R. Guerrini, E. Caselli, M. Rowińska-Żyrek and M. Remelli, *Sci. Rep.*, 2023, **13**, 18228.
14. D. Bellotti, M. Toniolo, D. Dudek, A. Mikołajczyk, R. Guerrini, A. Matera-Witkiewicz, M. Remelli and M. Rowińska-Żyrek, *Dalton Trans.*, 2019, **48**, 13740-13752.
15. D. Bellotti, M. D'Accolti, W. Pula, N. Huang, F. Simeliere, E. Caselli, E. Esposito and M. Remelli, *Gels (Basel, Switzerland)*, 2023, **9**.
16. D. Bellotti, A. Miller, M. Rowińska-Żyrek and M. Remelli, *Biomolecules*, 2022, **12**.
17. D. Bellotti, C. Tocchio, R. Guerrini, M. Rowińska-Żyrek and M. Remelli, *Metallomics*, 2019, **11**, 1988-1998.
18. D. Bellotti, D. Łoboda, M. Rowinska-Zyrek and M. Remelli, *New J. Chem.*, 2018, **42**, 8123-8130.

19. J. L. Alexander, Z. Thompson and J. A. Cowan, *ACS Chem. Biol.*, 2018, **13**, 844-853.
20. J.-C. Choi, M.-S. Kim, H.-Y. Choi, Y.-L. Kang, I.-Y. Choi, S.-W. Jung, J.-Y. Jeong, M.-C. Kim, A. Y. Cho, J.-H. Lee, D.-H. Lee, S.-W. Lee, S.-Y. Park, C.-S. Song, I.-S. Choi and J.-B. Lee, *Vet. Sci.*, 2023, **10**, 191.
21. D. Łoboda, H. Kozłowski and M. Rowińska-Żyrek, *New J. Chem.*, 2018, **42**, 7560-7568.
22. M. Wilson, L. Tillery, E. Tabaie, G. Beery, J. Preusker, I. Bhola and K. Frato, *JBIC Journal of Biological Inorganic Chemistry*, 2020, **25**, 489-500.
23. N. E. Wezynfeld, T. Frączyk and W. Bal, *Coord. Chem. Rev.*, 2016, **327-328**, 166-187.
24. E. I. Podobas, A. Bonna, A. Polkowska-Nowakowska and W. Bal, *J. Inorg. Biochem.*, 2014, **136**, 107-114.
25. L. D. Pettit, K. J. Powell, P. International Union of and C. Applied, 1 online resource.
26. H. Sigel and R. B. Martin, *Chem. Rev.*, 1982, **82**, 385-426.
27. G. D. Natale, C. A. Damante, Z. Nagy, K. Ősz, G. Pappalardo, E. Rizzarelli and I. Sóvágó, *J. Inorg. Biochem.*, 2008, **102**, 2012-2019.
28. A. Jancsó, Z. Paksi, N. Jakab, B. Gyurcsik, A. Rockenbauer and T. Gajda, *Dalton Trans.*, 2005, DOI: 10.1039/B507655B, 3187-3194.
29. J. Peisach and W. E. Blumberg, *Arch. Biochem. Biophys.*, 1974, **165**, 691-708.
30. C. Kállay, Z. Nagy, K. Várnagy, G. Malandrinos, N. Hadjiliadis and I. Sóvágó, *Bioinorg. Chem. Appl.*, 2007, **2007**, 030394.
31. H. F. Stanyon, X. Cong, Y. Chen, N. Shahidullah, G. Rossetti, J. Dreyer, G. Papamokos, P. Carloni and J. H. Viles, *The FEBS journal*, 2014, **281**, 3945-3954.
32. P. G. Daniele, E. Prenesti and G. Ostacoli, *Journal of the Chemical Society, Dalton Transactions*, 1996, DOI: 10.1039/DT9960003269, 3269-3275.
33. I. L. Alberts, K. Nadassy and S. J. Wodak, *Protein science : a publication of the Protein Society*, 1998, **7**, 1700-1716.
34. M. F. Powell, *Chapter 30. Peptide Stability in Drug Development: in vitro Peptide Degradation in Plasma and Serum*, in *Annu. Rep. Med. Chem.*, ed. J. A. Bristol, Academic Press, 1993, vol. 28, pp. 285-294.
35. E. Lenci and A. Trabocchi, *ChSRv*, 2020, **49**, 3262-3277.
36. S. M. Shi and L. Di, *Strategies to Optimize Peptide Stability and Prolong Half-Life*, in *Peptide Therapeutics: Fundamentals of Design, Development, and Delivery*, ed. S. D. Jois, Springer International Publishing, Cham, 2022, DOI: 10.1007/978-3-031-04544-8_4, pp. 163-182.
37. D. Bellotti and M. Remelli, *Molecules*, 2022, **27**, 4584.
38. M. Jeżowska-Bojczuk and K. Stokowa-Sołtys, *Eur. J. Med. Chem.*, 2018, **143**, 997-1009.
39. J. I. Lachowicz, K. Szczepski, A. Scano, C. Casu, S. Fais, G. Orrù, B. Pisano, M. Piras and M. Jaremko, *Int. J. Mol. Sci.*, 2020, **21**, 7349.
40. J. Wu, L. Wang, J. He and C. Zhu, *Contraception*, 2012, **85**, 509-518.
41. D. Bellotti, M. Rowińska-Żyrek and M. Remelli, *Dalton Trans.*, 2020, **49**, 9393-9403.
42. F. Comert, F. Heinrich, A. Chowdhury, M. Schoeneck, C. Darling, K. W. Anderson, M. D. J. Libardo, A. M. Angeles-Boza, V. Silin, M. L. Cotten and M. Mihailescu, *Sci. Rep.*, 2021, **11**, 12620.
43. A. Vaishampayan and E. Grohmann, *Microorganisms*, 2022, **10**, 61.
44. M. D. J. Libardo, S. Nagella, A. Lugo, S. Pierce and A. M. Angeles-Boza, *BBRC*, 2015, **456**, 446-451.
45. D. Boas and M. Reches, *Front. Bioeng. Biotechnol.*, 2021, **9**, 736679.
46. N. L. Benoiton, *Chemistry of Peptide Synthesis*, Taylor & Francis, 2005.
47. N. A. Sole and G. Barany, *The Journal of Organic Chemistry*, 1992, **57**, 5399-5403.
48. P. Gans, A. Sabatini and A. Vacca, *Journal of the Chemical Society, Dalton Transactions*, 1985, DOI: 10.1039/DT9850001195, 1195-1200.
49. P. Gans and B. O'Sullivan, *Talanta*, 2000, **51**, 33-37.
50. G. Gran, H. Dahlenborg, S. Laurell and M. J. A. C. S. Rottenberg, 1950, **4**, 559-577.
51. P. Gans, A. Sabatini and A. Vacca, *Talanta*, 1996, **43**, 1739-1753.
52. P. L. Brown and C. Ekberg, *First Transition Series Metals*, in *Hydrolysis of Metal Ions*, Wiley-VCH, Weinheim, 2016, pp. 499-716.
53. G. Arena, R. Cali, E. Rizzarelli and S. Sammartano, *Thermochimica Acta*, 1976, **16**, 315-321.
54. L. Alderighi, P. Gans, A. Ienco, D. Peters, A. Sabatini and A. J. C. C. R. Vacca, 1999, **184**, 311-318.
55. E. J. Billo, *Inorganic and Nuclear Chemistry Letters*, 1974, **10**, 613-617.
56. E. Prenesti, P. G. Daniele, M. Prencipe and G. Ostacoli, *Polyhedron*, 1999, **18**, 3233-3241.
57. D. E. Benovitz and A. F. Spatola, *Peptides*, 1985, **6**, 257-261.
58. I. Wiegand, K. Hilpert and R. E. W. Hancock, *Nat. Protoc.*, 2008, **3**, 163-175.
59. T. Mosmann, *J. Immunol. Methods*, 1983, **65**, 55-63.

Journal of Inorganic Biochemistry 262 (2025) 112761

Contents lists available at ScienceDirect

Journal of Inorganic Biochemistry

journal homepage: www.elsevier.com/locate/jinorgbio

# Positively charged residues play a significant role in enhancing the antibacterial activity of calcitermin

Silvia Leveraro [a], Maria D'Accolti [a,*], Erika Marzola [a], Elisabetta Caselli [a], Remo Guerrini [a], Magdalena Rowinska-Zyrek [b], Maurizio Remelli [a], Denise Bellotti [a,*]

[a] Department of Chemical, Pharmaceutical and Agricultural Sciences, University of Ferrara, L. Borsari 46, 44121 Ferrara, Italy
[b] Faculty of Chemistry, University of Wrocław, F. Joliot-Curie 14, 50-383 Wrocław, Poland.

ARTICLE INFO

*Keywords:*
Cryptides
Antimicrobial peptides
Calcitermin
Metal coordination
Spectroscopic methods
Antimicrobial activity

ABSTRACT

A systematic study on the human antimicrobial peptide calcitermin (VAIALKAAHYHTHKE) and its carefully designed derivatives was undertaken to verify the impact of divalent copper and zinc ions on the stability, coordination and antimicrobial activity of the formed complexes. In this work we investigate the calcitermin mutants where the alanine in position 7 and 8 is substituted with an arginine residue, with the aim of enhancing the antibacterial activity. Additionally, the analogue where alanine in position 7 is replaced with a histidine is considered, to obtain a chelating sequence with four histidines in alternate position; the aim of this change was to increase the cationic properties of the peptide under acidic conditions and possibly enhance its binding ability towards the metal ions. Through a comprehensive analytical approach involving potentiometric titrations, mass spectrometry, UV–Vis spectrophotometry, NMR and circular dichroism, we delved into the formation equilibria and coordination chemistry of the formed copper(II) and zinc(II) complexes. Antimicrobial assays are also performed to assess the bioactivity of the compounds against a broad spectrum of microorganisms, revealing the pivotal role of positively charged residues in enhancing the antibacterial activity of calcitermin. The obtained results serve as an important stepping stone towards the development of novel metal-based antimicrobial agents.

## 1. Introduction

Antimicrobial resistance (AMR) is one of the major threats to global health of the 21st century. Antibiotics are powerful life-saving drugs, but over time, they are losing their effectiveness due to the emerging growth of resistant pathogens. The excessive and often inappropriate use of antimicrobial drugs has triggered an evolutionary process in microorganisms, which have developed different resistance mechanisms. In order to slow the spread of AMR, there is an urgent need to design new drugs. Among several approaches, the use of antimicrobial peptides (AMPs) is one of the most promising. AMPs are fundamental components of the innate immune system. Indeed, they represent the first line of defense for plants and insects against pathogenic microorganisms. However, they possess a distinct function in higher eukaryotes, which includes the regulation of both innate and adaptive immune pathways [1]. Most eukaryotic AMPs are cationic and amphiphilic peptides presenting both lipophilic and hydrophilic domains [2]. Due to their amphiphilic nature and a net positive charge, the interaction with negatively charged groups on the bacterial membranes is facilitated. The interaction can lead to the insertion of the peptide into the membrane, causing the formation of pores or channels, resulting in the pathogen death [3,4]. Furthermore, AMPs are excellent candidates for the development of novel drugs due to their ability to act through diverse mechanisms of action, resulting into a lower susceptibility towards the development of resistance. Among the numerous mechanisms of action, nutritional immunity is of particular interest. According to this mechanism, AMPs can bind metal ions, such as copper, zinc, manganese or calcium, which are fundamental for pathogens survival and virulence [5]. Furthermore, the binding of metal ions may enhance AMPs antimicrobial activity, owing to modifications in structure and/or charge [5].

Noteworthy, all kingdoms of life are treasure troves repleted with biomolecules possessing potential antimicrobial properties. In recent decades many peptides originated from the cleavage of human proteins have shown antimicrobial activity, expanding the potential pool of novel peptide-based antimicrobial drugs [6–9]. These "cryptides", also known

* Corresponding authors.
*E-mail addresses:* dccmra@unife.it (M. D'Accolti), blldns@unife.it (D. Bellotti).

https://doi.org/10.1016/j.jinorgbio.2024.112761
Received 31 July 2024; Received in revised form 24 September 2024; Accepted 14 October 2024
Available online 16 October 2024

as encrypted or cryptic peptides, are the result of protein maturation processes which lead to the formation of waste products, i.e. peptides, which often exhibit biological activities. Numerous bioactive peptides with different functionalities are then produced by the cleavage of a precursor protein [10,11]. They can display a wide range of bioactivities, such as host defense, protease inhibition, antithrombotic, signaling, analgesic, and angiogenesis activity [11–14]. Examples of cryptides from human proteins include AMPs derived from hemoglobin fragmentation [15], and the 13-mer antifungal (against *Candida albicans*) peptide from the C-terminal domain of albumin [16].

In this work we focus on calcitermin (VAIALKAAHYHTHKE, **WT**), a 15 amino acids cryptide, corresponding to the C-terminal domain of calgranulin C, a pro-inflammatory protein of the S100 family [17]. Calcitermin presents an effective metal-binding domain encompassing three alternated histidine residues (His9, His11 and His13) in addition to its free terminal amino and carboxyl groups. Specifically, the coordination of metal ions, such as Cu(II) and Zn(II), has the potential to enhance the antimicrobial activity against common bacteria, like *Staphylococcus aureus* and *Enterococcus faecalis*, and against the yeast *Candida albicans* at acidic pH [18–20]. To further increase the antimicrobial power of calcitermin, we introduced modification to its native sequence aimed at enhancing the interaction with microbial cell membranes by increasing the number of positively charged residues. Literature provides many strategies to achieve this aim, however one of the most fruitful strategies is the introduction of arginine amino acid in the peptide sequence [21–26]. Also, there are evidence supporting the importance of this residue in the activity of AMPs with a membrane-permeabilization mechanism [25–28]. For this reason, we focused on Ala-to-Arg substitutions for the development of new calcitermin derivatives: VAIALKRAHYHTHKE (**A7R**) and VAIALKARHYHTHKE (**A8R**), in which alanine in position 7 or 8 has been substituted with one arginine residue. We have also investigated the **A7H** mutant (VAIALKHAHYHTHKE), in which the alanine in position 7 is replaced by a histidine residue. This modification affects the net charge of the peptide at acidic conditions (where histidines are expected to be protonated) and extends the number of possible coordination sites for Cu(II) and Zn(II) ions, giving a sequence with four alternated histidines (-HxHxHxHx).

The coordination ability, and thermodynamic and structural characterization of the new calcitermin derivatives (**A7R**, **A8R** and **A7H**) require a thorough analysis, in order to identify similarities and differences with the native peptide and understand how the modification of the peptide sequence affects the coordination property and antimicrobial activity, specifically against three classes of pathogens: a Gram-positive bacterium *Enterococcus faecalis*, a Gram-negative bacterium *Escherichia coli* and the yeast *Candida albicans*. This work therefore sheds light on the role of positively charged residues in affecting the formation of metal complexes and in enhancing the power of the antimicrobial peptide calcitermin.

## 2. Results and discussion

### 2.1. Protonation of the ligands

The potentiometric titrations of the peptides allow to determine the protonation *macro*-constants referred to the following equilibrium equation: $L + nH \leftrightarrows LH_n$ (charges omitted). The symbol L here indicates the ligand in its unprotonated form, i.e. when all the dissociable protons have been released. The net charge of L is −3 for **A7H**, and − 2 for **A7R** and **A8R** due to the presence of the positively charged arginyl guanidinium group, which is always protonated in the pH range here employed. The protonation constants are reported in Table 1 and show reasonable similarities with literature values of calcitermin and other derivatives [29,30] as well as with those of similar ligands [31].

In ligands **A7R** and **A8R** there are nine sites able to undergo acid-base reaction: the carboxyl groups of the C-terminal glutamic acid, the imidazole groups of the three histidine residues, the terminal amine, the phenolic group of tyrosine and two lysyl amino groups. In **A7H**, the substitution of an alanine residue with the histidine entails a further protonation step for the fourth imidazole group. Furthermore, the release of a proton from the amide groups of the peptide backbone cannot spontaneously occur in the pH range explored by potentiometry, since they are very weak acids ($pK_a \approx 15$) [32].

**Table 1**
Overall ($\beta$) and step ($K$) protonation constants for the investigated ligands at $T =$ 298 K and $I = 0.1$ M (KCl). $C_L = 0.5 \bullet 10^{-3}$ M.

| | VAIALKRAHYHTHKE (**A7R**) | | VAIALKARHYHTHKE (**A8R**) | |
|---|---|---|---|---|
| Species | log$\beta$ | log$K$ | log$\beta$ | log$K$ |
| $HL^{-}$ | 10.71(2) | 10.71 | 10.80(8) | 10.80 |
| $H_2L$ | 21.08(1) | 10.37 | 20.80(4) | 10.00 |
| $H_3L+$ | 30.61(2) | 9.53 | 30.04(7) | 9.24 |
| $H_4L^{2+}$ | 38.47(3) | 7.86 | 37.52(9) | 7.48 |
| $H_5L^{3+}$ | 45.32(3) | 6.85 | 44.40(8) | 6.87 |
| $H_6L^{4+}$ | 51.60(3) | 6.28 | 50.55(9) | 6.16 |
| $H_7L^{5+}$ | 57.27(3) | 5.67 | 56.19(8) | 5.64 |
| $H_8L^{6+}$ | 61.64(4) | 4.37 | 60.36(9) | 4.17 |
| $H_9L^{7+}$ | 64.54(4) | 2.90 | 63.60(9) | 3.24 |

| | VAIALKHAHYHTHKE (A7H) | |
|---|---|---|
| Species | log$\beta$ | log$K$ |
| $HL^{2-}$ | 10.77(4) | 10.77 |
| $H_2L^{-}$ | 21.05(3) | 10.28 |
| $H_3L$ | 30.25(5) | 9.21 |
| $H_4L^{+}$ | 37.70(7) | 7.45 |
| $H_5L^{2+}$ | 44.68(7) | 6.98 |
| $H_6L^{3+}$ | 50.95(8) | 6.28 |
| $H_7L^{4+}$ | 56.90(7) | 5.95 |
| $H_8L^{5+}$ | 62.03(7) | 5.13 |
| $H_9L^{6+}$ | 65.77(7) | 3.74 |
| $H_{10}L^{6+}$ | 68.56(7) | 2.79 |

The most acidic moieties are the carboxyl groups. Their log$K$ varies from 2.79 to 4.37, with the terminal -COOH being more acidic than the Glu sidechain. Histidine residues are characterized by log$K$ values ranging from 5.13 to 6.98, in good agreement with the expectation based on literature data. At slightly basic pH, the spontaneous deprotonation of the terminal amino group occurs with log$K$ values 7.86 (**A7R**), 7.48 (**A8R**) and 7.45 (**A7H**). Then, the three ligands show very similar log$K$ values for the phenolic functionality of Tyr (9.53, 9.24 and 9.21). Under basic conditions, the deprotonation of lysines occurres with log$K$ values ranging from 10.00 to 10.80.

### 2.2. Thermodynamic and spectroscopic characterization of metal complexes

The formation of Cu(II) and Zn(II) complexes has been studied by means of different experimental techniques, including potentiometric titrations, mass spectrometry, spectroscopic methods (UV–Vis absorption, circular dichroism (CD)) and nuclear magnetic resonance (NMR). The obtained experimental data were therefore comparatively analyzed, and the stoichiometry, coordination and structure of the complexes were inferred. Comparison with literature data on similar systems also supported the obtained characterization.

In the case of both Cu(II) and Zn(II), under the experimental conditions here employed, only variously protonated mononuclear complexes with metal/ligand stoichiometry of 1:1 have been detected by potentiometry and mass spectrometry. The overall complex-formation constants (log$\beta$) and the corresponding acid dissociation constants ($pK_a$) are reported in Tables 2 and 3. The corresponding species distribution diagrams, calculated from the experimental thermodynamic constants, are shown in Figs. S1-S6.

High resolution mass spectrometry supports the data obtained by potentiometry and the only detected $m/z$ signals correspond to

**Table 2**
Equilibrium constants for the formation of Cu(II) complexes with the investigated ligands at $T = 298$ K and $I = 0.1$ mol dm$^{-3}$ (KCl). $C_L = 0.5 \bullet 10^{-3}$ M and Cu:L = 0.8:1.

| | VAIALKRAHYHTHKE (**A7R**) | | VAIALKARHYHTHKE (**A8R**) | |
|---|---|---|---|---|
| Species | log$\beta$ | p$K_a$ | log$\beta$ | p$K_a$ |
| $[CuH_6L]^{6+}$ | 56.69(5) | 4.47 | 55.96(3) | – |
| $[CuH_5L]^{5+}$ | 52.22(3) | 5.13 | – | – |
| $[CuH_4L]^{4+}$ | 47.09(4) | 6.44 | 46.50(3) | 6.35 |
| $[CuH_3L]^{3+}$ | 40.65(5) | 6.85 | 40.15(7) | 6.74 |
| $[CuH_2L]^{2+}$ | 33.81(5) | 7.96 | 33.41(6) | 7.58 |
| [CuHL]+ | 25.85(6) | 9.53 | 25.83(6) | 9.25 |
| [CuL] | 16.32(7) | 10.13 | 16.58(9) | 9.97 |
| $[CuH_{-1}L]^{-}$ | 6.19(6) | – | 6.61(8) | – |
| $[CuH_{-3}L]^{3-}$ | −14.53(6) | – | −14.21(9) | – |

| | VAIALKHAHYHTHKE (A7H) | |
|---|---|---|
| Species | logβ | p$K_a$ |
| $[CuH_6L]^{5+}$ | 56.84(5) | 5.01 |
| $[CuH_5L]^{4+}$ | 51.84(8) | 5.06 |
| $[CuH_4L]^{3+}$ | 46.78(5) | 7.2 |
| $[CuH_3L]^{2+}$ | 39.6(1) | 7.3 |
| $[CuH_2L]^{+}$ | 32.33(8) | 7.82 |
| [CuHL] | 24.51(9) | 9.26 |
| $[CuL]^{-}$ | 15.25(9) | – |
| $[CuH_{-2}L]^{3-}$ | −5.2(1) | 10.8 |
| $[CuH_{-3}L]^{4-}$ | −16.0(2) | – |

**Table 3**
Equilibrium constants for the formation of Zn(II) complexes with the investigated ligands at $T = 298$ K and $I = 0.1$ M (KCl). $C_L = 0.5 \bullet 10^{-3}$ M and Zn:L = 0.8:1.

| | VAIALKRAHYHTHKE (**A7R**) | | VAIALKARHYHTHKE (**A8R**) | |
|---|---|---|---|---|
| Species | log$\beta$ | p$K_a$ | log$\beta$ | p$K_a$ |
| $[ZnH_5L]^{5+}$ | 49.14(8) | 6.03 | – | – |
| $[ZnH_4L]^{4+}$ | 43.11(4) | – | 42.45(2) | 7.43 |
| $[ZnH_3L]^{3+}$ | – | – | 35.02(6) | 7.56 |
| $[ZnH_2L]^{2+}$ | 27.57(5) | 9.52 | 27.37(4) | 8.64 |
| [ZnHL]+ | 18.04(9) | 9.60 | 18.72(5) | 9.15 |
| [ZnL] | 8.44(7) | – | 9.58(4) | – |
| $[ZnH_{-2}L]^{2-}$ | −13.0(1) | – | −11.10(4) | – |

| | VAIALKHAHYHTHKE (A7H) | |
|---|---|---|
| Species | logβ | p$K_a$ |
| $[ZnH_6L]^{5+}$ | 54.7(1) | – |
| $[ZnH_4L]^{3+}$ | 43.42(4) | 7.2 |
| $[ZnH_3L]^{2+}$ | 36.2(1) | 7.4 |
| $[ZnH_2L]^{+}$ | 28.79(7) | 8.36 |
| [ZnHL] | 20.43(9) | 9.18 |
| $[ZnL]^{-}$ | 11.26(9) | – |
| $[ZnH_{-2}L]^{3-}$ | −9.26(9) | – |

equimolar Cu(II) and Zn(II) complexes with different protonation states. Potassium and/or sodium adducts are also formed (Table S1). ESI-MS spectra and simulation of the isotopic patterns are reported in Figs. S7-S9.

The characterization of copper complexes also occurred with the support of spectroscopic techniques: Vis absorption spectra and CD spectra, recorded at different pH values, are shown in Figs. S10-S15, while spectroscopic data are summarized in Tables S2-S4. Being Zn(II) a diamagnetic ion and thus silent to the aforementioned techniques, we have deepened the study of its complexes by NMR (Figs. S18–S20).

### 2.2.1. Copper complexes

The formation of copper complexes in solution begins around pH 3 for all the studied peptides. However, their show slightly differences depending on the considered ligand.

In the case of **A7R** and **A8R** the first detected species is $[CuH_6L]^{6+}$. According to stoichiometry, in these complexes three acidic protons have been already released by the ligands (from His, Glu and terminal COOH). Hence, besides the histidine residue, one or both the carboxyl groups of *C*-terminal glutamic acid (sidechain and *C*-terminal $COO^-$ groups) can participate in the complexation, forming a macrocycle. The next species $[CuH_5L]^{5+}$ has been detected only for **A7R** system. It rapidly substitutes $[CuH_6L]^{6+}$ in solution, giving a ($2N_{Im}$, $COO^-$) complex. The coordination mode is confirmed by the Vis absorption band at pH 4.8 – where $[CuH_5L]^{5+}$ reaches its maximum of formation in solution – that shows a $\lambda_{max}$ value of 663 nm, (Fig. S10; predicted $\lambda_{max} = 663$ nm) [32,33]. The interaction with the *C*-terminus at acidic pH is also in agreement with the coordination behaviour of other calcitermin derivatives, and the obtained spectral results are consistent with literature data [29,30]. It is also important to consider that various macrochelated species may exist in solution, depending on the interacting His residues. Indeed, the determined p*K* value (4.47) is an equilibrium *macro*-constant that does not allow to identify which specific histidine is involved in the deprotonation step. Increasing the pH value, the Cu(II) ion can displace the acidic proton from a third histidine from both ligands **A7R** and **A8R**; the metal therefore coordinates three imidazoles forming a ($3N_{Im}$) species, which is prevalent in solution at around pH 5–6. The corresponding complex is $[CuH_4L]^{4+}$. The obtained wavelengths of maximum absorption at pH 5.5 and 5.8, respectively for the **A7R** and **A8R** solutions, are $\lambda_{max} = 640$ nm and $\lambda_{max} = 630$ nm and agree with the proposed coordination mode (expected $\lambda_{max} = 627$ nm) [32]. The slight deviation from the theoretical value in the case of **A7R** can be due to the copresence in solution of the species $[CuH_5L]^{5+}$, which is instead not detected for **A8R** system and that can cause the overlap of the absorbance bands of the ($2N_{Im}$, $COO^-$; $\lambda_{max} = 663$ nm) and ($3N_{Im}$; $\lambda_{max} = 627$ nm) species; or it can be due to a weak axial interaction of one of the *C*-terminal carboxylate groups, that can cause the shift of the $\lambda_{max}$ towards higher wavelengths (red-shift) [34]. The interconversion in solution between coordination mode ($3N_{Im}$) and ($3N_{Im}$, $COO^-_{(axial)}$) is also possible.

Increasing the pH value to the neutrality, $[CuH_3L]^{3+}$ and $[CuH_2L]^{2+}$ form by two subsequent deprotonation steps (p$K_a$ = 6.44 and 6.85 (**A7R**); p$K_a$ = 6.35 and 6.74 (**A8R**)). The analysis of Vis absorption spectra suggests that the binding of the terminal amino group and of a deprotonated backbone amide occurs to form a species with 4 N equatorial donor groups. For $[CuH_2L]^{2+}$, a mixture of isomers should therefore exist in solution. The equatorial positions of the complex can be occupied by two histidine residues, an ionized amide group, and the terminal amine ($2N_{Im}$, $NH_2$, $N^-$; theoretical $\lambda_{max} = 549$ nm) or three histidines and the backbone amide ($3N_{Im}$, $N^-$; theoretical $\lambda_{max} = 557$ nm). An axial donor group can also stabilize the coordination and cause a slight red-shift (≈ 10–15 nm) [34,35]. In fact, the experimental $\lambda_{max}$ value at pH 7.5 for **A7R** and 7.3 for **A8R** (where $[CuH_2L]^{2+}$ is predominant in solution) is 564 nm. The possible axial interaction can be due to the third histidine residue or to the terminal amino group, that move from the equatorial position. Circular dichroism data also suggest the binding of the backbone amides starting from pH 6, since changes in CD signals are observed (an intense band for d–d and CT transitions with negative and positive signs of the Cotton effect at 546 and 637 nm, respectively); therefore the coordination of an equatorial N-amide likely occurs in $[CuH_2L]^{2+}$ [33,36,37]. Above pH 8, the main species in solution is $[CuHL]^+$. It is formed by the deprotonation of $[CuH_2L]^{2+}$ with p$K_a$ values 7.96 (**A7R**) and 7.58 (**A8R**), attributable to the ionization and coordination of a second amide. Indeed, the formation of this complex is accompanied by significant changes of the absorption spectra, suggesting that the deprotonation step is not related to an hydroxo complex formation. Contextually, the intensity of CD bands increases, together with the square-planar character of the copper complex [36,38]. Vis absorption bands recorded in the pH range 8–9.5 are characterized by a $\lambda_{max}$ = 545–540 nm (Figs. S10 and S12) that also supports the

predominance in solution of a coordination isomer with a ($2N_{Im}$, 2 $N^-$) binding mode (expected $\lambda_{max}$ = 539 nm) [32]. d–d CD bands (Figs. S11, S13) also confirm the coordination of His side-chains and backbone amides [38]. The next deprotonation step, that leads to the formation of the species [CuL] (p$K_a$ = 9.53 (**A7R**) and 9.25 (**A8R**)), likely refers to the deprotonation of the tyrosine residue, which does not participate in the metal complexation. Indeed, the obtained constants are identical to those expected for the spontaneous release of the phenolic proton (Table 1) and no changes in the spectroscopic parameters (Tables S2, S3) are observed for the formation of [CuL]. When the pH is raised up to 10.5, a further hypsochromic shift to $\lambda_{max}$ = 528 nm is observed. Therefore, the formation of $[CuH_{-1}L]^-$ and $[CuH_{-3}L]^{3-}$ is due to the displacement of a third amide proton, giving rise to the ($N_{Im}$, 3 $N^-$) species (theoretical $\lambda_{max}$ = 525 nm) [32] and to the mere deprotonation of the non-coordinating Lys residues. Once again it is not possible to unequivocally establish which amide groups are involved in the metal coordination. Both the histidine residues and the *C*-terminal carboxyl groups are anchor sites at acidic pH, and then they can favour the metal ion-induced deprotonation and coordination of peptide nitrogens, giving rise to different coordination isomers [33,39–41]. For the **A7H** derivative the first detected complex is once again the exa-protonated species, $[CuH_6L]^{5+}$. In this case, however, the carboxyl groups and two histidine residues should be deprotonated to form a 2 N complex, as suggested by the obtained $\lambda_{max}$ = 688 nm. The participation of one or both the carboxylate groups to metal binding cannot be excluded. The next two deprotonation steps lead to the formation of $[CuH_5L]^{4+}$ and $[CuH_4L]^{3+}$; they are characterized by p$K_a$ values of 5.02 and 5.06, and can be ascribed to the two additional His residues. Since these p$K_a$ values are significantly lower than those measured for the free ligand (6.28 and 6.98), the involvement of further histidines in Cu(II) binding is strongly suggested. From the spectroscopic analysis, we observe a Vis band at 589 nm (Fig. S14, pH 6.4–7.1) which has a bathochromic deviation of +13 nm from the theoretical $\lambda_{max}$ = 576 nm [32,34] and that is consistent with the axial interaction of one of the four bound histidines, giving a distorted octahedral geometry. The sharp blue-shift of the Vis spectra above pH 7.6 ($\lambda_{max}$ < 554 nm) indicates a change in the coordination mode, which is also confirmed by the different shape of the obtained CD spectra from pH 7.6 to 10.5. As in the case of **A7R** and **A8R**, such spectroscopic changes suggest the increasing of the square-planar character of the complexes which occurs upon the coordination of the backbone amides. Indeed, the formation of the species $[CuH_3L]^{2+}$, $[CuH_2L]^+$, [CuHL] is accompanied by the deprotonation of the terminal amine and of two backbone amide groups (p$K_a$ values = 7.2, 7.3 and 7.82). The additive property of absorbance makes difficult the analytical assignment of a Vis band to each single species, giving their coexistence in solution. In fact, a broad band in the pH range 8.6–9.2 is observed. This can also indicate the presence of isomeric species, where the donor groups mutually exchange in the copper coordination sphere. Nevertheless, the $\lambda_{max}$ = 536 nm strongly suggests a ($2N_{Im}$, 2 $N^-$) donor set at pH 9.6, where $[CuL]^-$ is the main complex in solution. As for **A7R** and **A8R**, also in this case, the deprotonation of the tyrosine occurs without involvement in the complexation; in fact, the deprotonation constant of the complex (p$K_a$ = 9.26, Table 2) is almost identical to that of the free peptide (9.21, Table 1). The formation of the $[CuH_{-2}L]^{3-}$ species involves two deprotonation steps that likely refers to the binding of a third deprotonated amide and to the mere deprotonation of one Lys residue, to form a ($N_{Im}$, 3 $N^-$) square planar complex (experimental $\lambda_{max}$ = 529 nm; expected $\lambda_{max}$ = 525 nm) [32]. The last detected deprotonation step leads to the formation of $[CuH_{-3}L]^{3-}$ and occurs with p$K_a$ = 10.8, which strongly suggests the spontaneous deprotonation of the second lysine residue (p$K$ = 10.80 for free peptide, Table 1).

### 2.2.2. Zinc complexes

The formation of zinc complexes occurs at pH 4–4.5 with all the three ligands. The obtained thermodynamic data for the studied derivatives (Table 3) show very high consistency with those of wild-type calcitermin and derivatives [29,30]. According to the stoichiometry, the first detected species for **A7R** ($[ZnH_5L]^{5+}$) and **A7H** ($[ZnH_6L]^{5+}$) corresponds to a macrochelated zinc complex likely formed by two coordinated histidines and the glutamic acid. By contrast, the first detected complex for **A8R** is $[ZnH_4L]^{4+}$, which is likely characterized by a ($3N_{Im}$, $COO^-$) donor set. Increasing the pH, **A7R** ligand releases an acidic proton (p$K_a$ = 6.03) to form $[ZnH_4L]^{4+}$: this deprotonation step can be attributed to the binding of a third histidine residue. In fact, the p$K_a$ value is significantly lower than that obtained for the spontaneous deprotonation (6.85). For **A7H**, instead, the third and fourth histidine residues likely interact with Zn(II) ion in a cooperative mode, forming the $[ZnH_4L]^{3+}$ complex. The coordination of the histidine and glutamic acid residues in **A7R** and **A8R** complexes at pH ~ 7.4 is supported by NMR results, where $H_\delta$-$H_\varepsilon$ and $H_\alpha$-$H_\beta$ protons signals of all the histidine residues and the proton correlations of the glutamic acid are broadened to baseline in the presence of the metal ion (Figs. S18, S19). In the case of **A7H**, although the interaction with Glu is still an option, the broadening of its proton signals is less intense (Fig. S20) and may suggest the simultaneous presence of more than one coordination mode, where the species with four bound histidines ($4N_{Im}$) is prevalent in solution. Moreover, for all the three ligands, the involvement of the *N*-terminal amino group cannot be excluded, since we observed a significant shift of the $H_\alpha$-$H_\beta$ correlations of Val1 in NMR spectra (Figs. S18–20). At higher pH values, the deprotonation of tyrosine and lysine residues occurs without participating in the complex formation. This is confirmed by the comparison of the obtained thermodynamic constants for zinc complex formation and ligand protonation, which are consistent with the spontaneous release of the proton from the aforementioned acid-base sites. Hydrolysis of coordinated water molecules may also occur as a result of the zinc electron density withdrawing, with p$K_a$ values which are usually >7 [42–46], also for calcitermin and its derivatives [29,30]. Such behaviour is therefore confirmed also for the Ala-to-Arg and Ala-to-His derivatives investigated in the present work (Table 3). Moreover, although the attribution of such deprotonation steps to the coordination of backbone amides is plausible, it is strongly discouraged by recent data on zinc inability to ionized peptide nitrogens, which confirm the stronger tendency of Zn(II) to undergo hydrolysis than amide coordination [47].

### 2.2.3. Comparison of metal-binding ability

The determined thermodynamic constants for the complex-formation equilibria provide an effective tool to understand the capacity of the investigated peptides to stably coordinate metal ions. Such evaluation can be obtained comparing the metal-binding affinity of each system in the whole pH range by means of competition diagrams (Fig. 1). These diagrams allow to simulate the behaviour of the ligands in a solution containing equimolar amounts of each of them and of the metal ion, describing the formation of the binary metal complexes. In Fig. 1 we compared the stability of the complexes with the native calcitermin **WT** with respect to that of the derivatives **A7R**, **A8R** and **AH7**.

In the case of copper, we observed that **WT**, **A7R** and **A8R** behave very similarly in the considered pH range, with only maximum 20 % difference in the percentage of complex formation between the native peptide and the Ala-to-Arg derivatives. This data is consistent with the proposed speciation model, since arginine residues are not directly involved in the formation of the complex. However, it can be interesting to note that, in general, **A8R** somewhat proved to form slightly more stable complexes. This is not straightforward to explain, because the three ligands **WT**, **A7R** and **A8R** are characterized by the same coordination, which is mostly confirmed by spectroscopic results: three histidine residues bind the metal ion at acidic conditions, while the interaction with the terminal amino group and up to three backbone amides is expected to start at neutral pH. An effect of the arginine in position 8, that is not occurring when Arg substitutes Ala residue in position 7, is conceivable in accordance with recent literature that shows different metal-binding affinity of calcitermin derivatives where Ala-7

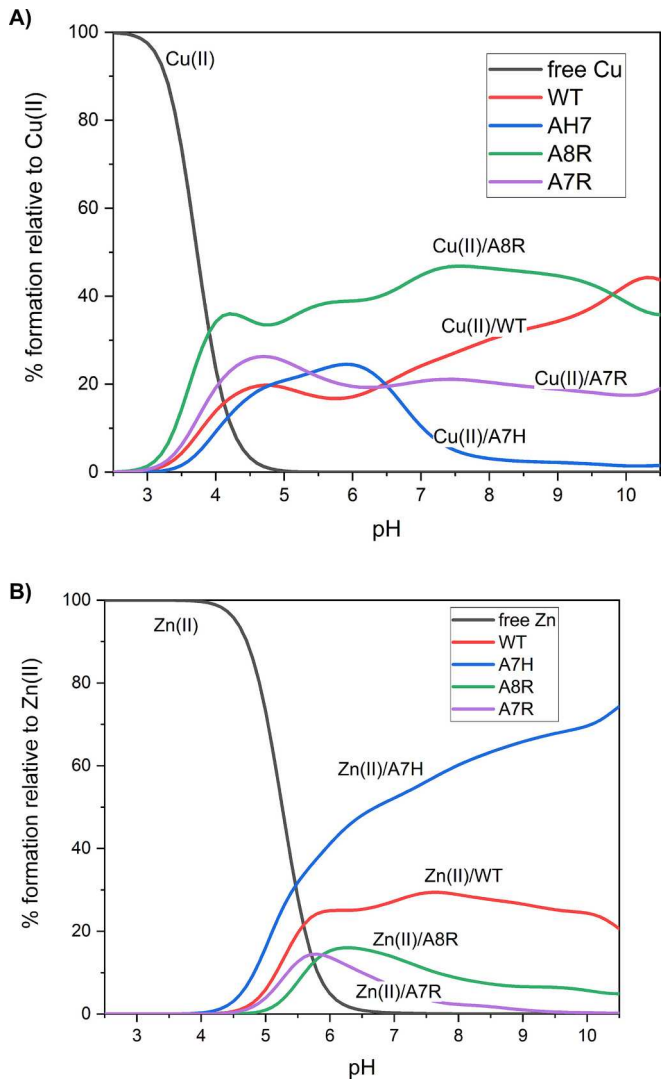


**Fig. 1.** Competition plots for a simulated solution containing equimolar concentrations of (A) Cu(II), (B) Zn(II), and **WT** [29], **A7R**, **A8R** and **A7H**.

and Ala-8 are substituted with non-coordinating polar residues [30]. Many hypotheses can be formulated (electrostatic effects, formation of a hydrogen bond with one of the deprotonated C-terminal carboxyl groups, weak interactions with coordinated solvent molecules, etc.) requiring further investigations. However, **A8R** noteworthy also displays higher proteolytic stability in human plasma (see Section "Peptide resistance to degradation in human plasma").

The analysis of the competition diagram in Fig. 1a also shows that **A7H** ligand displays a copper-binding affinity comparable to **WT** and **A7R** until pH 6.5, above which it becomes the less effective ligand. This is likely due to the presence of a fourth histidine able to bind the Cu(II) ion, which prevents the interaction with the backbone amides and moves their coordination to higher pH values [39,48]. By contrast, the presence of a fourth coordinating histidine in **A7H** peptide clearly increases the zinc binding affinity (Fig. 1b), due to either the formation of a thermodynamically stable complex, and the entropic effect that increases the number of potentially available donor groups and the possibility to form polymorphic binding states, in which at least two different sets of His imidazole residues are bound to the metal, where one of His residue is the same in two cases. The presence of such polymorphic binding states, in which the metal can move"back and forth" along the peptide binding sites, is well known to be the reason for the enhancement of metal complex stability [49–54].

### 2.3. Near-UV CD Structural Characterization

The obtained near-UV CD spectra for the **A7R**, **A8R** and **A7H** systems are very similar to the spectra of their Cu(II) and Zn(II) complexes depicted in Figs. S16, S17, therefore metal coordination has no effect on the secondary structure of the peptides. One negative absorption band at ~295–298 nm is obtained for both the apopeptides and metal complexes in water solution (Figs. S16), and this strongly suggests a random coil structure [55]. Fig. S17, instead, shows a slightly different structural conformation in 10 mM sodium dodecyl sulfate solution (SDS), that has been chosen as membrane-mimicking solvent. In particular, spectra in Fig. S17 display a positive absorption band at ~190 nm and two negative bands at ~202 nm and ~223 nm, which suggest the partial adoption of a helical conformation [56,57]. The observed structure variation from water solvent (unstructured systems) to a membrane-mimicking solvent (α-helical systems) may have significant implications on the bioactivity of the investigated compounds: peptides with helical structure usually afford stronger membrane activity and toxicity than the corresponding non-helical peptides, therefore the capability of undergoing smart transitions of the secondary structure provides a promising approach to enhance the selectivity towards pathogen cell membranes (e.g. by modulating the conditions of the delivery system) and limit toxicity against the host cells [58].

### 2.4. Peptide resistance to degradation in human plasma

The activity of antimicrobial peptides is subject to modulation or limitation by human proteolytic enzymes. In fact, many *endo-* and *exo-*peptidases can degrade high molecular weight peptides into shorter oligopeptides, making them inactive. The study of calcitermin degradation in human plasma showed that the main contribution to its degradation is due to aminopeptidases or dipeptidylaminopeptidases acting on the *N*-terminus. This results into a half-life of about 18 min.[30] Endo-peptidases can also affect the stability of calcitermin, and the study of the effect of Ala-to-Arg and Ala-to-His substitution on the calcitermin proteolytic stability has been carried on. In Fig. 2 the degradation profile of **A7R**, **A8R** and **AH7** is reported; **WT** is included for comparison. The substitution of alanine residue in position 7, either with an arginine or a histidine, does not affect the stability of calcitermin in plasma; indeed they display the same half-life period of **WT**: $t_{1/2} = 16 \pm 2$ min (**A7R**), $t_{1/2} = 16 \pm 3$ min (**A7H**). **A8R** is instead more resistant to degradation phenomena, and it reaches $t_{1/2} = 33 \pm 7$ min. This value is very similar

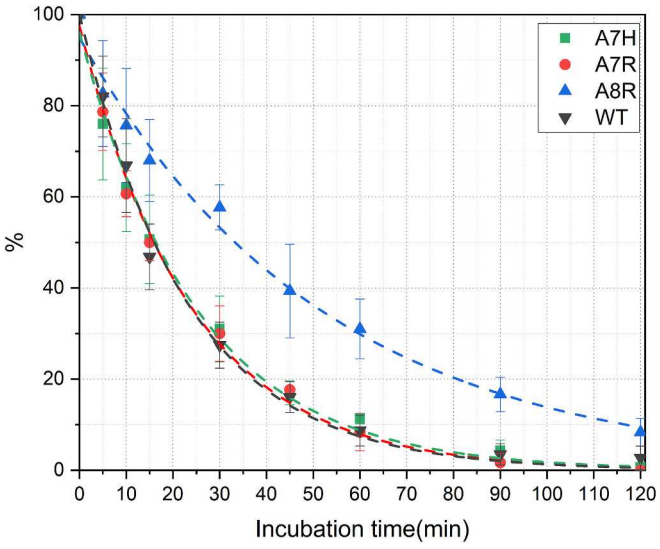


**Fig. 2.** Stability of wild-type calcitermin (**WT**) and its derivatives (**A7R**, **A8R**, **A7H**) in human plasma.

to that obtained for metal complexes with **WT** (33 min) [29]. Such results lead us to consider a scenario where the arginine residue in position 8 is able to exert a "protective" effect on the vicinal metal-binding site (-AHYHTHK-) that hinders the action of proteolytic enzymes in a way similar to the effect that would occur with the formation of a complex (the presence of the metal cation may therefore be comparable). By contrast, the residue in position 7, which is positioned on the opposite side of the peptide backbone with respect to residue-8, is likely ineffective. Certainly, the hypothesis requires further studies.

### 2.5. Antimicrobial activity of peptides and their Cu(II) and Zn(II) complexes

#### 2.5.1. Antifungal activity

Remarkable antifungal activity was not observed with any of the tested peptides, compared to untreated controls (Table S5).

More specifically, a slight decrease was observed after 3 h for **A8R**, although the results were not statistically significant (−5 % and − 17 % for 0.064 and 0.128 mg/mL, p = ns), and for **A7H** (−20 % at 0.128 mg/mL, p = ns).

By contrast, similarly to what observed in previous studies performed with other derivatives [29], a significant CFU reduction was observed with 0.128 mg/mL **A7R**, **A8R** and **A7H** in the presence of $Zn^{2+}$ (−37 %, −66 %, −76 %, $p < 0.05$ and $p < 0.0001$, respectively); a significant reduction was also observed with **A8R** in the presence of $Cu^{2+}$ at the highest concentration (−42 % decrease at 0.128 mg/mL, $p < 0.05$).

After 24 h of contact, the observed reduction values were maintained or increased in the presence of $Zn^{2+}$, especially at 0.128 mg/mL (−92 % for **A7R** + $ZnCl_2$, −85 % for **A8R** + $ZnCl_2$, and − 96 % for **A7H** + $ZnCl_2$, $p < 0.0001$) (Table 1). A similar reduction was detected also in presence of $Cu^{2+}$, with up to 30 % of reduction for **A7R** (0.128 mg/mL, $p < 0.01$) and up to 35 % for **A7H** (0.128 mg/mL, $p < 0.001$). $ZnCl_2$ alone, included as a control, however, exhibited a significant antifungal activity in all performed assays, reducing *C. albicans* CFUs up to 74 % at 3 h and to 93 % at 24 h ($p < 0.0001$). By contrast, negligible or no CFU reduction was observed in all conditions with $CuCl_2$ alone (Table S5). Fig. 3 summarizes the results obtained with *C. albicans* in a graphical way.

#### 2.5.2. Antibacterial activity

The antibacterial effect of peptides was analyzed by using the Gram-negative *Escherichia coli* and the Gram-positive *Enterococcus faecalis* strains as bacterial targets. Regarding *E. coli* (Table *S6*), the results at 3 h showed that **A7R** and **A8R** induced a 30 % ($p < 0.05$) and 40 % ($p < 0.01$) decrease of CFUs at the highest concentration (0.128 mg/mL). Both peptides exhibited a dose-dependent action, inducing −10 % (p = ns), −26 % ($p < 0.05$) and − 30 % ($p < 0.05$) at 0.032, 0.064, 0.128 mg/mL of **A7R**, and − 28 % ($p < 0.05$), −37 % ($p < 0.01$), −40 % ($p < 0.01$) at 0.032, 0.064, 0.128 mg/mL of **A8R**. The activity of the peptides was significantly increased by the presence of $ZnCl_2$ and $CuCl_2$, reaching −91 % ($p < 0.001$) and − 86 % ($p < 0.001$) CFU reduction for **A7R** (0.128 mg/mL), −95 % ($p < 0.001$) and − 76 % ($p < 0.001$) for **A8R** (0.128 mg/mL), and − 81 % ($p < 0.001$) and − 65 % ($p < 0.001$) for **A7H** (0.128 mg/mL), respectively. At 24 h, no significant reduction of CFUs was observed with any of the tested peptides, although a slight activity was evidenced when $Zn^{2+}$ was present, reaching an overall −20 % (p = ns), −28 % (p = ns) and − 37 % (p = ns) decrease for **A7R**, **A8R** and **A7H** (0.128 mg/mL), respectively. Similarly, the addition of $Cu^{2+}$ led to a − 24 % (p = ns), −30 % (p = ns) and − 54 % (p = ns) decrease of CFUs for **A7R**, **A8R** and **A7H** (0.128 mg/mL), respectively. Fig. 4 summarizes graphically the results obtained with *E. coli*.

Regarding *E. faecalis* (Table S7), the results at 3 h showed that **A7R** and **A8R** reduced CFU number of −15 % (p = ns) and − 40 % ($p < 0.05$) at the highest concentration (0.128 mg/mL). Some dose-dependent action was evidenced, being the reduction values corresponding to −6 % (p = ns) and − 15 % (p = ns) for 0.064, 0.128 mg/mL of **A7R**, respectively; −12 % (p = ns), −36 % (p = ns), −40 % ($p < 0.05$) for 0.032, 0.064, 0.128 mg/mL of **A8R** respectively. The peptides' activity was not significantly increased by the presence of $ZnCl_2$ after 3 h. Instead, a significant decrease of CFUs was observed with **A8R** (0.128 mg/mL) in the presence of $CuCl_2$, showing a − 70 % reduction ($p < 0.01$).

**A7H** at the highest concentration (0.128 mg/mL) was associated with a − 31 % decrease ($p < 0.05$) of CFUs, which was increased in the presence of $Zn^{2+}$ and $Cu^{2+}$, reaching −44 % ($p < 0.05$) and − 61 % ($p < 0.01$) respectively, at the highest peptide concentration. At 24 h, no significant reduction of the target CFU number was observed, being detected rather some increased proliferation of the bacterial target (Table *S7*). Fig. 5 summarizes graphically the results obtained with *E. faecalis*.

#### 2.5.3. Comparison of antimicrobial activity among calcitermin derivatives

To sum up the results and draw some conclusions, the collected data showed a certain antimicrobial activity of peptides after 3 h of contact, especially in the presence of bivalent metal ions. A CFU reduction was in fact observed for *C. albicans, E. coli*, and *E. faecalis* with **A7R**, **A8R**, and **A7H** at the highest concentration tested (0.128 mg/mL) (Fig. 6).

**A7R** exhibited an activity primarily directed against *E. coli* (up to −30 %) and *E. faecalis* (up to −15 %), whereas no antifungal effect after 3 h of contact.

**A8R** showed effect against *E. coli* (up to −40 %), *E. faecalis* (up to −40 %) and a slight action also against *C. albicans* (up to −17 %), at 3 h.

**A7H** was most effective against *E. faecalis* (up to −31 %), and secondly against *C. albicans* (up to −20 %) and *E. coli* (up to −7 %).

In most cases, the presence of zinc and copper increased the activity of the peptides: the effect was more evident against the Gram-negative bacterial target rather than towards the other targets. However, results showed that both Zn(II) and Cu(II) ions possess antimicrobial activity per se, similarly to what reported in previous studies (Fig. 6) [29,59,60]. This also suggests that a possible synergistic effect between the peptide and the metal ion can occur, since under the tested diluted conditions the metal complexes tend to dissociate (Fig. S21).

Finally, in the attempt to make a direct comparison between the different types of peptides tested so far, the data collected with **WT** calcitermin, its terminally protected derivatives **L1** (Ac-.

VAIALKAAHYHTHKE), **L2** (Ac-VAIALKAAHYHTHKE-$NH_2$), **L3** (VAIALKAAHYHTHKE-$NH_2$) [29], and **A7R**, **A8R**, **A7H** have been put together and shown in Fig. 7 (metal ions were not included in the figure, to focus exclusively on the comparison between individual peptides). To note, the Gram-positive bacterial target was represented by *S. aureus* for L1, L2, and L3 and by *E. faecalis* for **A7R**, **A8R**, and **A7H**. This because previous results showed that at 24 h of incubation in aqueous buffer at pH 5.4, no viable *S. aureus* bacteria were detectable even in untreated controls [29]; thus, *E. faecalis* was used in substitution of *S. aureus* in the last experiments. However, WT calcitermin was tested against both bacterial targets (Fig. S22): since no significant differences in the growth of *S. aureus* and *E. faecalis* were observed in the two independent experiments compared to untreated controls, the average value of CFU reduction percentage was included in the graph of Fig. 7.

Of note, results obtained after 3 h of contact showed that WT calcitermin displayed the highest antifungal activity, followed by L1, **A7H**, **A8R**, L3, **A7R** and L2. By contrast, WT calcitermin had no activity on both Gram-positive and Gram-negative bacteria, although a slight antimicrobial effect was exerted by some of its derivatives: specifically, L3, **A8R** and **A7H** were active against Gram-positive bacteria, whereas all derivatives, except for **A7H**, showed activity against *E. coli* (Fig. 7A).

After 24 h of incubation, WT calcitermin and derivatives generally lost their antibacterial activity, except for **A8R**, showing an anti-*E. faecalis* action causing up to −24 % CFUs decrease. Instead, the antifungal activity was maintained after 24 h by WT calcitermin (−41 %), L1 (−23 %), L3 (−14 %) and **A7H** (−14 %) (Fig. 7B). Taken together, the collected results showed that peptides alone are minimally

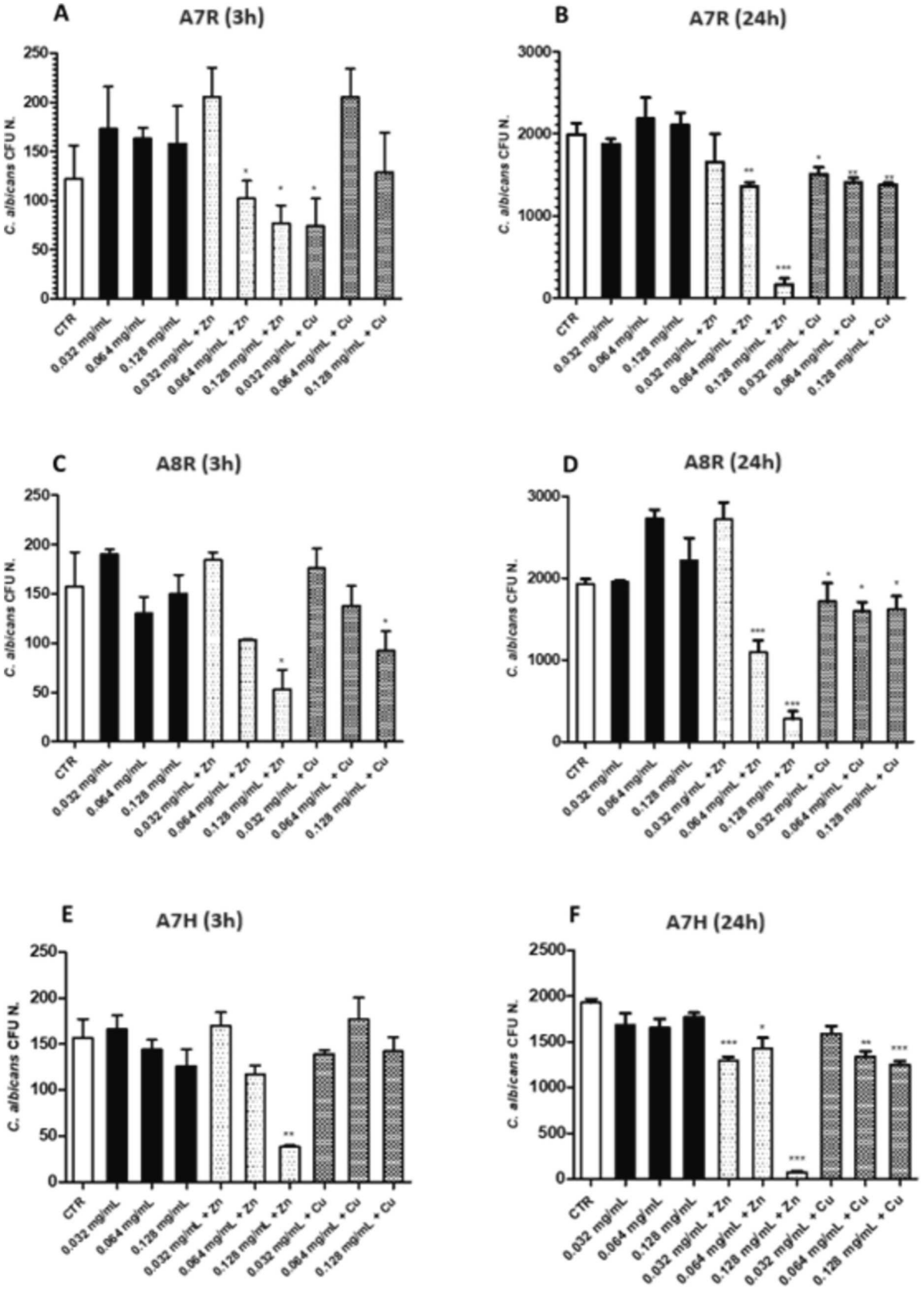


**Fig. 3.** In vitro activity of **A7R**, **A8R**, and **A7H** derivatives against *C. albicans*. All assays were performed in aqueous buffer (5.4 pH) in the presence or absence of $ZnCl_2$, or $CuCl_2$. A-B) **A7R** action after 3 and 24 h. C—D) **A8R** action after 3 and 24 h. *E*-F) **A7H** action after 3 and 24 h. Results are expressed as mean CFU N. ± SD per 0.1 mL of seeded suspension, obtained in triplicate samples from two independent experiments; CTR, untreated controls; * $p \leq 0.05$; ** $p \leq 0.01$; *** $p \leq 0.001$.

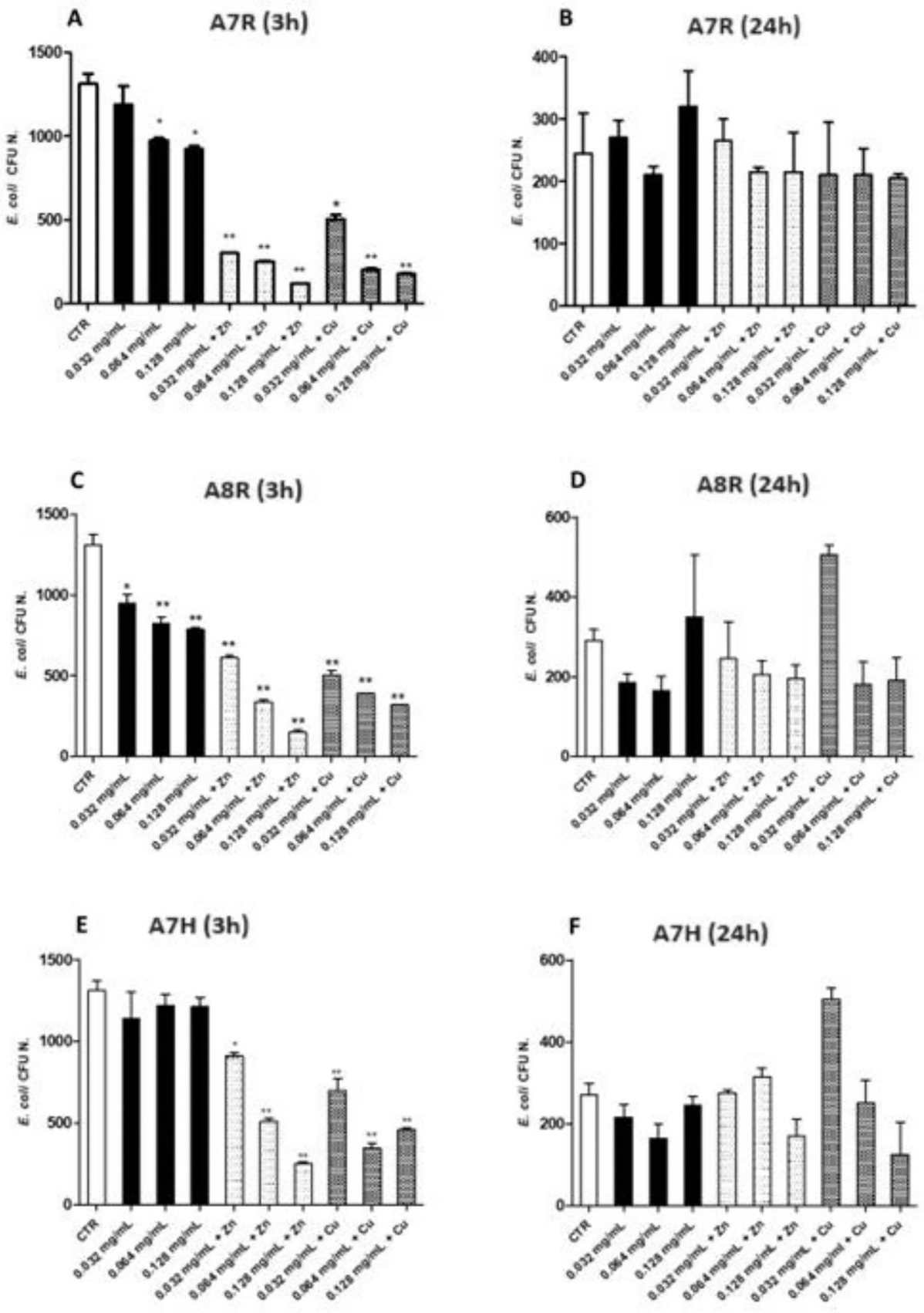


**Fig. 4.** In vitro activity of **A7R**, **A8R**, and **A7H** derivatives against *E. coli*. All assays were performed in aqueous buffer (5.4 pH) in the presence or absence of $ZnCl_2$, or $CuCl_2$. A-B) **A7R** action after 3 and 24 h. C—D) **A8R** action after 3 and 24 h. *E*-F) **A7H** action after 3 and 24 h. Results are expressed as mean CFU N. ± SD per 0.1 mL of seeded suspension, obtained in triplicate samples from two independent experiments; CTR, untreated controls; * $p \leq 0.05$; ** $p \leq 0.01$; *** $p \leq 0.001$.

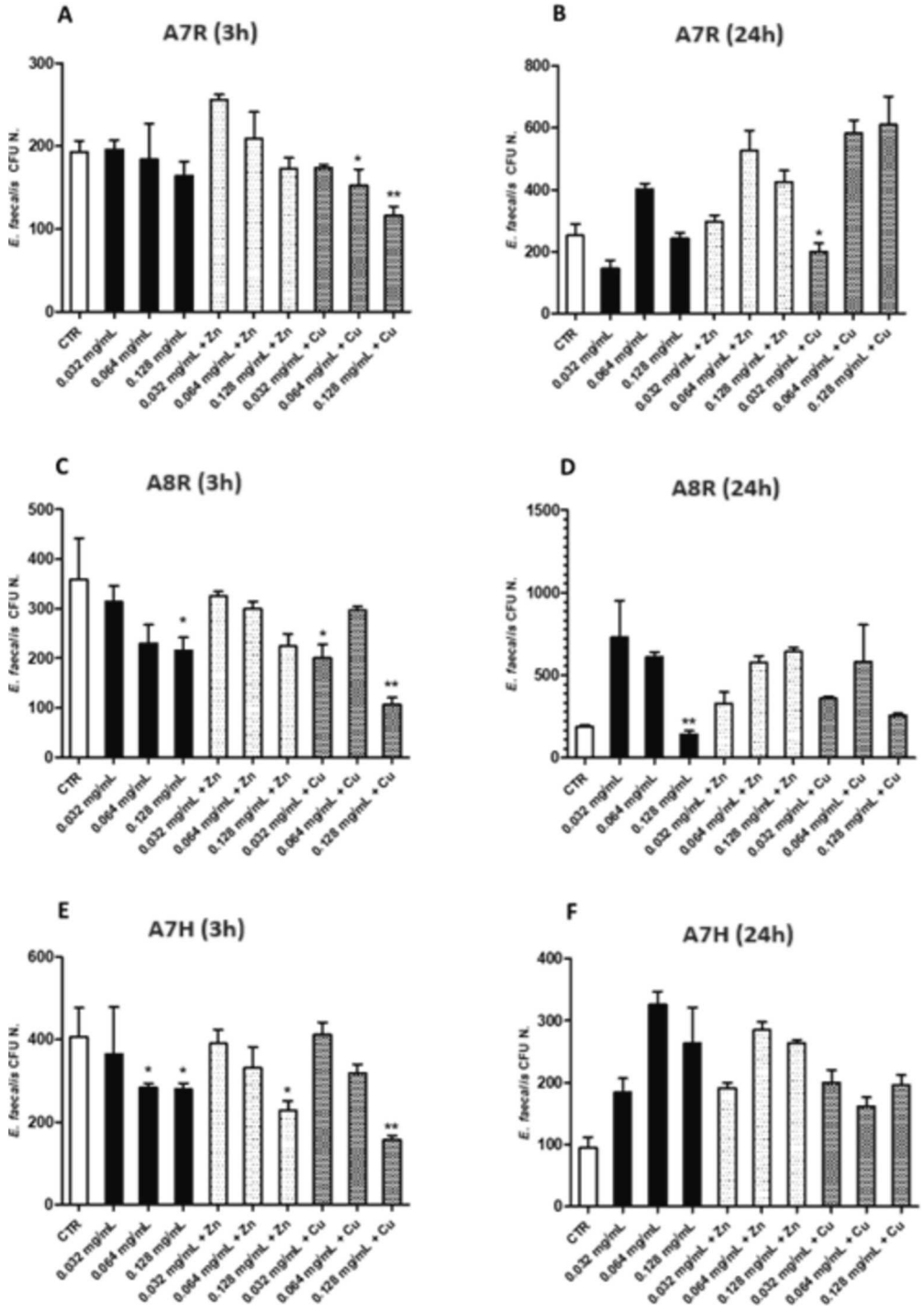


**Fig. 5.** In vitro activity of **A7R**, **A8R**, and **A7H** derivatives against *E. faecalis*. All assays were performed in aqueous buffer (5.4 pH) in the presence or absence of $ZnCl_2$, or $CuCl_2$. A-B) **A7R** action after 3 and 24 h. C—D) **A8R** action after 3 and 24 h. *E*-F) **A7H** action after 3 and 24 h. Results are expressed as mean CFU N. ± SD per 0.1 mL of seeded suspension, obtained in triplicate samples from two independent experiments; CTR, untreated controls; * $p \leq 0.05$; ** $p \leq 0.01$; *** $p \leq 0.001$.

effective even at the highest concentration tested (0.128 mg/mL), while their action is more apparent in the presence of metal ions. Further studies may be performed to evaluate higher concentration of WT calcitermin and derivatives.

## 3. Conclusions

In this study, we investigated the Zn(II) and Cu(II) complexes formation and the antimicrobial activity of three peptide derivatives of the antimicrobial peptide calcitermin: **A7R**, **A8R**, and **A7H**.

With respect to wild-type calcitermin, the investigated peptides do not exhibit significant differences in the metal coordination, expect for the **A7H** derivative, which forms most stable complexes with zinc, mostly due to the presence of one more histidine residue and the possibility to form polymorphic binding states.

The structural characterization highlights the possible occurrence of a transition from an unstructured system in water solvent to an α-helical system in a membrane-mimicking solvent, that could significantly impact the bioactivity of the studied compounds. This offers a promising strategy to enhance selectivity and activity towards pathogens: peptides

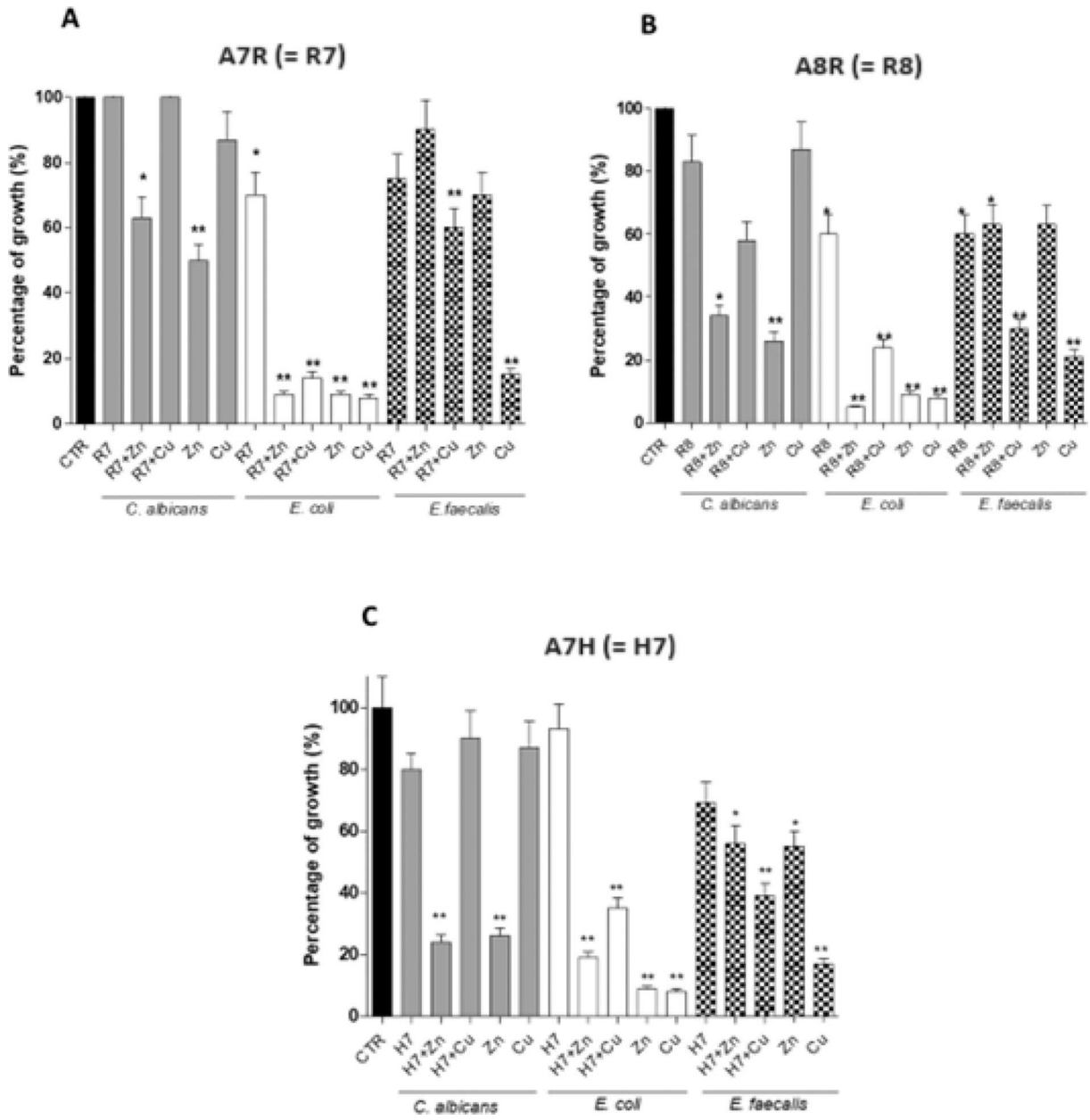


**Fig. 6.** Growth of the tested microbial targets in the presence of **A7R**, **A8R**, and **A7H** at the highest concentration used (0.128 mg/mL). The presence of added $ZnCl_2$, or $CuCl_2$ is also indicated. A) **A7R** action at 3 h incubation; B) **A8R** action at 3 h incubation; C) **A7H** action at 3 h incubation. Results are expressed as mean value of percentage of growth ± SD obtained in triplicate samples from two independent experiments; CTR, untreated controls; * $p \leq 0.05$; ** $p \leq 0.01$.

with a helical structure typically exhibit higher membrane-disrupting activity, but at the same time the less toxic unstructured conformation may be favoured by proper development and engineering of, for example, water-based delivery systems (e.g. smart hydrogels).

The substitution of the alanine residue at position 7 with either arginine or histidine does not affect the stability of calcitermin in plasma, as the **A7R** and **A7H** ($t_{1/2} = 16$ min) derivatives exhibit the same half-life as **WT** ($t_{1/2} = 18$ min). **A8R** showed instead a better performance ($t_{1/2} = 33$ min), which is comparable to that of **WT** metal complexes. Overall, the obtained half-life values are consistent with those of other known antimicrobial peptides (usually less than 30 min) [61]. Certainly, a possible strategy to increase the resistance to degradation of these derivatives relies on the protection of the amino-terminal end of the peptide, as already reported for wild-type calcitermin [29]. Such modification confers stability towards the action of aminopeptidases [62–64].

Finally, our findings also indicate that these peptides exhibit significant antimicrobial properties, particularly in the presence of bivalent metal ions, Zn(II) and Cu(II). Moreover, their antibacterial activity against the tested Gram-positive and -negative bacteria is higher than **WT** at pH 5.4, confirming the positive effect of the introduction of positively charged arginine and histidine residues in the peptide sequence. Such an effect is not exerted against *C. albicans*, against which **WT** is still a better antifungal agent.

Overall, we obtained calcitermin derivatives with better antibacterial activity, which is also enhanced by Cu(II) and Zn(II) ions. Our results contribute understanding the coordination behaviour and antimicrobial potential of native calcitermin and its Ala-to-Arg and Ala-to-His derivatives, providing a foundation for future research and potential therapeutic applications.

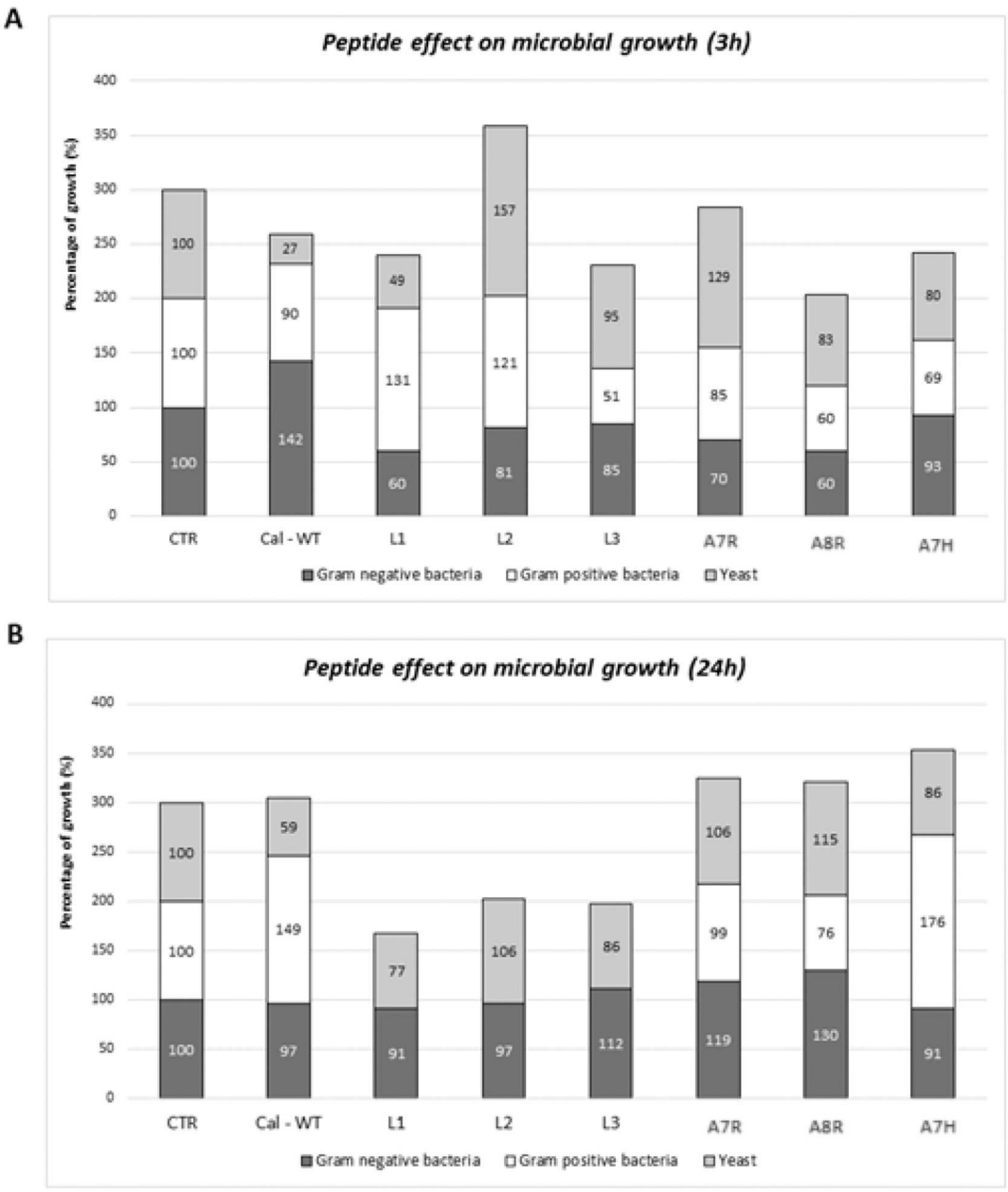


**Fig. 7.** Growth of microbial targets (Gram-negative and Gram-positive bacteria, and yeasts) in the presence of Cal-WT, L1, L2, L3, **A7R**, **A8R**, and **A7H** after 3 h (A) and 24 h (B) of incubation. The results are expressed as mean percentage values. CTR, untreated controls.

## 4. Experimental

### *4.1. Materials*

$ZnCl_2$ and $CuCl_2$ were extra pure products (Sigma-Aldrich); the concentrations of their stock solutions were standardized by EDTA titration. The carbonate-free stock solutions of KOH and HCl (Sigma-Aldrich) were prepared by diluting concentrated solutions (Sigma-Aldrich) and then potentiometrically standardized with primary standard (99.9 % purity) potassium hydrogen phthalate and sodium carbonate, respectively. All sample solutions were prepared with fresh Milli-Q® water. Soda lime traps were used to preserve solutions from atmospheric $CO_2$. The ionic strength was adjusted to 0.1 M by adding KCl (Sigma-Aldrich). Grade A glassware was always employed.

### *4.2. Peptide synthesis and purification*

Calcitermin derivatives (VAIALKRAHYHTHKE, **A7R**; VAIALKARHYHTHKE, **A8R** and VAIALKHYHTHKE, **A7H**) were synthesized according to published methods [65] using Fmoc/t-butyl chemistry with a Syro XP multiple peptide synthesizer (MultiSynTech GmbH, Written Germany). Wang resin preloaded with Fmoc-Glu(OtBu) was used as a solid support for the synthesis of the three peptides. Fmoc-amino acids (4-fold excess) were sequentially coupled to the growing peptide chain using DIPCDI/HOBt (N,N′-diisopropylcarbodiimide/1-hydroxybenzotriazole) (4-fold excess) as activating mixture for 1 h at room temperature. Cycle of deprotection of Fmoc (40 % piperidine/*N*,*N*-dimethylformamide) and coupling with the subsequent aminoacids were repeated until the desired peptide-bound resin was completed. N-terminal acetylation has been performed with acetic anhydride (0.5 M) with the presence of *N*-methylmorpholine (0.25 M) (3:1 *v*/v; 2 mL/0.2 g of resin) as the last synthetic step. The protected peptide-resin was

treated with trifluoroacetic acid (TFA)/H2O/triisopropylsilane 90:5:5; v/v; 10 mL per 0.2 g of resin [66] for 1.5 h at room temperature. After filtration of the resin, the solvent was concentrated in vacuo and the resin triturated with ethyl ether. Crude peptides were purified by preparative reversed-phase HPLC using a Water Delta Prep 3000 system with a Jupiter column C18 (250 × 30 mm, 300 A, 15 μm spherical particle size). The column was perfused at a flow rate of 20 mL/min with a mobile phase containing solvent A (water in 0.1 % TFA), and a linear gradient from 0 to 80 % of solvent B (60 % v/v, acetonitrile in 0.1 % TFA) over 35 min for the elution of peptides. Analytical HPLC analyses were performed on Beckman 116 liquid chromatograph equipped with a Beckman 166 diode array detector. Analytical purity of the peptides was assessed using a Zorbax C18 column (4.6 × 150 mm, 3 μm particle size) with the above solvent system (solvents A and B) programmed at a flow rate of 0.7 mL/min using a linear gradient from 0 % to 100 % B over 30 min. All analogues showed ≥95 % purity when monitored at 220 nm. Molecular weight of final compounds was determined by a mass spectrometer ESI Micromass ZMD-2000.

### 4.3. Potentiometry

Stability constants for proton and metal complexes were obtained from pH-metric titration curves registered at $T = 298$ K and ionic strength 0.1 M (KCl). The potentiometric apparatus was previously described [37]. High purity grade nitrogen was saturated with water vapors by prior passing through a solution of the same composition as the samples ($I = 0.1$ M KCl) to avoid concentration changes of the titrated solution due to water addition/removal, then the gas was gently blown over the test solution in order to maintain an inert atmosphere. Solutions of peptides ($[L]_{tot} = 5{\cdot}10^{-4}$ M) and metal complexes ($[L]_{tot} = 5{\cdot}10^{-4}$ M and M:L molar ratio 0.8:1) were titrated with standardized 0.1 M carbonate-free KOH. At least three titrations were performed for each peptide and its metal complex. The pH range considered for titrations and data treatment is from 2.5 to 10.5 to avoid acid and alkaline electrode errors. The electrode was daily calibrated for hydrogen ion concentration by titrating HCl with the standard base solution, under the same experimental conditions as above. The asymmetry potential and the slope of the electrode couple were computed by means of SUPERQUAD [67] and GLEE [68] programs. The purities and exact concentrations of the ligand solutions were determined by the Gran method [69]. The HYPERQUAD [70] program was employed for the overall formation constant (β) calculations, referred to the following equilibrium equation: $pM + qL + rH \leftrightarrows M_pL_qH_r$ (charges omitted; p is 0 in the case of ligan protonation; r can be negative). The computed standard deviations (referring to random errors only) were given by the program itself and are shown in parentheses as uncertainties on the last significant figure. Hydrolysis constants for metal ions were taken from the literature [71,72]. The distribution and competition diagrams were computed using HYSS program [73].

### 4.4. Mass Spectrometry

High-resolution mass spectra were obtained on the Bruker ESI-Q TOF spectrometer (Bruker Daltonics, Germany). The instrumental parameters were as follows: positive ion mode, scan range *m/z* 45–3000, dry gas nitrogen, temperature 180 °C and ion energy 5 eV. The capillary voltage was optimized to the highest S/N ratio and it was 3500 V. The sample ($[L]_{tot} = 0.2$ mM and M:L molar ratio = 0.8:1) were prepared in a 1:1 methanol-water mixture at pH 7.4. The variation of the solvent composition down to 5 % of methanol did not change the species composition. The instrument was externally calibrated with the Low Concentration Tuning Mix ESI-TOF (Agilent Technologies (SD ≤ 1 ppm) and sodium formate clusters (SD ≤ 1 ppm)). Data were processed using the Bruker Compass DataAnalysis 4.2 program. The mass accuracy for the calibration was better than 5 ppm, enabling together with the true isotopic pattern an unambiguous confirmation of the elemental composition of the obtained complex.

### 4.5. Spectroscopic measurements

The absorption spectra of $Cu^{2+}$ containing solutions were recorded on a Varian Cary50 Probe spectrophotometer, in the range 350–850 nm, using a quartz cuvette with an optical path of 1 cm. Circular dichroism (CD) spectra were recorded on a Jasco J-1500 spectrophotometer in the 180–800 nm range, using a quartz cuvette with an optical path of 1 cm in the UV–visible, and 0.01 cm in the 180–250 nm range. To describe the species present in solution, the observed spectroscopic parameters at a given pH were compared with the expected values obtained from literature [32,74,75]. The pH values where each species is predominant in solution were chosen for spectroscopic analysis. By means of the parameters of the average environment (Billo's method) [74] the wavelengths of maximum absorption ($\lambda_{max}$) are attributed to the presence of characteristic donor groups.

### 4.6. NMR measurements

$^1$H NMR spectra were collected on a Bruker AVANCE Neo 500 MHz spectrometer at $T = 298$ K. The temperature was controlled with an accuracy of ±0.1 K. All the samples were prepared in $D_2O$ (99.95 % from Merck). Proton resonance assignment was accomplished by 2D $^1$H—$^1$H total correlation spectroscopy (TOCSY) experiment, carried out with standard pulse sequences. Samples of analyzed zinc complexes (metal: ligand in a 0.8:1 stoichiometry, $[ligand]_{tot} = 1.0$ mM) were prepared by adding the metal ion to the solution of the ligand, and the pH was then adjusted to 7.4 by adding proper amount of NaOD (40 wt% in $D_2O$ from Merck). Spectral processing and analysis was performed using Bruker TOPSPIN 4.4.1 and MestRe Nova software [76]. Spectra were referenced to the residual HDO peak [77].

### 4.7. Peptide stability in human plasma

The persistence of **A7R**, **A8R** and **A7H** peptides in human plasma has been studied in vitro by means of the following procedure [78]. Each peptide ($C = 1{\cdot}10^{-4}$ M) was incubated in a sample containing 1 mL of human plasma (obtained as a pool of 40 individuals from the University Hospital of Ferrara) and 1 mL of ammonium acetate buffer (pH 7.4) at 37 °C. *L*-phenylalaninol was added as internal standard. At regular time intervals, 200 μL aliquots were taken and enzymatic reactions were blocked by adding 300 μL of $HClO_4$ 0.5 M. The sample was then centrifuged for 6 min at 14000 x*g*. The supernatant was then filtered and analyzed by HPLC. The analytical column was an Agilent Poroshell 120 SB-C18 (4.6 × 100 mm, 2.7 μm, pore size 120 Å). Flow rate = 0.5 mL/min, mobile phase $H_2O$:acetonitrile = 83:17 + 0.1 % *v*/v TFA, isocratic elution, temperature 25 °C, detection wavelength 214 nm. The reported results are the mean of three independent measurements.

### 4.8. Microbial strains

The potential antimicrobial activity of **A7R**, **A8R** and **A7H** derivatives of calcitermin was investigated by using the yeast *Candida albicans* (ATCC 10231), the Gram-positive bacterium *Enterococcus faecalis* (ATCC 51299), and the Gram-negative bacterium *Escherichia coli* (ATCC 25922) (all from American Type Culture Collection, ATCC, Thermo Scientific, Milan, Italy). All microbes were grown at 37 °C in Tryptic Soy Broth (TSB; Biolife, Milan, Italy) and seeded in Tryptic Soy Agar plates (TSA, Biolife, Milan, Italy). For antimicrobial tests, all strains were expanded in TSB at 37 °C under mild agitation for 12 h and then sub-cultured by 1:10 dilution in TSB under the same conditions until reaching $OD_{600nm} = 0.3$–0.4, as judged by spectrophotometric reading using a GENESYS 10S UV–Vis spectrophotometer (Thermo Scientific, Milan, Italy). This OD corresponded to 0.9–1.2 × $10^7$ colony forming units (CFU) per mL, 1.5–2 × $10^8$ CFU/mL and 2.4–3.2 × $10^8$ CFU/mL,

for *C. albicans, E. faecalis* and *E. coli* respectively.

### 4.9. Antimicrobial assays

Microbial subcultures reaching $OD_{600nm} = 0.3–0.4$ were centrifuged at 3,200 x*g* for 10 min washed with PBS pH 5.4, and finally suspended in 10 mL of PBS pH 5.4, to obtain a final concentration correspondent to $10^4$ CFU/mL. Aliquots of 100 μL (corresponding to $10^3$ CFU) were seeded in each well of a 96-wells plate, then 3 μL of TSB at pH 5.4 were added to each well to obtain a final 1.5 % TSB concentration in the culture medium. Peptides were tested at a final concentration C = 0.128, 0.064, 0.032 mg/mL, in the presence or absence of $ZnCl_2$ or $CuCl_2$, at a M:L molar ratio 0.9:1. To this purpose, peptides were serially diluted in PBS pH 5.4 to obtain a concentration corresponding to 0.257, 0.128, and 0.064 mg/mL, then $ZnCl_2$ or $CuCl_2$ solutions were added where requested. 100 μL of peptide ± $ZnCl_2$/$CuCl_2$ solution were then added to each well, obtaining the final 0.128, 0.064 and 0.032 mg/mL peptide concentrations in a total 0.2 mL volume. PBS alone and PBS + $ZnCl_2$/$CuCl_2$ solutions were included as controls. The plates were incubated at 37 °C on a platform rocker with slow stirring for 3 and 24 h. At the end of the incubation times, 100 μL aliquots were taken from each sample, appropriately diluted in PBS pH 5.4 and seeded on TSA plates. Specifically, *C. albicans*, *E. coli*, and *E. faecalis* aliquots were diluted 1:10 at 3 h, and 1:200, 1:1,000,000 and 1:10 at 24 h, respectively. After a further incubation for 24 h at 37 °C, CFUs grown on TSA plates were enumerated. Samples were assayed in triplicate in two independent experiments.

### 4.10. Statistics

Student's *t*-test was used for the statistical analysis of assays' results; a $p$ value $\leq 0.05$ was considered significant.

## CRediT authorship contribution statement

**Silvia Leveraro:** Investigation, Formal analysis. **Maria D'Accolti:** Writing – review & editing, Writing – original draft, Formal analysis, Data curation, Conceptualization. **Erika Marzola:** Formal analysis. **Elisabetta Caselli:** Writing – review & editing, Validation, Supervision. **Remo Guerrini:** Writing – review & editing, Validation. **Magdalena Rowinska-Zyrek:** Writing – review & editing, Resources, Data curation. **Maurizio Remelli:** Visualization, Methodology, Data curation. **Denise Bellotti:** Writing – review & editing, Writing – original draft, Validation, Supervision, Software, Project administration, Investigation, Funding acquisition, Data curation.

## Declaration of competing interest

The authors declare no competing interests.

## Data availability

Data will be made available on request.

## Acknowledgments

Financial support of the National Recovery and Resilience Plan (NRRP) Mission 4 Component 2 Investment 1.1 – European Union-NextGenerationEU (grant PRIN PNRR 2022-P2022EMY52; CUP F53D23008960001; project title: "EnzyMime – Biocompatible and sustainable enzyme mimics based on metal complexes with peptide derivatives: synthesis, characterization and potential biological applications") is gratefully acknowledged. M.R.-Z. is supported by the National Science Centre (Grant UMO-2017/26/E/ST5/00364). Staff exchange was possible due to Erasmus+ program.

## Appendix A. Supplementary data

Supplementary data to this article can be found online at https://doi.org/10.1016/j.jinorgbio.2024.112761.

## References

[1] K. Browne, S. Chakraborty, R. Chen, M.D. Willcox, D.S. Black, W.R. Walsh, N. Kumar, A new era of antibiotics: the clinical potential of antimicrobial peptides, Int. J. Mol. Sci. (2020) 21 (19).
[2] C.L. Chrom, L.M. Renn, G.A. Caputo, Characterization and antimicrobial activity of amphiphilic peptide AP3 and derivative sequences, Antibiotics (Basel, Switzerland) vol. 8 (1) (2019).
[3] G. Satchanska, S. Davidova, A. Gergova, Diversity and Mechanisms of Action of Plant, Animal, and Human Antimicrobial Peptides *Antibiotics* [Online], 2024.
[4] M. Rima, M. Rima, Z. Fajloun, J.M. Sabatier, B. Bechinger, T. Naas, Antimicrobial peptides: A potent alternative to antibiotics, Antibiotics (Basel, Switzerland) vol. 10 (9) (2021).
[5] D. Łoboda, H. Kozłowski, M. Rowińska-Żyrek, Antimicrobial peptide–metal ion interactions – a potential way of activity enhancement, NJCh 42 (10) (2018) 7560–7568.
[6] N. Malanovic, K. Lohner, Antimicrobial Peptides Targeting Gram-Positive Bacteria, Pharmaceuticals (Basel, Switzerland) vol. 9 (3) (2016).
[7] B. Vishnepolsky, G. Zaalishvili, M. Karapetian, T. Nasrashvili, N. Kuljanishvili, A. Gabrielian, A. Rosenthal, D.E. Hurt, M. Tartakovsky, M. Grigolava, M. Pirtskhalava, De Novo Design and in Vitro Testing of Antimicrobial Peptides against Gram-Negative Bacteria, Pharmaceuticals (Basel, Switzerland) vol. 12 (2) (2019).
[8] S. Chernysh, S.I. Kim, G. Bekker, V.A. Pleskach, N.A. Filatova, V.B. Anikin, V. G. Platonov, P. Bulet, Antiviral and antitumor peptides from insects, Proc. Natl. Acad. Sci. U. S. A. 99 (20) (2002) 12628–12632.
[9] K. Lugardon, R. Raffner, Y. Goumon, A. Corti, A. Delmas, P. Bulet, D. Aunis, M.-H. Metz-Boutigue, Antibacterial and antifungal activities of Vasostatin-1, the N-terminal fragment of chromogranin a*, J. Biol. Chem. 275 (15) (2000) 10745–10753.
[10] I.S.D. Costa, T. Junot, F.L. Silva, W. Felix, Fh. Cardozo, J. L.; Pereira de Araujo, A. F.; Pais do Amaral, C.; Gonçalves, S.; Santos, N. C.; Leite, J. R. S. A.; Bloch Jr, C.; Brand, G. D, Occurrence and evolutionary conservation analysis of α-helical cationic amphiphilic segments in the human proteome, FEBS J. 291 (3) (2024) 547–565.
[11] N. Ueki, K. Someya, Y. Matsuo, K. Wakamatsu, H. Mukai, Cryptides: functional cryptic peptides hidden in protein structures, Biopolymers 88 (2) (2007) 190–198.
[12] H.G. Boman, Antibacterial peptides: basic facts and emerging concepts, J. Intern. Med. 254 (3) (2003) 197–215.
[13] G. Satchanska, S. Davidova, A. Gergova, Diversity and mechanisms of action of plant, Animal, and Human Antimicrobial Peptides. 13 (3) (2024) 202.
[14] E. Pizzo, V. Cafaro, A. Di Donato, E. Notomista, Cryptic antimicrobial peptides: identification methods and current knowledge of their immunomodulatory properties, Curr. Pharm. Des. 24 (10) (2018) 1054–1066.
[15] C. Liepke, S. Baxmann, C. Heine, N. Breithaupt, L. Ständker, W.G. Forssmann, Human hemoglobin-derived peptides exhibit antimicrobial activity: a class of host defense peptides, J. Chromatogr. B Anal. Technol. Biomed. Life Sci. 791 (1–2) (2003) 345–356.
[16] T. Ciociola, P.P. Zanello, T. D'Adda, S. Galati, S. Conti, W. Magliani, L. Giovati, A Peptide Found in Human Serum, Derived from the C-Terminus of Albumin, Shows Antifungal Activity In Vitro and In Vivo, Microorganisms 8 (10) (2020).
[17] A.M. Cole, Y.H. Kim, S. Tahk, T. Hong, P. Weis, A.J. Waring, T. Ganz, Calcitermin, a novel antimicrobial peptide isolated from human airway secretions, FEBS Lett. 504 (1–2) (2001) 5–10.
[18] D. Bellotti, M. D'Accolti, W. Pula, N. Huang, F. Simeliere, E. Caselli, E. Esposito, M. Remelli, Calcitermin-loaded smart gels activity against Candida albicans: a preliminary in vitro study, Gels (Basel, Switzerland) 9 (2) (2023) 165.
[19] D. Bellotti, M. Toniolo, D. Dudek, A. Mikolajczyk, R. Guerrini, A. Matera-Witkiewicz, M. Remelli, M. Rowinska-Zyrek, Bioinorganic chemistry of calcitermin - the picklock of its antimicrobial activity, Dalton Trans. 48 (36) (2019) 13740–13752.
[20] D. Bellotti, A. Miller, M. Rowinska-Zyrek, M. Remelli, Zn(2+) and cu(2+) binding to the Extramembrane loop of Zrt2, a zinc transporter of Candida albicans, Biomolecules 12 (1) (2022) 121.
[21] J. Svenson, R. Karstad, G.E. Flaten, B.O. Brandsdal, M. Brandl, J.S. Svendsen, Altered activity and physicochemical properties of short cationic antimicrobial peptides by incorporation of arginine analogues, Mol. Pharm. 6 (3) (2009) 996–1005.
[22] K. Andreev, C. Bianchi, J.S. Laursen, L. Citterio, L. Hein-Kristensen, L. Gram, I. Kuzmenko, C.A. Olsen, D. Gidalevitz, Guanidino groups greatly enhance the action of antimicrobial peptidomimetics against bacterial cytoplasmic membranes, Biochim. Biophys. Acta 1838 (10) (2014) 2492–2502.
[23] J.S. Bahnsen, H. Franzyk, A. Sandberg-Schaal, H.M. Nielsen, Antimicrobial and cell-penetrating properties of penetratin analogs: effect of sequence and secondary structure, Biochim. Biophys. Acta 1828 (2) (2013) 223–232.
[24] K. Locock, T. Michl, H. Griesser, M. Haeussler, L. Meagher, Structure-activity relationships of Guanylated antimicrobial Polymethacrylates, Pure Appl. Chem. 86 (2014) 1281–1291.

[25] K.J. Cutrona, B.A. Kaufman, D.M. Figueroa, D.E. Elmore, Role of arginine and lysine in the antimicrobial mechanism of histone-derived antimicrobial peptides, FEBS Lett. 589 (24 Pt B) (2015) 3915–3920.
[26] N.W. Schmidt, K.P. Tai, K. Kamdar, A. Mishra, G.H. Lai, K. Zhao, A.J. Ouellette, G. C. Wong, Arginine in α-defensins: differential effects on bactericidal activity correspond to geometry of membrane curvature generation and peptide-lipid phase behavior, J. Biol. Chem. 287 (26) (2012) 21866–21872.
[27] Y. Huang, J. Huang, Y. Chen, Alpha-helical cationic antimicrobial peptides: relationships of structure and function, Protein Cell 1 (2) (2010) 143–152.
[28] Z. Jiang, A.I. Vasil, J.D. Hale, R.E. Hancock, M.L. Vasil, R.S. Hodges, Effects of net charge and the number of positively charged residues on the biological activity of amphipathic alpha-helical cationic antimicrobial peptides, Biopolymers 90 (3) (2008) 369–383.
[29] M. D'Accolti, D. Bellotti, E. Dzien, C. Leonetti, S. Leveraro, V. Albanese, E. Marzola, R. Guerrini, E. Caselli, M. Rowinska-Zyrek, M. Remelli, Impact of C- and N-terminal protection on the stability, metal chelation and antimicrobial properties of calcitermin, Sci. Report. 13 (1) (2023) 18228.
[30] S. Leveraro, K. Garstka, P. Śliwka, T. Janek, M. Rowińska-Żyrek, M. Remelli, D. Bellotti, Metal coordination governs the antimicrobial efficacy of calcitermin derivatives, Dalton Trans. 53 (2024) 12676–12687.
[31] L.D. Pettit, H.K.J. Powell, The IUPAC Stability Constants Database, Royal Society of Chemistry, London, 1992-2000.
[32] H. Sigel, R.B. Martin, Coordinating properties of the amide bond - stability and structure of metal-ion complexes of peptides and related ligands, Chem. Rev. 82 (4) (1982) 385–426.
[33] D. Sanna, G. Micera, C. Kallay, V. Rigo, I. Sovago, Copper(II) complexes of N-terminal protected tri- and tetra-peptides containing histidine residues, Dalton Trans. 17 (2004) 2702–2707.
[34] E. Prenesti, P.G. Daniele, M. Prencipe, G. Ostacoli, Spectrum-structure correlation for visible absorption spectra of copper(II) complexes in aqueous solution, Polyhedron 18 (25) (1999) 3233–3241.
[35] M. Perinelli, R. Guerrini, V. Albanese, N. Marchetti, D. Bellotti, S. Gentili, M. Tegoni, M. Remelli, Cu(II) coordination to his-containing linear peptides and related branched ones: equalities and diversities, J. Inorg. Biochem. 205 (2020) 110980.
[36] P.G. Daniele, E. Prenesti, G. Ostacoli, Ultraviolet–circular dichroism spectra for structural analysis of copper(II) complexes with aliphatic and aromatic ligands in aqueous solution, Dalton Trans. 15 (1996) 3269–3275.
[37] D. Bellotti, A. Sinigaglia, R. Guerrini, E. Marzola, M. Rowinska-Zyrek, M. Remelli, The N-terminal domain of helicobacter pylori's Hpn protein: the role of multiple histidine residues, J. Inorg. Biochem. 214 (2021) 111304.
[38] H.F. Stanyon, X. Cong, Y. Chen, N. Shahidullah, G. Rossetti, J. Dreyer, G. Papamokos, P. Carloni, J.H. Viles, Developing predictive rules for coordination geometry from visible circular dichroism of copper(II) and nickel(II) ions in histidine and amide main-chain complexes, FEBS J. 281 (17) (2014) 3945–3954.
[39] E. Székely, G. Csire, B.D. Balogh, J.Z. Erdei, J.M. Király, J. Kocsi, J. Pinkóczy, K. Várnagy, The Role of Side Chains in the Fine-Tuning of the Metal-Binding Ability of Multihistidine Peptides *Molecules* [Online], 2022.
[40] C. Kállay, K. Várnagy, G. Malandrinos, N. Hadjiliadis, D. Sanna, I. Sóvágó, Thermodynamic and structural characterization of the macrochelates formed in the reactions of copper(II) and zinc(II) ions with peptides of histidine, Inorg. Chim. Acta 362 (3) (2009) 935–945.
[41] D. Bellotti, C. Tocchio, R. Guerrini, M. Rowinska-Zyrek, M. Remelli, Thermodynamic and spectroscopic study of cu(ii) and Zn(ii) complexes with the (148-156) peptide fragment of C4YJH2, a putative metal transporter of Candida albicans, Metallomics 11 (12) (2019) 1988–1998.
[42] N.I. Jakab, A. Jancsó, T. Gajda, B. Gyurcsik, A. Rockenbauer, Copper(II), nickel(II) and zinc(II) complexes of N-acetyl-his-pro-his-his-NH2: equilibria, solution structure and enzyme mimicking, J. Inorg. Biochem. 102 (7) (2008) 1438–1448.
[43] G.E. Giacomazzo, D. Paderni, L. Giorgi, M. Formica, L. Mari, R. Montis, L. Conti, E. Macedi, B. Valtancoli, C. Giorgi, V. Fusi, A New Family of Macrocyclic Polyamino Biphenolic Ligands: Acid-Base Study, Zn(II) Coordination and Glyphosate/AMPA Binding 28 (5), 2023, p. 2031.
[44] J. Kamińska, A. Hecel, J. Słowik, A. Rombel-Bryzek, M. Rowińska-Żyrek, D. Witkowska, Characterization of four peptides from milk fermented with kombucha cultures and their metal complexes—in search of new biotherapeutics 11, 2024.
[45] K. Garstka, V. Dzyhovskyi, J. Wątły, K. Stokowa-Sołtys, J. Świątek-Kozłowska, H. Kozłowski, M. Barceló-Oliver, D. Bellotti, M. Rowińska-Żyrek, CH vs, HC—Promiscuous Metal Sponges in Antimicrobial Peptides and Metallophores. 28 (10) (2023) 3985.
[46] M. Mylonas, A. Krężel, J.C. Plakatouras, N. Hadjiliadis, W. Bal, Interactions of Zn (II) Ions with Three His-Containing Peptide Models of Histone H2A. 2 (1–2) (2004) 451012.
[47] S. Leveraro, V. Dzyhovskyi, K. Garstka, D. Bellotti, K. Stokowa-Sołtys, M. Remelli, M. Rowińska-Żyrek, Inorg. Chem., submitted, 2024.
[48] D. Bellotti, S. Leveraro, A. Hecel, M. Remelli, Investigation of metal interactions with YrpE protein of Bacillus subtilis by a polyhistidine peptide model, Anal. Biochem. 680 (2023) 115315.
[49] D. Bellotti, D. Loboda, M. Rowinska-Zyrek, M. Remelli, Investigation on the metal binding sites of a putative Zn(II) transporter in opportunistic yeast species, NJCh 42 (10) (2018) 8123–8130.
[50] D. Bellotti, M. Rowinska-Zyrek, M. Remelli, Novel insights into the metal binding ability of ZinT periplasmic protein from Escherichia coli and salmonella enterica, Dalton Trans. 49 (27) (2020) 9393–9403.
[51] M. Remelli, M. Peana, S. Medici, L.G. Delogu, M.A. Zoroddu, Interaction of divalent cations with peptide fragments from Parkinson's disease genes, Dalton Trans. 42 (17) (2013) 5964–5974.
[52] J. Watly, E. Simonovsky, N. Barbosa, M. Spodzieja, R. Wieczorek, S. Rodziewicz-Motowidlo, Y. Miller, H. Kozlowski, African viper poly-his tag peptide fragment efficiently binds metal ions and is folded into an alpha-helical structure, Inorg. Chem. 54 (16) (2015) 7692–7702.
[53] J. Watly, E. Simonovsky, R. Wieczorek, N. Barbosa, Y. Miller, H. Kozlowski, Insight into the coordination and the binding sites of cu(2+) by the histidyl-6-tag using experimental and computational tools, Inorg. Chem. 53 (13) (2014) 6675–6683.
[54] A. Hecel, J. Wątły, M. Rowińska-Żyrek, J. Świątek-Kozłowska, H. Kozłowski, Histidine tracts in human transcription factors: insight into metal ion coordination ability, JBIC J. Biol. Inorg. Chem. 23 (1) (2018) 81–90.
[55] K. Bakshi, M.R. Liyanage, D.B. Volkin, C.R. Middaugh, Circular dichroism of peptides, in: A.E. Nixon (Ed.), Therapeutic Peptides: Methods and Protocols, Humana Press, Totowa, NJ, 2014, pp. 247–253.
[56] N.J. Greenfield, Using circular dichroism spectra to estimate protein secondary structure, Nat. Protoc. 1 (6) (2006) 2876–2890.
[57] W.C. Johnson Jr., Protein secondary structure and circular dichroism: a practical guide, Proteins: Struct., Funct., Bioinf. 7 (3) (1990) 205–214.
[58] M. Xiong, Z. Han, Z. Song, J. Yu, H. Ying, L. Yin, J. Cheng, Bacteria-assisted activation of antimicrobial polypeptides by a random-coil to Helix transition, Angew. Chem. Int. Ed. Eng. 56 (36) (2017) 10826–10829.
[59] J. Pasquet, Y. Chevalier, J. Pelletier, E. Couval, D. Bouvier, M.A. Bolzinger, The contribution of zinc ions to the antimicrobial activity of zinc oxide, Colloids and Surfaces a-Physicochemical and Engineering Aspects 457 (2014) 263–274.
[60] S. Djearamane, L.-J. Xiu, L.-S. Wong, R. Rajamani, D. Bharathi, S. Kayarohanam, A. E. De Cruz, L.-H. Tey, A.K. Janakiraman, M. Aminuzzaman, S. Selvaraj, Antifungal Properties of Zinc Oxide Nanoparticles on *Candida albicans Coatings* [Online], 2022.
[61] D. Mathur, S. Prakash, P. Anand, H. Kaur, P. Agrawal, A. Mehta, R. Kumar, S. Singh, G.P.S. Raghava, PEPlife: a repository of the half-life of peptides, Sci. Rep. 6 (1) (2016) 36617.
[62] D. Li, Y. Yang, R. Li, L. Huang, Z. Wang, Q. Deng, S. Dong, N-terminal acetylation of antimicrobial peptide L163 improves its stability against protease degradation, J. Pept. Sci. 27 (9) (2021) e3337.
[63] L.H. Brinckerhoff, V.V. Kalashnikov, L.W. Thompson, G.V. Yamshchikov, R. A. Pierce, H.S. Galavotti, V.H. Engelhard, C.L. Slingluff, Terminal modifications inhibit proteolytic degradation of an immunogenic mart-127-35 peptide: implications for peptide vaccines, Int. J. Cancer 83 (3) (1999) 326–334.
[64] M. Powell, F., chapter 30. Peptide stability in drug development: in vitro peptide degradation in plasma and serum, in: J.A. Bristol (Ed.), Annu. Rep. Med. Chem 28, Academic Press, 1993, pp. 285–294.
[65] N.L. Benoiton, Chemistry of Peptide Synthesis, Taylor & Francis, 2005.
[66] N.A. Sole, G. Barany, Optimization of solid-phase synthesis of [Ala8]-Dynorphin-a, J. Organomet. Chem. 57 (20) (1992) 5399–5403.
[67] P. Gans, A. Sabatini, A. Vacca, Superquad - an improved general program for computation of formation-constants from potentiometric data, J. Chem. Soc. Dalton Trans. 6 (6) (1985) 1195–1200.
[68] P. Gans, B. O'Sullivan, GLEE, a new computer program for glass electrode calibration, Talanta 51 (1) (2000) 33–37.
[69] G. Gran, H. Dahlenborg, S. Laurell, M.J.A.C.S. Rottenberg, Determination of the Equivalent Point in Potentiometric Titrations. 4 (1950) 559–577.
[70] P. Gans, A. Sabatini, A. Vacca, Investigation of equilibria in solution. Determination of equilibrium constants with the HYPERQUAD suite of programs, Talanta 43 (10) (1996) 1739–1753.
[71] G. Arena, R. Cali, E. Rizzarelli, S. Sammartano, Thermodynamic study on the formation of the cupric ion hydrolytic species, Thermochim. Acta 16 (3) (1976) 315–321.
[72] P.L. Brown, C. Ekberg, First Transition Series Metals, in: Hydrolysis of Metal Ions, Wiley-VCH, Weinheim, 2016, pp. 499–716.
[73] L. Alderighi, P. Gans, A. Ienco, D. Peters, A. Sabatini, A. Vacca, Hyperquad simulation and speciation (HySS): a utility program for the investigation of equilibria involving soluble and partially soluble species, Coord. Chem. Rev. 184 (1999) 311–318.
[74] E.J. Billo, Copper(II) chromosomes and the rule of average environment, Inorg. Nucl. Chem. Lett. 10 (8) (1974) 613–617.
[75] E. Prenesti, P.G. Daniele, M. Prencipe, G. Ostacoli, Spectrum–structure correlation for visible absorption spectra of copper(II) complexes in aqueous solution, Polyhedron 18 (25) (1999) 3233–3241.
[76] M.R. Willcott, MestRe Nova, J. Am. Chem. Soc. 131 (36) (2009) 13180.
[77] H.E. Gottlieb, V. Kotlyar, A. Nudelman, NMR chemical shifts of common laboratory solvents as trace impurities, J. Organomet. Chem. 62 (21) (1997) 7512–7515.
[78] D.E. Benovitz, A.F. Spatola, Enkephalin pseudopeptides: resistance to in vitro proteolytic degradation afforded by amide bond replacements extends to remote sites, Peptides 6 (2) (1985) 257–261.

Analytical Biochemistry 700 (2025) 115784

Contents lists available at ScienceDirect

Analytical Biochemistry

journal homepage: www.elsevier.com/locate/yabio

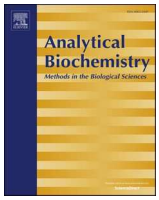

# A multi-technique approach to enlighten the role of metal coordination in calcitermin antiviral properties

Anna Caproni [a,1], Silvia Leveraro [a,1], Klaudia Szarszoń [b], Chiara Nordi [a], Riccardo Fontana [a], Mattia Buratto [a], Peggy Marconi [a], Maurizio Remelli [a], Mariaconcetta Sicurella [c,**], Denise Bellotti [a,*]

[a] Department of Chemical, Pharmaceutical and Agricultural Sciences, University of Ferrara, 44121, Ferrara, Italy
[b] Faculty of Chemistry, University of Wrocław, F. Joliot-Curie 14, 50-383, Wrocław, Poland
[c] Department of Environmental Sciences and Prevention, University of Ferrara, 441211, Ferrara, Italy

ARTICLE INFO

*Keywords:*
Potentiometry
Spectroscopic methods
Solution equilibria
Antiviral peptides
Herpes simplex
Calcitermin

ABSTRACT

In this work we presented how the use of suitable electroanalytical, thermodynamic and spectroscopic methods combined with proper experimental conditions can provide comprehensive information on the interaction between metal ions and peptides in solution, as a successful strategy for studying biological systems. Our candidate peptide is calcitermin, an effective metal chelator with significant anti-*Candida* and antibacterial activity in the presence of divalent metals. While the bioinorganic chemistry of calcitermin with zinc and copper is quite well described in the literature, no data about nickel complexes are available; we therefore deepened calcitermin ability to form nickel complexes by different analytical techniques, including potentiometry, ultraviolet–visible absorption spectrophotometry, circular dichroism and high-resolution mass spectrometry. Moreover, for the first time we have investigated the antiviral activity of calcitermin and its metal complexes towards *Herpes simplex* type 1. Despite the nickel-associated slow kinetics, which requires specific experimental precautions, calcitermin forms stable complexes with this cation at different pH conditions. Both the apopeptide and its metal complexes show a random coil secondary structure, which is often characteristic of viral cellular adhesion inhibition. This research highlights that calcitermin and its metal complexes can interfere with viral infections, particularly HSV-1, most likely by altering cell membrane permeability.

## 1. Introduction

When thinking about antimicrobial peptides and their mechanism of action, one is suddenly aware of the complexity of the investigation, due to the many factors affecting the biological environment where a peptide operates. If we consider metal-binding peptides, the complexity significantly increases, since one must consider the interactions between the peptide and the metal ion, but also the interference of other metal-chelators and competing metal ions. All this translates into the need for simplifications to study the mechanisms of metal interaction in detail and enlighten the underlying bioactivity.

To fully understand the system, various conditions must be considered during experimental investigations to gather information on species distribution, ligand coordination modes, and stoichiometry and geometry of the formed complexes in solution. In this work we aim at tackling the complexity of metal-peptide interactions, presenting a multi-technique approach that covers the most widely used thermodynamic and spectroscopic methods for investigating the interaction between metal ions and peptides in solution. A further effort is dedicated to the methodological study of the bioactivity of such systems, with a particular focus on the antiviral properties.

Indeed, antimicrobial peptides (AMPs), which lie between small molecules and biologic drugs, hold promise as a source for new, clinically relevant antiviral therapeutics. Traditionally recognized for their antibacterial and/or antifungal properties, many AMPs are now also known to possess antiviral activity. These peptides typically consist of short sequences of amino acids (from 10 to 100), with cationic and amphipathic properties. They exhibit antiviral activities by targeting

* Corresponding author.
** Corresponding author.
*E-mail addresses:* scrmcn@unife.it (M. Sicurella), blldns@unife.it (D. Bellotti).
[1] These authors equally contributed to the study.

https://doi.org/10.1016/j.ab.2025.115784
Received 24 December 2024; Received in revised form 7 January 2025; Accepted 23 January 2025
Available online 30 January 2025

various stages of the viral life cycle, for example by disrupting the membranes of enveloped viruses, blocking cellular penetration or intracellular trafficking, limiting viral transcription and translation, and/or preventing the budding of mature viral particles. Unlike traditional antiviral drugs, which often face challenges such as drug resistance and limited efficacy against emerging viral strains, AMPs offer a versatile and adaptable approach to antiviral therapy [1,2]. The multifaceted mechanism of action of AMPs not only enhances their antiviral efficacy but also reduces the likelihood of resistance development. Recent advances in peptide engineering and high-throughput screening techniques have accelerated the discovery and optimization of AMPs, leading to the identification of numerous candidates with broad-spectrum antiviral activities.

Moreover, analogously to antibacterial and antifungal peptides, the antiviral power can be enhanced or modulated by metal ions and formation of metal-complexes [3–5]. Metal ions are crucial components of life, playing important roles in various biological functions. They serve as essential cofactors for many enzymes and help regulate electrolyte balance, electron transfer, and oxygen transport. Additionally, they are involved in modulating the immune system and defending against pathogens. The diverse properties of metals, including their coordination numbers, geometries, redox states, reactivity, and thermodynamic behaviour, underline their significant role in medicine and their widespread use in the treatment and diagnosis of numerous diseases. In literature, many examples of metal complexes with antiviral activity can be found [5–13].

Calcitermin is a 15-mer AMP that has been isolated from the human airways [14]. Recently, it has been investigated in combination with metal ions to verify the ability to form stable metal complexes and how this can affect the antibacterial and anti-*Candida* activity. Interestingly, the presence of copper and zinc enhances the bioactivity of the peptide [15–18]. Here, we decided to extend the knowledge on calcitermin metal chelating ability, studying the coordination of nickel(II) ion. Indeed, the histidine residues in position 9, 10 and 11, and the amino- and carboxyl-ends of the peptide can function as binding sites not only for divalent zinc and copper ions but also for nickel [19–23]. The importance of nickel in bioinorganic chemistry has surged since the discovery of the nickel enzyme urease [24,25]. Subsequently, numerous nickel complexes have been identified with a wide range of activity against pathogens. This is likely due to their ability to penetrate microbial cells and influence enzyme activity [26]. Nickel is often recognized for its toxic potential, causing adverse effects like changes in metabolism, inflammation, oxidative stress, cell proliferation, and cell death. These effects are typically due to nickel non-specific interaction with metal-binding macromolecules and to the production of reactive compounds like radical oxygen species. It can also alter gene expression, mimicking oxygen deprivation and triggering immune responses. However, despite its toxicity, nickel is essential for various organisms (plants, bacteria, archaea, and unicellular eukaryotes). While not found in higher animals, it is considered a "possibly essential element" for humans for at least 50 years [27], potentially due to its role in mammal microbiota [26]. Moreover, the antimicrobial and antiviral role of nickel complexes is well documented in literature [6,7,28–32].

The investigation of the formation of Ni(II) complexes with calcitermin has been obtained through various techniques, including potentiometry, UV–Vis absorption spectrophotometry, circular dichroism (CD) and mass spectrometry (MS). Once the Ni(II) coordination behaviour has been unravelled, similarly to what has already been done for Zn(II) and Cu(II) [15,16], we aimed at testing the antiviral properties of calcitermin and its Cu(II), Zn(II) and Ni(II) complexes, since all these metal ions may influence the microbicidal properties of the peptide. In literature only data about antibacterial (against both Gram-positive and Gram-negative) and antifungal (against *C. albicans*) properties of calcitermin are available [14–18], but no information on its virucidal activity is known by far. In this regard, the viral model selected for this study is *Herpes simplex* type I (HSV1), one of the most common viruses responsible for a variety of clinical manifestations. HSV1 infection, mainly transmitted by oral contact, is characterized by the formation of epidermal lesions inside and around the mouth as well as in the nose or in other body zones, such as the fingers, with frequent recurrences [33,34]. HSV1 is a pathogen that establishes a latency in the sensory ganglia giving rise to periodic reactivation whose consequences, when not asymptomatic, range from cold sores to blindness, meningitis or encephalitis; HSV1 infections can range from mild to severe, depending on the area affected and the host's immune response [35]. It is an opportunistic pathogen that, despite the availability of antiviral therapies, continues to pose a significant public health challenge. A major reason for its persistence is the development of mechanisms of resistance to antiviral agents. The development of antiviral resistance has important clinical implications, in fact, resistant HSV infections can become chronic, causing increased morbidity and mortality, increased transmissibility – individuals infected with resistant strains can more easily transmit the infection to others – and treatment difficulties, since resistant HSV infections are more difficult to treat, requiring combination therapies or new drugs [36]. In this study the antiviral activity of calcitermin and its metal complexes were therefore evaluated and their inhibitive capacity on the plaque formation of HSV-1 in cultured cells was studied.

## 2. Materials and methods

### 2.1. Materials

Wild-type calcitermin (VAIALKAAHYHTHKE, **WT**) was purchased from KareBay Biochem (USA) with a certified purity of 98 % and it was used as received. $NiCl_2$, $ZnCl_2$ and $CuCl_2$ were extra pure products (Sigma-Aldrich); the concentrations of their stock solutions were standardized by EDTA titration. The carbonate-free stock solutions of 0.1 M KOH were prepared by diluting concentrated KOH (Sigma-Aldrich) and then potentiometrically standardized with potassium hydrogen phthalate (99.9 % purity), as primary standard. All sample solutions were prepared with fresh Milli-Q® water. The HCl stock solutions was prepared by diluting concentrated high purity, HCl and then standardized with standard KOH. The ionic strength was adjusted to 0.1 M by adding KCl (Sigma-Aldrich). Sample solutions of metal-peptide complexes were prepared with metal:ligand ratio 0.8:1. Grade A glassware was employed throughout.

### 2.2. Potentiometry

Stability constants for proton and metal complexes were obtained from pH-metric titration curves recorded at $T = 298$ K and ionic strength 0.1 M (KCl). The potentiometric apparatus was previously described [37]. Solutions of the ligand ($[L]_{tot} = 5 \times 10^{-4}$ M) and metal complexes ($[L]_{tot} = 5 \times 10^{-4}$ M and metal:ligand molar ratio 0.8:1) were titrated with 0.1 M carbonate-free KOH. The electrode was daily calibrated for hydrogen ion concentration by titrating HCl with the standard base solution, under the same experimental conditions as above. The asymmetry potential and the slope of the electrode couple were computed by means of SUPERQUAD [38] and Glee [39] programs. The purities and exact concentrations of the ligand solutions were determined by the Gran method [40]. The HYPERQUAD [41] program was employed for the overall formation constant ($\beta$) calculations, referred to the following equilibrium equation: $pM + qL + rH \leftrightarrows M_pL_qH_r$ (charges omitted; p is 0 in the case of ligand protonation; r can be negative). The computed standard deviations (referring to random errors only) were given by the program itself and are shown in parentheses as uncertainties on the last significant figure. Hydrolysis constants for metal ion were taken from the literature [42,43]. The distribution and competition diagrams were computed using the HYSS program [44]. Competition diagrams represent simulations of solutions containing the selected ligand(s) and metal ion(s) and are based on the binary speciation models, admitting that all

the components compete to form the respective binary complexes without mixed species formation [45,46].

### 2.3. Mass spectrometry

High-resolution mass spectra were obtained on the ESI-Q-TOF Maxis Impact (Bruker Daltonics) spectrometer. The instrumental parameters were set as follows: positive or negative ion mode, scan range *m/z* 150–2000, dry nitrogen gas, temperature 200 °C, capillary voltage of 3500 V and ion energy 5 eV. The samples ($[L]_{tot} = 1 \times 10^{-4}$ M and metal:ligand molar ratio = 0.8:1) were prepared in a 1:1 methanol-water mixture at pH about 7.4. The samples were infused at a flow rate of 3 μl/min. The instrument was calibrated externally with the Low Concentration Tuning Mix ESI-TOF (Agilent Technologies (SD ≤ 1 ppm) and sodium formate clusters (SD ≤ 1 ppm)). Data were processed using the Bruker Compass DataAnalysis 4.2 program. The mass accuracy for the calibration was <5 ppm, enabling together with the true isotopic pattern an unambiguous confirmation of the elemental composition of the obtained complex.

### 2.4. Spectroscopic measurements

The absorption spectra of Ni(II) containing solutions were recorded on a Varian Cary300 Bio spectrophotometer, in the range 250–800 nm, using a quartz cuvette with an optical path of 1 cm. Circular dichroism (CD) spectra were recorded on a Jasco J-1500 spectropolarimeter in the 200–800 nm range, using a quartz cuvette with an optical path of 1 cm in the UV–visible, and 0.01 cm in the 180–250 nm range. To describe the species, present in solution, the observed spectroscopic parameters at a given pH were compared with the expected values obtained from literature [20,47,48]. The pH values where each species is predominant in solution were chosen for spectroscopic analysis and the wavelengths of maximum absorption ($\lambda_{max}$) were attributed to the presence of characteristic donor groups and coordination geometries.

### 2.5. Cytotoxicity

Cell viability was assessed using a neutral red uptake assay. Vero cells were seeded in triplicate at a density of $20 \times 10^3$ cells/well in 100 μL of DMEM high glucose medium supplemented with 10 % FCS. The following day, cells were treated with various concentrations (50-10-1 μM) of $NiCl_2$, $ZnCl_2$, $CuCl_2$, or calcitermin (**WT**), either alone or in combination. After a 24-h incubation period, the medium was removed, and cells were gently washed with phosphate-buffered saline (PBS). Subsequently, 250 μL of neutral red (NR) dye solution (25 μg/mL NR concentration) was added to each well, and the plates were incubated at 37 ± 1 °C, 90 ± 5 % humidity, and 5.0 ± 1 % $CO_2$/air for 3 h. The NR medium was then removed, cells were rinsed with PBS, and 150 μL of a desorbing solution (50 % bi-distilled water, 49 % ethanol, 1 % acetic acid) was added to each well. The plates were shaken for 45 min to extract the NR dye from the cells, forming a homogeneous solution. The absorbance was measured at 540 nm using a spectrophotometric microplate reader (within 60 min of adding the desorbing solution) [49].

### 2.6. Cell culture

Vero cells (African green monkey kidney, ATCC-LGC Standards S.r.l., Milan, Italy) were maintained in Eagle's Minimum Essential Medium (DMEM) supplemented with 5 % fetal bovine serum (FBS), 100 μg/mL penicillin, and 100 μg/mL streptomycin. Cells were incubated at 37 °C in a humidified atmosphere containing 5 % $CO_2$. For plaque assays, cells were seeded at a density of $5 \times 10^5$ cells/well in six-well plates 24 h prior to infection.

### 2.7. Herpes virus stock Generation

Vero cells ($2 \times 10^7$ cells) were seeded into 175 $cm^2$ tissue culture flasks containing 10–20 mL of medium and incubated overnight at 37 °C in a humidified 95 % air–5% $CO_2$ incubator. The following day, the cells were infected with the herpes simplex virus strain KOS at a multiplicity of infection (MOI) of 0.01. Viral adsorption was performed for 1 h at 37 °C, with gentle mechanical agitation every 15 min to promote efficient virus-cell contact. After the adsorption period, the virus inoculum was aspirated, and fresh culture medium was added to each flask, bringing the final volume to 10–20 mL. The infected cells were further incubated at 37 °C in a humidified 95 % air–5% $CO_2$ atmosphere for 36–48 h, or until a complete cytopathic effect (CPE) was observed. After the CPE was reached, the cells and supernatant were harvested. The cell debris was removed by low-speed centrifugation, and the supernatant was subsequently centrifuged at 20,000 rpm for 30 min to pellet the virus. The resulting pellet was resuspended in 1 mL of culture medium, aliquoted, and stored at −80 °C until further use [49].

### 2.8. Titration of virus by plaque assay

To determine the viral titer, a plaque assay was performed on Vero cells. One day prior to the assay, 6-well plates were seeded with $0.5 \times 10^6$ Vero cells per well. A series of ten-fold dilutions ($10^{-2}$ to $10^{-10}$) of the viral stock was prepared in 1 mL of serum-free cell culture medium. Each dilution was added to a well containing Vero cells and incubated for 1 h at 37 °C to allow for viral adsorption. After incubation, the viral inoculum was removed, and the cells were overlaid with 3 mL of 1 % methylcellulose. The plates were incubated for 3–4 days until well-defined plaques formed. The methylcellulose overlay was removed, and the cells were stained with 2 mL of crystal violet solution for 10–20 min. The number of plaques in each well was counted, and the average plaque count for each dilution (n = 3) was multiplied by 10 to the power of the dilution to calculate the plaque-forming units per milliliter (PFU/mL) [49].

### 2.9. Infection treatment

Vero cells were treated with 10 μM of $NiCl_2$, $ZnCl_2$, $CuCl_2$ or **WT**, either alone or in combination, and simultaneously infected with the HSV-1 KOS strain $1 \times 10^5$ PFU/mL for 1 h. After 1 h at 35 °C, the viral inoculum was removed, and the cells were washed. The methylcellulose medium (1 %) was added. The number of plaques was determined as previously described [50,51], and the percentage of viral inhibition was calculated by comparison with viral control.

### 2.10. Post-infection treatment

Vero cell monolayers were infected with $1 \times 10^5$ PFU/mL concentrations of the HSV-1 KOS strain for 1 h at 35 °C. After the adsorption time, the viral inoculum was removed and 10 μM of $NiCl_2$, $ZnCl_2$, $CuCl_2$ or **WT**, either alone or in combination, were added for 1 h at 35 °C. The formulations were removed, and 1 % methylcellulose medium was added. The number of plaques was determined as previously described, and the percentage of viral inhibition was calculated by comparison with viral control [51].

### 2.11. Statistical analysis

All experiments were repeat three times. For all data analysis, GraphPad Prism 9 software (GraphPad Software Inc., San Diego, CA, USA) was used. ANOVA one-way nonparametric test- Kruskal-Wallis test provides a * *p*-values <0.05 considered statistically significant.

## 3. Results and discussion

### 3.1. Formation of Ni(II) complexes

Wild-type calcitermin (**WT**) has been previously investigated by our research group in aqueous solutions and ionic medium $NaClO_4$ [16] and KCl [15]. For the sake of comparison, in the present work, potentiometric studies of Ni(II)/**WT** complexes have been performed in ionic medium KCl. Potentiometric titrations of the ligand **WT** have been performed in order to control the ligand purity and confirm the previously determined protonation constants. The obtained experimental results show a very good agreement with literature data of **WT** protonation equilibria [15], with negligible differences between this work and literature results ($\Delta \log K < 0.2$, Table S1).

The equilibrium constants referring to Ni(II)/**WT** complex formation are reported in Table 1, and the corresponding species distribution diagram is shown in Fig. 1. Spectroscopic data are summarised in Table 2 and UV–Vis and CD spectra are depicted in Figs. 2 and 3. The speciation model obtained by potentiometric titrations is supported by MS results and it describes the formation in solution of 1:1 metal:ligand complexes under the employed experimental conditions. Long waiting times between each titrant addition were guaranteed (up to 15–20 min per point), due to slow kinetics of the Ni(II) complex formation [52,53]. No precipitation was observed in the explored pH range. High resolution mass spectra revealed the formation of mononuclear Ni(II) complexes under the employed experimental conditions (Fig. S1). Signals corresponding to various sodium and potassium adducts, together with the differently protonated free ligand and metal complexes have been detected. The most intense signals ($m/z = 563.65$, z = +3 and $m/z = 844.96$, z = +2) correspond to the free peptide, confirming its purity. Signals from the complex ($m/z = 872.92$, z = +2 and $m/z = 582.29$, z = +3) correspond to the species $[NiH_4L]^{3+}$ and $[NiH_3L]^{2+}$, which are also the major species in solution at the same pH condition (pH 7.4, Fig. 1). No poly-nuclear complexes or bis-complexes have been identified.

The potentiometric results show that the formation of Ni(II) complexes with **WT** starts at pH 4.5. The formed complex, $[NiH_5L]^{4+}$, is likely characterized by a ($2N_{Im}$) coordination, where two histidine residues should be already bound to the metal ion. Indeed, according to the stoichiometry, the ligand has already lost four acidic protons from its fully protonated form, and they correspond to its most acidic residues, *i.e.* the terminal carboxyl group, the glutamic acid and two histidine residues. Under such acidic condition, histidines do not spontaneously deprotonate, therefore the release of their acidic proton must be favoured by the metal coordination. It is also reasonable to consider the metal interaction with the carboxyl groups of Glu residue, enabling the interconversion among different coordination modes in an octahedral environment. The remaining coordination positions are saturated with water molecules. The speciation diagram plotted in Fig. 1 shows that the percentage of formation in solution of $[NiH_5L]^{4+}$ remains rather low (≈30 %) since this complex is quickly substituted by the $[NiH_4L]^{3+}$ species, that is by far the most abundant complex in solution from pH 6 until pH 7. The associated deprotonation step has a $pK_a$ value of 6.0,

**Table 1**
Overall and step formation constants for Ni(II)/**WT** complex formation at $T$ = 298 K and $I$ = 0.1 M (KCl). Values in parentheses are standard deviations on the last significant digit.

| Species | logβ | logK |
|---|---|---|
| $[NiH_5L]^{4+}$ | 49.5(1) | 6.0 |
| $[NiH_4L]^{3+}$ | 43.51(6) | 7.14 |
| $[NiH_3L]^{2+}$ | 36.37(9) | 8.2 |
| $[NiH_2L]^{+}$ | 28.1(1) | 8.9 |
| [NiHL] | 19.2(1) | 9.2 |
| $[NiL]^{-}$ | 10.0(1) | 9.7 |
| $[NiH_{-1}L]^{2-}$ | 0.3(1) | – |
| $[NiH_{-3}L]^{4-}$ | −20.6(1) | – |

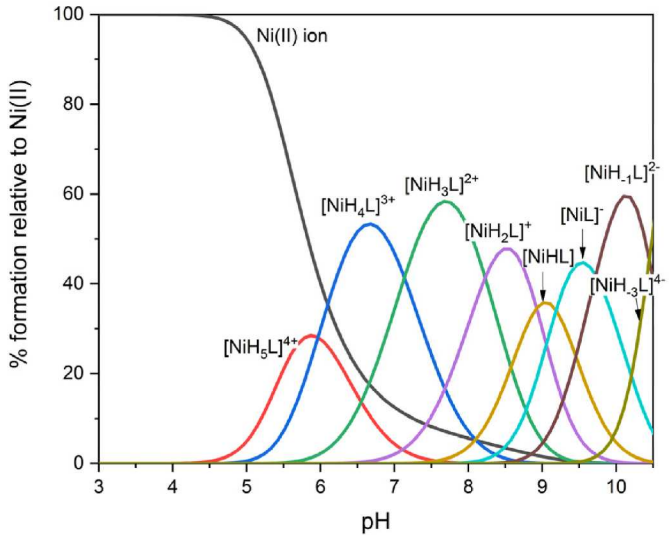


**Fig. 1.** Representative species distribution diagram of Ni(II)/**WT**; $C_L = 0.5 \times 10^{-3}$ M and Ni:L = 0.8:1.

**Table 2**
Spectroscopic data for Ni(II) complexes with ligand **WT**, at $T$ = 298 K and $I$ = 0.1 M (KCl). $C_L = 0.5 \times 10^{-3}$ M and Ni:L = 0.8:1.

| Species | pH | Vis absorption | | CD | |
|---|---|---|---|---|---|
| | | λ (nm) | ε ($M^{-1}cm^{-1}$) | λ (nm) | Θ (mdeg) |
| – | 3.5–5 | 390 | 24 | 240 | −0.92 |
| $[NiH_5L]^{4+}$ | 5.5 | 385 | 28 | 240 | −0.92 |
| | | 634 | 11 | | |
| | 6.0 | 380 | 38 | 240 | −0.92 |
| | | 634 | 14 | | |
| $[NiH_4L]^{3+}$ | 6.5 | 377 | 40 | 240 | −0.92 |
| | | 634 | 16 | | |
| $[NiH_4L]^{3+}$ | 7.0 | 377 | 38 | 240 | −0.92 |
| | | 634 | 16 | | |
| | 7.5 | 378 | 45 | 240 | −0.92 |
| | | 607 | 18 | | |
| $[NiH_3L]^{2+}$ | 8.0 | 480 | 25 | 252 | +0.77 |
| | | 615 | 20 | | |
| $[NiH_2L]^{+}$ | 8.5 | 465 | 50 | 252 | +2.28 |
| | | 615 | 20 | 290 | −0.45 |
| | | | | 431 | +0.27 |
| | | | | 510 | +0.48 |
| [NiHL] | 9.0 | 465 | 81 | 257 | +2.51 |
| | | | | 290 | −1.01 |
| | | | | 431 | +0.50 |
| | | | | 510 | +0.89 |
| $[NiL]^{-}$ | 9.5 | 461 | 105 | 261 | +1.70 |
| | | | | 294 | −1.26 |
| | | | | 431 | +0.40 |
| | | | | 510 | +0.98 |
| $[NiH_{-1}L]^{2-}$ | 10.0 | 457 | 110 | 261 | +1.33 |
| | | | | 294 | −1.26 |
| | | | | 431 | +0.22 |
| | | | | 513 | +0.84 |
| $[NiH_{-3}L]^{4-}$ | 10.5 | 445 | 120 | 265 | +1.05 |
| | | | | 294 | −1.03 |
| | | | | 463 | −0.16 |
| | | | | 520 | +0.67 |
| $[NiH_{-3}L]^{4-}$ | 11.0 | 445 | 127 | 267 | +1.11 |
| | | | | 294 | −0.55 |
| | | | | 446 | −0.37 |
| | | | | 520 | +0.54 |

attributable to the deprotonation and binding of a third imidazole group. For $[NiH_5L]^{4+}$ and $[NiH_4L]^{3+}$ a distorted octahedral coordination is likely conceivable due to the very low intensity of Vis absorption bands and the lack of significative CD signals until pH 8.0 (Table 2). This

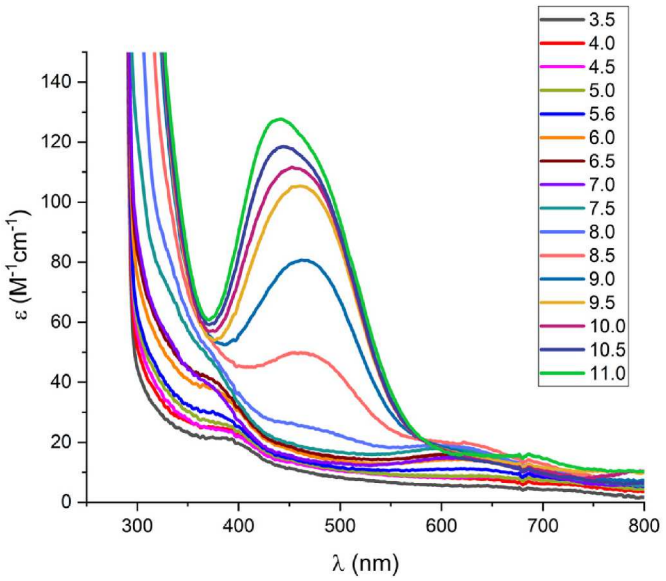


**Fig. 2.** Vis absorption spectra of Ni(II) complexes with **WT** at different pH values. $C_M = 0.4 \times 10^{-3}$ M; Ni:L 0.8:1; optical path 1 cm.

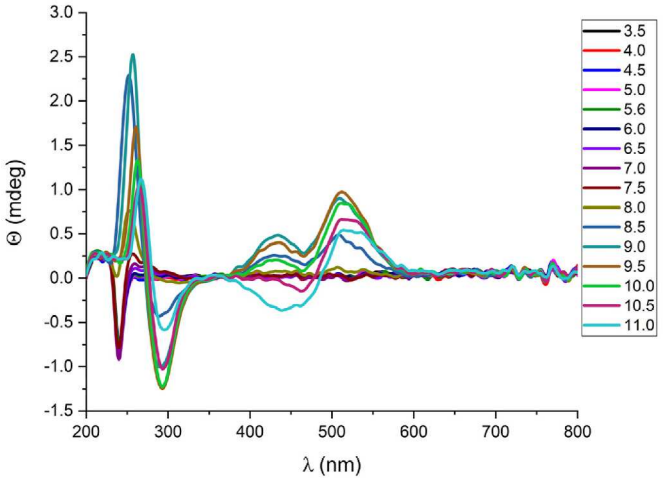


**Fig. 3.** CD spectra of Ni(II) complexes with **WT** at different pH values. $C_M = 0.4 \times 10^{-3}$ M; Ni:L 0.8:1; optical path 1 cm.

is consistent with previously studied Ni(II) complexes with His-containing peptides [19,54–58].

A further deprotonation step with $pK_a = 7.14$ leads to the $[NiH_3L]^{2+}$ species. In this case, the acidic proton is likely released by the terminal amino group. In these conditions, a mixture of coordination isomers should exist in solution and the terminal amine can also partially interact with Ni(II) and substitute a coordinated water molecule in the octahedral environment [20,59]. The formed $[NiH_3L]^{2+}$ complex progressively evolves to the classical yellow, square planar, low spin complex at alkaline pH, due to the coordination of deprotonated amide nitrogens of the backbone. This hypothesis is corroborated by the obtained equilibrium constants for the formation of $[NiH_2L]^{+}$ and [NiHL] ($pK_a$ = 8.2 and 8.9, respectively), and it is confirmed by the experimental Vis absorption spectra in the pH range 8.5–11.0 ($\lambda_{max}$ = 465–445 nm). Therefore, two backbone amides substitute the oxygen donor groups in the equatorial plane of Ni(II), giving a coordination mode which is likely ($2N_{Im}$, $2N^-$) for [NiHL]. Increasing the pH value, the species $[NiL]^-$ is formed ($pK_a$ = 9.2) and a slight hypsochromic shift (≈15–20 nm) from 465 nm to 445 nm of the maximum absorption is observed. The interaction of a third backbone amide can be then suggested, giving the coordination mode ($N_{Im}$, $3N^-$). The CD spectra confirm this hypothesis with a band near 250 nm corresponding to the $N^- \rightarrow$ Ni(II) transition [60–63]. Finally, the release of further protons at the most alkaline pH values, to form the species $[NiH_{-1}L]^{2-}$ ($pK_a = 9.7$) and $[NiH_{-3}L]^{4-}$, can be ascribed to the mere deprotonation of tyrosine and lysines residues, without any interaction with the metal ion. A similar behaviour has been also observed for the formation of Zn(II) and Cu(II) complexes of **WT** and its derivatives [15,16,18].

### 3.2. Near-UV CD Structural characterization

Secondary structure and hydrophobicity of the peptide play a significant role in determining its antiviral efficacy and specificity for targeting virulence factors (e.g. viral envelope, viral replication, viral cellular entry, etc.) [64]. The formation of metal complexes may affect both the secondary structure and the hydrophilic character of the ligand. The former aspect has been deepened by the circular dichroism technique. The obtained near-UV CD spectra for **WT** at three different pH values are very similar to the spectra obtained in the presence of Ni(II) ions, in water solution (Fig. 4). This behavior has been also observed for other calcitermin metal complexes and strongly suggests that the 3D arrangement of the apo-peptide is retained upon metal coordination. No specific conformations have been detected, and the random coil structure (typical negative CD band at 198 nm) [65,66] is predominant. Most of anti-HSV peptides acting by inhibiting the virus adhesion and cellular entry show higher content of random coil secondary structure [64].

### 3.3. Comparison of metal binding ability

Once the thermodynamic constants of complex formation equilibria are known, it is possible to compare the metal-binding affinity of **WT** for Ni(II) (studied in this work), Zn(II) and Cu(II), under the same conditions of temperature and ionic strength [15]. The competition diagrams in Fig. 5 show that the complexes formed with Cu(II) are always more stable than those formed with Zn(II) and Ni(II) throughout the explored pH range. The **WT** ability to bind Zn(II) and Ni(II) is instead comparable. These results are in perfect agreement with the Irving-Williams series that, on the basis of the metal ion electronic configuration, predicts a higher binding affinity for Cu(II) than Ni(II) and Zn(II) [67].

### 3.4. Citotoxicity Evaluation

Concentration and safety of $NiCl_2$, $ZnCl_2$, $CuCl_2$ or calcitermin (**WT**), either alone or in combination, were determined on Vero cell lines. The cell viability was tested after a 24 h incubation period with the neutral red assay. The neutral red assay determines the accumulation of the neutral red dye in the lysosomes, viable cells can release the incorporated dye under acidified extracted conditions. The data in Fig. 6 show the viability of cells after treatment at different concentrations (50-10-1 μM). The obtained results did not show alterations in viability. The range always remains above 60 %, considered as a threshold value.

### 3.5. In vitro antiviral activity

A plaque reduction assay was used to evaluate *in vitro* anti-HSV-1 activities of $NiCl_2$, $ZnCl_2$, $CuCl_2$ or calcitermin (**WT**), either alone or in combination. Different protocols were used in which the formulations were added during different stages of infection to determine the time and mode of action: (a) direct contact, in which the formulations and virus were in contact with the cells simultaneously; (b) pre-treatment, in which case the cells were pretreated with the formulations before to viral infection; and (c) post-infection, in which the addition of the formulations to the infected cells occurred after virus removal (Fig. 7). Percentual reduction was calculated compared with the amount of viral control in the absence of formulations. In the direct contact assay, no

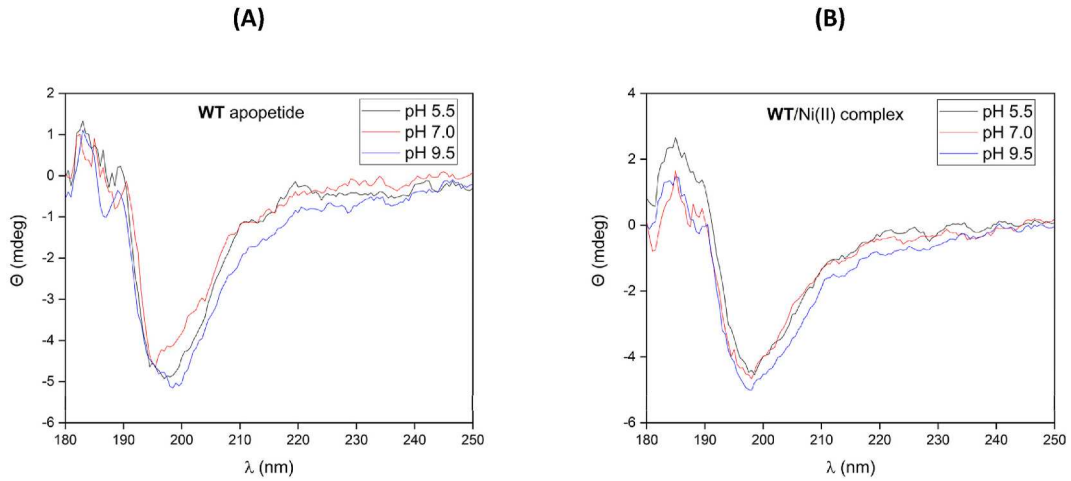


**Fig. 4.** CD spectra of (A) **WT** calcitermin and (B) its Ni(II) complexes at $T = 298$ K, in aqueous solution; M:L ratio 0.8:1, $C_L = 0.1 \times 10^{-3}$ M, optical path 0.01 cm.

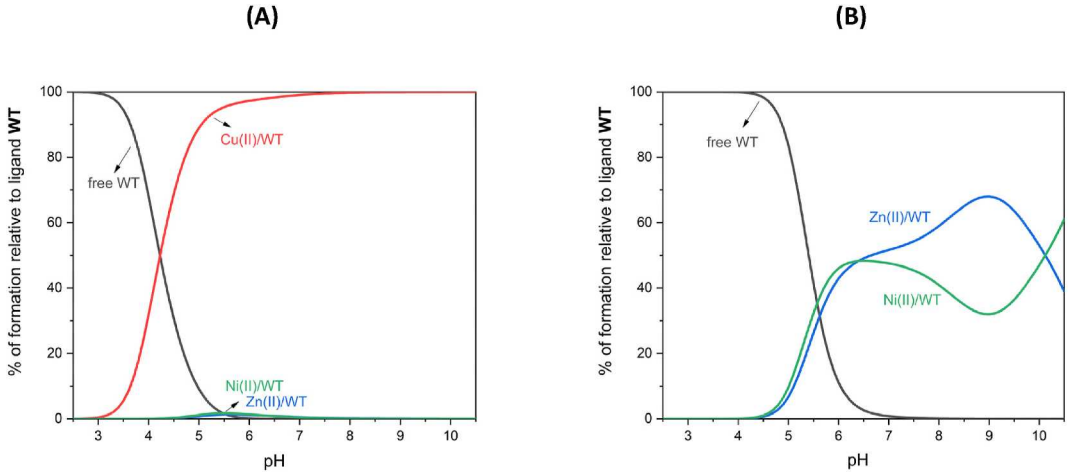


**Fig. 5.** Competition plots for simulated solutions containing equimolar concentrations (1 mM) of (A) **WT**, Cu(II) [15], Zn(II) [15], and Ni(II); and (B) **WT**, Zn(II) [15], and Ni(II).

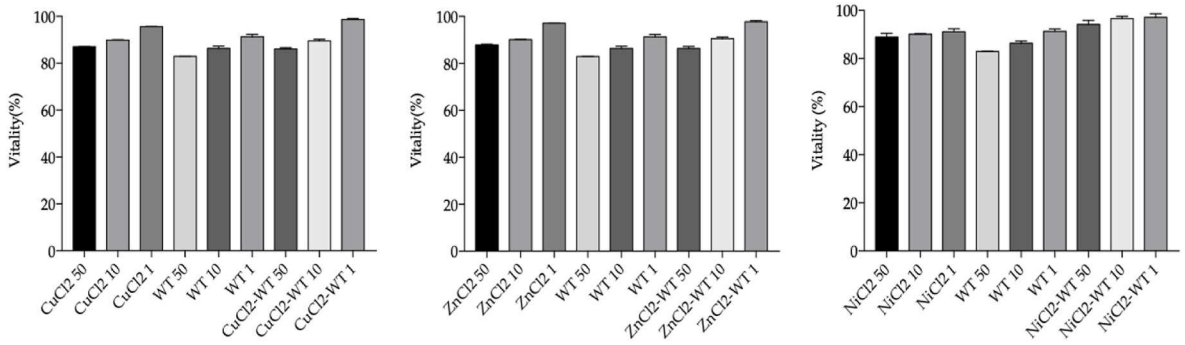


**Fig. 6.** Effects of formulations on the viability of Vero cell model. Treatment conducted using the formulations alone or in combination with calcitermin at different concentrations (50-10-1 μM). Cell viability was assessed by Neutral Red assay after 24h of treatment. Panel A shows the change in viability with $CuCl_2$ alone or in combination, panel B shows viability after treatment with $ZnCl_2$ alone or in combination and panel C is related to treatment with $NiCl_2$ alone or in combination.

reduction in plaque formation was observed compared to the untreated control with the formulations tested alone or in combination with **WT** (data not shown). Pre-treatment of cells with the formulations showed a reduction in the number of plaques. In fact, after 1 h of incubation at 35 °C and subsequent titration on the cell monolayer, a reduction in viral growth was observed in treatments with the formulations alone, 32 % for $CuCl_2$ and $ZnCl_2$ to 45 % for $NiCl_2$, 67 % in the **WT**. The formulations combined with **WT** showed a plaque reduction of 25 % for $CuCl_2$**WT**, 30 % for $ZnCl_2$**WT**, and 50 % for $NiCl_2$**WT**, suggesting that the metal-peptide combination may promote a slower and more prolonged action. In the treatment of cells with the formulations 1 h after infection, no reduction in plaques was observed for $CuCl_2$ and $ZnCl_2$ treatments; however, $NiCl_2$ treatment resulted in 30 % reduction, and **WT** alone showed a 45 % reduction. The combination of the formulations with the

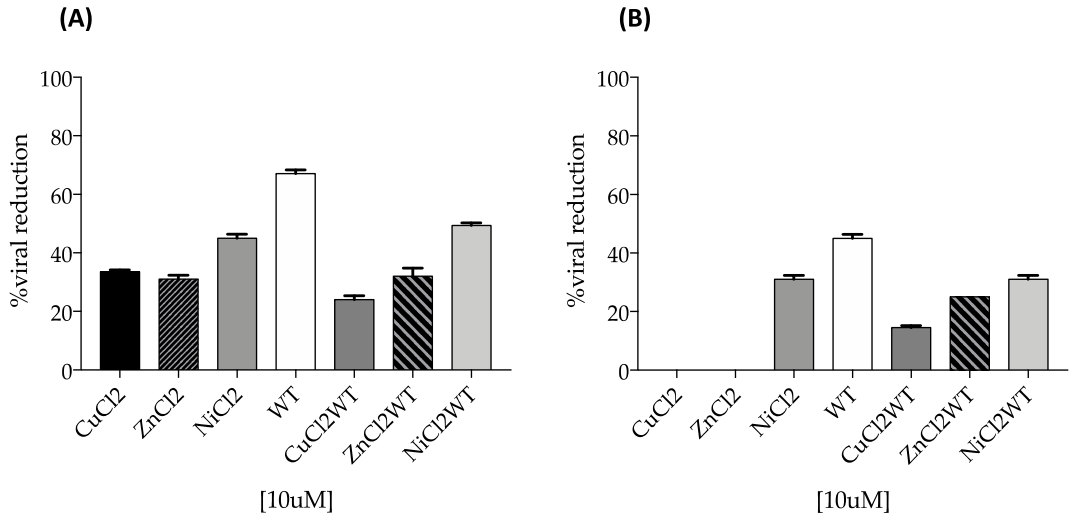


**Fig. 7.** Virucidal effect of $NiCl_2$, $ZnCl_2$ and $CuCl_2$ alone or in combination with calcitermin, against HSV-1 Kos strain 1 ($1 \times 10^5$ pfu/ml). Vero cells were treated with the formulations before (A) and after infection (B). A significant reduction was observed in the case of Vero cell treated before infection with **WT** alone or in combination with $NiCl_2$. The values were obtained by comparing the results with the untreated control. Data represents the mean of three independent experiments. ANOVA one-way nonparametric test- Kruskal-Wallis test provides a * $p$-values <0.05.

**WT** resulted in a plaque reduction of 15 % for $CuCl_2$**WT**, 25 % for $ZnCl_2$**WT**, and 30 % for $NiCl_2$**WT**. The **WT**-metal complexes do exhibit similar virucidal effects to the metal salts. However, the potential of these complexes as pharmaceutical agents lies beyond their direct virucidal activity. While the raw metal salts might possess significant antimicrobial properties, their potential for pharmaceutical applications can be limited by factors such as toxicity, covalently binding to essential biomolecules, undefined absorption and distribution. Metal complexes can offer advantages like increased solubility, reduced toxicity, and targeted delivery, making them more suitable for therapeutic use [68]. These results suggest that the action of the formulations combined with **WT** may influence the virus absorption and penetration phases into the cells, particularly when the formulation is applied prior to viral infection. It is well-known that metal complexes of nickel, copper, and zinc can interact with the lipids and proteins of the cell membranes [5,69]. This interaction can alter the structure and fluidity of the membrane, affecting and changing its permeability, which, in turn, may make it more difficult for the virus to penetrate the cell, thereby reducing the amount of virus that can infect the cells. The potential antioxidant properties of calcitermin, in particular when combined with copper and nickel (as already reported for histidine-containing antimicrobial peptides [13,70,71]), may also help reduce cellular damage and oxidative stress caused by the viral infection, improving cell health and their ability to withstand infection [72]. These characteristics may make calcitermin and its complexes promising as potential therapeutic agents, but the complexity of the mechanism of action requires further research to clarify these aspects.

## 4. Conclusions

This work represents an in-depth study of the metal coordination ability and antiviral properties of the antimicrobial peptide calcitermin. Its metal-binding site, consisting of three alternated histidines and the terminal amino and carboxyl groups, proved to be effective in coordinating not only divalent zinc and copper, but also nickel. The importance of nickel in bioinorganic chemistry arises from the discovery of the nickel enzyme urease, and nowadays many examples of antimicrobial and antiviral Ni(II) complexes are known. The present work shows that calcitermin is able to form octahedral complexes with Ni(II) at acidic and neutral pH values, while the diamagnetic, square planar configuration is obtained at alkaline pH due to the backbone amides coordination. The stability of the formed species is comparable to that of Zn(II) complexes.

It is also worth noting that the secondary structure of the investigated systems (both apopeptide and metal/peptide complex) proved to be prevalently random coil, and it is not affected by the pH. Most peptides that interfere with virus cellular adhesion and entry are hydrophilic and often form random coils or possess an unstable secondary structure. Such flexibility likely allows them to interact with multiple targets as required to exert this virucidal action. The formation of metal complexes usually causes changes in the molecule charge that may increase the hydrophilicity, even though the amphiphilic character of the ligand is maintained. Thus, the antiviral properties of calcitermin and its Zn(II), Cu(II) and Ni(II) complexes have been studied for the first time. They have shown potential in the treatment of HSV-1 infections, although the mechanism of action is not fully understood; in fact, their effectiveness depends on the timing of application, either before or after viral infection. When associated with metal ions, calcitermin has demonstrated the ability to influence the permeability of cell membranes. By altering membrane permeability, calcitermin can also influence intracellular signaling, which can modulate the immune response, contributing to the regulation of inflammation, for example potentially leading to an increase in cytokine production and better activation of immune cells, creating a less favorable environment for the virus [73]. Higher efficacy of calcitermin and its complexes incorporated into smart gels have also been observed [17]; this, along with the presented results, encourages the study of calcitermin to develop novel antiviral agents with topical administration to treat viral HSV infections.

## CRediT authorship contribution statement

**Anna Caproni:** Formal analysis. **Silvia Leveraro:** Formal analysis. **Klaudia Szarszoń:** Formal analysis. **Chiara Nordi:** Investigation. **Riccardo Fontana:** Writing – review & editing. **Mattia Buratto:** Visualization. **Peggy Marconi:** Writing – review & editing. **Maurizio Remelli:** Writing – review & editing, Visualization. **Mariaconcetta Sicurella:** Writing – review & editing, Writing – original draft, Supervision, Funding acquisition, Formal analysis, Data curation, Conceptualization. **Denise Bellotti:** Writing – review & editing, Writing – original draft, Validation, Supervision, Resources, Project administration, Methodology, Investigation, Funding acquisition, Formal analysis, Data curation, Conceptualization.

## Declaration of competing interest

The authors declare that they have no known competing financial interests or personal relationships that could have appeared to influence the work reported in this paper.

## Acknowledgments

This research was funded by the National Recovery and Resilience Plan (NRRP), Mission 4 Component 2 Investment 1.1 – NextGenerationEU (grant PRIN PNRR 2022 - P2022EMY52 - CUP F53D23008960001; project title "EnzyMime – Biocompatible and sustainable enzyme mimics based on metal complexes with peptide derivatives: synthesis, characterization and potential biological applications"); M.S. is supported by the University of Ferrara (grant FIRD 2022).

## Appendix A. Supplementary data

Supplementary data to this article can be found online at https://doi.org/10.1016/j.ab.2025.115784.

## Data availability

Data will be made available on request.

## References

[1] M.R. Loffredo, L. Nencioni, M.L. Mangoni, B. Casciaro, Antimicrobial peptides for novel antiviral strategies in the current post-COVID-19 pandemic, J. Pept. Sci. 30 (2024) e3534.
[2] Y.-C.J. Lee, J.D. Shirkey, J. Park, K. Bisht, A.J. Cowan, An Overview of antiviral peptides and Rational Biodesign Considerations, BioDesign Res. 2022 (2022) 9898241.
[3] D.W. Hutchinson, Metal chelators as potential antiviral agents, Antiviral Res 5 (1985) 193–205.
[4] A.M. Pinkham, Z. Yu, J.A. Cowan, Attenuation of west nile virus NS2B/NS3 Protease by amino terminal copper and nickel binding (ATCUN) peptides, J. Med. Chem. 61 (2018) 980–988.
[5] C. Abate, F. Carnamucio, O. Giuffrè, C. Foti, Metal-based compounds in antiviral therapy, Biomolecules 12 (2022) 933.
[6] D.M.J. Houston, J.J. Bugert, S.P. Denyer, C.M. Heard, Potentiated virucidal activity of pomegranate rind extract (PRE) and punicalagin against Herpes simplex virus (HSV) when co-administered with zinc (II) ions, and antiviral activity of PRE against HSV and aciclovir-resistant HSV, PLoS One 12 (2017) e0179291.
[7] R. Ahmad, M. Choudhary, Design and synthesis of copper(ii) and nickel(ii) complexes as potential inhibitors against SARS-CoV-2 viral RNA binding protein and Omicron RBD protein, New J. Chem. 48 (2024) 15053–15076.
[8] D. Boas, M. Reches, A novel copper-binding peptide that Self-Assembles into a Transparent antibacterial and antiviral Coating, Front. Bioeng. Biotechnol. 9 (2021) 736679.
[9] S.A. Galal, A.S. Abd El-All, K.H. Hegab, A.A. Magd-El-Din, N.S. Youssef, H.I. El-Diwani, Novel antiviral benzofuran-transition metal complexes, Eur. J. Med. Chem. 45 (2010) 3035–3046.
[10] K. Mulder, L.A. Lima, V. Miranda, S.C. Dias, O.L. Franco, Current scenario of peptide-based drugs: the key roles of cationic antitumor and antiviral peptides, Front. Microbiol. 4 (2013).
[11] C.M. Agbale, J.K. Sarfo, I.K. Galyuon, S.A. Juliano, G.G.O. Silva, D.F. Buccini, M. H. Cardoso, M.D.T. Torres, A.M. Angeles-Boza, C. de la Fuente-Nunez, O.L. Franco, Antimicrobial and Antibiofilm activities of Helical antimicrobial peptide sequences incorporating metal-binding Motifs, Biochemistry 58 (2019) 3802–3812.
[12] J.L. Alexander, Z. Thompson, J.A. Cowan, Antimicrobial Metallopeptides, ACS Chem. Biol. 13 (2018) 844–853.
[13] M. Jezowska-Bojczuk, K. Stokowa-Soltys, Peptides having antimicrobial activity and their complexes with transition metal ions, Eur. J. Med. Chem. 143 (2018) 997–1009.
[14] A.M. Cole, Y.H. Kim, S. Tahk, T. Hong, P. Weis, A.J. Waring, T. Ganz, Calcitermin, a novel antimicrobial peptide isolated from human airway secretions, FEBS Lett. 504 (2001) 5–10.
[15] M. D'Accolti, D. Bellotti, E. Dzien, C. Leonetti, S. Leveraro, V. Albanese, E. Marzola, R. Guerrini, E. Caselli, M. Rowinska-Zyrek, M. Remelli, Impact of C- and N-terminal protection on the stability, metal chelation and antimicrobial properties of calcitermin, Sci. Rep. 13 (2023) 18228.
[16] D. Bellotti, M. Toniolo, D. Dudek, A. Mikolajczyk, R. Guerrini, A. Matera-Witkiewicz, M. Remelli, M. Rowinska-Zyrek, Bioinorganic chemistry of calcitermin - the picklock of its antimicrobial activity, Dalton Trans. 48 (2019) 13740–13752.
[17] D. Bellotti, M. D'Accolti, W. Pula, N. Huang, F. Simeliere, E. Caselli, E. Esposito, M. Remelli, Calcitermin-loaded smart gels activity against Candida albicans: a Preliminary in vitro study, Gels (Basel, Switzerland) 9 (2023) 165.
[18] S. Leveraro, K. Garstka, P. Śliwka, T. Janek, M. Rowińska-Żyrek, M. Remelli, D. Bellotti, Metal coordination governs the antimicrobial efficacy of calcitermin derivatives, Dalton Trans. 53 (2024) 12676–12687.
[19] D. Bellotti, A. Sinigaglia, R. Guerrini, E. Marzola, M. Rowinska-Zyrek, M. Remelli, The N-terminal domain of Helicobacter pylori's Hpn protein: the role of multiple histidine residues, J. Inorg. Biochem. 214 (2021) 111304.
[20] M. Rowińska-Żyrek, H. Kozłowski, Nickel binding sites – coordination modes and thermodynamics, in: The Biological Chemistry of Nickel, The Royal Society of Chemistry, 2017, pp. 43–59.
[21] Y. Altun, F. Köseoglu, Stability of copper(II), nickel(II) and zinc(II) binary and ternary complexes of histidine, histamine and glycine in aqueous solution, J. Solution Chem. 34 (2005) 213–231.
[22] G. Pappalardo, G. Impellizzeri, R.P. Bonomo, T. Campagna, G. Grasso, M.G. Saita, Copper(II) and nickel(II) binding modes in a histidine-containing model dodecapeptide, New J. Chem. 26 (2002) 593–600.
[23] E. Farkas, É.A. Enyedy, G. Micera, E. Garribba, Coordination modes of hydroxamic acids in copper(II), nickel(II) and zinc(II) mixed-ligand complexes in aqueous solution, Polyhedron 19 (2000) 1727–1736.
[24] E.M. Jouad, G. Larcher, M. Allain, A. Riou, G.M. Bouet, M.A. Khan, X.D. Thanh, Synthesis, structure and biological activity of nickel(II) complexes of 5-methyl 2-furfural thiosemicarbazone, J. Inorg. Biochem. 86 (2001) 565–571.
[25] S. Svane, J.J. Sigurdarson, F. Finkenwirth, T. Eitinger, H. Karring, Inhibition of urease activity by different compounds provides insight into the modulation and association of bacterial nickel import and ureolysis, Sci. Rep. 10 (2020) 8503.
[26] B. Zambelli, V.N. Uversky, S. Ciurli, Nickel impact on human health: an intrinsic disorder perspective, Biochim. Biophys. Acta 1864 (2016) 1714–1731.
[27] F.H. Nielsen, D.A. Ollerich, Proceedings: nickel: a new essential trace element, Fed, SAVE Proc. 33 (1974) 1767–1772.
[28] A. Das, A. Rajeev, S. Bhunia, M. Arunkumar, N. Chari, M. Sankaralingam, Synthesis, characterization and antimicrobial activity of nickel(II) complexes of tridentate N3 ligands, Inorg. Chim. Acta. 526 (2021) 120515.
[29] T.M. Hunter, I.W. McNae, D.P. Simpson, A.M. Smith, S. Moggach, F. White, M. D. Walkinshaw, S. Parsons, P.J. Sadler, Configurations of nickel–Cyclam antiviral complexes and protein Recognition, Chem. Eur J. 13 (2007) 40–50.
[30] R.D. Graham, D.R. Williams, The synthesis and screening for anti-bacterial, -cancer, -fungicidal and -viral activities of some complexes of palladium and nickel, J. lnorg. Nucl. Chem. 41 (1979) 1245–1249.
[31] B. Atasever Arslan, B. Kaya, O. Şahin, S. Baday, C.C. Saylan, B. Ülküseven, The iron (III) and nickel(II) complexes with tetradentate thiosemicarbazones. Synthesis, experimental, theoretical characterization, and antiviral effect against SARS-CoV-2, J. Mol. Struct. 1246 (2021) 131166.
[32] N. Sarı, S.Ç. Şahin, H. Öğütcü, Y. Dede, S. Yalcin, A. Altundaş, K. Doğanay, Ni(II)-tetrahedral complexes: characterization, antimicrobial properties, theoretical studies and a new family of charge-transfer transitions, Spectrochim. Acta Mol. Biomol. Spectrosc. 106 (2013) 60–67.
[33] R.D. Everett, HSV-1 Biology and life cycle, in: R.J. Diefenbach, C. Fraefel (Eds.), Herpes Simplex Virus: Methods and Protocols, Springer New York, New York, NY, 2014, pp. 1–17.
[34] J.B. Epstein, C. Scully, Herpes simplex virus in immunocompromised patients: Growing evidence of drug resistance, Oral Surg. Oral Med. Oral Pathol. 72 (1991) 47–50.
[35] F. Nicoli, E. Gallerani, C. Skarlis, M. Sicurella, A. Cafaro, B. Ensoli, A. Caputo, P. C. Marconi, R. Gavioli, Systemic immunodominant CD8 responses with an effector-like phenotype are induced by intravaginal immunization with attenuated HSV vectors expressing HIV Tat and mediate protection against HSV infection, Vaccine 34 (2016) 2216–2224.
[36] I. Roca, M. Akova, F. Baquero, J. Carlet, M. Cavaleri, S. Coenen, J. Cohen, D. Findlay, I. Gyssens, O.E. Heure, G. Kahlmeter, H. Kruse, R. Laxminarayan, E. Liébana, L. López-Cerero, A. MacGowan, M. Martins, J. Rodríguez-Baño, J. M. Rolain, C. Segovia, B. Sigauque, E. Tacconelli, E. Wellington, J. Vila, The global threat of antimicrobial resistance: science for intervention, New Microbes and New Infections 6 (2015) 22–29.
[37] D. Bellotti, A. Miller, M. Rowinska-Zyrek, M. Remelli, Zn(2+) and Cu(2+) binding to the Extramembrane Loop of Zrt2, a zinc transporter of Candida albicans, Biomolecules 12 (2022) 121.
[38] P. Gans, A. Sabatini, A. Vacca, SUPERQUAD: an improved general program for computation of formation constants from potentiometric data, J. Chem. Soc., Dalton Trans. (1985) 1195–1200.
[39] P. Gans, B. O'Sullivan, GLEE, a new computer program for glass electrode calibration, Talanta 51 (2000) 33–37.
[40] G. Gran, Determination of the Equivalent point in potentiometric titrations. Part II, Analyst (1952) 661–671.
[41] P. Gans, A. Sabatini, A. Vacca, Investigation of equilibria in solution. Determination of equilibrium constants with the HYPERQUAD suite of programs, Talanta 43 (1996) 1739–1753.
[42] P.L. Brown, C. Ekberg, First Transition Series Metals, Hydrolysis of Metal Ions, Wiley-VCH, Weinheim, 2016, pp. 499–716.
[43] H. Gamsjäger, J. Bugajski, T. Gajda, R.J. Lemire, W. Preis, Chemical Thermodynamics of Nickel, Chemical Thermodynamics, OECD Nuclear Energy Agency Data Bank, Eslevier, Amsterdam, 2005.
[44] L. Alderighi, P. Gans, A. Ienco, D. Peters, A. Sabatini, A. Vacca, Hyperquad simulation and speciation (HySS): a utility program for the investigation of

equilibria involving soluble and partially soluble species, Coord. Chem. Rev. 184 (1999) 311–318.
[45] D. Bellotti, S. Leveraro, A. Hecel, M. Remelli, Investigation of metal interactions with YrpE protein of Bacillus subtilis by a polyhistidine peptide model, Anal. Biochem. 680 (2023) 115315.
[46] D. Bellotti, D. Loboda, M. Rowinska-Zyrek, M. Remelli, Investigation on the metal binding sites of a putative Zn(II) transporter in opportunistic yeast species, New J. Chem. 42 (2018) 8123–8130.
[47] E. Székely, G. Csire, B.D. Balogh, J.Z. Erdei, J.M. Király, J. Kocsi, J. Pinkóczy, K. Várnagy, The role of Side Chains in the Fine-Tuning of the metal-binding ability of multihistidine peptides, Molecules (2022).
[48] M. Perinelli, R. Guerrini, V. Albanese, N. Marchetti, D. Bellotti, S. Gentili, M. Tegoni, M. Remelli, Cu(II) coordination to His-containing linear peptides and related branched ones: Equalities and diversities, J. Inorg. Biochem. 205 (2020) 110980.
[49] M. Sicurella, M. Sguizzato, P. Mariani, A. Pepe, A. Baldisserotto, R. Buzzi, N. Huang, F. Simelière, S. Burholt, P. Marconi, E. Esposito, Natural Polyphenol-containing gels against HSV-1 infection: a Comparative study, Nanomaterials 12 (2022) 227.
[50] M. Sicurella, W. Pula, K. Musiał, K. Cieślik-Boczula, M. Sguizzato, A. Bondi, M. Drechsler, L. Montesi, E. Esposito, P. Marconi, Ethosomal gel for topical administration of Dimethyl Fumarate in the treatment of HSV-1 infections, Int. J. Mol. Sci. 24 (2023) 4133.
[51] M. Sicurella, M. Sguizzato, R. Cortesi, N. Huang, F. Simeliere, L. Montesi, P. Marconi, E. Esposito, Mangiferin-loaded smart gels for HSV-1 treatment, Pharmaceutics 13 (2021) 1323.
[52] R.B. Martin, M. Chamberlin, J.T. Edsall, The association of nickel(II) ion with peptides 1, J. Am. Chem. Soc. 82 (1960) 495–498.
[53] L.D. Pettit, S. Pyburn, H. Kozlowski, B. Decock-Le Reverend, F. Liman, Coordination of nickel(II) ions by angiotensin II and its peptide fragments. A potentiometric, proton nuclear magnetic resonance and circular dichroism spectroscopic study, J. Chem. Soc., Dalton Trans. (1989) 1471–1475.
[54] I. Turi, C. Kállay, D. Szikszai, G. Pappalardo, G. Di Natale, P. De Bona, E. Rizzarelli, I. Sóvágó, Nickel(II) complexes of the multihistidine peptide fragments of human prion protein, J. Inorg. Biochem. 104 (2010) 885–891.
[55] H. Kozlowski, A. Lebkiri, C.O. Onindo, L.D. Pettit, J.F. Galey, The influence of aspartic or glutamic acid residues in tetrapeptides on the formation of complexes with nickel(II) and zinc(II), Polyhedron 14 (1995) 211–218.
[56] K. Garstka, V. Dzyhovskyi, J. Wątły, K. Stokowa-Sołtys, J. Świątek-Kozłowska, H. Kozłowski, M. Barceló-Oliver, D. Bellotti, M. Rowińska-Żyrek, CH vs. HC—Promiscuous metal Sponges in antimicrobial peptides and Metallophores, Molecules 28 (2023) 3985.
[57] M. Peana, K. Zdyb, S. Medici, A. Pelucelli, G. Simula, E. Gumienna-Kontecka, M. A. Zoroddu, Ni(II) interaction with a peptide model of the human TLR4 ectodomain, J. Trace Elem. Med. Biol. 44 (2017) 151–160.
[58] D. Witkowska, R. Politano, M. Rowinska-Zyrek, R. Guerrini, M. Remelli, H. Kozlowski, The coordination of NiII and Cu(II) ions to the polyhistidyl motif of Hpn protein: is it as strong as we think? Chemistry (Easton) 18 (2012) 11088–11099.
[59] W. Bal, H. Kozlowski, R. Robbins, L.D. Pettit, Competition between the terminal amino and imidazole nitrogen donors for coordination to Ni(II) ions in oligopeptides, Inorg. Chim. Acta. 231 (1995) 7–12.
[60] K. Garstka, D. Bellotti, J. Wątły, H. Kozłowski, M. Remelli, M. Rowińska-Żyrek, Metal coordination to solute binding proteins – exciting chemistry with potential biological meaning, Dalton Trans. 52 (2023) 16140–16150.
[61] K. Ősz, B. Bóka, K. Várnagy, I. Sóvágó, T. Kurtán, S. Antus, The application of circular dichroism spectroscopy for the determination of metal ion speciation and coordination modes of peptide complexes, Polyhedron 21 (2002) 2149–2159.
[62] W. Bal, J. Lukszo, M. Jezowska-Bojczuk, K.S. Kasprzak, Interactions of nickel(II) with Histones. Stability and solution structure of complexes with CH3CO-Cys-Ala-Ile-His-NH2, a putative metal binding sequence of Histone H3, Chem. Res. Toxicol. 8 (1995) 683–692.
[63] D. Bellotti, M. Rowinska-Zyrek, M. Remelli, Novel insights into the metal binding ability of ZinT periplasmic protein from Escherichia coli and Salmonella enterica, Dalton Trans. 49 (2020) 9393–9403.
[64] U.L. Urmi, A.K. Vijay, R. Kuppusamy, S. Islam, M.D.P. Willcox, A review of the antiviral activity of cationic antimicrobial peptides, Peptides 166 (2023) 171024.
[65] K. Bakshi, M.R. Liyanage, D.B. Volkin, C.R. Middaugh, Circular dichroism of peptides, in: A.E. Nixon (Ed.), Therapeutic Peptides: Methods and Protocols, Humana Press, Totowa, NJ, 2014, pp. 247–253.
[66] W.C. Johnson Jr., Protein secondary structure and circular dichroism: a practical guide, Proteins: Struct., Funct., Bioinf. 7 (1990) 205–214.
[67] H. Irving, R.J.P. Williams 637, The stability of transition-metal complexes, J. Chem. Soc. (1953) 3192–3210.
[68] K.H. Thompson, C. Orvig, Boon and Bane of metal ions in medicine, Sci 300 (2003) 936–939.
[69] H.M. Abd El-Lateef, T. El-Dabea, M.M. Khalaf, A.M. Abu-Dief, Development of metal complexes for treatment of Coronaviruses, Int. J. Mol. Sci. 23 (2022) 6418.
[70] A. Miller, A. Mikołajczyk, D. Bellotti, K. Garstka, J. Wątły, A. Hecel, R. Wieczorek, A. Matera-Witkiewicz, M. Rowińska-Żyrek, Zn(II) and Cu(II) coordination enhances the antimicrobial activity of Piscidin 3, but not that of Piscidins 1 and 2, Inorg. Chem. 63 (2024) 12958–12968.
[71] K. Szarszoń, N. Baran, P. Śliwka, M. Wiloch, T. Janek, J. Wątły, Bioinorganic chemistry Meets Microbiology: copper(II) and zinc(II) complexes doing the Cha-Cha with the C-t-CCL-28 peptide, Dancing till the end of Microbes, Inorg. Chem. 63 (2024) 19105–19116.
[72] T. Elias, L.H. Lee, M. Rossi, F. Caruso, S.D. Adams, In vitro analysis of the antioxidant and antiviral activity of Embelin against herpes simplex virus-1, Microorganisms 9 (2021) 434.
[73] S.A. Read, S. Obeid, C. Ahlenstiel, G. Ahlenstiel, The role of zinc in antiviral Immunity, Adv. Nutr. 10 (2019) 696–710.